SAINT PETERSBURG STATE UNIVERSITY

Published as manuscript

Ruchkin Maksim Vladimirovich

CHRONOLOGY AND DEPOSITION CONDITIONS OF THE MGA MARINE INTERGLACIAL FORMATION IN THE NEVA LOWLAND

Translation from Russian

1.6.14. Geomorphology and paleogeography

Thesis for the Candidate Degree in Geography

Supervisor:

Doctor in Geology
and Mineralogy,
Candidate in Chemistry
V. Yu. Kuznetsov

Saint Petersburg - 2024

Content

Introduction

Motivation

The Last Interglacial (LIG, Mikulino, Eemian) was climatically similar to the present Holocene period. It approximately correlates with marine isotope stage (MIS) 5e (LIGA Members, 1991; CAPE-LIP Members, 2006), which lasted from 130 to 115 ka ago (Shackleton et al., 2002; Lisiecki and Raymo, 2005), though its precise age bounds have been a subject of discussions (Govin et al., 2015). The LIG paleogeography has implications for the ongoing global natural processes, especially important in view of the current global warming. Already at present, the global mean annual ground surface temperature is 1°C above that of the pre-industrial era, and the excess may reach 1.5 to 5 °C by the end of the 21st century, according to different scenarios (IPCC, 2022). In this respect, the global climate will be ever more similar to that of the LIG, when the mean annual temperature during the optimum was 1–2 °C higher than it is now (CAPE-LIP Members, 2006; Turney and Jones, 2010).

The onset of the LIG was marked by extremely rapid eustatic sealevel rise, up to ~6 m above the present stand (Murray-Wallace and Woodroffe, 2014). The interglacial transgression deposits in the northwestern East European Plain belong to the Mga Formation (Malakhovsky et al., 1989), the thickest (≥30 m) within the Neva Lowland (Znamenskaya and Cheremisinova, 1962). The Mga Fm. in the Neva Lowland consists of clay and silt with marine mollusc fauna and the clay is of industrial value as raw material for production of bricks. The Mga marine deposits have easily recognizable Mikulino pollen spectra (Znamenskaya, 1959; Lavrova and Grichuk, 1960), which makes them a reliable stratigraphic marker for the Pleistocene division of Northwestern European Russia. Furthermore, the deposits of the Mga (Boreal, Eemian) transgression can be used as reference for inter-regional stratigraphic correlations.

The present study is based on data collected from the Mga deposits cropping out in the quarry of the Etalon (formerly Sverdlov) brick factory located in the central Neva Lowland. This is the only section in Northwestern European Russia where the Mga Fm., together with the underlying and overlying sediments, is exposed in outcrops and thus can provide age and stratigraphic constraints for the formation itself, as well as for the evolution stages of the Mga Sea and pre- and post-Mga continental paleobasins. The large thickness of the interglacial deposits allows tracing in detail the depth-dependent paleographic changes in the area.

The level of development of the subject

A significant contribution to the study of the problem of chronology and deposition conditions of the Mga marine interglacial formation in the Neva Lowland was made by N. V. Potulova, M. A. Lavrova, O. M. Znamenskaya, E. A. Cheremisinova, M. P. Grichuk, D. B Malakhovsky, E. S. Pleshivtseva and A. N. Molodkov.

The Mga Fm. in the Neva Lowland and surrounding territories has undergone extensive research. Spore-pollen and diatom analyses successfully determined the Mikulino age of the Mga Fm. and identified the main phases of the Mga Sea evolution during the LIG. However, some paleogeographic methods, such as geochemical analysis, were not applied to deposits. The chronology of the Mga Fm. deposition has been studied insufficiently. Four ESR ages based on mollusc shells have been obtained but fail to constrain its chronostratigraphic volume.

Chocolate varved clay of the Late Moscow age, formed in a glacial lake during two stadials separated by the Kasplya Interstadial, underlie the Mga deposits in the territory of the Neva Lowland. Brackish diatoms identified in interstadial sediments mark the first inflow of seawater into the Mga Basin. Although the presence of varve deposits under the Mga Fm. has been recognized since long ago, varve chronological studies are yet to be conducted.

The Mga deposits displays limited species and poor quantitative diversity of marine molluscs compared to the coeval deposits of the Boreal and Eemian transgressions. Anoxic conditions were widespread in the bottom waters of the Mga Sea, but no data are currently available on the anoxia chronology in the Mga Basin.

The lack of knowledge about the chronology and deposition conditions of the Mga marine interglacial formation in the Neva Lowland determined the main focus, goal, and objectives of the study.

The studies were performed using clay, silt, and sand samples from the sequence between two major moraines in the Neva Lowland.

The *main focus* of the research was on geochronology and stratigraphy of sediments, as well as on paleogeography of their deposition basins.

Principal goal and objectives

The main goal of the research consisted in constraining the chronological volume of the Mga Fm. in the territory of the Neva Lowland, reconstructing the deposition conditions and main evolution phases of the Mga Sea.

The principal objectives accomplished in order to achieve the goal included:

1. Inventory of the available published data and archived geological and technical reports on the conditions and time of the Mga Fm. deposition.

2. Field work in the Etalon quarry for documenting local geology and sampling for further analytical work.

3. Reconstructing the vegetation history in the Neva Lowland during the Mikulino Interglacial and Moscow Late Glacial on the basis of pollen analysis.

4. Optically stimulated luminescence (OSL) dating of intermorainic sediments sampled from the quarry.

5. Diatom analysis for reconstructing main events in the evolution of the Mga Sea.

6. Elucidating sedimentation patterns in the Neva basin of the Mga Sea from grain size data.

7. Updating the history of the Neva basin of the Mga Sea and reconstructing the near-bottom deposition conditions on the basis of geochemical analytical data.

8. Correlating the phases of the LIG vegetation history within the Baltic and Onego-Ladoga regions.

Methodology and methods

The dissertation research objectives were conducted using geological and paleogeographic methods. These included lithological (facial and grain size analyses), paleontological (pollen and diatom analyses), geochronometric (OSL dating and varve chronology), and geochemical (X-ray fluorescence and CN analyses) methods.

Novelty

In the course of the work, the following achievements were performed for the first time:

– Several methods were used jointly to study the Mga marine interglacial deposits of the Mikulino regional stage, as well as sediments above and below the Mga Fm.: analyses of sedimentary facies, spore and pollen spectra, contents of chemical elements, particle sizes and diatom taxonomy, as well as OSL dating and varve chronology;

– The relative salinity and oxygenation of water in the Mga Sea and the basin history were reconstructed using geochemical analyses of samples;

– The age of the Mikulino Interglacial was constrained by means of Bayesian age-depth modeling based on the OSL ages of the Mga Fm. samples;

– The boundary between the brackish and marine phases in the evolution of the Baltic and Mga Seas was proven to be isochronous during the LIG throughout the area and was used for reference to estimate the lag of vegetation evolution phases behind the respective phases in Central Europe, in northern and northeastern directions.

Theoretical and practical significance

The presented study shed more light on the duration and intensity of climate events in the northwestern East European Plain during the Moscow Late Glacial and Mikulino Interglacial. Good agreement between geochemical and diatom data indicates that element contents can be a reliable proxy of deposition conditions, along with such classical proxies as pollen spectra and diatom taxonomy. The integrated approach of using jointly the spore-pollen analysis, OSL dating, and Bayesian modeling has demonstrated high efficiency in estimating the age bounds of Late Pleistocene climate-stratigraphic units. The boundary between the brackish and marine phases in the evolution of the Baltic and Mga

Seas, inferred to be isochronous throughout the area, provides ties for precise correlation of Eemian (Mikulino) sections within the Baltic and Onego-Ladoga regions.

Contribution of the author

Maksim Ruchkin, the author, organized and conducted field campaigns of 2020 and 2021 at the quarry of the Etalon (Sverdlov) Brick Factory. The field work included clearing and photographing sediment exposures, detailed lithological description of the exposed sediments, sampling for palynological, diatom, geochemical, grain-size, and macrofossil analyses and OSL dating. OSL ages were obtained for thirty three samples of soft sediments; additionally, seventy seven samples were analyzed for geochemistry (XRF and CN methods) and particle-size distribution. M. Ruchkin studied varve chronology of the Upper Moscow sediments, interpreted all analytical results, designed the structure of the thesis, and formulated main postulates and conclusions.

The reliability of the results is due to the extensive factual material obtained by the author on marine interglacial deposits of the Neva Lowland. The main scientific principles and conclusions are based on geochronological data (OSL dating), as well as data from pollen, diatom, geochemical, and grain size analyses obtained in accredited laboratories.

Testing

The data and results of the study were reported and discussed at meetings of the Geomorphology Department of the St. Petersburg State University, as well as at domestic and international conferences, including "Geochronology of the Quaternary Period: Instrumental Dating Methods of Recent Deposits" dedicated to the 90th anniversary of L. D. Sulerzhitsky (All-Russian Conference with International Participation, Moscow, 2019); “The Markov Readings in 2020 Year”, on the 115th Anniversary of Academician K. K. Markov (All-Russian Conference with International Participation, Moscow, 2020); Trends in Evolution Geography (All-Russian Scientific Conference in Memory of Professor A. A. Velichko, Moscow, 2021); "Geochronology of the Quaternary Period: Instrumental Dating Methods of Recent Deposits " (2nd All-Russian Conference with International Participation), Moscow, 2022); Methods of Absolute Chronology (14th International Conference, Gliwice, 2023).

Publications

The results of the study were reported in 23 publications: 9 papers (3 papers from the list of the State Commission for Academic Degrees and Titles and 6 papers in Scopus rated peer reviewed journals and) and 14 publications in proceeding volumes of conferences. Two more papers have been submitted to Scopus rated peer reviewed journals.

Content and scope of work

The thesis consists of Introduction, seven Chapters, Conclusion, and a list of references (398 references, among which 264 in foreign languages and 16 archived geological and technical reports).

The main text is in 155 pages (original text in Russian) and contains 50 figures and 9 tables; the reference list is in 33 pages.

Main scientific results

As part of the dissertation work, the author's methodological developments for dating Quaternary deposits of various genesis using the optically stimulated luminescence (OSL) were applied, including:

– dating LIG marine sediments using quartz and K-feldspars aliquots;

– dating poorly bleached glaciofluvial and glaciolacustrine deposits using aliquots and single grains of quartz and K-feldspar;

– dating deposits of different origins using quartz aliquots with high (> 200 Gy) equivalent doses.

These developments have been presented in a number of publications:

1) *Zaretskaya N.E., Taldenkova E.E., Ovsepyan Ya.S.,* ***Ruchkin M.V.****, Baranov D.V., Rudenko O.V., Stepanova A.Yu.* First Data on the Paleogeographical Settings and Chronology of the Last Interglacial on the Zimnii Coast of the White Sea // Doklady Earth Sciences. 2023. Vol. 512. P. 1059–1064 (pp. 1060-1061).

2) *Novikov I.S., Nazarov D.V., Mikharevich M.V., Gladysheva A.S.,* ***Ruchkin M.V.****, Prudnikov S.G.* The Azas ice sheet and its role in the formation of Late Pleistocene ice-dammed lakes in southern Siberia: case study of Upper Kharal paleolake // Geology and Geophysics. 2023. Vol. 64, No. 5. P. 595–606 (pp. 597–598).

3) *Zaretskaya N.E., Baranov D.V.,* ***Ruchkin M.V.****, Lugovoy N.N.* The Southeastern White Sea Coast in the Late Pleistocene // Izvestiya RAN (Akad. Nauk SSSR). Seriya Geograficheskaya. 2022. Vol. 86, No. 6. P. 898–913 (in Russian, pp. 900–901).

4) *Nazarov D.V., Nikolskaia O.A., Gladysheva A.S., Zhigmanovskiy I.V.,* ***Ruchkin M.V.****, Merkuljev A.V., Thomsen K.J.* Evidence for the intrusion of marine Atlantic waters into the West Siberian Arctic during the Middle Pleistocene // Boreas. 2022. Vol. 51, No. 2. P. 402–425 (pp. 406–412).

5) *Nazarov D.V., Nikolskaia O.A., Zhigmanovskiy I.V.,* ***Ruchkin M.V.****, Cherezova A.A.* Lake Yamal, an ice-dammed megalake in the West Siberian Arctic during the Late Pleistocene, ~60–35 ka // Quaternary Science Reviews. 2022. Vol. 289. 107614 (p. 5).

6) *Zaretskaya N.E., Korsakova O., Molodkov A.N.,* ***Ruchkin M.V.****, Baranov D.V., Rybalko A., Lugovoy N.N., Merkuljev A.V.* Early Middle Weichselian in the White Sea and adjacent areas: Chronology, stratigraphy and palaeoenvironments // Quaternary International. 2022. Vol. 632. P. 65–78 (pp. 68–69).

7) *Shvarev S.V., Zaretskaya N.E.,* ***Ruchkin M.V.****, Lugovoy N.N., Zazovskaya E.P., Subetto D.A.* Cross-OSL and 14C Dating of Young Subaerial Deposits in the Sambia (Kaliningrad) Peninsula // Doklady Earth Sciences. 2021. Vol. 499, No. 2. P. 639–642 (p. 641).

8) *Panin P.G., Filippova K.G., Bukhonov A.V., Karpukhina N.V., Kalinin P.I.,* ***Ruchkin M.V.*** High-resolution analysis of the Likhvin loess-paleosol sequence (the central part of the East European Plain, Russia) // Catena. 2021. Vol. 205. 105445 (p. 5).

Main defended postulates

1. The Mga marine interglacial deposition in the territory of the Neva Lowland lasted within a period corresponding to Mikulino pollen zones M_2–M_8, from 133±8 to 109±7 ka ago. The beginning of the Mikulino Stage in the Neva Lowland coincides roughly with the top of the Sverdlov varved clay.

2. The evolution of the Mga Sea comprised four main phases of glaciomarine (pollen zones Ms_3–Ms_1), brackish (M_2–M_3), marine (M_4–M_6), and regressive (M_6–M_8) environments. Seawater penetrated into the Late Moscow periglacial basin in the territory of the present Neva Lowland no later than ~1100 years before the Mikulino Interglacial. Between ~1030 and ~350 years before the LIG, the Mga Sea became much less saline (or freshwater), but then the connection with the ocean resumed.

3. The bottom water of the Mga Sea became anoxic in the beginning of pollen zone M_5, and these conditions lasted till the end of zone M_8. The lack of oxygen in the bottom water accounts for low numbers and poor diversity of molluscs in the Mga sediments.

Acknowledgements

I wish to express my sincere gratitude to V. Yu. Kuznetsov, my supervisor and to M. V. Sheetov (VSEGEI, St. Petersburg) and D. V. Nazarov (VSEGEI), my advisers. I also thank my colleagues who made analytical work and shared their data. The work would be incomplete without analyses of pollen spectra (palynologist E. S. Nosevich, VSEGEI) and diatoms (analyst Z. V. Pushina, VSEGEI). The magnetic susceptibility data are courtesy of V. I. Dudanova (Moscow State University, Moscow). I greatly appreciate valuable advice on the OSL dating methods by A. S. Murray (Aarhus University, Denmark), D. Brill and T. Reimann (Cologne University, Germany), as well as the overall support by S. Opitz (Cologne University, Germany) who supervised measurements of grain sizes and geochemical analyses of samples. More thanks go to R. S. Shukhvostov (Moscow State University, Moscow) and P. Yu. Belyaev (VNIIOkeangeologiya Institute, St. Petersburg) for assistance in sampling, A.V. Merkuliev (VSEGEI) for mollusc identification, P.A. Kosintsev (IAPE, Yekaterinburg) for identification of mammal bones, and I. V. Timofeeva (VSEGEI), V. Hansen, W. Thompson (Technical University of Denmark, Denmark), A. Zander, H. Ketges, and L. Dünn (Cologne University, Germany) for assistance in preparation of samples for OSL dating. Special gratitude is due to S. V. Krivonos, the director of the

Etalon quarry, for support in the field work. Thanks are extended to T. I. Perepelova for aid with translations.

OSL dating at the Nordic Center for Luminescence Research (DTU Risø Campus, Roskilde, Denmark) was supported by the Danish Government Scholarship under the Cultural Agreements Programme. Luminescence, geochemical, and grain-size analyses conducted at the Cologne University (Germany) were supported jointly by the German Academic Exchange Service (DAAD) and Saint Petersburg University within the “Dmitrij Mendeleev” Programme.

Chapter 1. Local geology and geomorphology

The Neva Lowland located in the drainage basin of the Neva River between the Neva Bay (Gulf of Finland, Baltic Sea) and Lake Ladoga is a part of the Fore-Klint Lowland (Fig. 1.1). It borders the Baltic Klint in the south and the Lembolovo-Toksovo hilly (kame) area and the Central Upland of the Karelian Isthmus in the north. The Neva Lowland is a terraced plain distinctly expressed in the surface topography, with elevations from 0 to 40 m above the sea level (asl) and outliers reaching locally 78 m asl. The lowland area belongs to the pre-Quaternary topographic low at the junction between the Fennoscandian shield and the sedimentary cover of the East European Craton. The lowland developed upon ~400 m thick Vendian-Cambrian sediments lying almost horizontally above a basement dipping

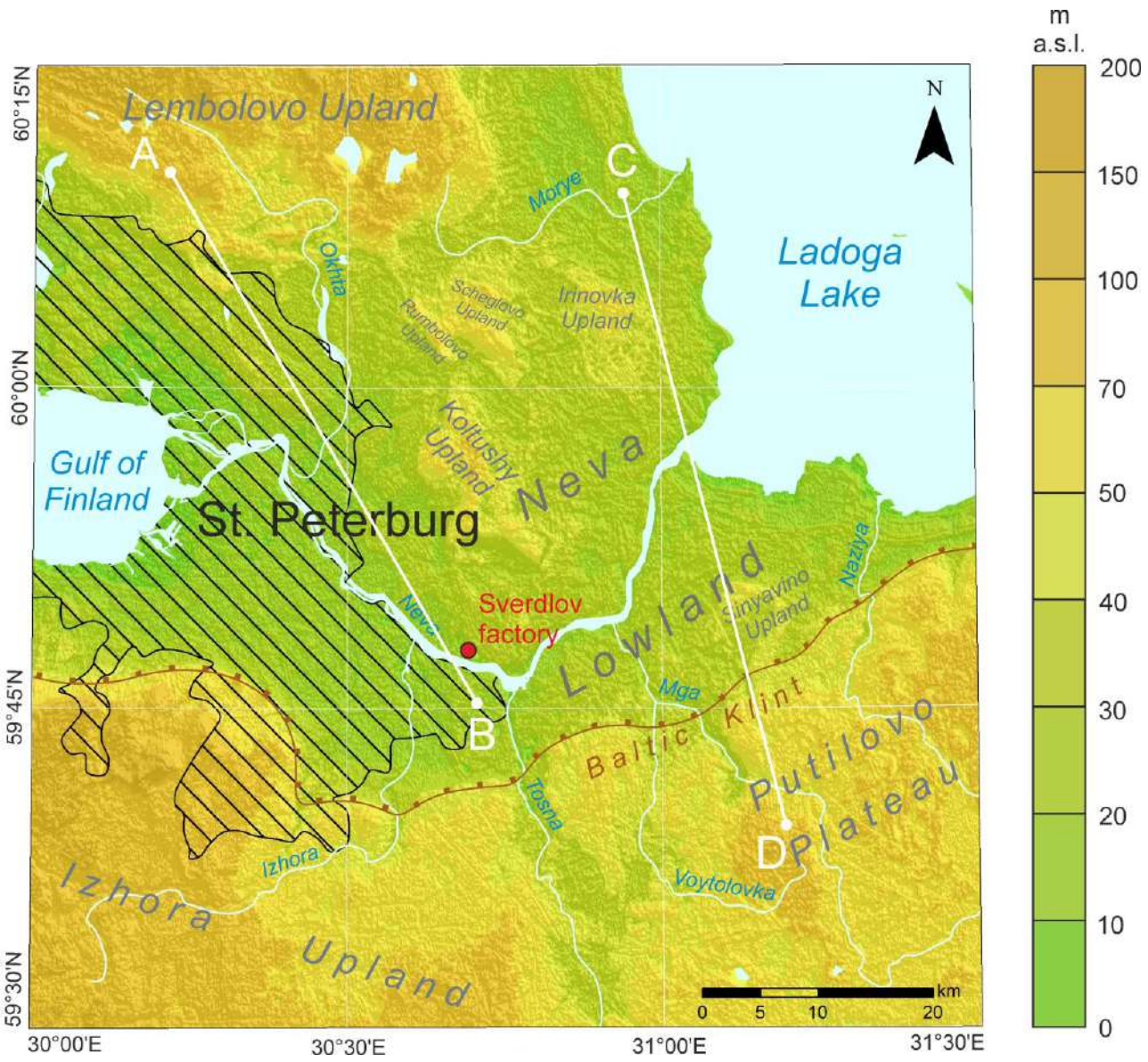

Fig. 1.1. Digital elevation model of the Neva Lowland and its surroundings (SRTM 1 Arc-Second). A–B and C–D are approximate locations of profiles corresponding to cross sections shown in Figs 1.2 and 1.3, respectively.

southward (Selivanova, 1962; Verbitsky et al., 2012). The pre-Quaternary rocks are overlain by Quaternary sediments reaching a thickness of 110 m or more (Nasonova et al., 1995; Auslender and Pleshivtseva, 2011).

The Quaternary sediments in the area of the Neva Lowland (Figs 1.2, 1.3) consist of three moraines, two inter-moraine beds, as well as Late Glacial and Holocene sediments over the upper moraine (Yakovlev, 1926; Auslender and Pleshivtseva, 2011). The upper (Ostashkov) and lower (Moscow) moraines extend almost throughout the area, except for a few eroded zones, whereas the lower moraine is of sporadic occurrence restricted to pre-glacial topographic lows and pre-Quaternary valleys (Auslender, 1998). The lower moraine is most often assigned to the Vologda (Dnieper) Stage of the regional stratigraphy, though there is no enough data for its reliable correlation (Auslender and Pleshivtseva, 2011). The sediments over the Vologda moraine are mainly coarse-grained fluvioglacial facies (Auslender and Pleshivtseva, 2011). The intermorainic Moscow-Valdai sequence is composed of the Upper Moscow glaciolacustrine and glaciomarine, Mga marine, as well as Lower and Middle Valdai lacustrine and alluvial facies. The Mga marine unit of the Mikulino Stage is an essential marker for the stratigraphic division of Pleistocene sediments. No intermorainic marine deposits of other ages have been found in the area of the Neva Lowland. The Pleistocene sequence is topped by late-glacial fluvioglacial sediments and glaciolacustrine deposits of the Baltic Ice Lake. They, in turn, lay under Holocene marine deposits of the Littorina and modern Baltic Seas in the Neva Delta and Neva Bay coast, respectively, deposits of the Ladoga transgression in the Neva headwaters, alluvium in river valleys and organic-bearing lacustrine-boggy facies.

The Neva Lowland is an area of smooth topography sloping gently toward the Gulf of Finland and Lake Ladoga. It consists of several terraced steps composed of the Baltic Ice Lake, Littorina Sea, modern Baltic Sea, and Lake Ladoga deposits. In addition, the topographic pattern includes beaches, sand pits, and sand ridges that record the stages of water level fall in the local lakes and seas. The highest elevated zones of the area are remnant topographic highs composed of the Upper Valdai kame (Koltushi and Rumbolovo) and moraine (Scheglovo, Irinovka, Vaganovo, Sinyavino, Kelkolovo, Gory) deposits (Fig. 1.1). The elongate zone along the Baltic Klint bears signatures of thrust-like glacial deformation (Nasonova et al., 1995).

The Neva River valley is a key topographic element of the Neva Lowland. It is 74 km long, 400 to 1250 m wide, up to 24 m deep, with steep sides, 6–9 m of average height (Nezhikhovsky, 1981). Unlike the classical plainland river valleys, the Neva valley lacks terraces and meanders. Near the Neva mouth, it splays into numerous arms forming a broad delta produced by erosion rather than by deposition. The river arms are incised into marine and glaciolacustrine deposits forming an incision delta (Nasonova

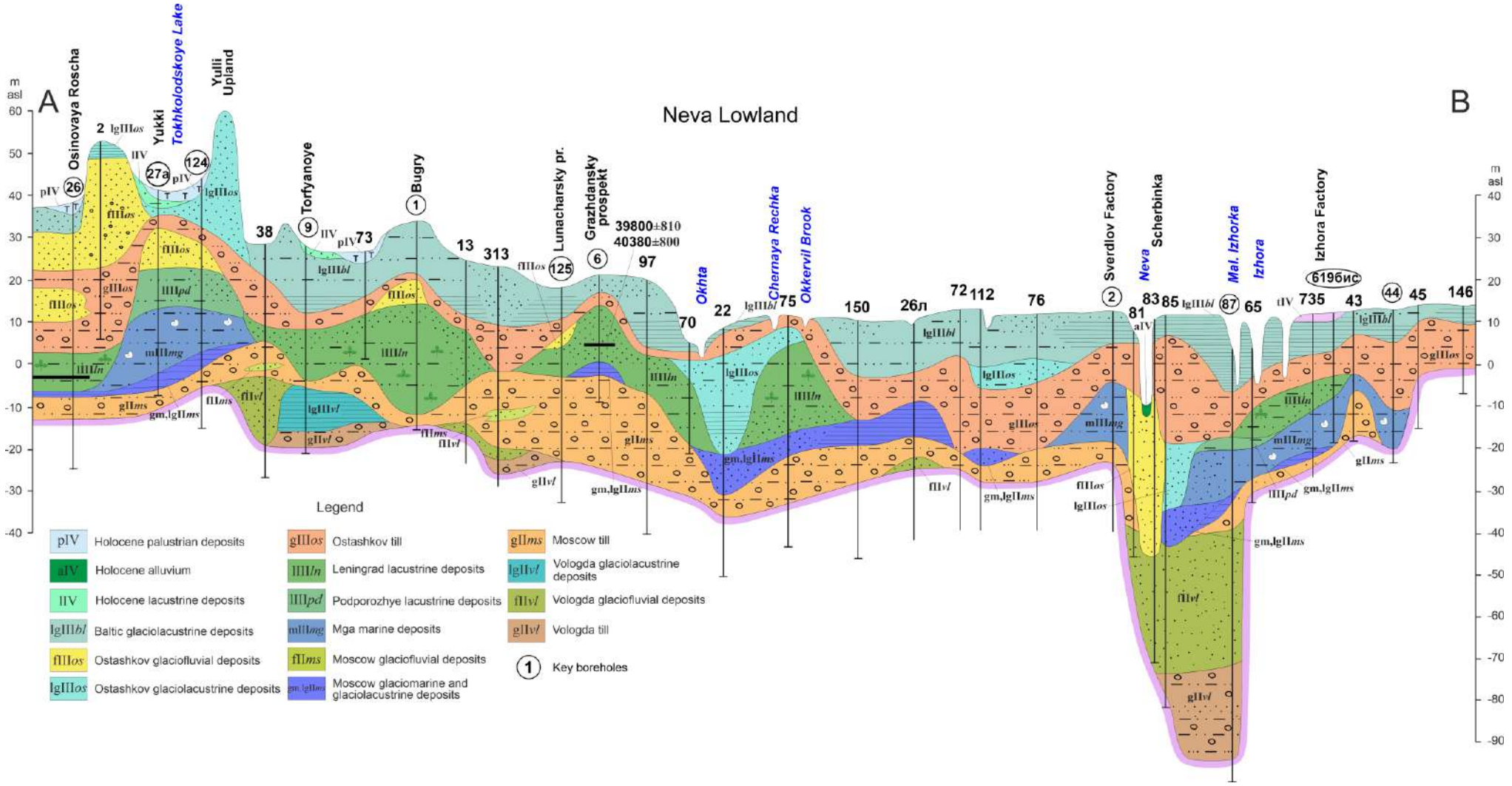

Fig. 1.2. Cross section of Quaternary sediments, western Neva Lowland (A–B, Figure 1.1), modified after Auslender and Pleshivtseva (2011).

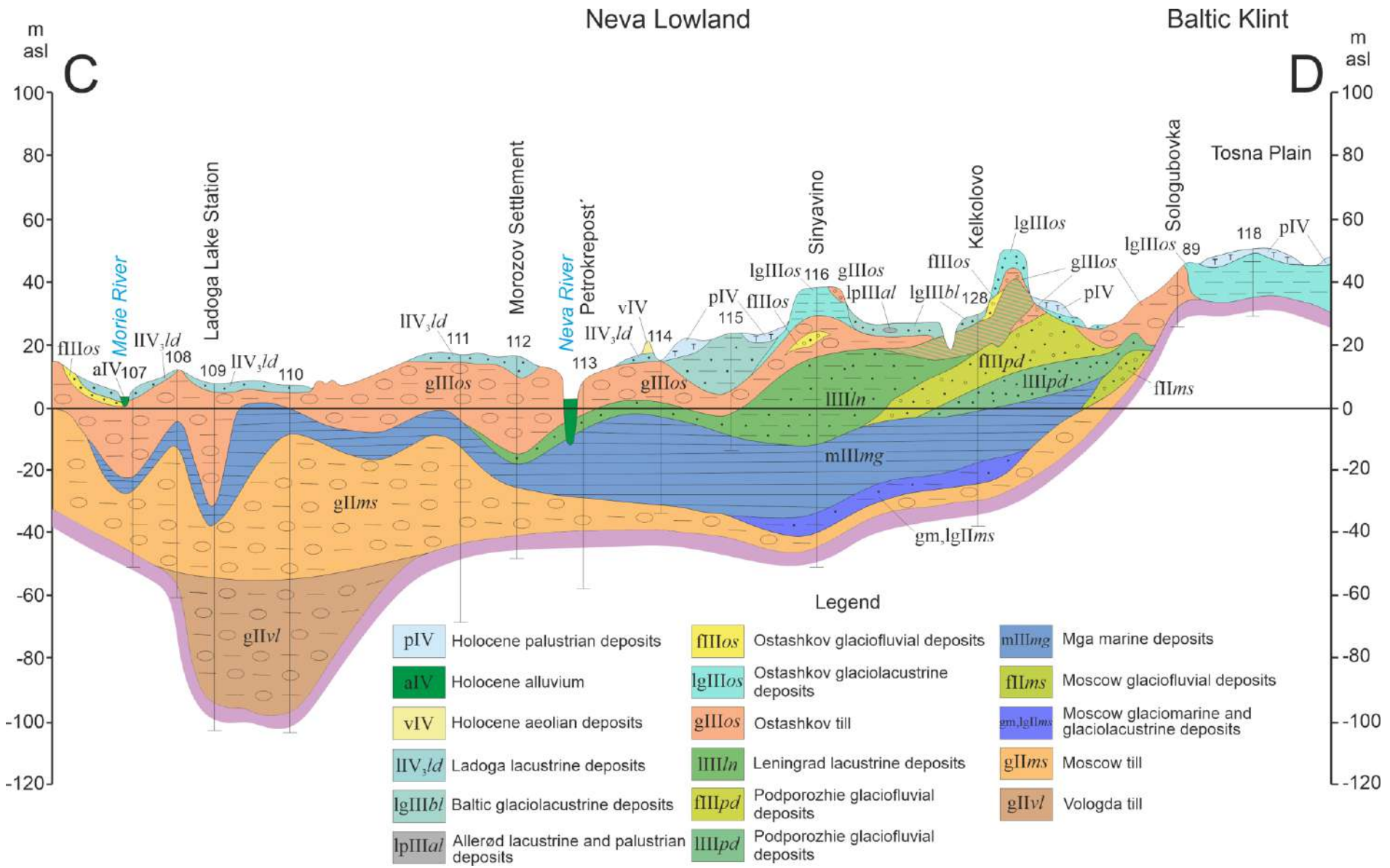

Fig. 1.3. Cross section of Quaternary sediments, eastern Neva Lowland (A–B, Figure 1.1), modified after Nasonova et al. (1995).

et al., 1995). The particular morphology of the Neva River valley shaped up about 3350 cal BP (Saarnisto, 2012) when waters broke through the watershed in the area of the modern Ivanovskie Rapids during the Ladoga transgression (Ailio, 1915, cited from Dudanova et al., 2020). Alternatively, the Neva may have existed already in the earliest Holocene (Verzilin et al., 1997; Dudanova et al., 2020).

Chapter 2. Last Interglacial deposits in the Neva Lowland: historic background

2.1. Mga section and Mga Formation

The studies of the LIG deposits in the Neva Lowland (Fig. 2.1) began in 1921, when black layered clay with marine mollusc fossils was discovered in the course of geological survey in an outcrop on the left bank of the Mga River, downstream of the Voitolovka mouth in the vicinity of Petrograd (St. Petersburg) (Fig. 2.2) (Potulova, 1921). The marine sediments were first interpreted as deposits of the Yoldia Sea, as no overlying moraine was found then (Potulova, 1921), but more detailed later studies showed that the Mga Formation (Fm.) was sandwiched between two moraines (Potulova, 1922). The Mga marine clay contained mollusc shell remnants of *Tellina (Macoma) calcarea*, *Yoldia (Portlandia) arctica*, *Mytilus edulis* (identified by N. Knipovich) and *Littorina littorea* (found by E. Abakumova)

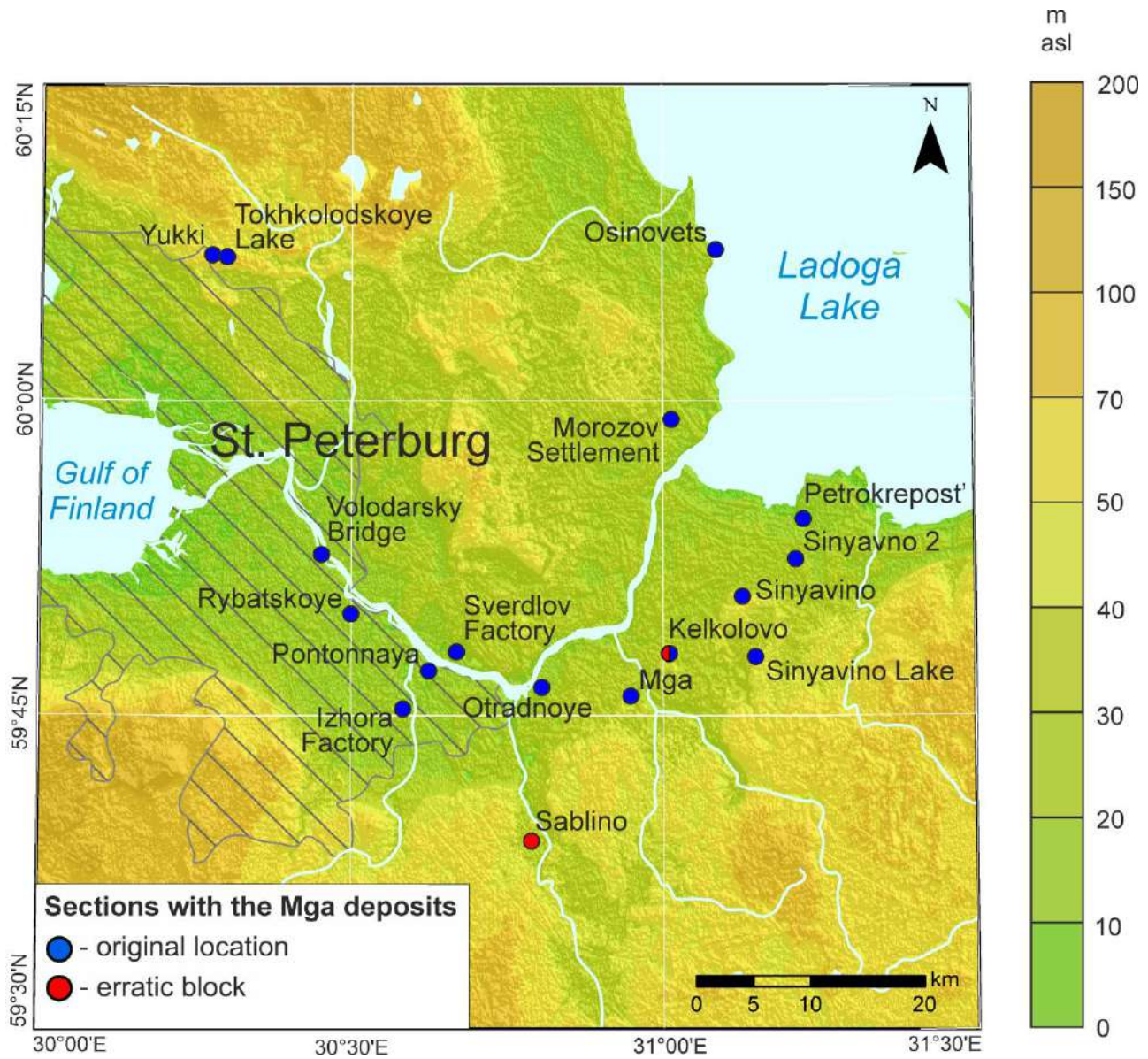

Fig. 2.1. Location map of the Mga interglacial deposits in the Neva Lowland and surrounding areas.

(Potulova, 1922; 1924). The Mga Fm. bearing marine fauna were timed as pre-glacial from the data of geological surveys in 1923 performed for 10 verst mapping of European Russia (Yanishevsky, 1924). However, Yakovlev (Jakowleff, 1923; Yakovlev, 1926) placed the Mga deposits between the Danish Glacial (15–11.5 ka ago) and an earlier glaciation of an uncertain age represented, respectively, by the middle and lower moraines of Leningrad and its vicinities. The position of the Mga Fm. between the middle and lower moraines was supported in another model (Potulova, 1924, 1932) attributing the marine clay to the Mindel-Riss interglacial and correlating the Mga Fm. with the deposits of the Boreal transgression in northern Russia, as well as with the interglacial marine sediments of Europe.

The Mga Fm. was first unambiguously correlated with the Riss-Würm interglacial by Yanishevsky (1931) who also described brown varved clay under the marine sediments in a borehole drilled by P. Kumpan in 1925 on the right side of the Mga River, 300 m downstream of the railway bridge. That interpretation was favored by data from a large collection of fossils from the Mga clay

Fig. 2.2. The Mga interglacial deposits containing mollusc shells in the stratotype section located on the left bank of the Mga River, near the “45 km” railway station, 30 m downstream of the footbridge (photograph by M. Ruchkin).

(Skorokhod, 1932), which included *Yoldia arctica aestuariorum (Portlandia aestuariorum)*, *Yoldia*

arctica siliqua (Portlandia siliqua), *Cardium ciliatum (Ciliatocardium ciliatum ciliatum)* and *Cardium (Cerastoderma) edule* molluscs besides the previously identified species, as well as bones of Cyprinidae fishes (identified by V. Shtylko), remnants of Cyperaceae leaves, and a branch of a Pinaceae tree (identified by A. Krishtofovich). The observed depth-dependent variations in the taxonomic composition of molluscs recorded changes from a freshened shallow gulf to a gradually shoaling sea (Skorokhod, 1932). The mollusc collection of Skorokhod (1932) was supplemented by the discovery of *Anomia (Heteranomia) squamula*, as described by Lavrova (1939). The Riss-Würm timing of the Mga Fm. was largely supported at that time (Lavrova, 1939; Gerasimov and Markov, 1939; Goretsky, 1949).

The first pollen spectra for the Mga clay (Pokrovskaya, 1936) revealed several phases in the vegetation history different from those in other known interglacial deposits of the Leningrad region. The pollen data and the presence of cold-water mollusc and diatom assemblages enabled Pokrovskaya to conclude that the marine sediments had an interstadial origin, a view supported by other researchers (Zemlyakov, 1936; Sukachev, 1936; Hyyppä, 1937).

V. Zans (1936) and G. Brander (Brander, 1937a,b) posited that the interglacial transgression consisted of two phases: the Eemian and the "Portlandia". In accordance with their views, the Eemian transgression took place during the earlierwarmer half of the interglacial period (pollen zones c–i, Jessen and Milthers, 1928), while the Portlandia transgression occurred during the later cooler half (pollen zones l–m, Jessen and Milthers, 1928). The Mga clay sequence is considered to have formed during the Portlandia transgression. Additionally, V. Zans hypothesized the presence of a connection between the Baltic and White Seas during the Portlandia interglacial transgression. The idea of a two-stage transgression was later disproved though, but the hypothesis of the Baltic-White Sea connection in the LIG was justified and developed in later studies (Cleve-Euler, 1940, cited from Cheremisinova, 1959; Lavrova, 1946; 1948; Goretsky, 1949).

The studies of diatoms in the Mga section began in the 1930-1940s by Zans, Brander, and Anisimova (Zans, 1936; Brander, 1937a; Sheshukova, 1949). The more complete lists of Brander and Anisimova included 100 species; the diatoms identified by Anisimova were mainly diverse fresh- and brackish species, with fewer marine taxa (Sheshukova, 1949).

A new model of glaciations and northern transgressions in the Russian Plain suggested in the 1940s by Yakovlev (1947; 1956) comprised four glacial and four interglacial events in the Late Pleistocene. According to his ideas, the Mga deposits were formed during the "4th New Interglacial," which existed approximately 20 thousand years ago. Similar ideas were put forward by Pokrovskaya (1954) and Apukhtin (Apukhtin et al., 1960, cited from Lavrova, 1962). The age of the Mga clay was further constrained by two radiocarbon dates for humus (36.5±1.0 ka BP) and mollusc shell (47.4±1.4 ka BP) samples (Starik et al., 1964). The dates were considered as the upper bound for high probability

of contamination with modern carbon, but were used as reliable reference (Apukhtin and Ekman, 1967) to correlate the Mga Fm. with the Mologa-Sheksna Interglacial of Moskvitin (1947) or Yakovlev's (1947) 3th Interglacial, corresponding to the 50–30 ka ago interval; the same timing for the Mga Fm. was suggested by Moskvitin (1965).

In 1947, Znamenskaya (1959) conducted a comprehensive study of the Mga section. Her findings from borehole (BH) 3 on the right bank of the Mga River and outcrop No. 4 on the left bank, located below the railway bridge, were used to create a composite geological model. In BH 3, the marine interglacial deposits are underlain by varved clay and sand more than 9 m thick. The Mga Fm. consists of marine mollusc shells and fragments of *Zostera marina* grass. Its thickness measures ~10 metres, and it can be found at 0-10 m asl.

Cheremisinova (1952; 1959; 1960) performed diatom analysis on samples taken from Znamenskaya's section. The diatom flora of the Mga section is highly diverse comprising over 200 species. Data on diatom assemblages along the section, allowed Cheremisinova to identify four evolutionphases of the Mga Sea.

Phase I corresponds to the initial penetration of seawater into the glacial lake. It was identified in varved deposits and named the *glaciomarine* phase by Cheremisinova (1952). The diatom assemblage of the glaciomarine phase comprises freshwater, cold-water, and multiple marine species. The domination of benthic diatoms indicates that the basin was shallow, around 20 meters.

Phase II is characterised by the condition of a freshened sea lagoon, with a depth of at least 30–40 meters and predominance of species that thrive at a water temperature of 1–3°C and a salinity of 4–8‰. The phase was called the *lagoon* phase (Znamenskaya and Cheremisinova, 1962), or the *lower lagoon* phase (Malakhovsky et al., 1969a).

Phase III encompasses strata where marine planktonic neritic and littoral diatoms are prevalent, whereas the brackish and euryhaline diatoms are absent. This assemblage indicates that the Mga Sea had a high salinity level (25–30‰) and a minimum depth of 50–75 m. This phase corresponds to the *highstand* of the Mga Sea (Cheremisinova, 1959) and is otherwise known as the *marine* phase (Malakhovsky et al., 1969a).

During Phase IV, several species of planktonic marine diatoms vanished while the percentages of freshwater, brackish and euryhaline species increased. The change in diatom assemblages indicates the regression of the Mga Sea, which commenced during the interglacial climatic optimum (Lavrova, 1948; Cheremisinova, 1952). This evolution stage of the Mga Basin is referred to as the *onset of sea regression* (Cheremisinova, 1959), or the *upper lagoon* phase (Cheremisinova, 1960).

The determinations of foraminiferal shells within the core of BH 3 (Nedesheva, 1972) confirm the conclusions derived from diatom analysis.

Pollen analysis by E. Malyasova (Cheremisinova, 1952) showed that varved clay and sand, as well as the Mga sediments cored in BH 3, were deposited within interglacial pollen zones b–g (Jessen and Milthers, 1928). However, the Mikulino (Eemian) age of the Mga Fm. was mainly inferred from the pollen diagram of M. Grichuk (Znamenskaya, 1959). The vegetation history reconstructed from the Mga sediments suggests similarities with the LIG pollen zones identified in Denmark and North Germany (Jessen and Milthers, 1928). Furthermore, the pollen diagram of the Mga section was correlated with those for continental lacustrine-boggy deposits of the Dnieper-Valdai (Mikulino) Interglacial in the Russian Plain (Znamenskaya, 1959).

Synthesis of data available by the end of 1950s for marine interglacial sediments in the northern Europe and USSR territories (Lavrova, 1961) showed that the deposits of the Boreal, Mga, and Eemian transgression events made up a single geological unit. Lavrova (1961) was the first to infer that the Mga basin became saline during the Moscow (Saalian) Late Glacial, while no Saalian Late Glacial marine sediments were known from Poland and North Germany. Lavrova (1962) posited that during the Late Glacial, seawater apparently entered the Baltic Basin via the tectonically formed Vänern and Vättern lakes in Central Sweden. During the LIG, the Baltic and North Sea basins became connected via the Danish Straits as a result of glacioisostatic uplift in Central Sweden and a global rise in sea level.

The review of the Mga sections by Znamenskaya and Cheremisinova (1962) highlighted an abrupt change of diatom ecosystems in the beginning of the regression event, possibly, caused by greater isolation of the Mga Sea upon rapid uplift of the western Gulf of Finland (Prangli Island area). More data came from outcrop 976 in the right bank of the Mga River, 4.3 km west of the Mga railway station (Nedrigailova et al., 1965), sampled as part of 1:200 000 geological and hydrogeological surveys (sheet O-36-II). The spore-pollen spectra of the samples included pollen zones M_6–M_8 (after Grichuk, 1961) of the Mikulino Interglacial (identified by P. Bichurina), while diatom data (E. Cheremisinova and M. Travina) showed a lagoonal deposition environment.

A new collection of data was obtained from reference Quaternary sections drilled by the Leningrad Geological Survey in 1981–1982 before the XI INQUA Congress. Those data included geological and paleo-phytological evidence from the core samples of boreholes 6a and 6 (Pleshivtseva et al., 1984; 2011a) located on the floodplain terrace in the left bank of the Mga River near the 45 km railway station, 1.5 km downstream of the railway bridge (BH 6a) and 500 m farther to the north on the high terrace of the Mga River (BH 6). The two boreholes complemented each other and made up a composite section of the Quaternary strata. The Mga clay and clayey silt, with a smell of hydrogen sulfide, bearing valves of *Portlandia arctica* and plant remnants, were stripped at -3 to -11 m asl elevations. This interval comprises a complete sequence of regional pollen zones M_1–M_8 of the Mikulino Interglacial (palynologists G. Abakumenko and E. Pleshivtseva). The Mga Beds lying over ~13 m of

brown varved clay with pollen of zones Ms_1–Ms_3 corresponded to the Moscow Late Glacial (Malakhovsky et al., 1969a). Diatom analysis (S. Gorshkova) allowed an inference that the varved clay were deposited in a cold freshwater basin that shoaled in the beginning of zone M1. Interglacial deposition occurred in the Mga Sea in lagoonal, marine, and regression conditions.

Different age estimates for the samples of Mga Fm. range from ~71 ka to ~157 ka: ~71 ka thermoluminescence (TL) age obtained in 1980 by Punning (Malakhovsky et al., 1989); 135.3±12.5 ka and 137.6±12.7 ka electron spin resonance (ESR) ages for *Portlandia arctica* shells (Molodkov and Krasnov, 1998); and 156.6±13.1 ka ESR age for marine mollusc shells from an outcrop on the Mga River, determined by A. Molodkov (Bolshiyanov et al., 2016). Shells of five marine and four freshwater mollusc species (*Arctica islandica*, *Cerastoderma glaucum*, *Musculus niger*, *Modiolus modiolus*, *Macoma balthica* and *Margaritifera margaritifera*, *Pisidium amnicum*, *Corbicula fluminalis*, *Sphaericum solidum*, respectively) were discovered in the Mga clay by A. Krylov (Bolshiyanov et al., 2016).

The data on the Mga Fm. synthesized by Malakhovsky et al. (1969a; 1989) included the results of particle size distribution and mineralogical studies by E. Rukhina (Malakhovsky et al., 1989) for the Rybatskoye, Sinyavino, White Lake (Apukhtin and Sammet, 1967) and some other sections. The sediments showed a homogeneous composition, without prominent size peaks and a <1% average yield of the heavy fraction, mainly composed of metallic minerals (~86%). The heavy fraction of the lower strata included 74–76% of siderite; hornblende decreased upward, to the contents 5–9% lower on average. The light fraction mainly consisted of quartz, feldspar, hydromica phases and carbonates.

The review of sections with the Mikulino marine deposits in the northwestern East European Plain (Ikonen and Ekman, 2001) included results of diatom and spore-pollen (palynologist Ya. Elovicheva) analyses of interglacial deposits in the Petrozavodsk area indicating that the Baltic and White Seas were connected during the interval of pollen zones M_2–M_3 (*Pinus-Betula*) till the beginning of zone M7 (*Picea-Pinus*).

According to the review of hydrography and mollusc fauna of the Baltic Sea, Baltic-White Sea connection, and White Sea (Funder et al., 2002), only eight species of marine molluscs were identified in LIG marine deposits (without those found by A. Krylov): arctic *Ciliatocardium ciliatum*, *Portlandia arctica* and *Portlandia aestuariorum*, subarctic *Heteranomia squamula* and *Mytilus edulis*, boreal *Cerastoderma glaucum* and *Littorina littorea* and ubiquitous *Macoma calcarea*. The poor taxonomy of molluscs during that interval, unlike the rich Eemian and Boreal fauna of the area with ~200 species, as well as the localization of molluscs within banks, high contents of organic carbon in the sediments, and scarcity of benthic and attached diatom species, provide evidence of frequent anoxic episodes intermittent with oxic excursions in the bottom water of the Mga Sea. The mollusc shell identified

previously as *Cardium (Cerastoderma) edule* (Skorokhod, 1932) was re-identified as *Cerastoderma glaucum* (Funder et al., 2002). Furthermore, the Baltic-White Sea connection was inferred (Funder et al., 2002) to have existed from the beginning of zone M_3 to the end of zone M_4 (palynologist Ya. Elovicheva), or ~2.5 ka according to the chronology of the Bispingen section in Germany (Müller, 1974). The lifespan estimate for the Baltic-White Sea strait by Funder et al. (2002) differed from that by Ikonen and Ekman (2001) because the two studies were based on different data sources: molluscs and diatoms, respectively.

Relatively recent studies of Pleshivtseva (2007; 2011b) provided an informative historic background for the Mga sediments and revealed several regional features of their spore-pollen spectra (Pleshivtseva, 2011a). Namely, the palynological data were reported to record

(1) a well-defined, though low and long, *Picea* maximum in the lower part of the section, with *Picea obovata*, *Picea abies* and *Abies* in the northwestern Leningrad Oblast;

(2) optimum of the Mikulino Interglacial corresponding to pollen zones M_{4-5} and M_6, with *Quereus*, *Ulmus*, *Corylus* and *Alnus* culminating in zone M_{4-5}, at low percentages of *Tilia*, a considerable contribution of *Picea* in zone M_6 in the northwestern Leningrad Oblast, second maximum of *Carpinus* coinciding with zone M_7 but resulting from redeposition of zone M_6 pollen during regression;

(3) *Picea* maximum in the upper part of the section, especially prominent in the eastern and northeastern Leningrad Oblast as a record of conifer taiga vegetation including *Picea obovata*, often overlapping with the *Carpinus* zone (M_{6-7}) in the northwest;

(4) halophytic pollen of sea coast in the beginning of the interglacial (zones M_1–M_3): *Salsola kali*, *Salicornia herbaceae* and *Suaeda maritime*;

(5) hypo-arctic taxa, including within the optimum: *Betula nana*, *Alnus fruticosus*, *Polygonum viviparum* etc.;

(6) Siberian species *Pinus sibirica*, *Athyrium crenatum*, *Lonicera palassii*, *Cystopteris sudetica* etc.

2.2. Key Mga sections in the Neva Lowland

2.2.1. Osinovets

In the first half of the 1930s, thirty four boreholes (Fig. 2.1) were drilled from ice in Lake Ladoga along a line 3 km eastward from the Osinovets lighthouse (Krasnov and Reineke, 1936). Some boreholes stripped up to 3 m thick bituminous clay, with vivianite concretions, shells of sea molluscs, and marine diatoms, wherefrom some gas occurrences were inferred to originate. Up to 99% of diatoms from the Mga sediments from two boreholes were planktonic species indicating interglacial deposition in the neritic zone (Cheremisinova, 1952, 1957). The predominant species of diatoms and silicoflagellates were cold-loving.

2.2.2. Sablino

Intermorainic marine clay with the top at 32 m asl were found (Ansberg and Znamenskaya, 1941) in the vicinities of Sablino (Ulyanovka) Village, south of the Baltic Klint (Fig. 2.1). The clay sequence was studied in boreholes 42 and 43 on the Tosna-Sablinka watershed between Maloye Gertovo and Kozlovka Villages, slightly upstream of the latter. The core samples contained *Portlandia* sp., *Yoldia (Portlandia) arctica* and *Tellina (Macoma) calcarea* molluscs (identified by M. Lavrova) and very poorly preserved diatoms of 27 species, mostly (93%) marine (Sheshukova, 1949), which recorded deposition in a shelf zone. The Mga Fm. stripped in the Sablino section was attributed to a glacial outlier, proceeding from the high hypsometric position (Malakhovsky et al., 1969a).

2.2.3. Otradnoye

One poorly known section of the Mga Fm. was sampled in 1956 as part of an engineering geological campaign at Otradnoye Village, on the left bank of the Neva River (Rzhonsnitskaya and Kurochkina, 1959), where BH 700 tapped 19 m thick marine sediments at -12 to 7 m asl. (Fig. 2.1). Spore-pollen analysis (by L. Korotkevich) showed that the Mga sediments were deposited during pollen zones d–i (Jessen and Milthers, 1928), while diatom analysis (by I. Kuptsova) revealed the lagoonal, marine, and regressive phases in the deposition history.

2.2.4. Kelkolovo

The Mga deposits were also stripped by BH 976 at the base of the Kelkolovo Heights (Fig. 2.1) as part of 1:50 000 comprehensive engineering-geological surveys in 1958 (Sokolova et al., 1959). The section included dark grey and black clay at -15 to -2 m asl, with vivianite concretions and shells of *Portlandia arctica* and *Mytilus edulis* (identified by M. Lavrova). The spore-pollen spectra recorded a succession of plant communities (identified by E. Malyasova): conifer (pine) forests → conifer-deciduous forests → conifer forests. The diatom assemblage was dominated by marine and brackish marine species (identified by M. Chizhikova).

More detailed evidence of the Mga sediments in the Kelkolovo site was obtained from a sand quarry for production of silica bricks (Krasnov et al., 1995). Bituminous clay with vivianite concretions and shells of *Portlandia arctica* occurred in the section as glacial layers and outliers (Fig. 2.3). The spore-pollen spectra of the Mikulino Interglacial (zones M_6–M_8) were studied in a cut of one such glacial layer (palynologist E. Pleshivtseva). According to diatom analysis (by V. Fyodorova), the Mga sediments were deposited in freshened water during a regression. *Portlandia arctica* shells from the section gave a 137.2±15.6 ka ESR age (Molodkov and Krasnov, 1998).

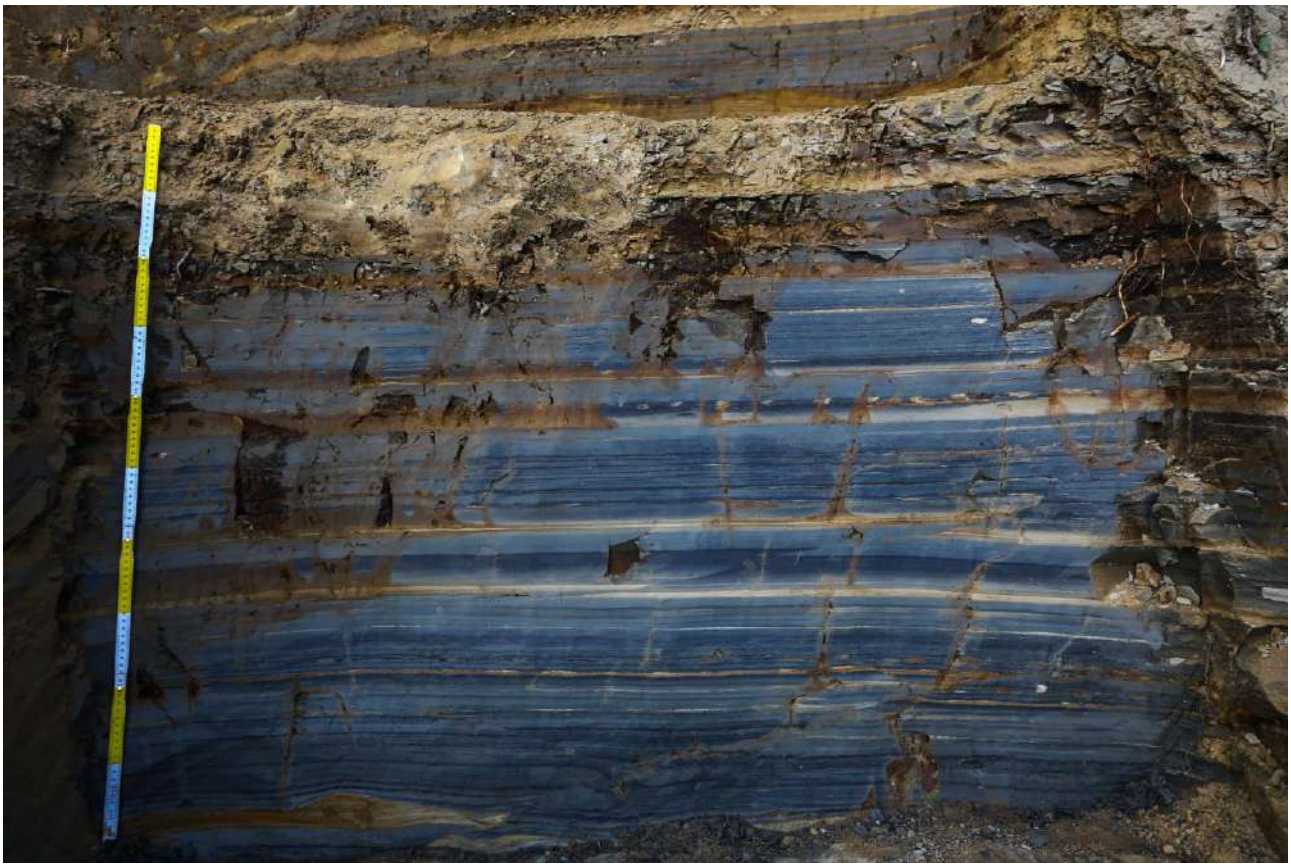

Fig. 2.3. The Mga marine interglacial deposits in the Kelkolovo quarry (photograph by M. Ruchkin).

2.2.5. Morozov Settlement

One more section of the Mga Fm. (Fig. 2.1) was stripped in BH 977 in Morozov Settlement during the comprehensive 1:50 000 engineering-geological surveys (Sokolova et al., 1959; Sokolova and Mokrienko, 1960). The core samples were composed of clay containing shells of *Yoldia (Portlandia) arctica* and *Mytilus* sp. molluscs (identified by S. Troitsky) and carbonized plant remnants at -24 to -16 m asl. The Mga deposits were observed to overlie 3.5 m of chocolate-brown varved clay. The spore-pollen spectra recorded three phases in the local vegetation history (identified by E. Malyasova), from bottom to top: (1) *Picea* maximum; (2) deciduous taxa (*Quereus* subphase); (3) mixed *Pinus-Betula* forests.

2.2.6. Rybatskoye

A classical section of the Mga Fm. (Fig. 2.1) was studied near Rybatskoye Village (Lavrova and Grichuk, 1960), where BH 47 penetrated all Quaternary strata till Cambrian clay. The ~33 m thick Mga deposits in the Rybatskoye section were stripped at -36 to -3 m asl (Lavrova and Grichuk, 1960; Malakhovsky et al., 1969a) over ~2 m thick varved clay. The Mga Fm. mainly consisted of clay with vivianite concretions and shells of *Portlandia arctica*, *Tellina (Macoma) calcarea* and *Mytilus edulis* molluscs, grass *Zostera* and algae. Diatom analysis (by E. Cheremisinova) revealed the lagoonal, marine, lagoonal, and littoral phases (bottom to top) of the sea history (Znamenskaya and Cheremisinova, 1962). Spore-pollen analysis of samples from BH 47 (by M. Grichuk) showed spectra typical of the Mikulino

Interglacial (Lavrova and Grichuk, 1960), zones M_2–M_8 (after Grichuk, 1961). Together with the pollen data from the Mga section, the spectra from the Rybatskoye section were critical for the final timing of the Mga Fm. The results from BH 47 generally agreed with the pollen and diatom data from BH 1 drilled in the right bank of the Neva River near Rybatskoye Village (Sokolova et al., 1959; Malyasova, 1960).

2.2.7. Sinyavino 2

The Mga Fm. composed of layered clayey silt with *Portlandia* sp., *Mytilus edulis* and *Macoma* sp. molluscs (identified by M. Lavrova) was also encountered at -32 to -30 m asl in BH 3361 in Sinyavino 2 Village (Fig. 2.1) during the comprehensive 1:50 000 engineering-geological surveys of 1962–1963 (Mokrienko et al., 1963).

2.2.8. Lake Sinyavino

Another BH 3365 as part of the comprehensive 1:50 000 engineering-geological surveys of 1962–1963 (Mokrienko et al., 1963) was drilled 2 km east of Lake Sinyavino (Fig.. 2.1) and stripped the Mga bituminous clayey silt with shells of marine molluscs *Portlandia arctica*, *Mytilus edulis*, *Astarte borealis* and *Macoma calcarea* (identified by M. Lavrova) at 5–11 m asl. It was the first finding of *Astarte borealis* in the Mga sediments.

2.2.9. Volodarsky Bridge

BH 1470 (Fig. 2.1) stripped the Mga greenish-grey humus-bearing clayey silt with vivianite concretions and *Mytilus edulis*, *Portlandia arctica*, and *Macoma calcarea* mollusc shells (identified by M. Lavrova) near Volodarsky Bridge in Leningrad (St. Petersburg), at -24 to -20 m asl (Usikova and Malyasova, 1965; Malakhovsky et al., 1969a). The diatom assemblage found in the sediments consisted of 78 species, including marine and brackish varieties. The Mga Fm. in the BH overlaid 2.5 m thick glaciolacustrine sediments with predominant periglacial pollen species, whereas the pollen spectra of marine deposits contained a phase of *Pinus-Picea* forests with some percentages of *Betula* and *Alnus* (identified by E. Malyasova). The sediments in the section were most likely deposited in the beginning of the Mikulino Interglacial (zone M_1).

2.2.10. Petrokrepost'

The Mga deposits were also sampled from BH 7 (Fig. 2.1) during the 1:200 000 geological and hydrogeological surveys (sheet O-36-II), east of Shlisselburg (Petrokrepost'), 3 km north of Sinyavino 2 Village (Nedrigailova et al., 1965). The BH stripped silty clay with vivianite concretions, plant remnants and *Portlandia arctica* shells at -26 to -20 m asl. All pollen zones of the Mikulino Interglacial (M_1–M_8) were distinguished (by R. Bichurina) in that section (Pleshivtseva, 2011b). No diatoms were found though, possibly, because the frustules were dissolved during deposition, as hypothesized by E. Cheremisinova.

2.2.11. Sinyavino

The Mga Fm. under 55 m of the Valdai sediments was described (Malakhovsky et al., 1969a) in BH 7 drilled on the Sinyavino Heights near the upper edge of an abrasion terrace near abandoned Sinyavino Village, south of a peat mining site (Fig. 2.1). According to spore-pollen analysis (by V. Grichuk), marine clay with plant remnants, vivianite concretions, shells *Portlandia arctica*, *Mytilus edulis* and *Macoma calcarea* molluscs (identified by M. Lavrova), and prints of *Zostera marina* grass in the interval from -29 to -11 m asl were deposited during the interval of pollen zones M_2–M_8 in the Mikulino Interglacial. The interglacial sediments lying over the Moscow Late Glacial deposits corresponded to pollen zones Ms_1–Ms_3 (top to bottom). In that model, zone Ms_3 represents birch open woods with elements of periglacial plant communities. Zone Ms_2 corresponds to the Kasplya Interstadial (Buslovich et al., 1969) and comprises three subzones (bottom to top) of birch-pine (a), spruce-pine (b), and pine-birch (c). Zone Ms_1, with predominant birch and periglacial plants in the pollen spectra, records cold climate conditions. Diatoms in the core samples (identified by E. Cheremisinova) showed the lower lagoon (1), marine (2), and upper lagoon (3) phases in the Mga Sea history, with a glaciomarine subphase in the lagoon phase (1). Marine molluscs and diatoms appeared for the first time in the Kasplya Interstadial deposits.

2.2.12. Yukki

BH 27a in the Yukki Heights north of the Neva Lowland (Fig. 2.1) stripped the Mga marine clayey silt and silt, with shells of *Portlandia arctica* and *Macoma calcarea* molluscs (identified by M. Lavrova) and prints of *Zostera* grass at elevations of 1–14 m asl (Malakhovsky et al., 1969a; Vishnevskaya et al., 1973) lying over ~6 m of varved clayey silt. The spore-pollen spectra recorded deposition during pollen zones M_3–M_8 (palynologist E. Malyasova). Diatom analysis (E. Vishnevskaya) revealed the glaciomarine, maximum transgression and lagoon deposition phases.

2.2.13. Sverdlov Factory

In the early 1980s, several boreholes were drilled through all Pleistocene strata in the area for exploration of the Cambrian Siverskaya clay lying under the Quaternary at the Sverdlov Factory site (Fig. 2.1). Core samples from three boreholes (2, 8, 10) were studied for spore-pollen spectra and diatoms (Pleshivtseva et al., 1984; Pleshivtseva, 2023). The most complete section (BH 10) stripped a glacial unit of the Moscow age including a till and overlying Late Moscow varved clay, ~10 m thick, over the bedrock. Up the section, at -21 to -5 m asl, there followed the Mga marine clay of the Mikulino Interglacial, the Ostashkov till and the glaciolacustrine deposits of the Baltic Ice Lake on the top. The varved clay was deposited during the Moscow Late Glacial (pollen zones Ms_1–Ms_3), while the Mga Fm. displayed a complete record of all regional Mikulino pollen zones M_1–M_8 (palynologist E. Pleshivtseva). The diatom analysis (by S. Gorshkova) showed that inputs of saline seawater into the glacial lake began during the Kasplya Interstadial (Ms_2). The taxonomic changes of diatom assemblages allowed

reconstructing the complete sequence of the glaciomarine, lagoonal, marine, and regressive phases of the Mga Sea evolution.

Later the Mga sediments were stripped in a quarry at Sverdlov Settlement (Malakhovsky et al., 2000) and, together with the underlying varved clay, were sampled in a quarry outcrop for spore-pollen spectra (Borisova and Novenko, 2014). The spectra of the Mga deposits encompassed pollen zones M_1–M_4, while the Moscow Late Glacial deposits were correlated with the Zeifen-Kattegat climate oscillation of Western Europe (Borisova and Novenko, 2014). The mollusc fauna found in the quarry included eight marine species, identified by A. Krylov (Bolshiyanov et al., 2016): *Arctica islandica*, *Cerastoderma glaucum*, *Clinocardium ciliatum (Ciliatocardium ciliatum ciliatum)*, *Macoma balthica*, *Macoma calcarea*, *Mytilus edulis*, *Portlandia aestuariorum*, *Portlandia siliqua*, as well as one freshwater species (*Corbicula fluminalis*). Shells sampled at -11 m asl gave an ESR age of 109.8±9.4 ka (dated by A. Molodkov).

A record of the Blake geomagnetic excursion was found in the upper strata of the Mga Fm. exposed in the quarry (Dudanova et al., in press), with syngenetic greigite produced by metabolism of magnetoactive bacteria as a carrier of the characteristic remanent magnetization (ChRM) component in the marine interglacial deposits. The Blake excursion lasted for 3 to 6 ka: it began within pollen zones $M_{6\text{-}7}$ and coincided with the transgression maximum followed by the onset of regression of the Mga Sea (Dudanova, 2023).

2.2.14. Lake Tokhkolodskoye

BH 124 in the southeastern side of Lake Tokhkolodskoye (Fig. 2.1) was drilled in 1981–1982 to prepare reference Quaternary sections before the XI INQUA Congress (Pleshivtseva et al., 1984). It stripped clayey silt and silt with marine molluscs at 3.5 to 19.5 m asl lying over 5 m of varved clay. The Mga interval comprised regional pollen zones M_1–M_8 of the Mikulino Interglacial (palynologist E. Pleshivtseva). The diatom analysis (by S. Gorshkova) revealed the marine and regressive phases of the Mga Sea. Diatoms found in sand beds over the Mga Fm. were of freshwater origin.

2.2.15. Izhora Factory

More than a thousand engineering-geological boreholes were drilled in different years in the territory of the Izhora Factory in Kolpino (Fig. 2.1). BH 619-bis stripped the Mga Fm. with mollusc shells at -24 to -7 m (Auslender et al., 2001) and with pollen spectra corresponding to zones M_3–M_6 (palynologist E. Pleshivtseva).

2.2.16. Pontonnaya

BH 87-bis drilled south of the Pontonnaya railway station in the left bank of the Malaya Izhorka River (Fig. 2.1) stripped coarse to fine silty sand with marine shell detritus at depths 31.5–25 m asl (Auslender et al., 2001). The Mga Fm. contained 111 species of diatoms (identified by S. Gorshkova),

including 80 marine and 25 freshwater species. The sedimentary record displayed all main phases of the Mga Sea evolution. The spore-pollen spectra encompassed pollen zones M_3–M_8 (palynologist E. Pleshivtseva).

Chapter 3. Methods

Lithological, paleontological, geochronological, and geochemical analytical methods were used to constrain the time span of the Mga deposition in the Neva Lowland and to reconstruct the history of the Mga Sea.

3.1. Lithological methods

3.1.1. Facies analysis

The Quaternary stratigraphy was studied from the sedimentary architecture, structure, and texture features in the quarry of the Sverdlov (Etalon) Brick Factory. The exposed section was documented, photographed, and sampled in stepped cut walls to determine the orientation of the cuts, color and moisture contents of sediments, particle sizes, bedding patterns, inclusions, and secondary alteration signatures. Special focus was made on elevations of bed contacts and related possible deposition gaps. Structural measurements were applied to document the directions and lengths of faults and folds that disturb the primary sedimentary bedding.

3.1.2. Grain size analysis

Grain sizes were measured in 77 samples from intermorainic deposits at elevations from -21.9 to -1.5 m asl in the Sverdlov Factory quarry. The measurements were performed by the author under supervision of S. Opitz at the University of Cologne (Germany), using a Beckman Coulter LS 13320 Laser Particle Analyzer (<2 mm; Brea, CA, USA). Prior to analysis, the samples were treated with H_2O_2 (30%) to remove organic carbon and in 0.5N $Na_4P_2O_7$ (55.7 g/l) in order to disperse aggregates.

The parameters of the particle size distribution were calculated in GRADISTAT v9.1 (Blott and Pye, 2001). The particles were classified using a modified size classification of Udden (2014) and Wentworth (1922). The statistics (mean values, sorting, skewness, and kurtosis) were estimated following Folk and Ward (1957).

3.2. Paleontological methods

3.2.1. Pollen analysis

3.2.1.1. Method

Pollen analysis of samples from intermorainic deposits in the Sverdlov Factory quarry was carried out at A.P. Karpinsky Russian Geological Research Institute (VSEGEI, St. Petersburg, Russia), by analyst E. Nosevich. The samples were preconditioned following the enhanced technique of V. Grichuk (Grichuk and Zaklinskaya, 1948). Carbonate-free sediments, from 80 g to 150 g, were treated with sodium pyrophosphate, centrifuged in heavy liquid (2.28-2.30 g/cm^3), examined under an Olympus CX31P microscope, and photographed using a Zeiss 105 Axiocam color camera. The interpretation was based on published pollen identification guides (Pokrovskaya, 1950; Kupriyanova and Alyoshina, 1972; 1978; Moore et al., 1994). Spore-pollen diagrams were plotted in TILIA v3.7 (E. Grimm).

3.2.1.2. Trans-regional correlation of vegetation history

The LIG vegetation history followed the same trends in East, Central, and West Europe: birch (*Betula*) and conifer forests in the beginning of the period, then mixed and deciduous forests with domination of oak (*Quercus*), elm (*Ulmus*), hazel (*Corylus*), alder (*Alnus*), and hornbeam (*Carpinus*) during the optimum, and finally taiga vegetation in the end of the LIG. The stages of taxonomically similar predominant species are distinguished as pollen zones. The first chart of LIG pollen zones was based on data from Jutland and northwestern Germany (Jessen and Milthers, 1928); later such charts were compiled for many other regions of Europe (Grichuk, 1961; Zagwijn, 1961; Selle, 1962; Devyatova, 1982; Menke and Tunni, 1984; Mamakova, 1988; Liivrand, 1991; Eriksson, 1993).

The identified pollen zones are well pronounced in regional spore-pollen diagrams and can be correlated with zones from other regions (Table 3.1). However, the correlation may be disturbed by local features of vegetation patterns. For instance, the *Picea* zone was present in the East European Plain of the earliest interglacial time (Grichuk, 1961) but was absent in West Europe, i.e., the spruce vegetation had limited westward extent. Other examples are from West and Central Europe: a small peak of *Juniperus* in southern West Europe in the beginning of the interglacial (Woillard, 1978; Menke and Tunni, 1984) and high percentages of *Taxus* and *Abies* in the interglacial forest communities of West and Central Europe, as far eastward as the Polish Plain and the Eastern Carpathians (Grichuk, 1982; Menke and Tunni, 1984).

Note that the correlation of pollen zones in Table 3.1 is approximate as the boundaries are asynchronous, especially in the first half of the interglacial period (Chepurnaya, 2009a,b), depending on climate gradient and distance to refugium. The vegetation phases in the East European Plain in the early-middle interglacial lagged behind those of other European areas in the NE direction, while the difference in the life span of broad-leaved forests between southwestern and northeastern areas of the East European Plain could reach 2 to 4 ka (Chepurnaya, 2009a,b).

3.2.2. Diatom analysis

Diatom analysis of 77 samples from intermorainic deposits in the Sverdlov Factory quarry was carried out at VSEGEI, St. Petersburg (analyst Z. Pushina). The samples were preconditioned following the standard technique (Zhuze et al., 1974) and the permanent preparations were mounted in the Elyashev medium (n = 1.67–1.68) and analyzed under a biological microscope at a magnification of ×1500.

Table 3.1. Correlation of Eemian (Mikulino) pollen zones across Europe (after Menke and Tunni, 1984; Liivrand, 1991; Zagwijn, 1996; Kristensen et al., 2000; Velichko et al., 2005; Head et al., 2005).

Netherlands (Zagwijn, 1961)	**Denmark** (Jessen and Milthers, 1928; Andersen, 1975)	**Northwestern Germany** (Selle, 1962)	**Western and Central Europe** (Menke and Tunni, 1984)	**Poland** (Mamakova, 1988; 1989)	**Estonia** (Liivrand, 1991)	**East European Plain** (Grichuk, 1961; Velichko et al., 2005)
E6b *Pinus*	**E7 (i)** *Pinus*	**VI** *Pinus*	**E7** *Pinus*	**E7** *Pinus*	**E8** *Pinus*	**M8** *Pinus-Picea-Betula*
E6a *Picea*	**E6 (h)** *Picea-Pinus-Alnus*	**Vb** *Pinus-Picea-Abies*	**E6** *Pinus-Picea-Abies*	**E6** *Picea- Abies-Alnus*	**E7** *Picea*	**M7** *Picea*
		Va *Pinus-Picea-Carpinus*				
E5 *Carpinus*	**E5 (g)** *Picea-Carpinus-Alnus*	**IV** *Carpinus*	**E5** *Carpinus-Picea*	**E5** *Carpinus-Corylus-Alnus*	**E6** *Carpinus*	**M6** *Carpinus*
E4b *Taxus*	**E4 (f)** *Quercus-Corylus-Alnus*	**IIIc** *Tilia-Ulmus-Corylus*	**E4b** *Corylus-Taxus-Tilia*	**E4** *Corylus-Quercus-Tilia*	**E5** *Tilia*	**M5** *Tilia-Quercus-Ulmus* (second half of *Corylus* maximum)
E4a *Corylus*		**IIIb** *Corylus*	**E4a** *Quercetum mixtum-Corylus*		**E4** *Quercus-Ulmus*	**M4** *Quercus-Ulmus* (first half of *Corylus* maximum)
E3b *Quercus-Corylus*		**IIIa** *Corylus-Quercetum mixtum*				
E3a *Quercus*	**E3 (e)** *Quercus-Fraxinus*	**IIb** *Pinus-Quercetum mixtum*	**E3** *Pinus-Quercetum mixtum*	**E3** *Quercus-Fraxinus-Ulmus*	**E3** *Pinus-Betula-Quercus-Ulmus*	
E2b *Pinus-Quercus*						
E2a *Pinus-Ulmus*	**E2 (d)** *Betula-Pinus-Ulmus*	**IIa** *Pinus-Betula*	**E2** *Pinus-Betula*	**E2** *Pinus-Betula-Ulmus*	**E2** *Pinus-Betula*	**M3** *Pinus-Betula* (*Quercus-Ulmus-Corylus)*
				E1 *Pinus-Betula*		
E1 *Betula-Pinus*	**E1 (c)** *Betula*	**I** *Betula*	**E1** *Betula*		**E1** *Betula-Pinus*	**M2** *Betula*
						M1 *Picea*

3.3. Geochronometry

3.3.1. Optically stimulated luminescence dating

3.3.1.1. Physical background

Optically stimulated luminescence (OSL) is a dating technique that uses minerals as natural dosimeters which can absorb radiation dose and thus show how long ago mineral grains were last exposed to sunlight or heating. Other techniques of dosimetric dating include electron spin resonance (ESR), thermoluminescence (TL), radiofluorescence (RF), and photoluminescence (PL) methods. The minerals that are measured in OSL dating are usually quartz or K-feldspar, though dating may be applied to other minerals as well: plagioclase (Krause et al., 1997; Barré and Lamothe, 2010; Sohbati et al., 2013), zircon (Smith, 1988), calcite (Liritzis, 1994; Liritzis et al., 1997), etc.

The luminescence ability of quartz and K-feldspar is explained in terms of the band theory of solids implying the existence of discrete energy levels (bands) in the radiation spectra of electrons in solids. Electrons can have any energy within allowed bands separated by forbidden intervals, and each band can accommodate a finite number of electrons. The most important energy bands in solids are valence bands filled with electrons, conduction bands free from electrons, and forbidden bands corresponding to the energy gap between the two bands in semiconductors and dielectrics. The valence and conduction bands in conductors overlap and make up a single shared zone half-filled with electrons that can move freely within its limits. The forbidden band is narrow in semiconductors (<2 eV) and wider (> 2 eV) in dielectrics, i.e., higher-energy electrons can easily penetrate into the conduction band

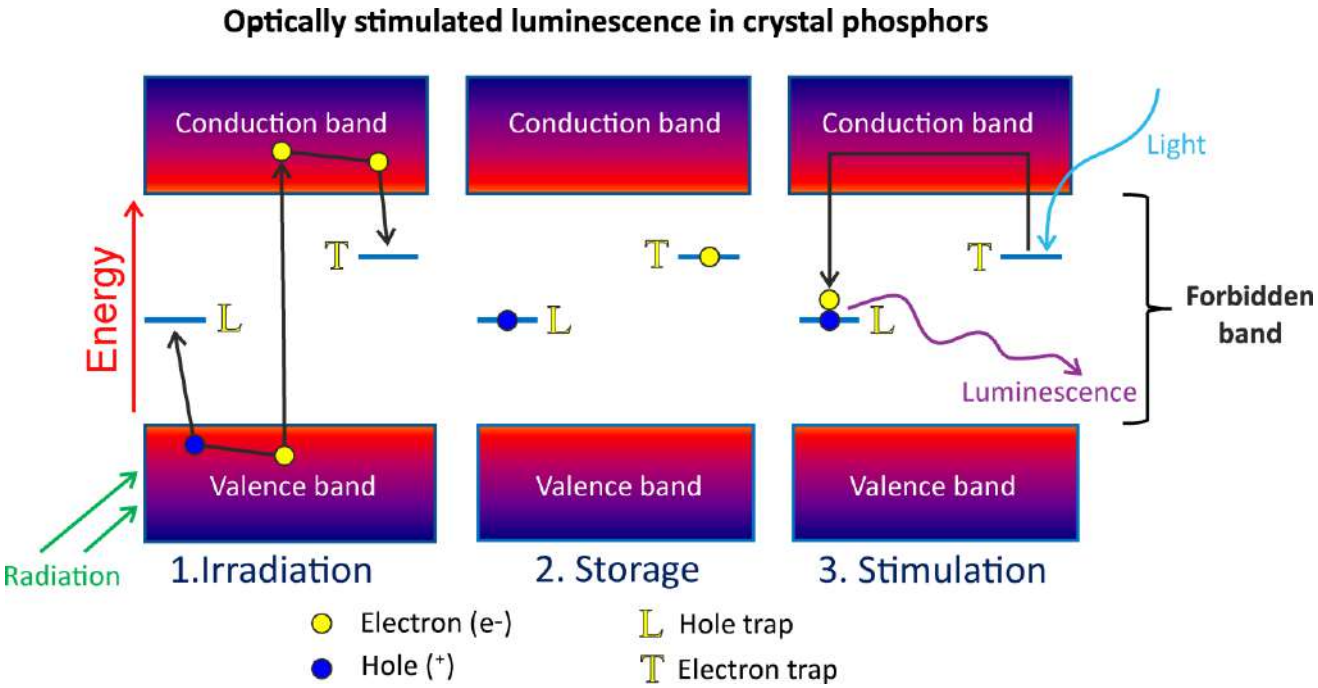

Fig. 3.1. Sketch of OSL mechanism in crystal phosphors (e.g., quartz and feldspar crystals), modified after Aitken (1985).

in the former case but cannot in dielectrics, unless having sufficient energy at higher temperatures (Ashkroft and Mermin, 1976).

Quartz and feldspar are dielectrics, with ~11.7 eV (Lysakov, 2003) and ~7.7 eV (Jain and Ankjærgaard, 2011) widths of the forbidden band, respectively. The low-energy electrons can cross the forbidden band only if they gain energy from α-, β- and γ-radiation, which is accompanied by ionization, Compton recoil, and other exothermic effects. These effects produce pairs of negatively charged electrons and positively charged holes left by liberated electrons; the charges can move freely over the crystal lattice (Wagner, 1998).

Natural radiation comes from ^{238}U, ^{232}Th, ^{235}U and their progeny, as well as ^{40}K, ^{87}Rb and from cosmic rays. The radionuclides are present in different amounts in any rocks; ^{40}K and ^{87}Rb (Rb isomorphically substitutes for K) exist in the feldspar structure, and their decay energy is absorbed internally in the crystals.

Natural minerals can have lattice defects formed either during or after the crystal growth (Ashkroft and Mermin, 1976), especially vacancies (vacant lattice nodes) and interstitial atoms (extra ions between nodes). The structure defects lack positive or negative charges and become traps for freely moving charges (Fig. 3.1): the holes are captured by negatively charged hole traps while the electrons that gain energy from radiation and can penetrate into the conduction band across the forbidden band fall into positively charged electron traps (Wagner, 1998) (Fig. 3.1). The trap depth varies proportionally to the energy of electrons required for being entrapped and is equivalent to the distance to the conduction (valence) band in the OSL model for crystal phosphors (Fig. 3.1). The deeper the trap the more stable the entrapped electron because escaping requires significant energy from heating or insolation. The electrons that escape from traps return to the conduction band, while some reach recombination centres where they recombine with holes and then move back to the valence band. Recombination (Fig. 3.1) is accompanied by heat and/or light emission (Aitken, 1985). Recombination centres where light is emitted are called luminescence centres.

The OSL signals of quartz and feldspar used for dating correspond to anti-Stokes luminescence (according to the law of Stokes (1852), the emission wavelengths are always longer that those of absorption). For quartz, blue, at ~465 nm (Bøtter-Jensen et al., 1999), or green, at ~520 nm (Huntley et al., 1985), excitation wave lengths are most often used while the luminescence intensity is the highest in the UV (~365 nm) region (Huntley et al., 1991). In the case of K-feldspar, it is infrared excitation at ~850 nm (Hütt et al., 1988) and violet emission is measured at ~410 nm (Huntley et al., 1991). The emitted signals are recorded by a photomultiplier tube (PMT) equipped with optical light filters, at a narrow transmission band to prevent penetration of the exciting photons. The measured signals are fitted

to laboratory dose response curves, and projection of natural signals onto these curves yields the total absorbed radiation dose, or equivalent dose.

The emitted signals are initially accumulated in mineral grains after crystallization from a magmatic melt (Fig. 3.2). Mineral grains released from eroded igneous rocks can be exposed to sunlight,

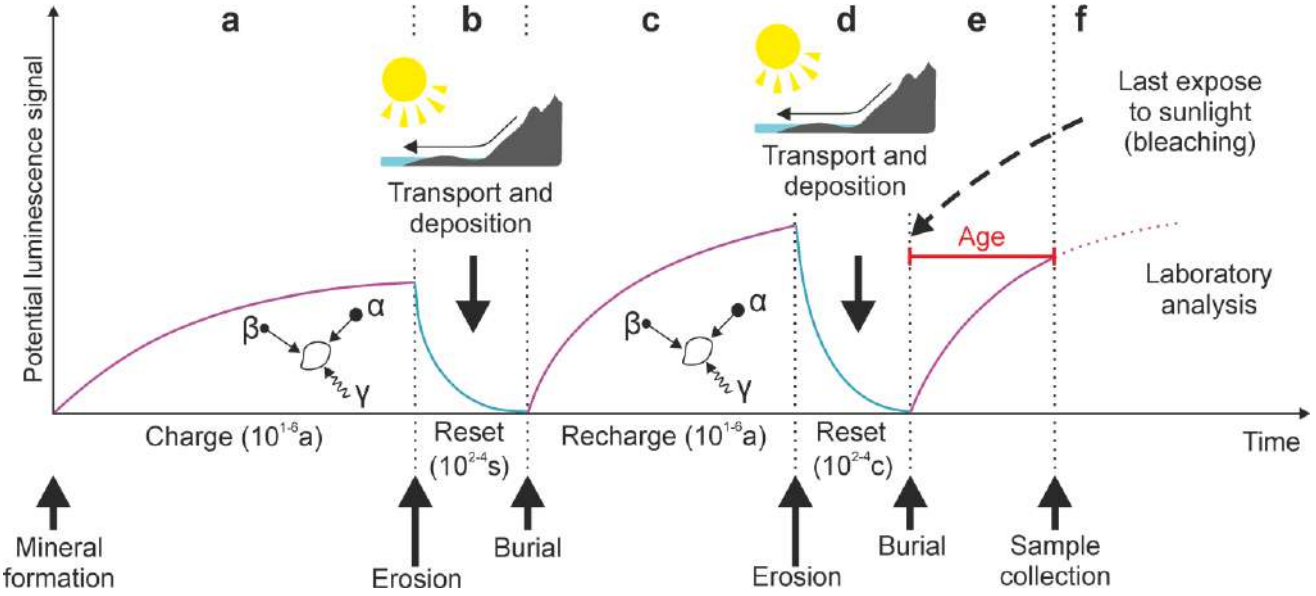

Fig. 3.2. a – increase of potential OSL signal in a bedrock mineral exposed to radiation; **b** – bleaching of OSL signal as the mineral grain is transported from eroded bedrock under sunlight; **c** – repeated increase of OSL signal upon deposition; **d** – repeated erosion-induced bleaching; **e** – repeated increase of OSL signal during the last deposition episode; **f** – time elapsed after the last exposure to sunlight, calculated in samples from sediments as an equivalent dose/dose rate ratio (after Mellet, 2014).

which leads to signal bleaching. The mineral grains liberated by erosion can be redeposited, and the accumulation of luminescence resumes. Each grain can undergo several erosion-deposition cycles, but the accumulated signal is bleached upon each subsequent daylight exposure, i.e., the OSL method records the latest exposure events. The total absorbed radiation dose and the respective equivalent dose are used to estimate the age of the sample as

$$A = \frac{D_e}{D_r}, \quad (3.1)$$

where A is the OSL age in ka; D_e is the equivalent dose in Gy; D_r is the dose rate, Gy/ka.

3.3.1.2. OSL dating procedure

3.3.1.2.1. Sampling, laboratory preparation, and instruments

Sediments for OSL dating were sampled from intermorainic deposits at the Sverdlov Factory quarry by two methods. Some samples were placed in 30 cm long opaque plastic or steel tubes, 5 cm in diameter, while others were collected as 15×10 cm clayey-silty monoliths and packed in opaque black bags. The samples were unpacked under red LED light in the OSL Laboratory at VSEGEI (St. Petersburg, Russia). The 3–5 cm portions of sediments from tube ends and 1–2 cm outer layers of monoliths, which could be bleached while sampling, were used for measuring water contents and for

gamma spectrometry, whereas the inner parts of the samples were used for luminescence analysis after sieving, chemical treatment, and heavy-liquid separation.

The samples were sieved to grain-size fractions from 63 to 250 μm, treated by 10% HCl to remove carbonates and 10% H_2O_2 to dissolve any reactive organic material (e.g., Murray et al., 2021). Then the samples were etched with 10% HF for 15 min (Porat et al., 2015) to clean the grain surfaces and remove an α-irradiated outer layer from K-feldspar grains. Coarse K-feldspar grains were separated in HPS-W heavy liquid (heteropolyoxotungstates) with a density of 2.58 g/cm^3 (Mejdahl, 1985). The quartz heavy (> 2.58 g/cm^3) fraction was etched with 40% HF for 40–60 min without stirring to remove plagioclase and an α-irradiated outer layer (Fleming, 1969, cited from Duval et al., 2018). Finally, the separated K-feldspar and quartz coarse fractions were treated with 10% HCl to remove fluorides (e.g., Murray et al., 2021), dried at 50℃ and sieved again. The 4–11 μm fraction of polymineral grains was prepared from three samples, following the procedure of Frechen et al. (1996).

The luminescence measurements were performed in the Cologne Luminescence Laboratory (CLL) at the University of Cologne (Cologne, Germany) and in the Nordic Laboratory for Luminescence Dating (NLL) (then part of Aarhus University, now the Technical University of Denmark, DTU Risø Campus, Denmark). All analyses were carried out using Risø TL/OSL readers, with blue stimulation (λ=470 nm, 35–100 mW/cm^2) and photon detection through a 7.5-mm Hoya U-340 glass filters for quartz (340±40 nm) and infrared stimulation (λ=870–875 nm, 135–180 mW/cm^2) and photon detection through a Schott BG39/BG3 filter combination (2 and 3mm, respectively), with a transmission band of 400±70 nm filters for K-rich feldspar (Bøtter-Jensen et al., 2000; 2003; 2010; Lapp et al., 2015). In the CLL, an AT405/30X filter with a 405±30 nm transmission band was used for K-rich feldspar instead. The signals were recorded using an ET EMD-9107 detector providing high performance in the 160–630 nm range. All aliquots (1–2 mm K-rich feldspar and 2–8 mm quartz) mm were measured on stainless steel discs or in cups. Laboratory irradiation was with ^{90}Sr/^{90}Y beta sources calibrated for both discs and cups using 180–250 mm Risø calibration quartz (Autzen et al., 2022).

The 100–200 g samples for gamma spectrometry were dried, packed in plastic double dishes (10 × 1.5 cm), sealed with wax to prevent radon leakage and stored for at least 20 days to ensure radioactive equilibrium between ^{226}Ra and its daughter isotopes. The measurements were conducted in the OSL Laboratory at VSEGEI on a high-resolution gamma spectrometer with a high-purity germanium (HPGe) radiation detector (Canberra BE3825).

3.3.1.2.2. Dosimetry

The specific activities of the natural radionuclides were measured on a gamma spectrometer for 24 hours, assuming equivalence between ^{238}U and ^{234}Th activities. The ^{226}Ra activity was computed as the weighted average of the ^{214}Pb and ^{214}Bi activities. The ^{232}Th activities were calculated as the

weighted average of the ^{228}Ac, ^{212}Pb, ^{212}Bi, and ^{208}Tl activities considering the ^{212}Bi branching coefficient. The presence or absence of ^{222}Rn exhalation during the interment period was ascertained by utilizing the ratio of ^{210}Pb and ^{226}Ra activities. Dose rates were calculated on the basis of the Dose Rate and Age Calculator (DRAC) (Durcan et al., 2015) using the disintegration energies given by Liritzis et al. (2013) and Cresswell et al. (2018). The grain size dependent beta dose attenuation factors were taken from Cunningham et al. (2022), assuming an etch depth of 10 µm. The internal beta dose rates in K-rich feldspar were calculated based on K concentrations of 12.5±0.5% (Huntley and Baril, 1997) and Rb concentrations of 400±100 ppm (Huntley and Hancock, 2001). Internal alpha dose rates were 0.10±0.05 Gy ka-1 in K-rich feldspar (Mejdahl, 1987) and 0.010±0.002 Gy ka-1 in quartz (Vandenberghe et al., 2008). The attenuation factors depending on water content were in accordance with Zimmerman (1971) and Cunningham et al. (2022). To calculate the contribution of α-radiation to total dose rates for fine-grain polymineral grains, we employed a-values of 0.08±0.02 (Rees-Jones, 1995) and 0.11±0.02

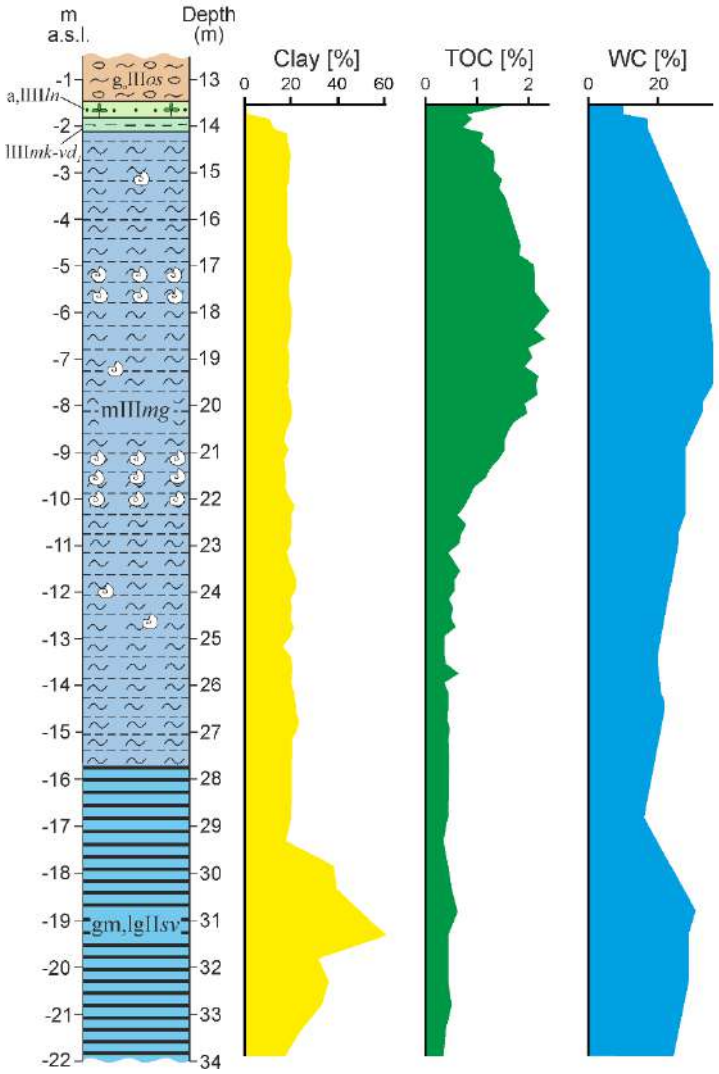

Fig. 3.3. Comparison of clay, total organic carbon (TOC), and modern water (WC) contents in the Sverdlov glaciomarine/glacolacustrine, Mga marine, Mikulino/Lower Valdai lacustrine, and Leningrad alluvial/lacustrine deposits.

(Kreutzer et al., 2014) for the IR_{50} and $pIRIR_{225}$ signals respectively. An uncertainty of 5% was applied to the assumed water contents. The contribution from cosmic rays to the dose rates was calculated according to Prescott and Hutton (1994).

For the sandy Leningrad sediments, we assumed an average burial water content of 75% of saturation. The saturation water content was measured using the syringe method (Murray et al. 2021). For silty and clayey deposits, another approach was applied. Modern water content in the Sverdlov and Mga clayey-silty deposits positively correlates with TOC and clay content (Fig. 3.3). It means that water content reflects real hydrogeologic conditions, i.e. the outcrops studied were quite fresh and saved the original moisture. At the same time, the Sverdlov and Mga deposits probably lost some percentage of porosity and, correspondingly, water content during the Scandinavian Ice Sheet expansion in the Late Valdai because of the compaction process. To accommodate this effect, we added 10% to the modern water content values and used the new values for dose rate calculations.

3.3.1.2.3. Quartz luminescence

Quartz OSL measurements were conducted using the single-aliquot regenerative-dose (SAR) protocol (Murray and Wintle, 2000; 2003) (Table 3.1). Before measurement, we checked quartz purity in three aliquots per sample applying the OSL IR depletion ratio (Duller, 2003). If an OSL IR depletion ratio was inconsistent with unity (at two standard deviations, Jacobs et al., 2003), a sample was additionally etched with 40% HF. In cases when it was not possible to achieve a satisfactory OSL IR depletion ratio with etching, the post-IR OSL SAR protocol (Banerjee et al., 2001) (Table 3.1) was used to minimize the effects of any feldspar contamination. Fig. 3.4 demonstrates that despite the fact that some aliquots showed poor OSL IR depletion ratios there is no correlation of D_e with the OSL IR depletion ratio.

Table 3.1. The single-aliquot regenerative-dose (SAR) protocol (Murray and Wintle, 2000; 2003) and the post-IR OSL SAR protocol (Banerjee et al., 2001) applied for quartz grains dating.

SAR		**post-IR OSL SAR**	
Step	Procedure	Step	Procedure
1	Give dose (natural or regenerated)	1	Give dose (natural or regenerated)
2	Preheat (260°C, 10 s)	2	Preheat (260°C, 10 s)
3	OSL (125°C, 40 s) → L_i	3	IRSL (125°C, 40 s)
4	Give test dose	4	OSL (125°C, 40 s) → L_i
5	Cutheat (220°C, 10 s)	5	Give test dose
6	OSL (125°C, 40 s) → T_i	6	Cutheat (220°C, 10 s)
7	OSL (280°C, 40 s)	7	IRSL (125°C, 40 s)
8	Return to step 1	8	OSL (125°C, 40 s) → T_i
		9	OSL (280°C, 40 s)
		10	Return to step 1

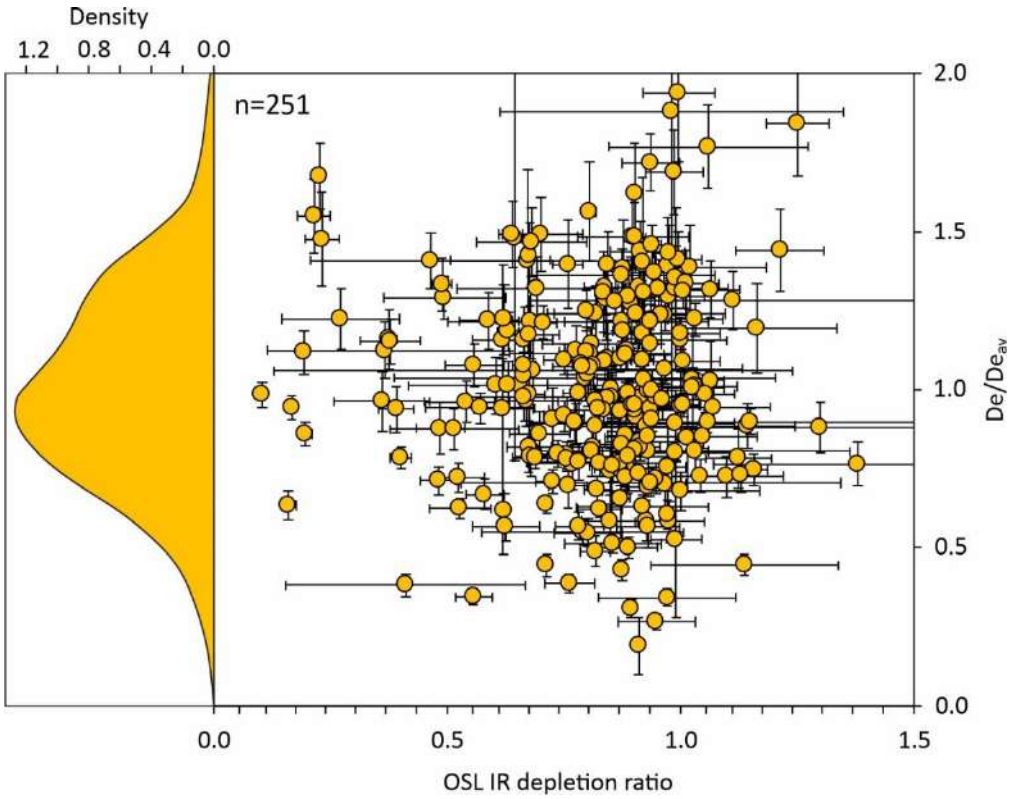

Fig. 3.4. Dependence of the ratio of individual aliquot D_e to sample average D_e on the OSL IR depletion ratio and Kernel density estimation of the ratios.

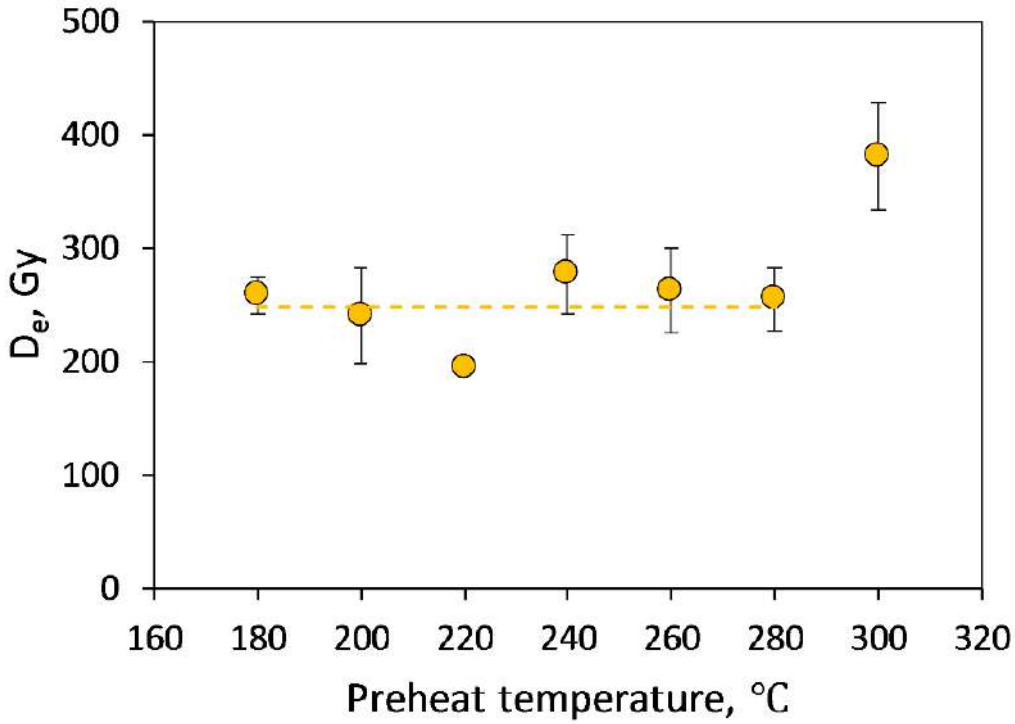

Fig. 3.5. Preheat plateau test results for sample 2103-28. A plateau between 180°C and 280°C indicates thermal stability of OSL in this range of preheat temperatures.

Preheat plateau tests (Huntley et al., 1985; Aitken, 1994) were performed to choose acceptable preheat and cutheat temperatures (Fig. 3.5). Twenty one aliquots from each of five samples from different sedimentary formations were divided into seven groups of three aliquots. D_e values were measured in each group applying different preheat temperatures from 180°C to 300°C, at a step of 20°C. Cutheat temperatures were always 40°C lower than preheat temperatures. As a result, a preheat temperature of 260°C and a cutheat temperature of 220°C were chosen for all quartz D_e measurements.

Dose recovery tests (Folz and Mercier, 1999; Murray and Wintle, 2003) were undertaken for five samples. Given doses varied from 50 to 355 Gy. Before giving a dose, quartz was bleached twice at room temperature by blue LEDs for 40 s each time with a 10 000 s pause between stimulations (Murray and Wintle, 2003). The given doses were regenerated using the SAR protocol and dose recovery ratios were calculated. Fig. 3.6 demonstrates that dose recovery ratios are consistent with unity within 10% in a range 50–355 Gy, i.e. our SAR protocol successfully measures the doses given before any prior thermal treatment over this dose range.

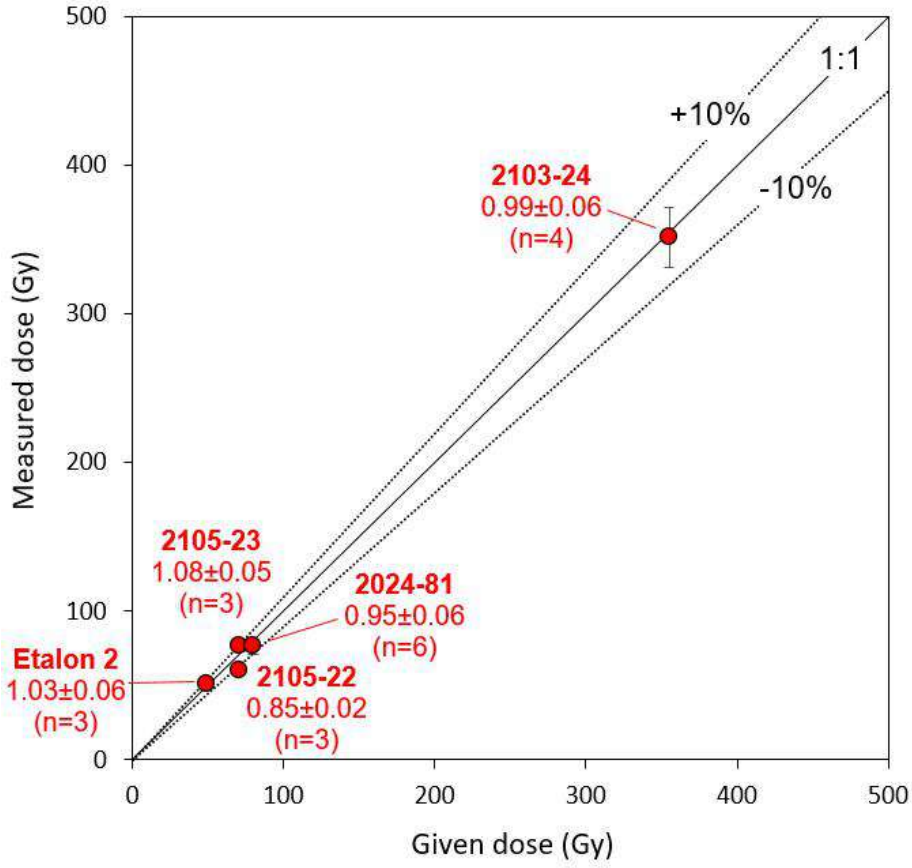

Fig. 3.6. Results of dose recovery test for five quartz samples. Dose recovery ratios and numbers of aliquots measured are shown.

The preliminary analysis of OSL data was done using the Analyst software package v4.57 (Duller, 2015). Quartz dose-response curves were fitted by a sum of two exponential functions or an exponential function with a linear component (Fig. 3.7). In Fig. 3.7 we compare OSL decay curves of

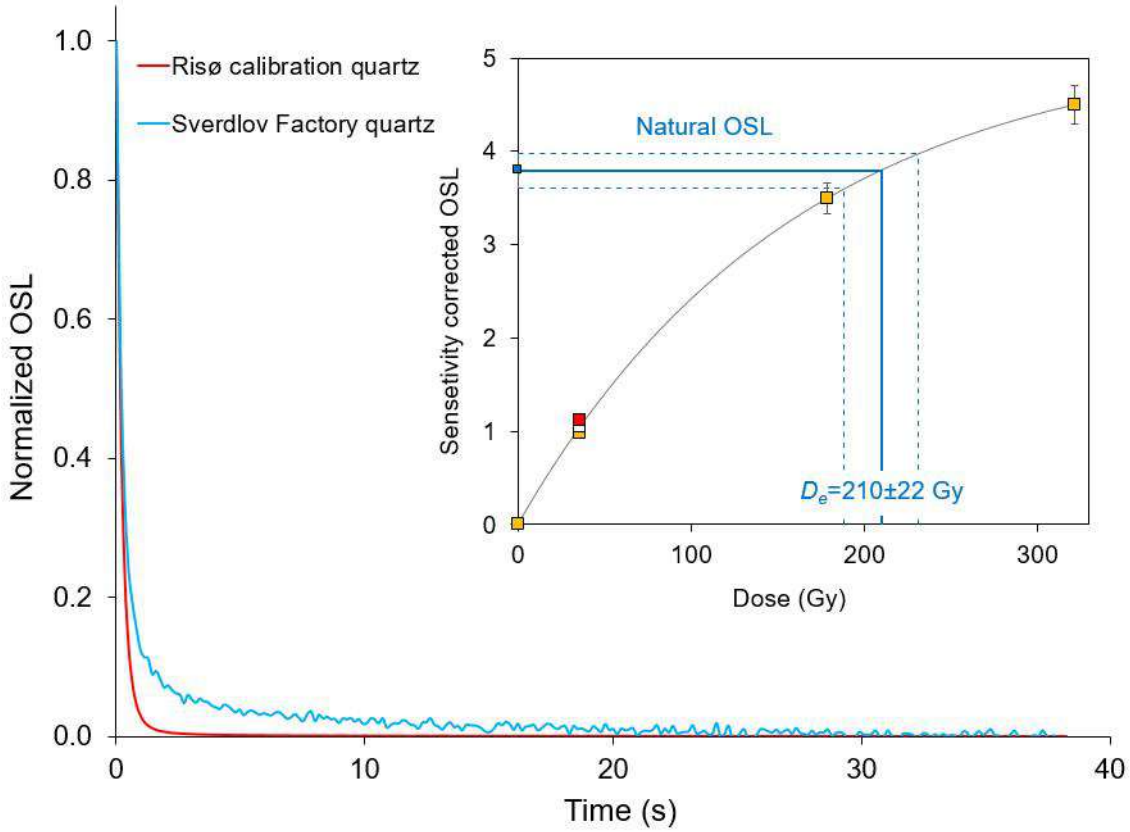

Fig. 3.7. Comparison of averaged OSL decay curves of Sverdlov Factory quartz (n=12) and Risø calibration quartz (n=6) measured on the same reader with the same blue-LEDs stimulation power. OSL signals are normalized and background is subtracted. The inset shows a typical quartz dose-response curve for sample 2103-28. The white marker is a recycling point and the red marker is a purity check point.

Sverdlov Factory quartz and Risø calibration quartz (Hansen et al., 2015), measured on the same reader with the same stimulation power, to show that the fast component (Bailey et al., 1997; Jain et al., 2003) dominates in our quartz. It is known that more than 99% of the Risø calibration quartz OSL signal is derived from the fast component (Hansen et al., 2015). Although the fast component dominates the OSL signals from Sverdlov Factory quartz, a contribution of the unwanted medium and slow components (Tsukamoto et al., 2003; Li and Li, 2006) is visible (Fig. 3.7). To maximize the fast component contribution to the quartz OSL, the initial signal was summed over the first 0.32 s and the background was summed over the subsequent 0.8 s (early background subtraction, EBG) (Ballarini et al., 2007; Cunningham and Wallinga, 2010). Moreover, six OSL decay curves of Risø calibration quartz were fitted by an exponentially decaying function (Bailey et al., 1997) to find the average detrapping probability. Then, twelve OSL decay curves of Sverdlov Factory quartz were fitted by a sum of three exponentially decaying components, and the detrapping probability found earlier was used as a constant for the fast component. This modelling showed that the fast component contributes an average of 89±3% (n=12) to the OSL signal within the above integration intervals. Additionally, we found that the shape of natural OSL decay curve does not depend on the natural D_e value and that there is no significant

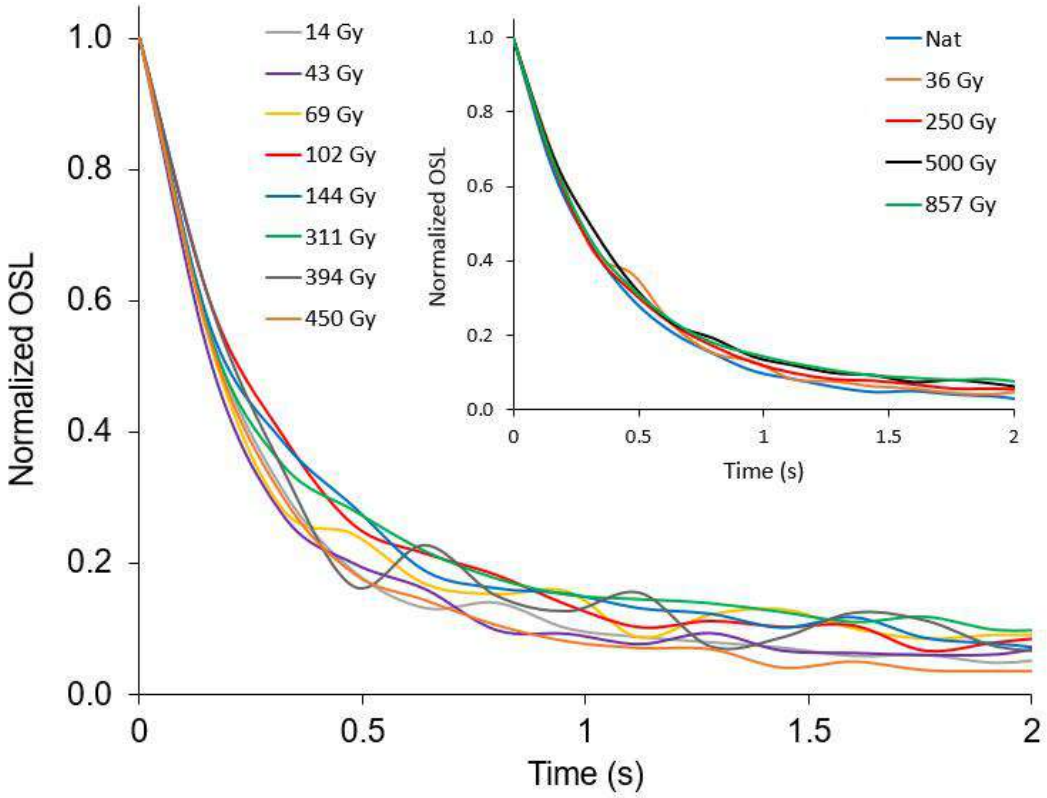

Fig. 3.8. Comparison of normalized and background subtracted natural OSL decay curves from individual aliquots of different samples with De values in a range 14–450 Gy. The inset shows comparison of normalized and background subtracted natural and regenerated OSL decay curves from a typical aliquot of sample 2103-12. Regenerated signals are obtained after artificial irradiation of the aliquot by doses in a range 36–857 Gy.

difference in decay shape between individual natural and corresponding regenerated OSL signals (Fig. 3.8).

3.3.1.2.4. K-rich feldspar luminescence

K-rich feldspar luminescence measurements were carried out using post-IR $IR_{225}SL$ SAR ($pIRIR_{225}$) (Table 3.2) (Buylaert et al., 2009) and post-IR $IR_{290}SL$ SAR ($pIRIR_{290}$) (Table 2) (Thiel et al., 2011) protocols. Dose recovery tests were performed using a Hönle SOL2 solar simulator for bleaching. Six aliquots from each of six samples were bleached for 24 or 48 hours and then residual doses were measured in three aliquots per sample. The remaining aliquots were irradiated with β-doses in the range 359–1076 Gy, and then the doses were measured using the $pIRIR_{225}$ and $pIRIR_{290}$ protocols. Residual doses (4–29 Gy) were subtracted from the measured doses, and dose recovery ratios were calculated. The results are summarized in Fig. 3.9, which shows that the dose recovery ratios for all signals ($pIRIR_{225}$, $IR_{50,225}$, $pIRIR_{290}$, $IR_{50,290}$) decrease as the given dose increases. The $pIRIR_{225}$, $IR_{50,225}$ and $pIRIR_{290}$ signals satisfactorily recover low given doses but not higher than 500 Gy. The $IR_{50,290}$ signal fails to provide a satisfactory dose recovery at any dose.

Table 3.2. The post-IR IR225SL SAR (Buylaert et al., 2009) and the post-IR IR290SL SAR (Thiel et al., 2011) protocols applied for K-rich feldspar and polymineral single-aliquot dating.

post-IR IR_{225}SL SAR		**post-IR IR_{290}SL SAR**	
Step	Procedure	Step	Procedure
1	Give dose (natural or regenerated)	1	Give dose (natural or regenerated)
2	Preheat (250°C, 60 s)	2	Preheat (320°C, 60 s)
3	IRSL (50°C, 200 s) → L_n	3	IRSL (50°C, 200 s) → L_n
4	IRSL (225°C, 200 s) → L_i	4	IRSL (290°C, 200 s) → L_i
5	Give test dose	5	Give test dose
6	Cutheat (250°C, 60 s)	6	Cutheat (250°C, 60 s)
7	IRSL (50°C, 200 s) → T_n	7	IRSL (50°C, 200 s) → T_n
8	IRSL (225°C, 200 s) → T_i	8	IRSL (290°C, 200 s) → T_i
9	IRSL (270°C, 40 s)	9	IRSL (325°C, 40 s)
10	Return to step 1	10	Return to step 1

K-rich feldspar dose-response curves were fitted by a sum of two exponential functions. An initial signal was summed over the first 0.8 s of OSL and a signal averaged over the last 10 s was subtracted as background. The measurements were conducted using test doses approximate to 40% of the D_e (Yi et al., 2016). We measured anomalous fading of the signals $pIRIR_{225}$, $IR_{50,225}$, $pIRIR_{290}$, $IR_{50,290}$ in several samples and calculated average g_{2days} values (Table 3.3). The determinations were

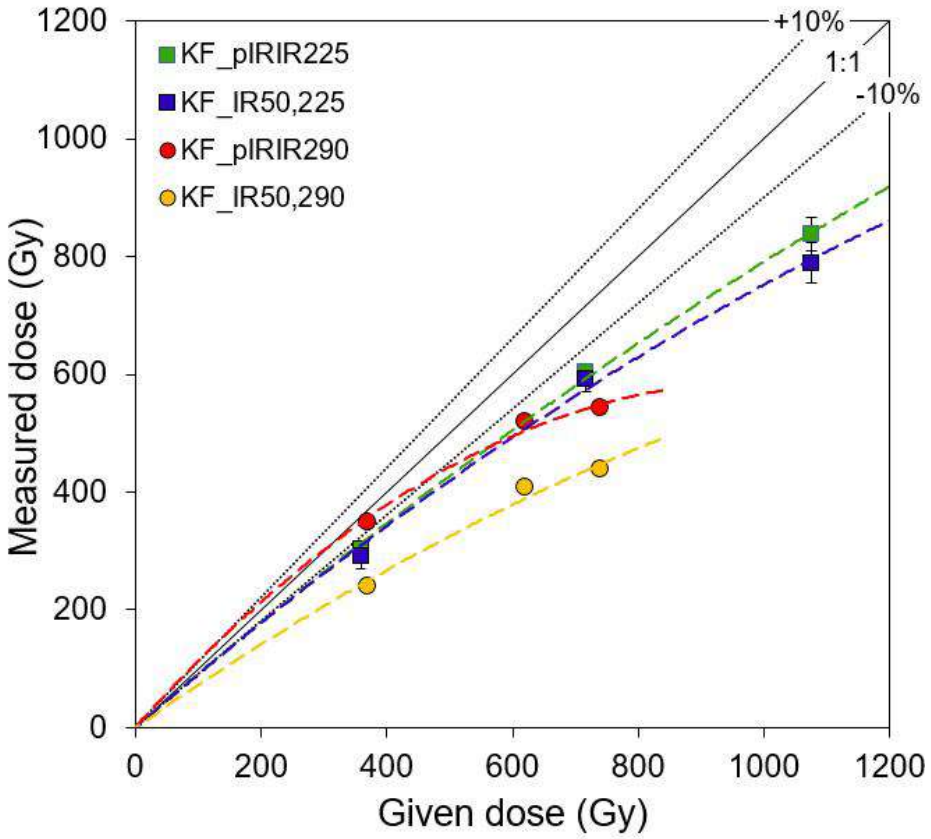

Fig. 3.9. Dose recovery test results for six K-rich feldspar (KF) coarse-grained samples bleached in a Hönle SOL2 solar simulator for 24h before measurements. The measured doses were computed using the signals $pIRIR_{225}$, $IR_{50,225}$, $pIRIR_{290}$ and $IR_{50,290}$, and the respective residual doses were subtracted. Each marker corresponds to the average of three aliquots.

performed using three prompt measurements and three delayed measurements (~50 min, ~8 h and ~33 h after irradiation). The g_{2days} values were computed in Analyst v4.57.

Table 3.3. Anomalous fading rates (g_{2days}) of the signals $pIRIR_{225}$, $IR_{50,225}$, $pIRIR_{290}$, $IR_{50,290}$ from K-rich feldspar coarse-grained and polymineral fine-grained aliquots

Mineral	Grain size (μm)	Protocol	Signal	g_{2days} (%/decade)	n
K-rich feldspar	Coarse (63–250)	post-IR IR_{290}SL SAR	$pIRIR_{290}$	0.55±0.33	3
			$IR_{50,290}$	1.55±0.34	3
		post-IR IR_{225}SL SAR	$pIRIR_{225}$	1.46±0.10	21
			$IR_{50,225}$	3.04±0.15	22
Polymineral	Fine (4–11)	post-IR IR_{225}SL SAR	$pIRIR_{225}$	1.63±0.07	8
			$IR_{50,225}$	2.85±0.05	8

3.3.1.2.5. Luminescence of polymineral fine (4–11 μm) grains

Equivalent doses in polymineral fine grains were measured using the $pIRIR_{225}$ protocol (Table 3.2). Dose recovery tests were carried out in the same manner as for K-rich feldspar coarse grains (Fig. 3.10). The dose recovery ratios are stable but low in a range of given doses 448–1076 Gy; 0.841±0.008 (n=9 aliquots) and 0.851±0.002 (n=9 aliquots) for $pIRIR_{225}$ and $pIRIR_{50,225}$ signals respectively. The

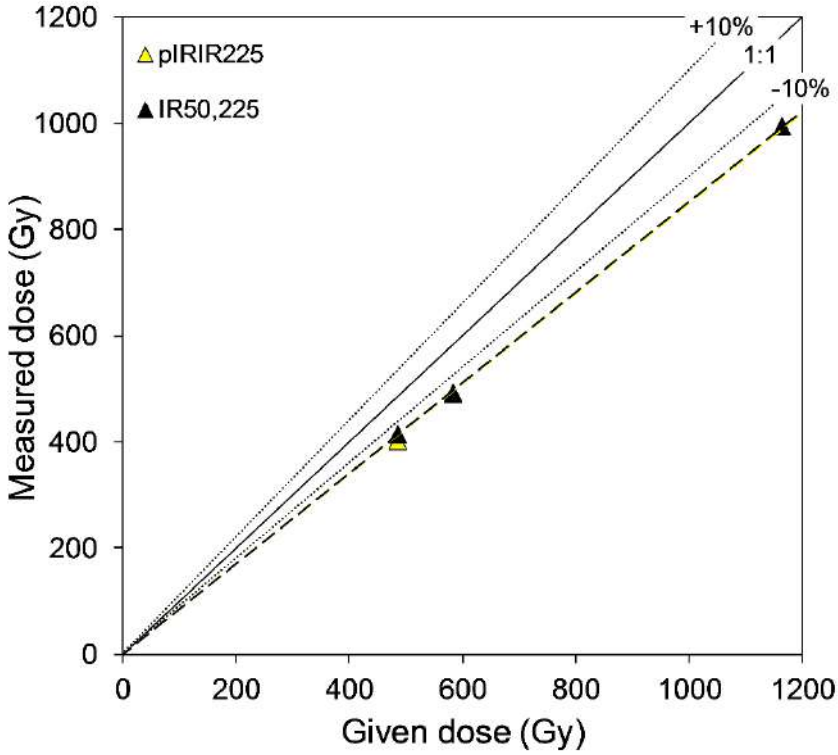

Fig. 3.10. Dose recovery test results for three polymineral fine-grained samples bleached in a Hönle SOL2 solar simulator for 24h before measurements. The measured doses were computed using the signals $pIRIR_{225}$, $IR_{50,225}$ and the respective residual doses were subtracted. Each marker corresponds to the average of three aliquots.

g_{2days} values in polymineral samples for all signals were measured in the same manner as in K-rich feldspar samples (Table 3.3).

3.3.1.2.6. Criteria for selection of aliquots

Equivalent dose values in aliquots were selected in two steps. First (in *Analyst v4.57*), aliquots were rejected if the signal was absent, reached the saturation limit or did not increase with given dose. At the next step, the rejection criteria (applied in *Microsoft Excel*) were: >20% relative error of test dose signal in the first cycle of the SAR protocol (Feathers, 2003); >5% recuperation (Murray and Olley, 2002); >2σ deviation from unity in recycling ratio (Thomsen, 2004); >30% relative error in individual D_e (Feathers, 2003); >2σ deviation from unity in OSL reduction after infrared excitation (Jacobs et al., 2003); <20 fast ratio (Durcan and Duller, 2011); individual D_e outside the (Q1-1.5IQR; Q3+1.5IQR) range, where Q1 and Q3 are, respectively, the 1st and 3rd quartiles, and IQR is the interquartile range (Tukey, 1977). The latter criterion was applied to all samples, while the others were used only if they could provide >1σ change in average D_e or improve its accuracy. The fast ratio criterion was not applied to K-feldspar aliquots.

3.3.2. Varve chronology

Varves in varved clay were calculated in the field in cut quarry walls and then recalculated in laboratory from photographs. Each varve was assumed to consist of two layers deposited in summer and winter seasons: a light-color coarse-grained layer below and a dark-color fine-grained one above respectively.

3.4. Geochemical methods

3.4.1. X-ray fluorescence analysis

Non-destructive X-ray fluorescence (XRF) spectrometry was used to determine element concentrations in 77 samples. The measurements were performed by the author at the Institute of Geography, University of Cologne (Germany), under supervision of S. Opitz. The samples selected for measurements were dried, homogenized, mixed with a wax binder (CEREOX Licowax at a ratio of 4 to 1) and pressed into 32-mm pellets. All measurements were performed on an Energy-Dispersive Polarisation XRF (EDPXRF) SPECTRO XEPOS (SPECTRO Analytical Instruments Ltd.) analyzer in a helium gas atmosphere, simultaneously for 60 elements and Fe_2O_3.

3.4.2. Measurement of carbon and nitrogen concentrations

Total organic carbon (TOC) and total nitrogen (TN) were measured in 77 samples on a C/N element analyzer (Elementar vario EL Cube; Elementar UK Limited, Stockport, UK), by the author at the Institute of Geography, University of Cologne (Germany), under supervision of S. Opitz. The TOC was determined in samples treated with HCl while heating to 90°C to eliminate inorganic carbon.

Chapter 4. Results and interpretation

4.1. Stratigraphy

The section stripped in the Scerdlov Factory quarry comprises seven lithostratigraphic units, described from bottom to top (Figs. 4.1, 4.2).

Unit 1

Description

Alternated glaciolacustrine dark brown silty clay and light grey silt varves in the lower part of the quarry, ~6.2 m of visible thickness, were documented in cuts 7 and 9 (Figs. 4.1, 4.2, 4.3, 4.4). Sediments at the bottom of the unit enclose abundant bedrock and mudrock gravel, pebble and boulders up to 0.5 m in size (Figs. 4.4C, 4.5D), as well as disc-shaped carbonate concretions (so-called Imatra stones), 1-3 cm thick and up to 10 cm in diameter (Fig. 4.5C); the boulders may be dropstones judging by typical downwarping of the sedimentary layers (Fig. 4.5E). The varves are the thickest (10 cm) in the lower part of cut 6 (Fig. 4.5A) but become thinner up the section, to a few mm near the unit top (Fig. 4.5B). Some varves are folded (Fig. 4.4B) and some silt layers bear current ripples, up to ~2 cm high and ~35 cm long (Fig. 4.4E). The top of the varved unit lies at -10.0 m asl in cut 9 and at -15.7 m asl in cut 7. The unit grades smoothly into unit 2 where sediments acquire bluish and blackish hues, while the varved bedding disappears (Figs. 4.4B, 4.5B).

Interpretation

The unit can be correlated to the Moscow Stage of the regional stratigraphy (Table 4.1). The varved bedding, along with ice rafted debris (dropstones) and Imatra stones (Tarr, 1935; Salmi, 1959; Astakhov et al., 2005), is evidence of deposition in a glacial basin. Diatom data (Pleshivtseva et al., 1984) reveal two episodes of saline water influx to the lake. The gradual upward thinning of the varves indicates ice retreat. The Upper Moscow glaciomarine/glaciolacustrine deposits were identified by the author as the Sverdlov Fm. The Sverdlov Factory quarry is the only place where the formation is exposed and can be documented in detail. The Sverdlov deposits are prevalent in the Neva Lowland and surrounding areas. The deposits exhibit a distinctive appearance and comprise brown (chocolate) varved clay and silt (e.g., Yanishevsky, 1931; Sokolova et al., 1959; Lavrova and Grichuk, 1960; Malakhovsky et al., 1966; Nedrigailova et al., 1971; Pleshivtseva et al., 1984). These deposits are typically underlain by the Moscow till and overlain by the Mga interglacial deposits.

Unit 2

Description

The unit, up to 16 m thick, is composed of laminated clayey silt (Fig. 4.6C, D) looking bluish black in fresh sections (Fig. 4.6). In cut 9 (Figs. 4.1, 4.3), the bluish hue also appears in varves, 30 cm below the lithological boundary revealed from the disappearance of varve bedding (Fig. 4.4C). Clayey

Table 4.1. Correlation of sedimentary formations described in this paper with marine isotope stages (MIS) (Lisiecki and Raymo, 2005) officially approved in Russia: North-West Russian Stages (Resolutions…, 2002) and North-West European Stages (Mangerud, 1991). The Middle/Late Pleistocene and the Pleistocene/Holocene boundaries are after Head et al. (2021).

<table>
<tr><th>Subseries</th><th>Age (ka)</th><th>MIS</th><th>Age (ka)</th><th>Sedimentary formations in this work</th><th colspan="2">North-West Russian Stages (Zhamoida, 2002)</th><th colspan="2">North-West European Stages (Mangerud, 1991)</th></tr>
<tr><td>Holocene</td><td rowspan="9">11.7</td><td>1</td><td rowspan="9">14</td><td>–</td><td colspan="2">Holocene</td><td colspan="2">Holocene</td></tr>
<tr><td rowspan="8">Late Pleistocene</td><td rowspan="2">2</td><td>Baltic glaciolacustrine</td><td rowspan="8">Valdai</td><td rowspan="2">Ostashkov</td><td rowspan="8">Weichselian</td><td>Upper</td></tr>
<tr><td>Ostashkov till</td><td rowspan="2">Middle</td></tr>
<tr><td rowspan="2">3</td><td rowspan="2">Leningrad alluvial/ lacustrine</td><td rowspan="2">Leningrad</td></tr>
<tr><td rowspan="2">29</td></tr>
<tr><td rowspan="2">4</td><td rowspan="3">Lower Valdai lacustrine</td><td rowspan="3">Podporozhye</td></tr>
<tr><td rowspan="2">57</td><td>Lower</td></tr>
<tr><td>5a-d</td><td rowspan="2">71</td></tr>
<tr><td rowspan="2">129</td><td>5e</td><td rowspan="2">115</td><td>Mga marine</td><td colspan="2">Mikulino</td><td colspan="2">Eemian</td></tr>
<tr><td>Middle Pleistocene</td><td>6</td><td>130</td><td>Sverdlov glaciolacustrine</td><td colspan="2">Moscow</td><td colspan="2">Saalian</td></tr>
</table>

silt contains numerous bivalve shells at 2–3 levels (Fig. 4.6A, B), but rare visible shells were observed between the levels (Fig. 4.6C, D). Two levels with bivalves in cut 7 (Figs. 4.1, 4.3) lie in the depth intervals -10 m to -9 m asl and -6 m to -5 m asl. Most of the shells are deformed and crumbly (Fig. 4.6B). Only few specimens of *Portlandia arctica* could be identified (by A. Merkuliev, Zoological Institute, St. Petersburg) in the poorly preserved shells from cut 8 at -5 m asl. Other fossils found in the unit were right foreleg bones (Figs. 4.6E, 4.7) of an adult individual *Cervus elaphus* (identified by P.A. Kosintsev, Institute of Plant and Animal Ecology, IPAE, Ekaterinburg). Furthermore, clay silt encloses a wood fragment, about 30 cm long. The section of cut 9 bears signatures of sediment deformation and an unconformity at -7 to -6 m asl (Fig. 4.6A). Clayey silt is folded near the unit top in cut 4 (Figs. 4.1, 4.3). The upper >1.5 m of the unit stripped in cut 5 (Figs. 4.1, 4.8D) are composed of diamicton (gravel and pebble debris in massive black clayey silt). The top of the unit lies at -3 m to 0 m asl.

Interpretation

The appearance and stratigraphy of the unit, along with the found marine fossils, allow reliable correlation with the Mga Fm.. deposited during the Mikulino interglacial (Table 4.1). The Mikulino age of the unit is supported by palynological (see section 3.2.1) and OSL (see section 3.3.1) data.

Unit 3

Description

The unit, ~0.5 m of true thickness, is exposed only in cut outcrop 4 (Figs. 4.1, 4.3, 4.5A) between -2.4 m and -0.7 m asl. It consists of grey parallel-bedded clayey silt folded concordantly with deformation in the upper part of unit 2.

Interpretation

Sedimentary structure, texture, absence of marine fossils (present in unit 2), as well as geochemical composition of deposits (see section 3.4), indicate that the unit was deposited in a freshwater lake. According to OSL ages (see section 3.2.1), the lacustrine deposition occurred during the latest Mikulino Interglacial or the earliest Early Valdai (Table 4.1).

Unit 4

Description

The unit is exposed in cut outcrops 4 and 8 (Figs. 4.1, 4.3), with its top at -1.9 m to 0.4 m asl. It is composed of parallel-bedded light brown sand with plant detritus (Figs. 4.8A, B). The primary sedimentary structure is disturbed by folds and faults. The maximum visible thickness is 1.5 m.

Interpretation

Grain size and sedimentary structure and texture indicate lacustrine or alluvial origin of the sediments. According to stratigraphy and OSL dating (see section 3.2.1), the unit correlates with the Leningrad Stage of regional stratigraphy (Table 4.1).

Unit 5

Description

The unit is exposed only in cut outcrop 5 (Figs. 4.1, 4.3, 4.8D) and consists of parallel-bedded light gray fine sand and dark gray silt, within 0.4 m thick, deformed by faulting.

Interpretation

The unit was deposited in a lake, judging by parallel bedding and grain sizes of the sediments. It was previously assigned to the Ostashkov Stage (Ruchkin e t al., 2021) and interpreted as an intra-glacial unit proceeding from the presence of diamicton of uncertain origin below the base. However, later OSL data (see section 3.2.1) rather support correlation with the Leningrad Stage.

Unit 6

Description

The grey-brown clayey silt and sandy silt diamicton of the unit, 3 to 10 m thick, with pebbles and boulders up to 1.5 m, is widespread throughout the quarry (Figs. 4.1, 4.7A, C). The elevations vary from 1 to 5–6 m asl. The sediments are laminated in the lower part of the unit in cut 5 (Figs. 4.1, 4.3, 4.6C) but are massive at higher levels.

Interpretation

The rocks in cut 5 show a typical succession grading upward into subglacial till (Banham, 1977; Hart and Boulton, 1991; Bennett and Glasser, 2009): (1) undeformed Mga clayey silt; (2) folded marine and lacustrine/alluvial sediments; (3) diamicton with tectonic lamination; (4) homogeneous diamicton. Judging by the structure and texture of rocks, as well as the stratigraphy of diamicton, the unit represents the subglacial till of the Ostashkov Stage(Table 4.1).

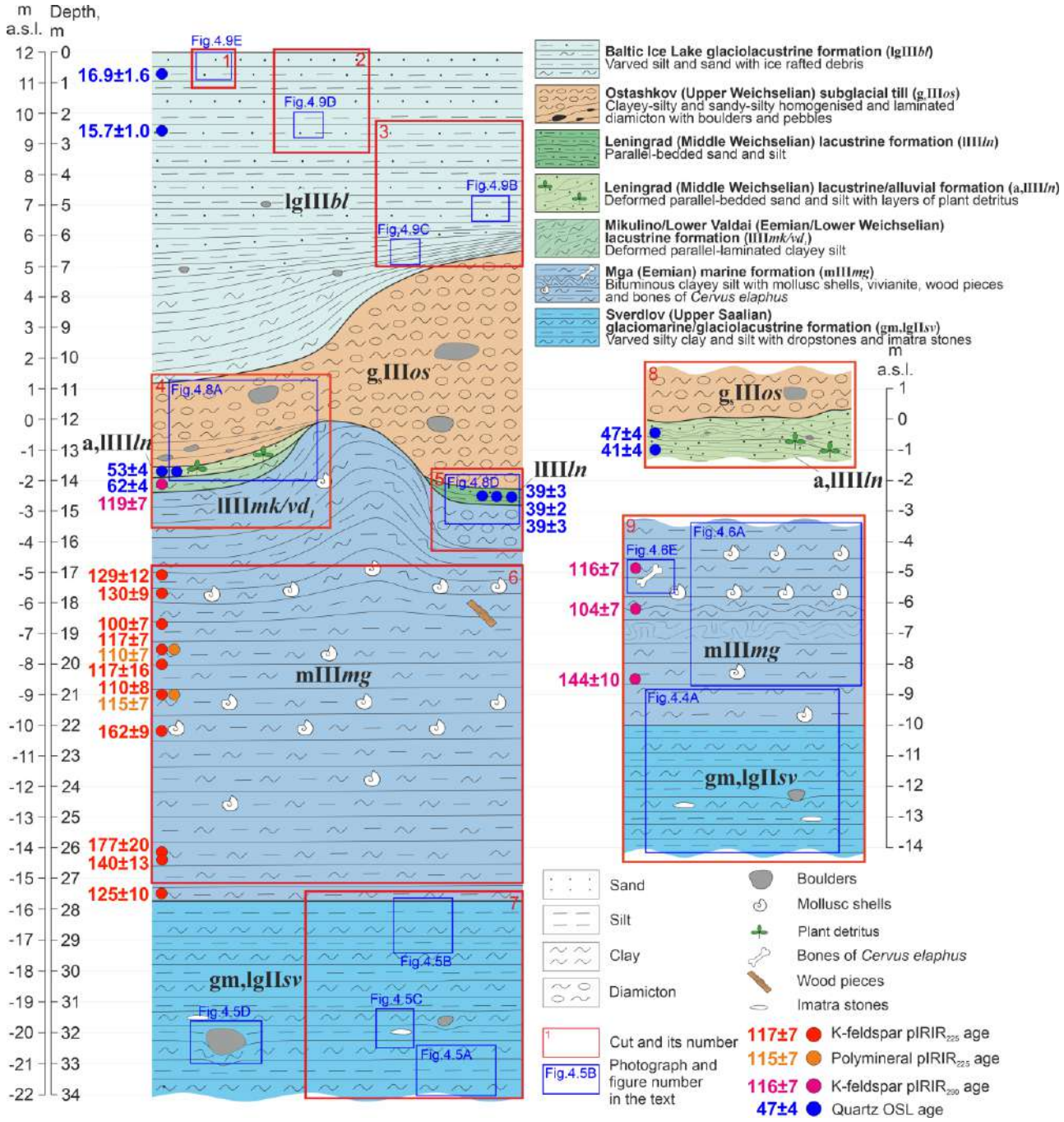

Fig. 4.1. Stratigraphy of the Sverdlov Factory quarry.

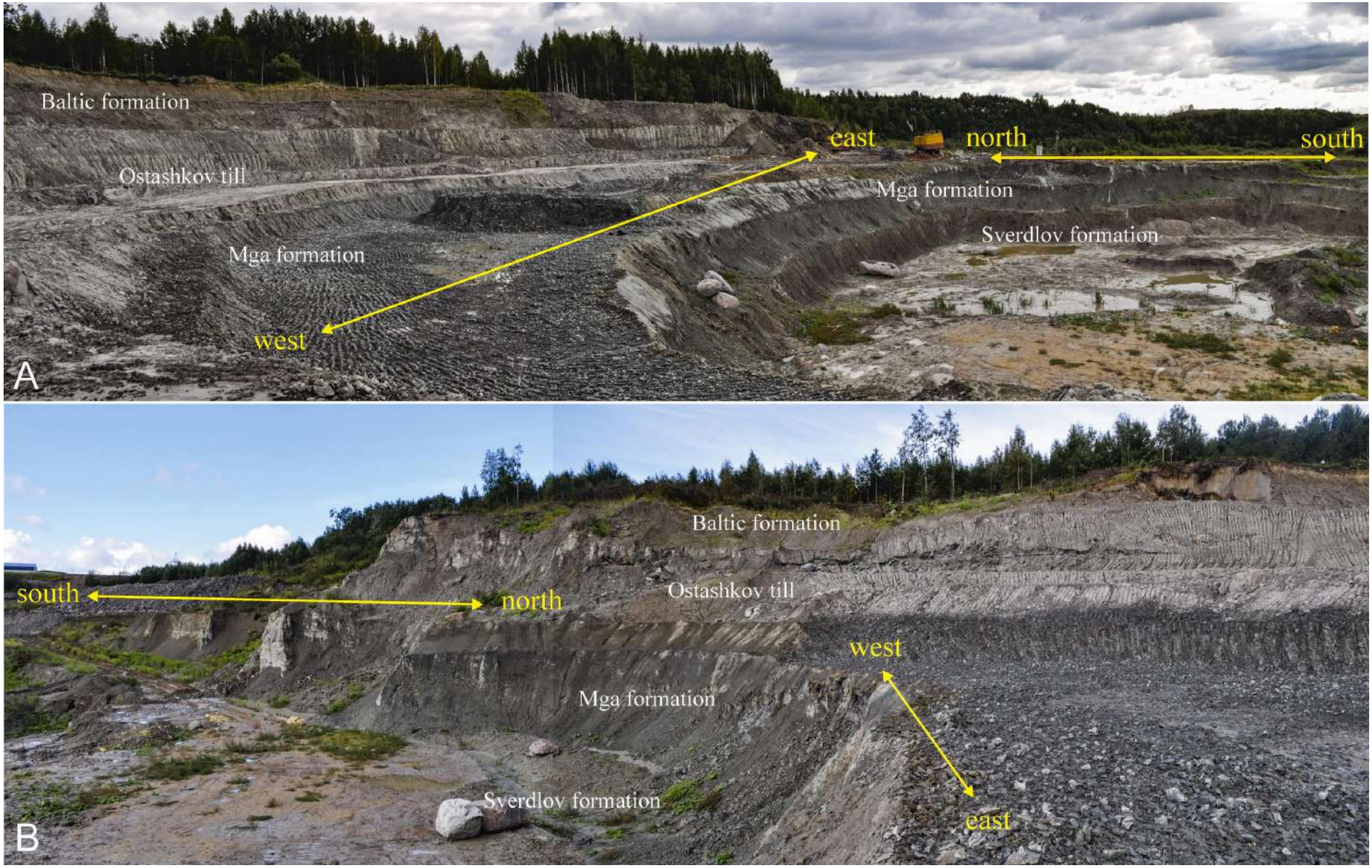

Fig. 4.2. Sverdlov (Etalon) Factory quarry: general view. **A** – Eastern and northeastern walls. **B** – Western and northwestern walls. Photographs by V. Dudanova.

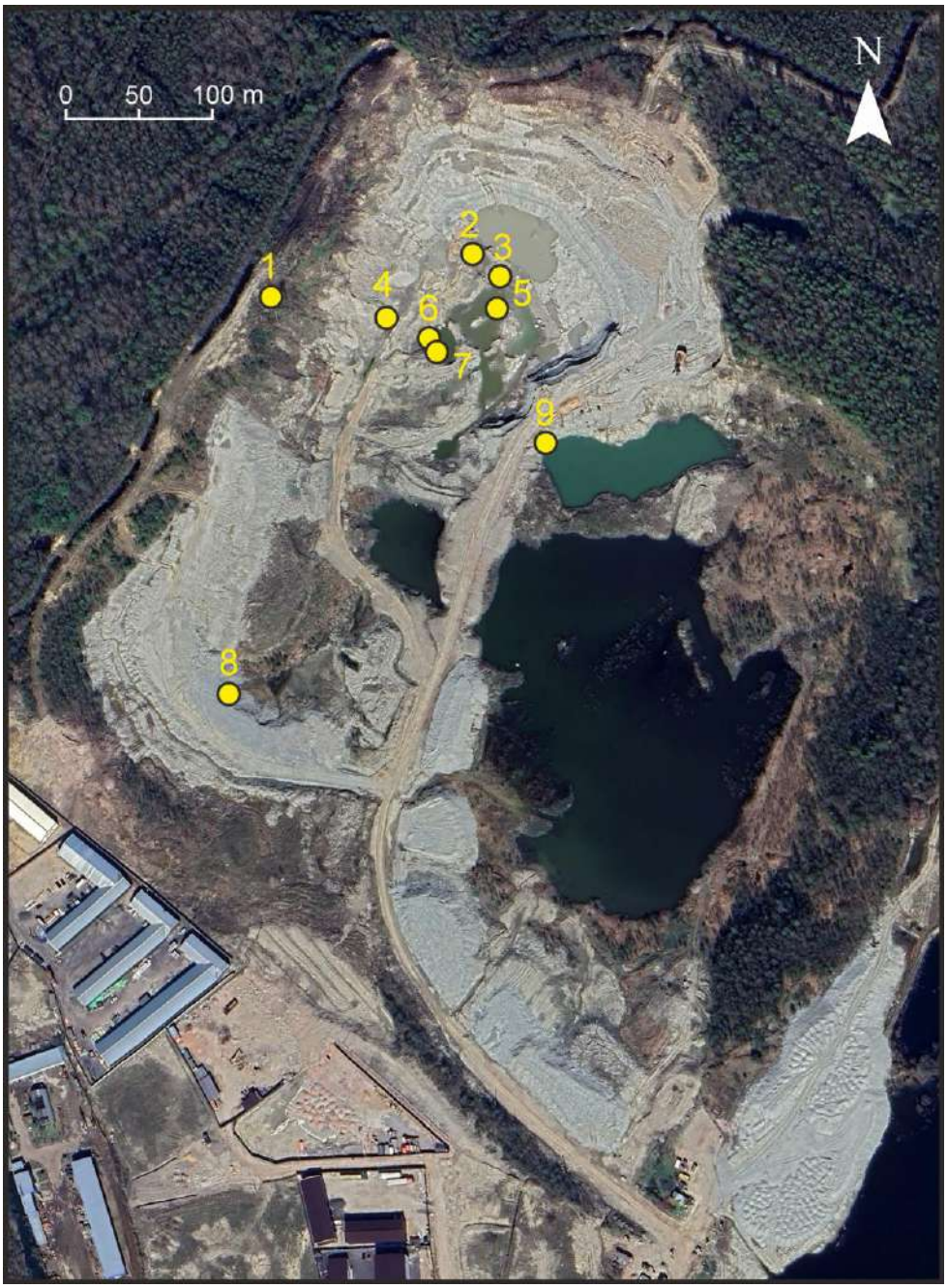

Fig. 4.3. Location of cut outcrops in Sverdlov quarry (Fig. 4.1), based on a Google Earth image (Image © 2023 Airbus, shot on 08.05.2023).

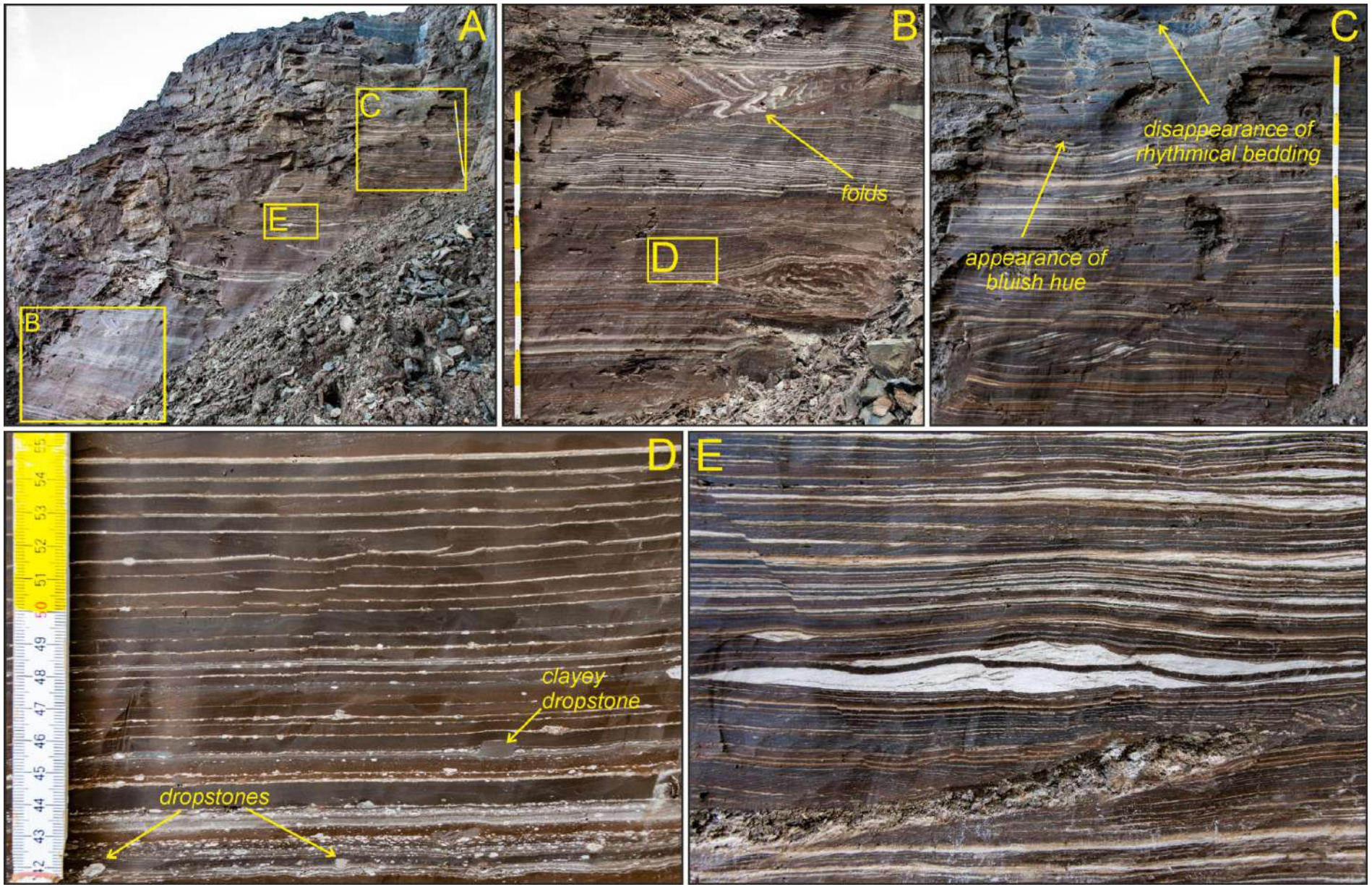

Fig. 4.4. **A** – General view of the Sverdlov glaciomarine/glaciolacustrine varved sediments in cut 9 (Figs. 4.1, 4.3). **B** – The lower part of the Sverdlov formation in cut 9 (Fig. 4.1, 4.3). **C** – The boundary between the Sverdlov glaciomarine/glaciolacustrine and Mga marine interglacial formations. **D** – Ice rafted debris in the Sverdlov glaciomarine/glaciolacustrine varves. **E** – Current ripples in the Sverdlov deposits.

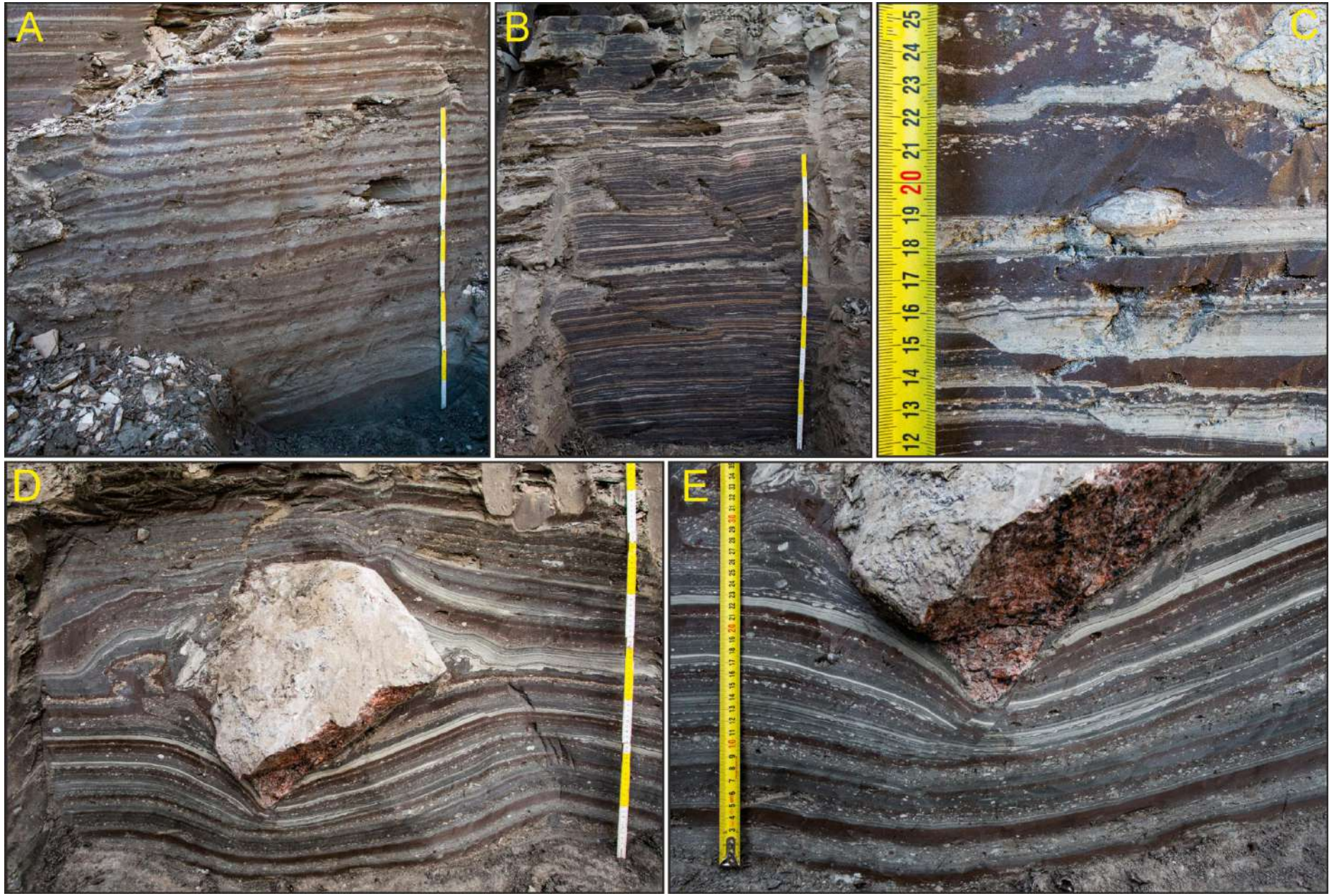

Fig. 4.5. **A** – The lower part of the Sverdlov formation in cut 7 (Figs. 4.1, 4.3). **B** – The upper part of the Sverdlov formation in cut 7 (Fig. 10, 14). **C** – Imatra stone in the Sverdlov varves. **D** – Giant dropstone in the Sverdlov formation. **E** – Buckling of varves under the giant dropstone.

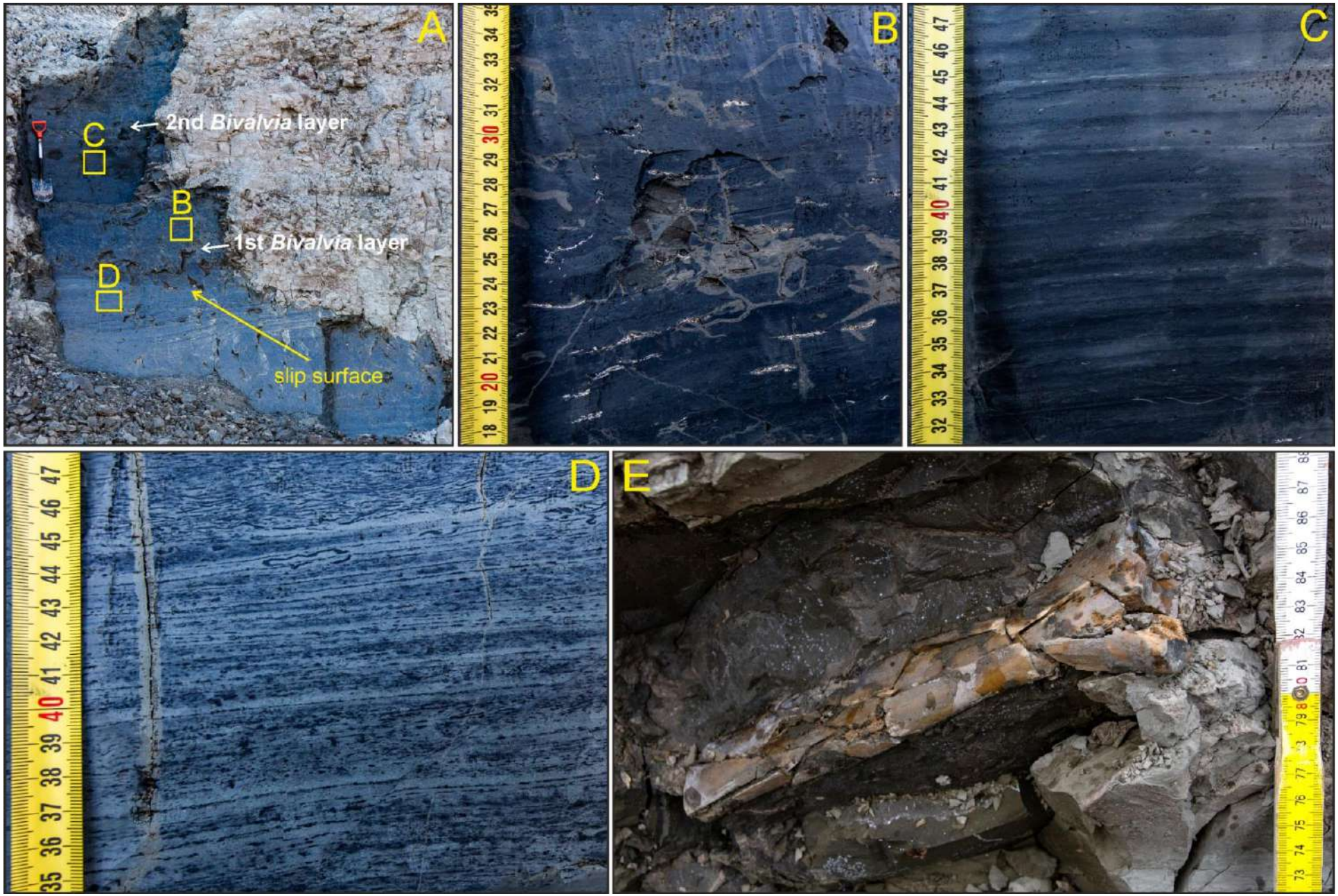

Fig. 4.6. A – General view of the Mga marine clayey silt in cut 9 (Fig. 4.1, 4.3). **B** – Squashed *Bivalvia* shells in the Mga deposits. **C, D** – Thin lamination of the Mga clayey silt. **E** – A bone of the off fore leg of an adult specimen *Cervus elaphus* (defined by P. Kosintsev, IPAE, Ekaterinburg).

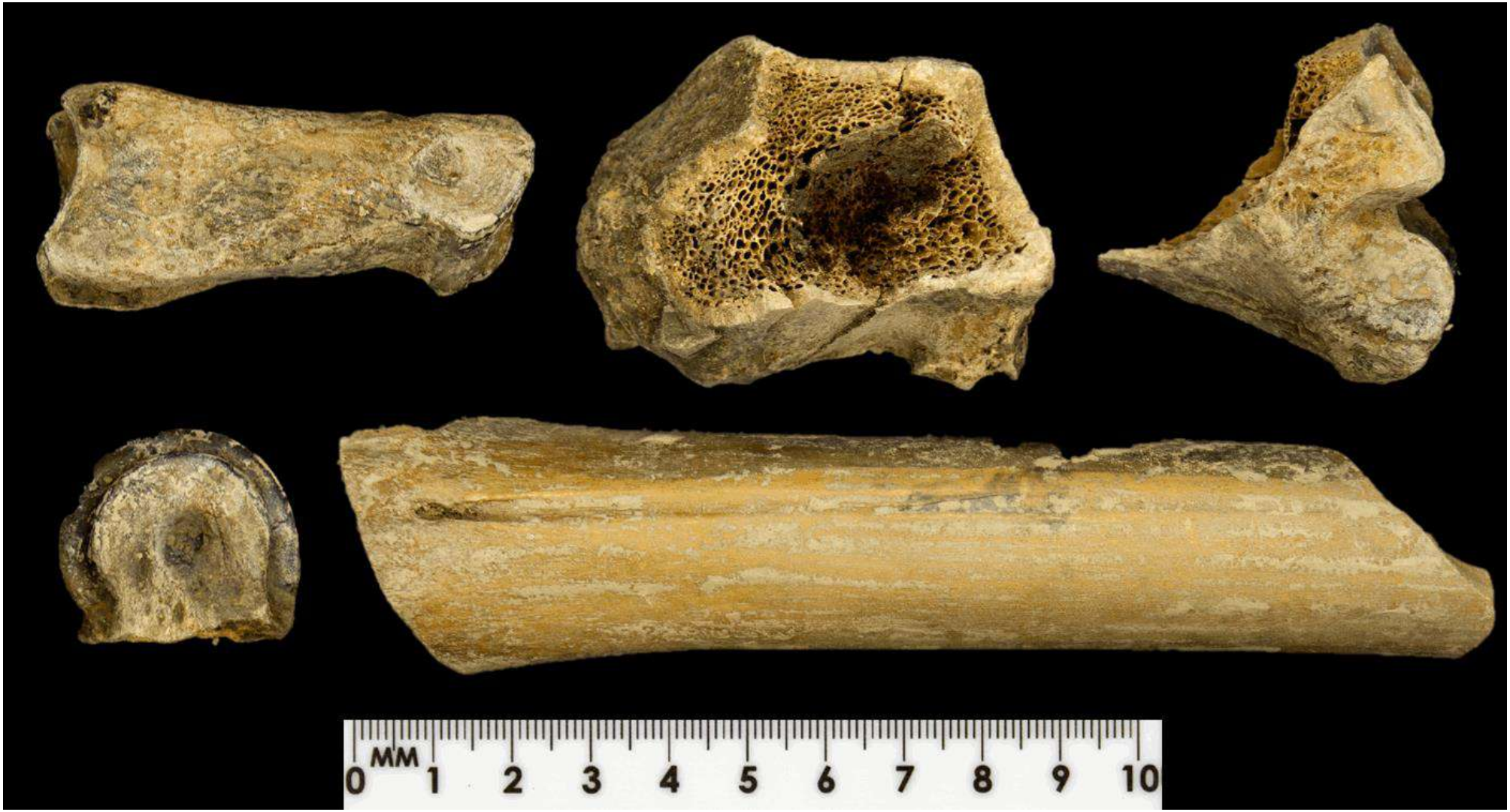

Fig. 4.7. Right foreleg bones of an adult *Cervus elaphus* individual (identified by P. Kosintsev, IPAE, Ekaterinburg).

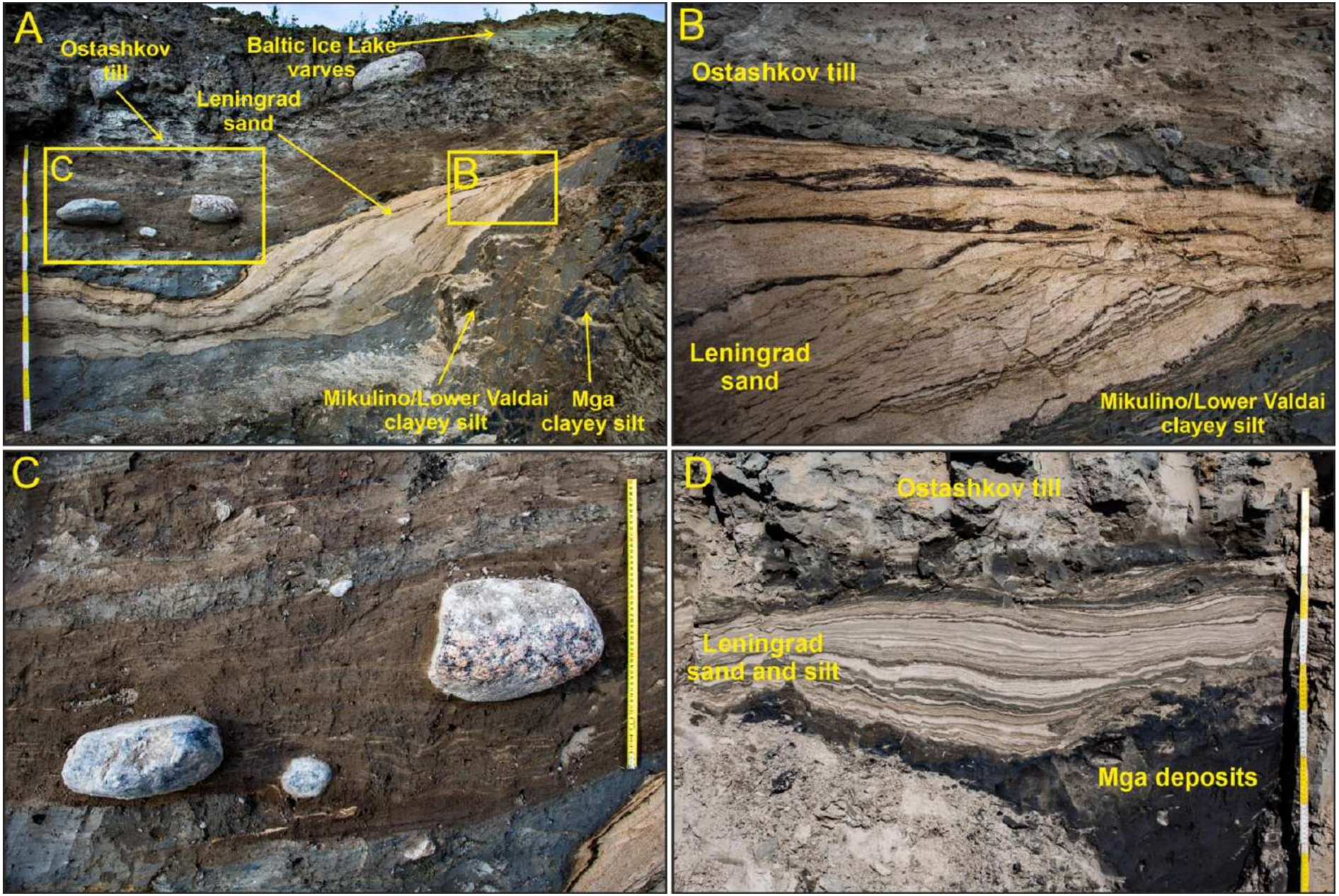

Fig. 4.8. **A** – General view of the succession in cut 4 (Figs. 4.1, 4.3). **B** – The deformed Leningrad sand sandwiched between the Mikulino/Lower Valdai clayey silt and Ostashkov till. **C** – The Ostashkov subglacial till with sandy-silty matrix, tectonic lamination and boulders of crystalline rocks. **D** – A lens of the Leningrad sand and silt sandwiched between the Mga deposits and Ostashkov till in cut 5 (Figs. 4.1, 4.3).

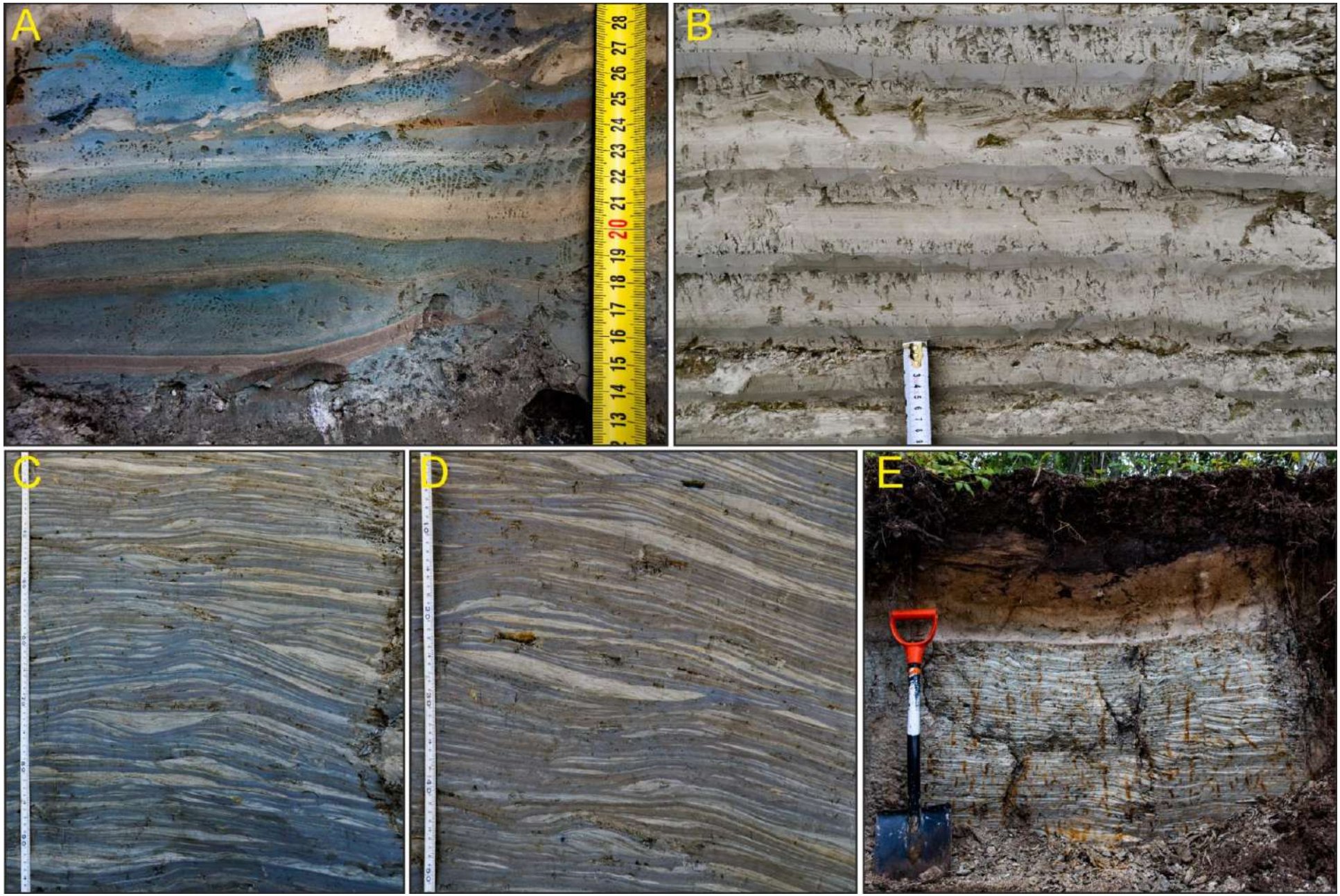

Fig. 4.9. The base of the Baltic formation in cut 4 (Figs. 4.1, 4.3). **B** – Varves of the Baltic Ice Lake in cut 3 (Figs. 4.1, 4.3). **C, D** – Lenticular bedding in the Baltic formation in cuts 3 and 2 respectively (Figs. 4.1, 4.3). **E –** The top of the Baltic varves in cut 1 (Figs. 4.1, 4.3).

Unit 7

Description

The varved sand and gray silt of the unit are widespread throughout the quarry (Figs. 4.1, 4.9). Winter layers at the base are bluish (Fig. 4.9A). The unit includes a bed of bedrock and mudrock pebbles and gravel. The varved sediments, 6.5 m to 11 m thick, build a terrace at 12–13 m asl. Varves vary in thickness from ~10 cm at the base to 1–2 cm at the top of the section (Fig. 4.9B, E). The sediments show lenticular bedding in some parts of the quarry (Fig. 4.9C, D). At the top, there are vertical traces of iron staining along plant roots (Fig. 4.9E).

Interpretation

According to the stratigraphy and sedimentary structure and texture, the unit was deposited in the Baltic Ice Lake (Table 4.1). This interpretation is consistent with results of OSL dating (see section 3.2.1). Coarse material at the base likely results from ice rafting. The upward thinning of varves records gradual ice retreat.

4.2. Varve chronology

Annual varves were counted in cuts 7 and 9 (Figs. 4.1, 4.3). The visible part of the Sverdlov Fm. includes at least ~1100 varves in cut 7, where it is 6.2 m thick, and ~1050 varves in cut 9, over 4.0 m thick. This is the minimum varve count as some varves are too thin (~1 mm) to be visually distinguishable, and a special study is required for more exact estimates.

4.3. OSL chronology

4.3.1. Dosimetry

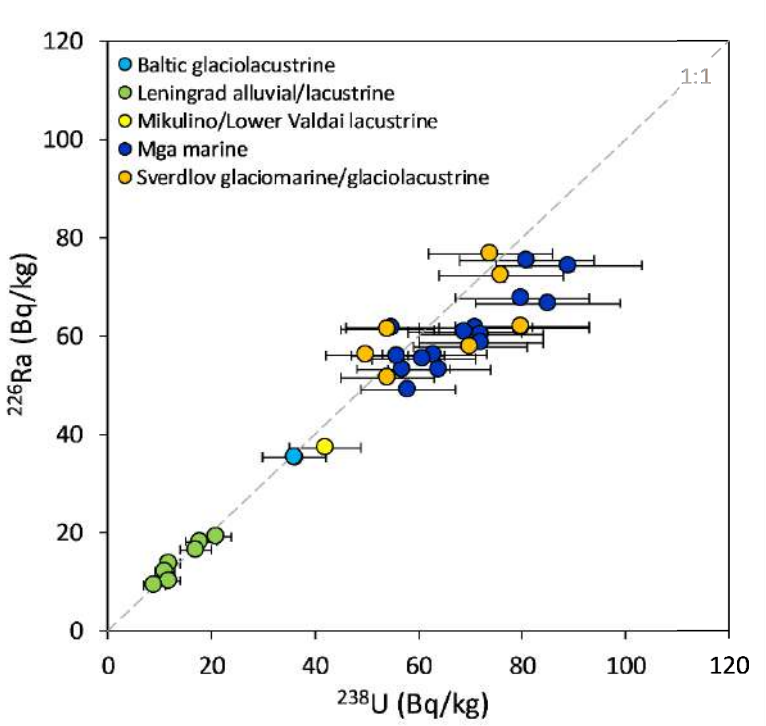

Fig. 4.10. Correlated ^{238}U and ^{226}Ra activities in different facies from the Sverdlov Factory quarry.

Activities of ^{238}U, ^{226}Ra, ^{232}Th and ^{40}K radionuclides were measured in 33 samples by high-resolution gamma spectrometry (Table 4.2). The clay-silt sediments of Sverdlov, Mga, and Mikulino/Lower Valdai Fms. are highly radioactive, with dose rates from 3.59 to 4.68 Gy/ka in quartz (Table 4.3). The dose rates are lower in the Baltic Ice Lake deposits (3.45–3.52 Gy/ka, quartz) and the lowest in the Leningrad sand (1.39–2.45 Gy/ka).

The gamma spectrometry data were confirmed by XRF results for the Sverdlov, Mga, and Mikulino/Lower Valdai deposits (Fig. 4.11). The K depth profiles obtained by the two methods are almost identical. The curves for U and Th differ slightly, possibly because the gamma spectrometry and XRF measurements were applied to different groups of samples: rocks for OSL dating were sampled at every 1 m, and samples for XRF were collected separately at every 0.2 to 0.5 m. XRF gave slightly

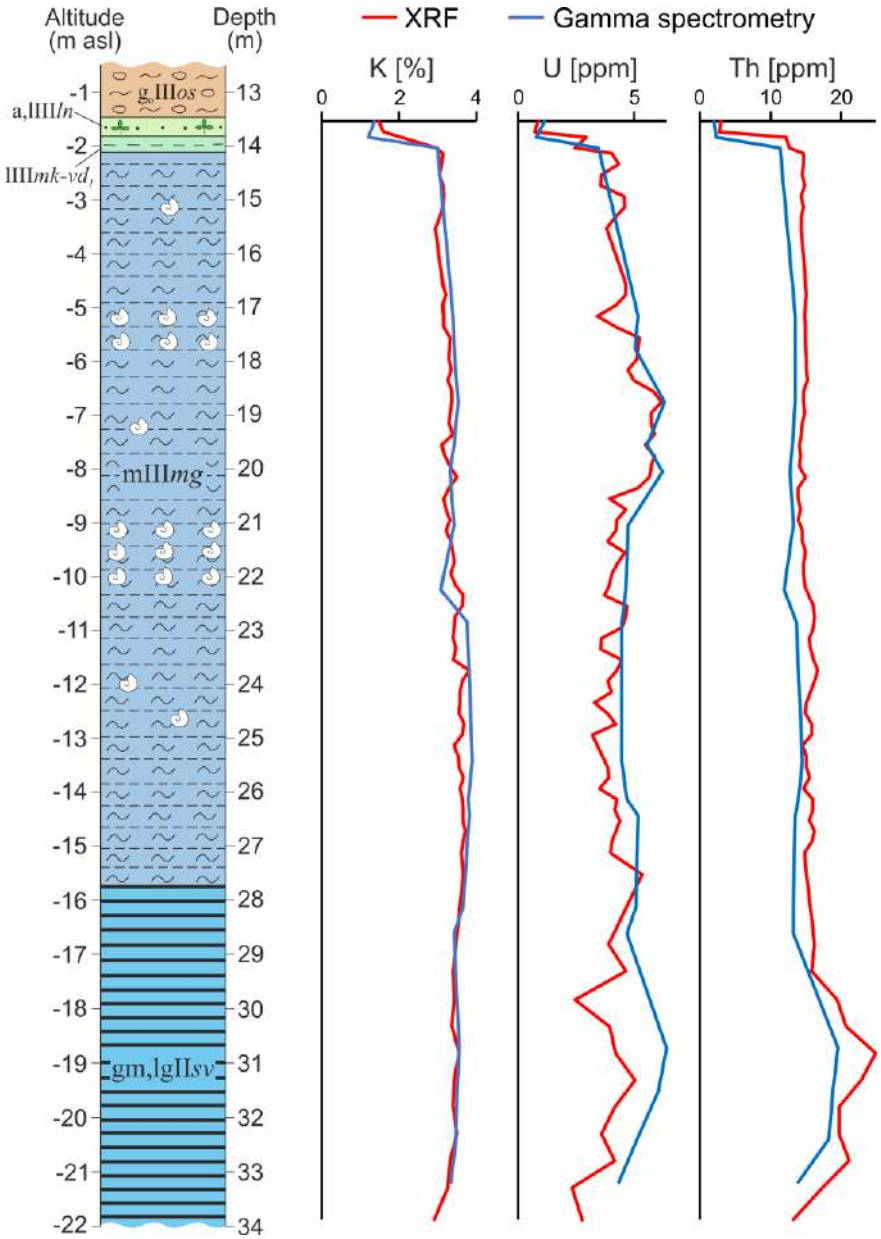

Fig. 4.11. Depth profiles of K, U, and Th concentrations measured by gamma spectrometry and XRF analysis in samples from the Sverdlov Factory quarry.

lower U and higher Th concentrations than gamma spectrometry, but the difference was commonly within 15% and the values balanced one another in the dose rate calculations.

Table 4.2. Activity of natural radionuclides in samples from Sverdlov Factory quarry

No	Sample	Depth (m)	Water content (%)	Specific activity (Bq/kg)			
				^{238}U	^{226}Ra	^{232}Th	^{40}K
1	Etalon 3	0.7	18±5	36±6	35.2±0.7	39.1±0.6	810±38
2	Etalon 2	2.5	30±5	36±6	35.4±0.7	45.6±0.7	898±41
3	2105-23	15	20±5	21±3	19.0±0.4	19.6±0.4	650±30
4	2105-22	15	23±5	18±3	18.1±0.4	18.1±0.4	632±29
5	2105-21	15	21±5	17±3	16.5±0.4	16.0±0.3	607±28
6	2104-14	12.5	17±5	12±2	13.6±0.3	11.2±0.3	414±20
7	2104-13	13	17±5	11±2	12.1±0.3	10.5±0.2	438±21
8	2024-81	13.5	20±5	12±2	10.2±0.2	9.5±0.2	385±21
9	2024-79	13.8	20±5	9±2	9.3±0.2	8.3±0.2	429±20
10	2024-82	14	27±5	42±7	37.2±0.7	46.1±0.7	954±44
11	2103-29	17.1	45±5	71±11	61.7±1.1	54.8±0.9	1080±50
12	2103-19	17.7	45±5	72±12	60.3±1.0	55.3±0.8	1090±51
13	2103-27	18.7	46±5	81±13	75.3±1.3	55.2±0.9	1120±52
14	2103-28	19.6	46±5	85±14	66.6±1.1	53.3±0.8	1090±51
15	2103-21	20	43±5	89±14	74.3±1.3	51.9±0.8	1056±49
16	2103-25	21	38±5	63±10	56.2±1.0	53.7±0.8	1086±50
17	2103-26	22.2	38±5	61±10	55.3±0.9	48.6±0.7	979±45
18	2103-17	25.4	30±5	64±10	53.1±1.0	59.4±0.9	1238±57
19	2103-12	26.1	31±5	56±9	55.9±1.0	56.5±0.8	1207±56
20	2103-18	26.4	32±5	55±9	61.6±1.1	55.2±0.8	1210±56
21	2102-9	27.5	29±5	69±11	60.8±1.0	53.8±0.8	1161±54
22	2021-77	17.5	47±5	80±13	67.7±1.2	55.9±0.8	1115±51
23	2021-76	19	35±5	72±12	58.5±1.1	61.5±0.9	1250±57
24	2021-75	20.5	31±5	58±9	49.1±0.9	59.4±0.9	1263±58
25	2102-20	28.6	26±5	50±8	56.0±1.0	53.8±0.8	1090±50
26	2102-11	31.5	41±5	76±12	72.2±1.2	76.6±1.1	1110±51
27	2102-8	31.7	39±5	74±12	76.6±1.3	79.5±1.1	1130±52
28	2102-10	32.4	39±5	54±9	61.2±1.0	74.2±1.1	1101±51
29	2102-6	33.2	36±5	54±9	51.4±0.9	56.9±0.8	1060±50
30	2021-71	23	29±5	70±11	57.8±1.0	57.9±0.9	1147±52
31	2021-70	24	29±5	80±13	61.5±1.1	65.6±1.0	1117±51
32	2021-69	26	37±5	80±13	61.8±1.1	74.6±1.2	1100±52
33	2103-24	22.8	36±5	57±9	53.2±0.9	55.8±0.8	1194±56

Table 4.3. Optically stimulated luminescence (OSL) summary for quartz (Q) K-rich feldspar (KF) and polymineral (PM) extracts. Depth is the current burial depth and n is the number of accepted (a) and rejected (r) aliquots. The K-rich feldspar and polymineral $pIRIR_{225}$ and $pIRIR_{290}$ ages are corrected for anomalous fading according to Huntley and Lamothe (2001). All uncertainties are given at 1σ (~ 68% confidence interval).

Subseries	Stage	Formation	No	Field code	Lab. code	Depth (m)	Water content (%)	Grain size (μm)	Dose rate (Gy/ka)	Mineral	Signal	n (a/r)	Equivalent dose uncorrected (Gy)	OSL age uncorrected (ka)	OSL age corrected (ka)	Quartz is reset? and KF/Q
Upper Pleistocene	Ostashkov	Baltic glaciolacustrine	1	Etalon 3	RGI-813 C-L5323	0.7	18±5	90-180	3.52±0.14	Q	post-IR OSL	20/7	59±5	**16.9±1.6**	–	**?**
								90-180	4.23±0.22	KF	$pIRIR_{225}$	3/0	328±25	78±7	–	4.62±0.56
											$IR_{50,225}$	3/0	225±39	53±10	–	3.14±0.64
			2	Etalon 2	RGI-814 C-L5324	2.5	30±5	90-180	3.45±0.13	Q	post-IR OSL	18/0	54±3	**15.7±1.0**	–	**?**
								90-180	4.17±0.22	KF	$pIRIR_{225}$	3/0	210±13	50±4	–	3.18±0.29
											$IR_{50,225}$	3/0	129±11	31±3	–	1.97±0.21
	Leningrad	Leningrad lacustrine	3	2105-23	RGI-863 C-L5327	15	17±5	90-180	2.45±0.11	Q	post-IR OSL	25/9	95±7	**39±3**	–	**?**
								90-180	3.16±0.21	KF	$pIRIR_{225}$	3/0	259±29	82±11	–	2.10±0.31
											$IR_{50,225}$	3/0	176±14	56±6	–	1.44±0.18
			4	2105-22	RGI-863 C-L5327	15	17±5	90-180	2.35±0.10	Q	post-IR OSL	27/0	91±5	**39±3**	–	✓
								90-180	3.06±0.20	KF	$pIRIR_{225}$	3/0	194±22	63±8	–	1.62±0.23
											$IR_{50,225}$	3/0	126±12	41±5	–	1.05±0.14
			5	2105-21	RGI-863 C-L5327	15	20±5	90-180	2.17±0.09	Q	post-IR OSL	27/10	84±7	**39±4**	–	✓
								90-180	2.88±0.20	KF	$pIRIR_{225}$	3/0	237±11	82±7	–	2.10±0.26
											$IR_{50,225}$	3/0	163±35	57±13	–	1.46±0.36
		Leningrad alluvial/lacustrine	6	2104-14	RGI-866 C-L5325	12.5	23±5	180-250	1.46±0.06	Q	post-IR OSL	15/3	68±5	**47±4**	–	✓✓
								180-250	2.49±0.16	KF	$pIRIR_{225}$	3/0	155±23	62±10	–	1.32±0.23
											$IR_{50,225}$	3/0	87±11	35±5	–	0.74±0.12
			7	2104-13	RGI-866 C-L5325	13	21±5	90-180	1.55±0.07	Q	post-IR OSL	16/2	64±6	**41±4**	–	✓✓
								180-250	2.54±0.16	KF	$pIRIR_{225}$	3/0	132±8	52±4	–	1.27±0.14
											$IR_{50,225}$	3/0	92±7	36±3	–	0.88±0.10
			8	2024-81	RGI-868 Risø 202595	13.5	20±5	90-180	1.39±0.06	Q	OSL	16/1	74±4	**53±4**	–	✓✓
								180-250	2.39±0.16	KF	$pIRIR_{290}$	3/0	164±12	69±7	–	1.30±0.15
											$IR_{50,290}$	3/0	110±4	46±3	–	0.87±0.08
			9	2024-79	RGI-868 Risø 202593	13.8	20±5	180-250	1.43±0.06	Q	OSL	17/2	89±5	**62±4**	–	–

Subseries	Stage	Formation	No	Field code	Lab. code	Depth (m)	Water content (%)	Grain size (μm)	Dose rate (Gy/ka)	Mineral	Signal	n (a/r)	Equivalent dose uncorrected (Gy)	OSL age uncorrected (ka)	OSL age corrected (ka)	Quartz is reset? and KF/Q
Upper Pleistocene	Mikulino/ Lower Valdai	Mikulino/ Lower Valdai lacustrine	10	2024-82	RGI-870 Risø 202596	14	27±5	63-90	4.16±0.16	KF	$pIRIR_{290}$	6/0	469±19	113±6	**119±7**	–
											$IR_{50,290}$	5/1	281±10	68±4	–	–
	Mikulino	Mga marine	11	2103-29	RGI-871 C-L5330	17.1	45±5	90-150	4.50±0.18	KF	$pIRIR_{225}$	6/1	504±41	112±10	**129±12**	–
											$IR_{50,225}$	5/2	444±55	99±13	–	–
			12	2103-19	RGI-873 C-L5331	17.7	45±5	150-250	4.74±0.23	KF	$pIRIR_{225}$	5/0	537±30	113±8	**130±9**	–
											$IR_{50,225}$	4/1	404±21	85±6	–	–
			13	2103-27	RGI-874 C-L5332	18.7	46±5	90-250	3.99±0.15	Q	post-IR OSL	12/0	381±30	95±8	–	–
								90-180	4.75±0.22	KF	$pIRIR_{225}$	5/6	417±22	87±6	**100±7**	–
											$IR_{50,225}$	8/3	306±21	65±5	–	–
			14	2103-28	RGI-876 C-L5333	19.6	46±5	63-250	3.87±0.15	Q	post-IR OSL	23/1	278±18	72±5	–	–
								90-150	4.57±0.18	KF	$pIRIR_{225}$	4/2	468±23	102±6	**117±7**	–
											$IR_{50,225}$	4/2	436±33	96±8	–	–
								4-11	5.68±0.28	PM	$pIRIR_{225}$	6/0	535±19	94±6	**110±7**	–
									5.28±0.26		$IR_{50,225}$	6/0	389±14	74±5	–	–
			15	2103-21	RGI-877 C-L5334	20	43±5	90-250	3.93±0.14	Q	post-IR OSL	13/2	295±23	75±6	–	–
								150-250	4.87±0.24	KF	$pIRIR_{225}$	5/0	495±66	102±14	**117±16**	–
											$IR_{50,225}$	3/2	287±10	59±4	–	–
			16	2103-25	RGI-879 C-L5335	21	38±5	90-150	4.62±0.19	KF	$pIRIR_{225}$	5/1	444±28	96±7	**110±8**	–
											$IR_{50,225}$	6/0	319±54	69±12	–	–
								4-11	5.64±0.26	PM	$pIRIR_{225}$	6/0	556±20	99±6	**115±7**	–
									5.26±0.25		$IR_{50,225}$	5/1	401±15	76±5		–

Subseries	Stage	Formation	No	Field code	Lab. code	Depth (m)	Water content (%)	Grain size (μm)	Dose rate (Gy/ka)	Mineral	Signal	n (a/r)	Equivalent dose uncorrected (Gy)	OSL age uncorrected (ka)	OSL age corrected (ka)	Quartz is reset? and KF/Q
Upper Pleisocene	Mikulino	Mga marine	17	2103-26	RGI-880 C-L5336	22.2	38±5	90-250	3.59±0.14	Q	post-IR OSL	16/1	242±25	67±7	–	–
								63-90	4.16±0.15	KF	$pIRIR_{225}$	6/0	585±27	141±8	**162±9**	–
											$IR_{50,225}$	6/0	408±15	98±5	–	–
			18	2103-17	RGI-882 C-L5338	25.4	30±5	63-250	4.61±0.19	Q	post-IR OSL	13/2	276±33	60±7	–	–
			19	2103-12	RGI-883 C-L5339	26.1	31±5	90-250	4.43±0.18	Q	post-IR OSL	12/0	486±52	110±12	–	–
								90-180	5.19±0.24	KF	$pIRIR_{225}$	6/0	798±78	154±17	**177±20**	–
											$IR_{50,225}$	6/0	500±32	96±8	–	–
			20	2103-18	RGI-884 C-L5340	26.4	32±5	90-250	4.43±0.18	Q	post-IR OSL	3/0	348±70	78±16	–	–
									5.29±0.35	KF	$pIRIR_{225}$	9/2	645±42	122±11	**140±13**	–
											$IR_{50,225}$	10/1	540±55	102±12	–	–
			21	2102-9	RGI-888 C-L5341	27.5	29±5	90-180	5.21±0.24	KF	$pIRIR_{225}$	5/1	568±37	109±9	**125±10**	–
											$IR_{50,225}$	6/0	635±129	122±25	–	–
			22	2021-77	RGI-872 Risø 202592	17.5	47±5	90-180	4.65±0.22	KF	$pIRIR_{290}$	5/1	510±18	110±6	**116±7**	–
											$IR_{50,290}$	6/0	326±12	70±4	–	–
			23	2021-76	RGI-875 Risø 202591	19	35±5	90-180	5.31±0.24	KF	$pIRIR_{290}$	6/0	524±25	99±6	**104±7**	–
											$IR_{50,290}$	6/0	354±12	67±4	–	–
			24	2021-75	RGI-878 Risø 202590	20.5	31±5	90-180	5.31±0.25	KF	$pIRIR_{290}$	4/2	727±22	137±8	**144±10**	–
											$IR_{50,290}$	4/2	438±14	83±5	–	–

Subseries	Stage	Formation	No	Field code	Lab. code	Depth (m)	Water content (%)	Grain size (μm)	Dose rate (Gy/ka)	Mineral	Signal	n (a/r)	Equivalent dose uncorrected (Gy)	OSL age uncorrected (ka)	OSL age corrected (ka)	Quartz is reset? and KF/Q
Middle Pleistocene	Moscow	Sverdlov glaciomarine/glaciolacustrine	25	2102-20	RGI-889 C-L5342	28.6	26±5	90-180	5.03±0.24	KF	$pIRIR_{225}$	6/0	838±80	167±18	192±21	–
											$IR_{50,225}$	6/0	674±70	134±15	–	–
			26	2102-11	RGI-890 C-L5344	31.5	39±5	90-250	5.23±0.34	KF	$pIRIR_{225}$	5/1	1234±87	236±23	272±27	–
											$IR_{50,225}$	5/1	893±44	170±14	–	–
								4-11	6.56±0.32	PM	$pIRIR_{225}$	6/0	1196±44	182±11	213±13	–
									6.07±0.30		$IR_{50,225}$	5/1	735±27	121±7	–	–
			27	2102-8	RGI-891 C-L5343	31.7	41±5	90-150	5.14±0.19	KF	$pIRIR_{225}$	7/0	1178±119	229±25	264±29	–
											$IR_{50,225}$	7/0	914±92	178±19	–	–
			28	2102-10	RGI-892 C-L5345	32.4	39±5	63-250	4.14±0.16	Q	post-IR OSL	3/0	264±24	64±6	–	–
			29	2102-6	RGI-893 C-L5346	33.2	36±5	150-250	4.79±0.24	KF	$pIRIR_{225}$	6/0	1104±119	230±27	265±32	–
											$IR_{50,225}$	5/1	834±43	174±13	–	–
			30	2021-71	RGI-885 Risø 202589	23	29±5	63-90	4.59±0.16	Q	OSL	8/4	443±23	95±6	–	–
								63-180	5.18±0.28	KF	$pIRIR_{290}$	3/0	923±101	178±22	187±24	–
											$IR_{50,290}$	3/0	403±19	78±6	–	–
			31	2021-70	RGI-886 Risø 202588	24	29±5	63-90	4.68±0.17	Q	OSL	7/0	386±41	82±9	–	–
								63-180	5.28±0.28	KF	$pIRIR_{290}$	6/0	832±51	158±13	166±15	–
											$IR_{50,290}$	6/0	375±17	71±5	–	–
			32	2021-69	RGI-887 Risø 202587	26	37±5	90-180	4.39±0.15	Q	OSL	4/13	578±110	132±26	–	–
								90-180	5.10±0.23	KF	$pIRIR_{290}$	3/0	1286±63	252±17	265±20	–
											$IR_{50,290}$	3/0	699±24	137±8	–	–

Probability of quartz reset prior to burial:

? – unknown ✓ – probably poorly reset ✓✓ – probably well reset

Errors in dose rates may result from the lack of equilibrium in the ^{238}U decay chain (Krbetschek et al., 1994; Olley et al., 1996). The equilibrium in the ^{238}U series was checked by the ^{226}Ra /^{238}U ratios (Fig. 4.10), which varied from 0.77 to 1.13 but approached unity within two standard deviations. Equilibrium was observed in the Leningrad (1.00±0.05, n=7) and Baltic (0.98±0.03, n=2) samples, while ^{238}U excess appeared in the Sverdlov varves (0.94±0.06, n=8) and the Mga sediments showed the highest disequilibrium (0.89±0.04, n=15).

4.3.2. Quartz OSL age of the Sverdlov and Mga deposits

Results

The ages of the Sverdlov and Mga deposits were constrained by ten OSL dates on quartz, all calculated with D_e above 200 Gy. Most of the ages turned out to be younger than expected: from 132 to 60 ka (Table 4.3), except for two dates of 132±26 ka for sample 2021-69 from the Sverdlov Fm. and 110±12 ka for sample 2103-12 from the Mga Fm.

Interpretation

The quartz age is often underestimated at a high equivalent dose (D_e) above 200 Gy, (e.g., Buylaert et al., 2007; Murray et al., 2007; Moska et al., 2012) due to signal saturation. This effect is especially prominent in “infinity old” sediments with paleodoses above 2000 Gy. The OSL signal in such sediments should achieve saturation, but some published dates (Buylaert et al., 2007; Timar-Gabor et al., 2012; Zander and Hilgers, 2013; Anechitei-Deacu et al., 2018; Lowick and Valla, 2018) were much younger than expected. On the other hand, OSL dates for the coarse fraction (63–180 μm) of quartz were reported in many cases to agree with independent estimates at D_e from 200 to 600 Gy (Murray et al., 2002, 2008; Watanuki et al., 2005; Astakhov and Nazarov, 2010; Pawley et al., 2010; Nazarov, 2011; Constantin et al., 2014; Schielein et al., 2015; Panin et al., 2021; Nazarov et al., 2022)

To identify potential age underestimation in quartz dating, Chapot et al. (2012) suggested the concept of a natural DRC that illustrates the relationship between sensitivity corrected OSL and expected natural D_e. They found out that in contrast to the laboratory-generated DRCs which are often best fitted by a sum of two exponential functions, the natural DRC can be well described by a single exponential function with lower saturation. Based on this observation, they concluded that the upper limit for quartz OSL measurements at Luochuan section (Chinese Loess Plateau) is ~150 Gy and higher D_e obtained are likely underestimations.

Natural DRCs were plotted for samples from the Sverdlov Factory quarry in order to check the saturation of the OSL signal. The age of the Baltic Ice Lake deposits was estimated to be ~13 ka (Gromig et al., 2019), while the expected age of the Mga deposits was based on the chronology of the Eemian pollen zones (Müller, 1974; Lambeck et al., 2006). The quartz ages of the Leningrad sediments were expected to be reliable proceeding from their agreement with published radiocarbon dates for the

Leningrad deposits in the Leningrad Oblast (Malakhovsky et al., 1969b; Arslanov et al., 1981; Krasnov et al., 1995). The natural DRC for samples from the Sverdlov Factory quarry was approximated by a single saturating exponential function ($R^2 = 0.85$), as well as by a double saturating exponential function ($R^2 = 0.86$) (Fig. 4.12). Both curves saturate at sensitivity corrected OSL ~3.3, while the laboratory curve is growing further. Therefore, the quartz OSL signals from the Sverdlov and Mga samples are apparently in saturation and the respective OSL ages may underestimate the true geological ages of the sediments.

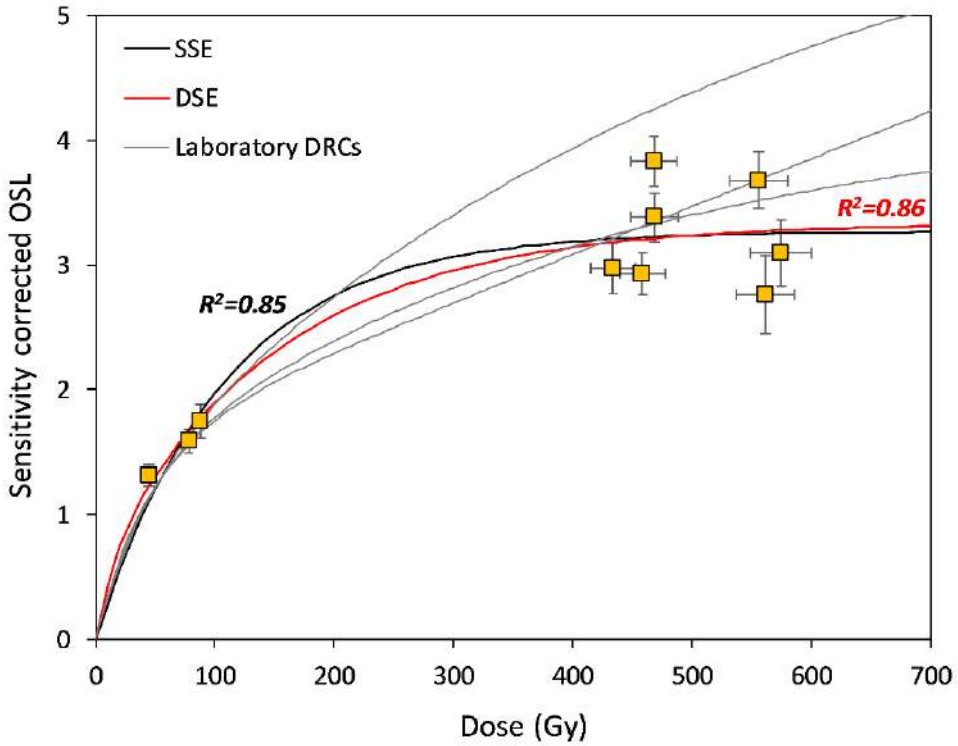

Fig. 4.12. A natural DRC for measured quartz samples fitted with both a single saturating exponential (SSE) function and a double saturating exponential (DSE) function as well as examples of laboratory-constructed DRCs.

4.3.3. Quartz OSL age of the Leningrad and Baltic deposits

Results

The Leningrad deposits from the Sverdlov Factory quarry comprise two visibly different units: light brown sand with layers of plant detritus (Figs. 4.1, 4.8A, B) and grey interbedded fine sand and silt without organic matter (Figs. 4.1, 4.8D). The light brown unit was characterized by four quartz OSL of of 62±4, 53±4, 47±4 and 41±4 ka (Table 4.3). Two first ages may be overestimated because of underestimated dose rates, as the samples were collected from a ~0.3 m sand bed sandwiched between two more radioactive beds. The grey unit was dated from three OSL quartz ages of 39±4, 39±3 and 39±3 ka (Table 4.3). The deposits of Baltic Ice Lake received two OSL quartz ages: 16.9±1.6 and 15.7±1.0 ka BP (Table 4.3).

Interpretation

Bleaching of quartz grains was estimated using the method of Murray et al. (2012) based on bleaching rate difference between OSL signal in quartz and IRSL signal in K-feldspar, as quartz is bleached much faster by both natural sunlight (Godfrey-Smith et al., 1988; Sanderson et al., 2007) and artificial light (Thomsen et al., 2008; Buylaert et al., 2012; Murray et al., 2012). K-feldspar grains are commonly bleached incompletely before deposition and often yield older ages than quartz, especially at fast burial, as in the case of fluvioglacial and glaciolacustrine deposits (e.g., Alexanderson and Murray, 2012; Murray et al., 2012; Möller and Murray, 2015; Novikov et al., 2023). Thus, similar K-feldspar and quartz ages indicate that both were bleached completely before deposition (Murray et al., 2012), whereas the K-feldspar ages notably older than the quartz ages evidence for incomplete bleaching of feldspar grains and, possibly, also the grains of quartz. Möller and Murray (2015) suggested that quartz should be considered 'well-reset' if the ratio of a feldspar $pIRIR_{225}$ age to the corresponding quartz age is lower than unity or approaches it within 2σ. When this condition is not fulfilled, but nevertheless the ratio of a feldspar IR_{50} age to the quartz age is lower than unity or consistent with it within 2σ, the quartz signal should be considered as 'probably well-reset'. Should neither condition be fulfilled, the degree of bleaching of the quartz at deposition is unknown. The two levels of confidence in quartz bleaching are based on the observation that pIRIR signals are bleached more slowly than the IR_{50} signal (Li and Li, 2011; Buylaert et al., 2012, Murray et al., 2012). However, one should bear in mind that the IR_{50} signal in feldspar usually suffers from significant anomalous fading (Spooner, 1992; 1994), and the well-bleached feldspar IR_{50} ages not corrected for fading are usually ~30% younger than the respectivequartz ages (Möller and Murray, 2015).

The KF/Q age ratios (Table 4.3) were calculated for eight samples collected from the Leningrad and Baltic deposits. The approach was not applied to older samples given their underestimated quartz OSL ages. Judging by the resulting ratios, quartz was most likely completely bleached before deposition in the Leningrad deposits but the bleaching was incomplete in the Baltic Fm. The latter inference is consistent with data for Lake Ladoga (Gromig et al., 2019) indicating the onset of deposition at 13 910±140 cal. a BP. Therefore, the quartz OSL ages from the Baltic glaciolacustrine sediments of 16.9±1.6 and 15.7±1.0 ka (Table 4.3) are probably overestimated.

4.3.4. OSL ages of Sverdlov, Mga, and Mikulino/Lower Valdai deposits: K-feldspar and polymineral fractions

The time of the Sverdlov, Mga and Mikulino/Lower Vladai deposition was constrained by sixteen OSL ages for coarse-grained K-feldspar ($pIRIR_{225}$ protocol), seven OSL ages for coarse F-feldspar grains ($pIRIR_{290}$ protocol), and three OSL ages for fine-grained polymineral fraction (Table 4.3). All ages were corrected for anomalous fading (Huntley and Lamothe, 2001), using the *calc_FadingCorr* function from the R package *Luminescence* software (Kreutzer, 2022). In addition,

two other techniques of fading correction were tested (Lamothe et al., 2003; Kars et al., 2008), but the results yielded overestimated ages and were not included into Table 4.3 to avoid overcharging.

The Sverdlov Fm. deposition was timed from nine ages between 272 and 166 ka. They all must be older than the true ages, for several reasons. First, the dated portion of the Sverdlov Fm. is composed of varved clay, with about 1100 annual layers. Second, varved sediments grade into the Mga Fm. marine clayey silt without visible deposition gaps. Therefore, the Sverdlov deposition occurred during the latest Moscow cryochron, at the transition to interglacial, ~132–131 ka ago (Lambeck et al., 2006). Third, OSL K-feldspar ages for fluvioglacial deposits are often overestimated (e.g., Alexanderson and Murray, 2012; Murray et al., 2012; Möller and Murray, 2015; Novikov et al., 2023). Finally, K-rich feldspar $pIRIR_{225}$ ages of 78±7 and 50±4 ka obtained from the deposits of the Baltic Ice Lake is evidence that the residual dose in K-feldspar from glaciolacustrine deposits in this area can be as high as 250 Gy.

Other obtained dates are fifteen ages from 177 to 100 kyr BP (123±10 ka, 2σ, on average) for the Mga Fm. and one 119±7 ka ka for the Mikulino/Lower Vladai deposits.

4.3.5. Age-depth model of the Mga deposits

The duration of the Mga Fm. deposition was estimated from an age-depth model based on data from the Sverdlov Factory quarry, with the R package *rbacon v2.5.8* software using the Bayesian

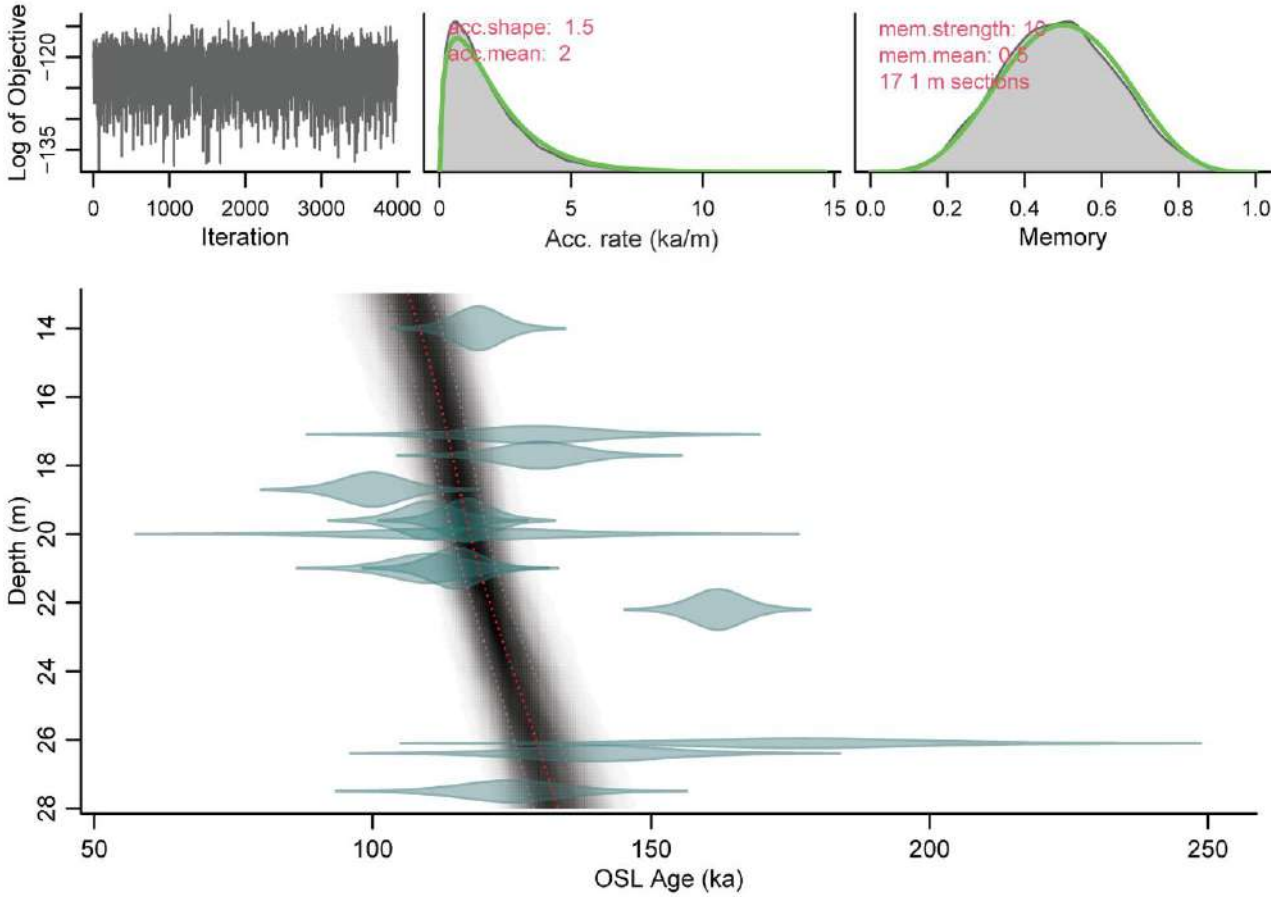

Fig. 4.13. Bayesian age-depth model of the Mga Fm. at Sverdlov Factory based on K-rich feldspar and polymineral post-IR IRSL ages.

statistics (Blaauw and Christen, 2011; Blaauw et al., 2022). For modelling, K-rich feldspar and polymineral post-IR IRSL ages from cuts 4 and 6 (Fig. 4.1, 4.3, 4.11) corrected for anomalous fading according to Huntley and Lamothe (2001) were used. Uncertainties in the age-depth model correspond to the 68% confidence interval. Shared errors (Rhodes et al., 2003) were excluded from age uncertainties before modeling and recombined after the analysis. They include errors associated with conversion factors, beta source calibration, gamma spectrometer calibration, and TL/OSL reader reproducibility and are typically ~5%. A mean accumulation rate of 2 ka/m was applied, following the value suggested by the software. The combination of the age-depth model with pollen zones allowed us to estimate the duration of the Mikulino Interglacial (Fig. 4.13), from the boundary between regional pollen zones M_1 and M_2 to the end of zone M_8 (after Grichuk, 1961). Therefore, the Mga clayey silt accumulation and Mikulino Interglacial began 133±8 ka ago and ended 109±7 ka ago. At least two ages from the Mga Fm. (177±20 and 162±9 ka) are significantly overestimated presumably due to incomplete bleaching. They, however, were not excluded from the model to avoid subjectivity in the age estimation.

4.4. Pollen analysis

The palynological data for samples from cut outcrops 9 and 6, 7 (Figs. 4.1, 4.3) in the Sverdlov Factory quarry were presented in two pollen diagrams. Local pollen zones (LPZ) were distinguished and described by E. Nosevich (VSEGEI, St. Petersburg).

4.4.1. Pollen diagram 1

Diagram 1 was obtained for 32 samples from cut 9 (Figs. 4.1, 4.3) and comprised two local pollen zones (Figs. 4.14, 4.15).

LPZ1 (-14.5 to -10.0 m asl)

Description

The upper limit of local pollen zone (LPZ) 1 coincides with the boundary between the Sverdlov Fm. and Mga Fm. Generally, the spore-pollen spectra represent well preserved grains. Tree taxa predominate everywhere (up to 80.1% of the spore+pollen total), with up to 53.2% *Picea*. The zone includes three subzones:

Subzone 1a (-14.5 to -12.6 m asl), about 350 annual varves: within 26.4% *Pinus*, 11.4% *Betula* and 9.7% *Betula nana*, as well as few *Alnus glutinosa* and *Alnus incana* pollen grains. Herbs (≤16.8%) are within 7.5% Poaceae and 8.4% *Artemisia*. No thermophilic flora was found. Spores belong to *Lycopodium complanatum* (≤4.7%).

Subzone 1b (-12.6 to -11.2 m asl), about 400 varves: 27.3% *Pinus*, 9.8% *Alnus glutinosa* and *Alnus incana* (in total); few grains of *Corylus*. Among the grass species, *Artemisia* reduced to 4.1%, while Asteraceae increased to 7.4%; Cyperaceae decreased from 7.1% in subzone 1a to few percent in 1b, *Salix* disappears from the spectra in the same way.

Subzone 1c (-11.2 to -10.0 m asl), about 200 varves: no *Corylus*, within 2.1% *Alnus*, 16.9% *Pinus*, up to 47.6% *Picea*; *Salix* (≤2.8%), and Cyperaceae (≤3.1%) reappear; *Artemisia* is up to 6.8%; *Sphagnum* spores reach 8.8%.

Interpretation

The LPZ records climate change from cold and relatively wet to slightly warmer and drier and back to harsher conditions. Subzone 1a may be correlated with regional pollen zone (RPZ) Ms_3 (Malakhovsky et al., 1969a), subzone 1b with regional palynozone Ms_2 (Malakhovsky et al., 1969a) and the Kasplya Interstadial (Buslovich et al., 1969). Subzone 1c corresponds to RPZ Ms_1 (Malakhovsky et al., 1969a) and to the Kattegat Stadial (Seidenkrantz, 1993). The whole LPZ1 also fits the lower zone of highest *Picea* percentages (M_1) (after Grichuk, 1961). The correlation of the Kasplya Interstadial and the Kattegat Stadial with zone M_1 was reported earlier from Prangli (Liivrand, 1987) and Nizhnyaya Boyarschina (Novenko, 2016) sections.

LPZ2 (-10.0 to -8.1 m asl)

Description

Tree species predominate (up to 77.4 %), with lower percentages of *Picea* (12.3%) and higher *Pinus* (44.5%) than in LPZ1; up to 10.9% *Betula* and 2.7% *Betula nana*; few grains of *Corylus* pollen; The grass communities (up to 20.1%) include mainly Poaceae (up to 10.2%) and diverse boreal species; rare spores belong to *Selaginella*.

Interpretation

The spore-pollen spectra record a climate milder than in LPZ1. The high percentages of *Pinus* and *Betula*, along with few *Corylus* grains, allow correlating the zone with Grichuk's (1961) regional zone M_{2-3}.

4.4.2. Pollen diagram 2

The diagram encompasses four local pollen zones (Figs. 4.16, 4.17).

LPZ1 (-21.3 to -15.9 m asl)

Description

The pollen spectra mainly consist of tree taxa (up to 77.9% of spore+pollen total), with high percentages of *Picea* (28.6%), *Pinus* (≤19.6%), and *Betula* (≤19.1%), within 11.2% *Betula nana* and few grains of Siberian conifers: *Abies*, *Pinus sibirica*, *Picea omorica*, *Picea obovata* and *Larix*. Herbs (≤28.8% of spore+pollen total) are mainly Poaceae (4.6– 8.0%) and some *Artemisia* (≤4.5%); Cyperaceae are no higher than 4.0%. No thermophilic species were observed, while *Polemonium* was

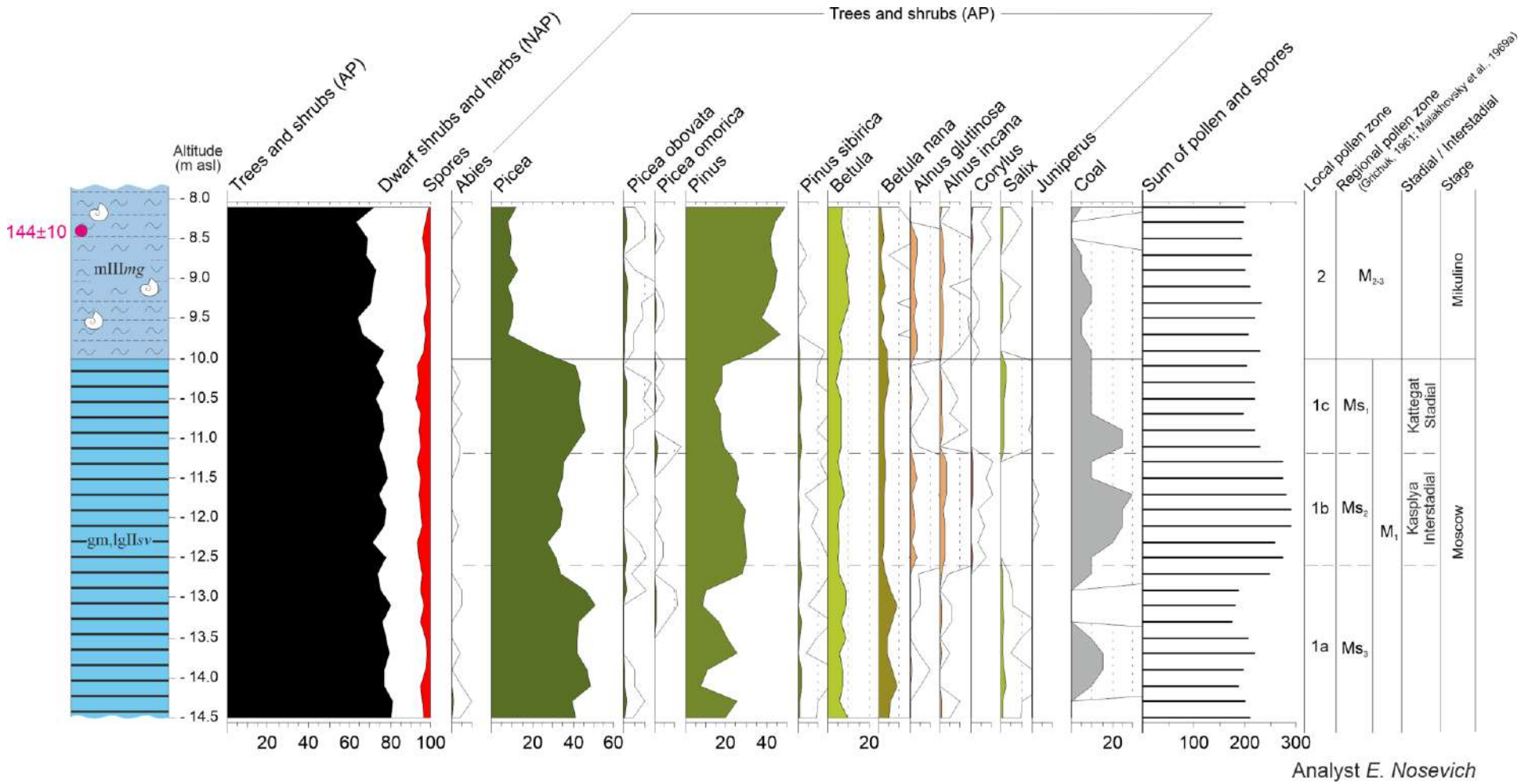

Fig. 4.14. Pollen diagram for the Sverdlov and Mga Fms. sampled in cut 9 (Figs. 4.1, 4.3). Tree and shrubs pollen. Percentages are quoted relative to sum of pollen and spores. For lithology legend see Fig. 4.1.

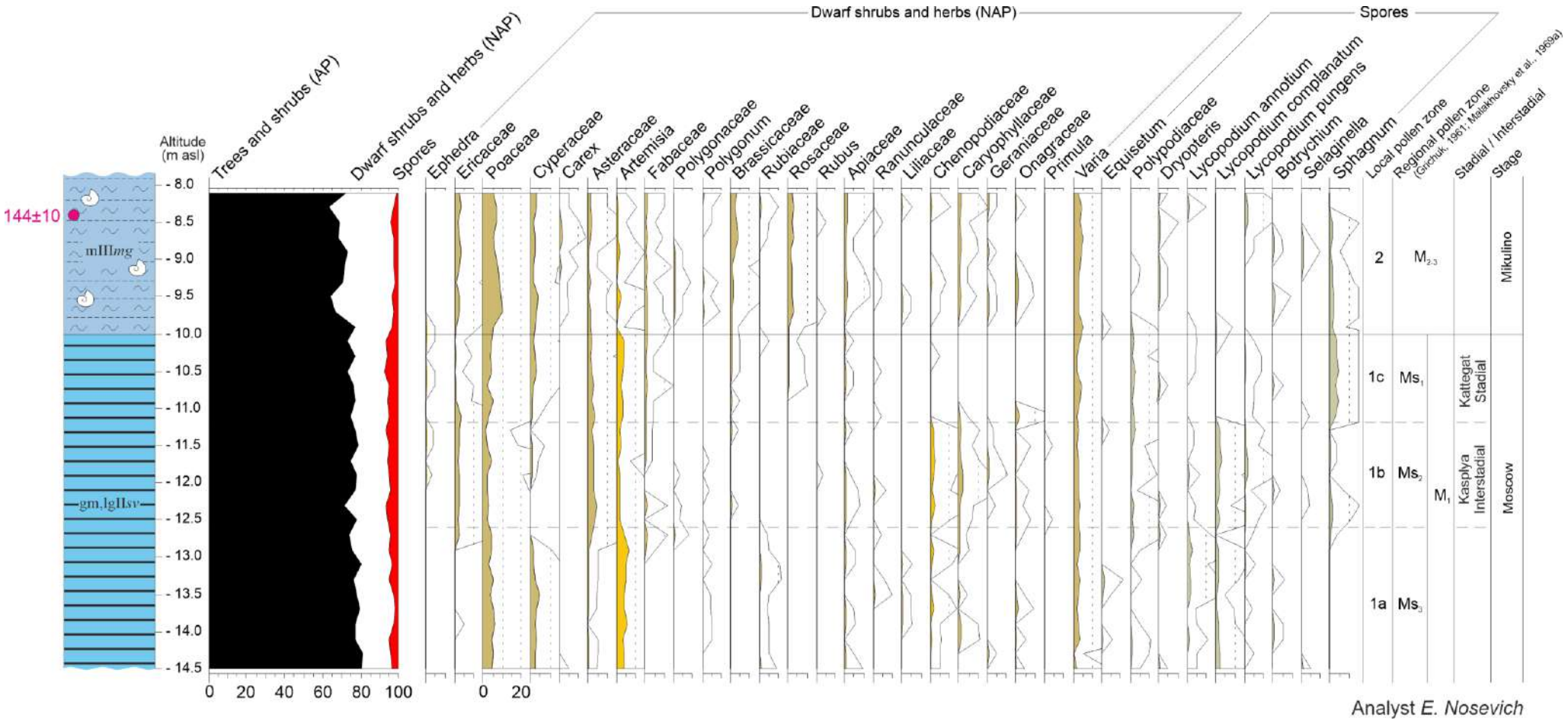

Fig. 4.15. Pollen diagram for the Serdlov and Mga Fms. sampled in cut 9 (Figs. 4.1, 4.3). Herbs pollen and spores. Percentages are quoted relative to sum of pollen and spores. For lithology legend see Fig. 4.1.

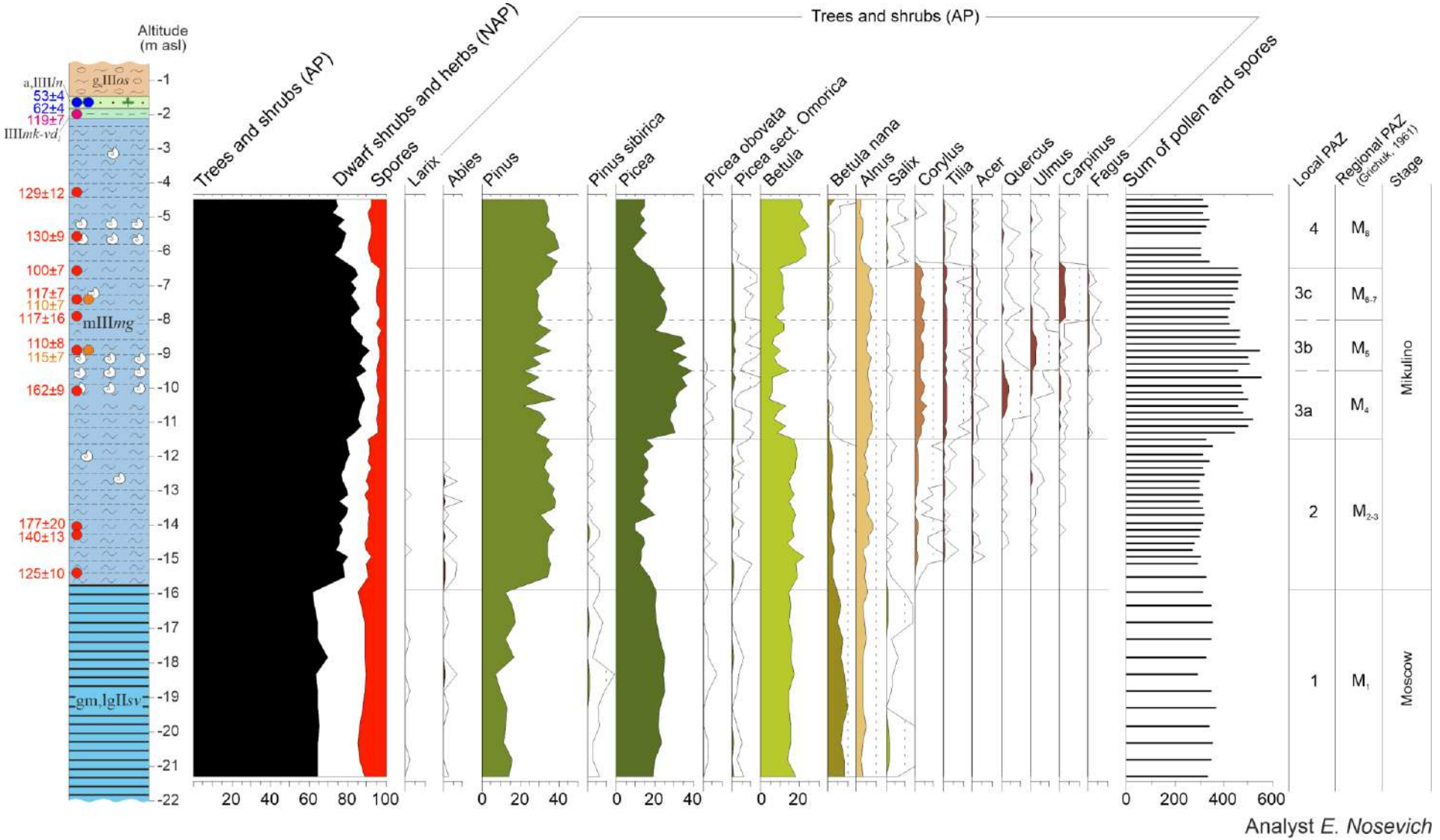

Fig. 4.16. Pollen diagram of the Sverdlov and Mga Fms. sampled in cuts 6 and 7 (Figs. 4.1, 4.3). Tree and shrubs pollen. Percentages are quoted relative to sum of pollen and spores. For lithology legend see Fig. 4.1.

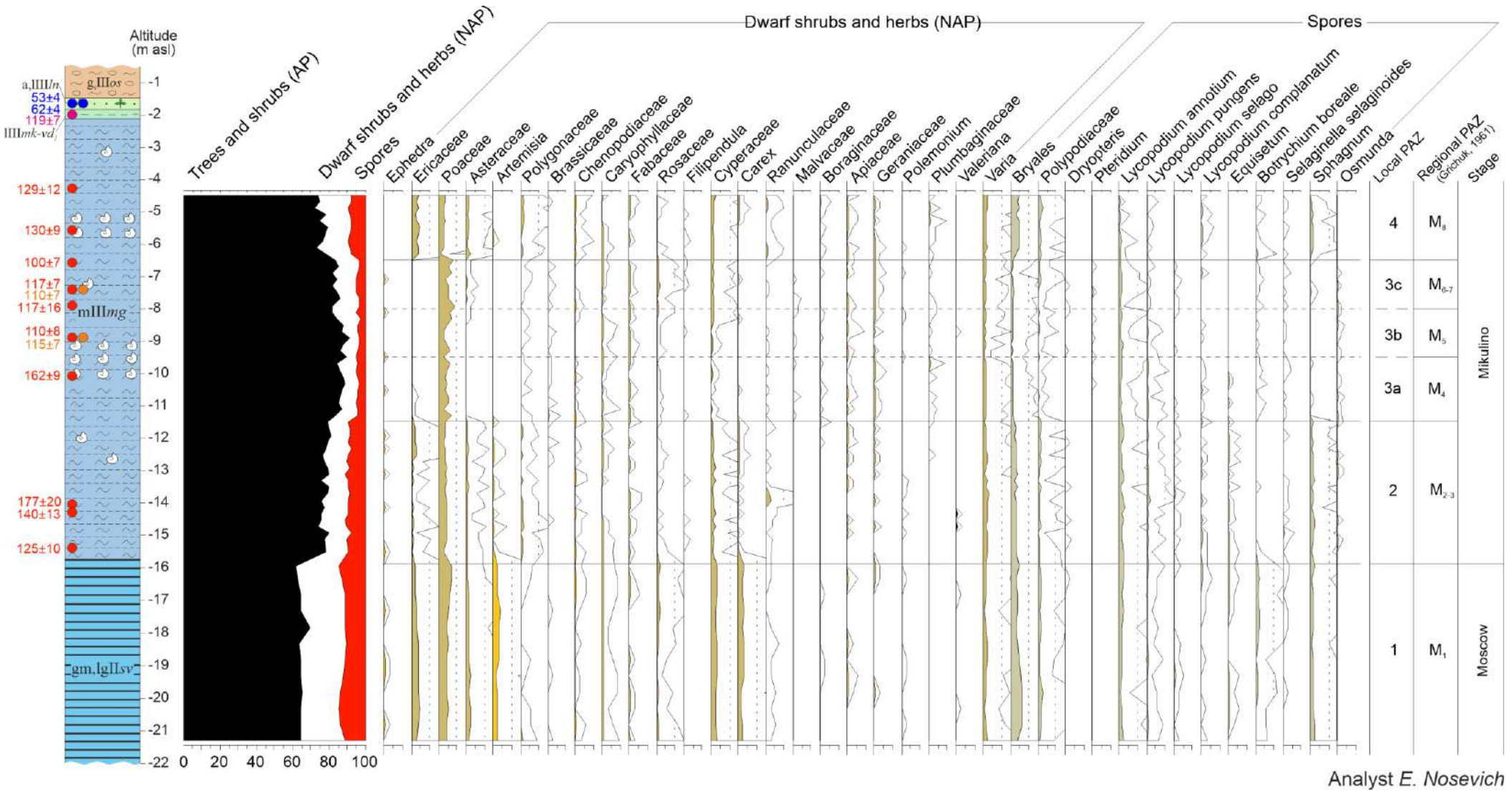

Fig. 4.17. Pollen diagram of the Sverdlov and Mga Fms. sampled in cuts 6 and 7 (Figs. 4.1, 4.3). Dwarf shrubs and herbs pollen pollen and spores. Percentages are quoted relative to the sum of pollen and spores. For lithology legend see Fig. 4.1.

encountered. The spores represent *Botrychium*, *Sphagnum*, and *Lycopodium annotium* species. Palynomorphs include few fungi spores and fine coal particles.

Interpretation

The spectra characterize conifer plant communities that lack thermophilic taxa. According to combined palynological and geological data, the LPZ2 interval can be correlated with the end of the Moscow Glacial and the lower zone of maximum *Picea* percentages, M_1 zone of Grichuk (1961).

LPZ2 (-15.9 to -11.5 m asl)

Description

The percentages of tree pollen reach 90.2%, while *Pinus* and *Picea* are up to 40.6% and 24.6%, respectively; *Betula nana* reduces to 3.7% and *Betula* is ≤20.8%. Pollen of broad-leaved species (mainly *Tilia* and *Ulmus*) is present throughout the zone, especially in its upper part; some *Abies* and *Larix* pollen species were encountered as well. The grass communities (≤18.1% of spore+pollen total) include Poaceae (≤5.3%) and diverse Boreal species; *Artemisia* appears as few grains. Spores represent Bryales and *Sphagnum*. Other forms found in the zone are phytoliths, stomata of conifers (*Pinus* and *Picea*), cysts of colonial algae, and fungi spores.

Interpretation

The spectra confirm the trend toward a milder climate. The high percentages of *Pinus* and *Betula*, along with the presence of broad-leaved species, allow correlating the zone with regional zone $M_{2\text{-}3}$ (Grichuk, 1961).

LPZ3 (-11.5 to -6.5 m asl)

Description

The zone comprises three subzones. Pollen and spores show the highest counts (up to 553 grains). Palynomorphs include abundant phytoliths, stomata of conifers, diverse fauna fragments, algae cysts, and few poorly preserved dinoflagellates. Tree pollen reaches 94.0% of the spore+pollen total, including up to 39.9% *Pinus* and 40.6% *Picea*, 13.1% *Betula* and minor percentages of *Pinus sibirica*, *Picea omorica* (≤2.5%) and *Picea obovata*. Subzones were distinguished according to successively changing peaks of *Quercus* (subzone 3a, -11.5 to -9.5 m asl, up to 3.8%), *Ulmus* (subzone 3b, -9.5 to -8.0 m, up to 3.5%) and *Carpinus* (subzone 3c, -8.0 to -6.5 m, up to 3.9%). *Corylus* and *Tilia* are ubiquitous. The total percentage of broad-leaved pollen exceeds 10%. Herbs (6.0–15.0%) are mainly Poaceae (up to 9.0%) and small percentages of Malvaceae and other Mediterranean taxa. The percentages of spores are within 4.7%, including *Lycopodium annotium* and *Osmunda*.

Interpretation

The spectra correspond to warm and dry conditions unusual for the Neva Lowland, which were crucial for penetration of thermophilic and drought-tolerant plant taxa. The successive peaks of *Quercus*,

Ulmus and *Carpinus* provide reliable evidence of the Mikulino Interglacial. Subzones 3a, 3b and 3c can be correlated, respectively, with regional pollen zones M_4, M_5 and M_{6-7} (Grichuk, 1961). Note that *Ulmus* has a peak in zone M_5 while *Tillia* is evenly distributed over the climate optimum and shows no peaks. The correlation of *Carpinus* (M_6) and upper zone of maximum *Picea* percentages (M_7) is common to marine deposits in the Leningrad Oblast (Pleshivtseva, 2007; 2011a).

LPZ4 (-6.5 to -4.5 m asl)

Description

The samples from the zone contain less abundant and less diverse pollen and spores than in the lower zones and fewer palynomorphs, with few coarse coal particles and phytoliths. Tree pollen (up to 85.7%) is dominated by *Pinus* (up to 44.5%), *Picea* reduces to 9.6–16.6%, *Betula* reaches 26.9%; *Picea omorica* appears in the lower part of the zone, while broad-leaved species disappear from the upper strata and are limited to few grains of *Corylus*; meanwhile, *Betula nana* increases. Grass communities (up to 20.0%) include Ericaceae (up to 4.1%), Poaceae (≤4.1%), and Cyperaceae (≤2.4%). Spores represent *Sphagnum*.

Interpretation

The spectra record a cooling after the climate optimum. The zone can be correlated with regional zone M_8 (Grichuk, 1961) on the basis of widespread pine and birch.

4.4.3. Correlation of the pollen diagrams

The Sverdlov Fm. has a chronological volume of ~1050 years in diagram 1 and encompasses three RPZ (Ms_3, Ms_2 and Ms_1), while diagram 2 comprises ~1100 annual varves. The varves underlie the Mga Fm. in both cuts and lack visible discordant boundaries. Diagram 2 likewise presumably corresponds to three Late Moscow regional zones. The monotonic patterns in diagram 2 may be due to lower sampling density: at every 0.5 m in cut 7 but at 0.2 m in cut 9 (Figs. 4.1, 4.3). The two pollen diagrams were cross correlated on the basis of lithology and varve chronology, in order to make the Late Moscow palynozones comparable with other data obtained for cut 7 only. According to the correlation, the Ms_3/Ms_2, and Ms_2/Ms_1 boundaries should be in cut 7 at -18.0 and -17.2 m asl respectively.

4.5. Grain size analysis

Grain size data for the intermorainic deposits sampled in cut outcrops 7, 6 and 4 at the Sverdlov Factory site were plotted as depth profiles of sizes and statistical parameters (mean, sorting, skewness, and kurtosis) (Fig. 4.18). The section comprises five grain size zones (GSZ).

GSZ1 (-21.9 to -21.0 m asl)

Description

The zone corresponds to the bottom of the visible Sverdlov Fm. section (Fig. 4.3A) composed mainly of silt (58–67%) and clay (18–25%). It differs from sediments above in a high percentage of sand (15–17%), bimodal distribution of grain sizes, with peaks at ~3 and ~11 μm in the clay-silt fraction (Fig. 4.19), and poor sorting, with σ_1 = 2.5–2.7 (Folk and Ward, 1957). Varves within the zone are 3–10 cm thick and become thinner upsection. The sediments near the zone top enclose a ~0.5 m dropstone (Fig. 4.5D). The total number of varves within the zone is 20.

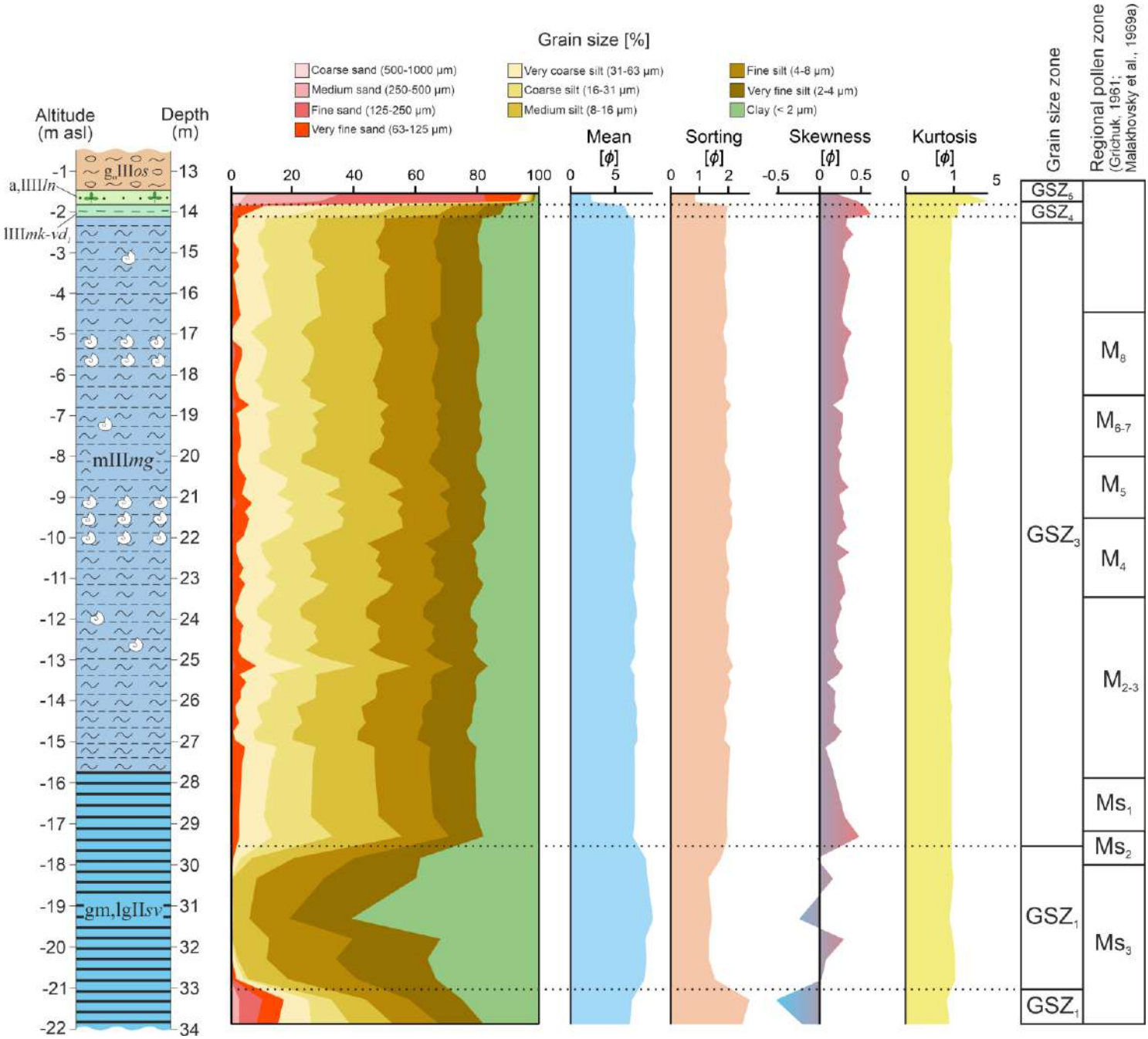

Fig. 4.18. Particle size distribution of intermorainic deposits sampled in the Sverdlov Factory quarry in cuts 4, 6 and 7 (Figs. 4.1, 4.3). For lithology legend see Fig. 4.1.

Interpretation

The sediments of the zone were deposited in a glacial basin. High sand percentages, the presence of dropstones, and poor sorting indicate active ice rafting. The interval may be correlated with 11th Heinrich event (Heinrich, 1988; McManus et al., 1998).

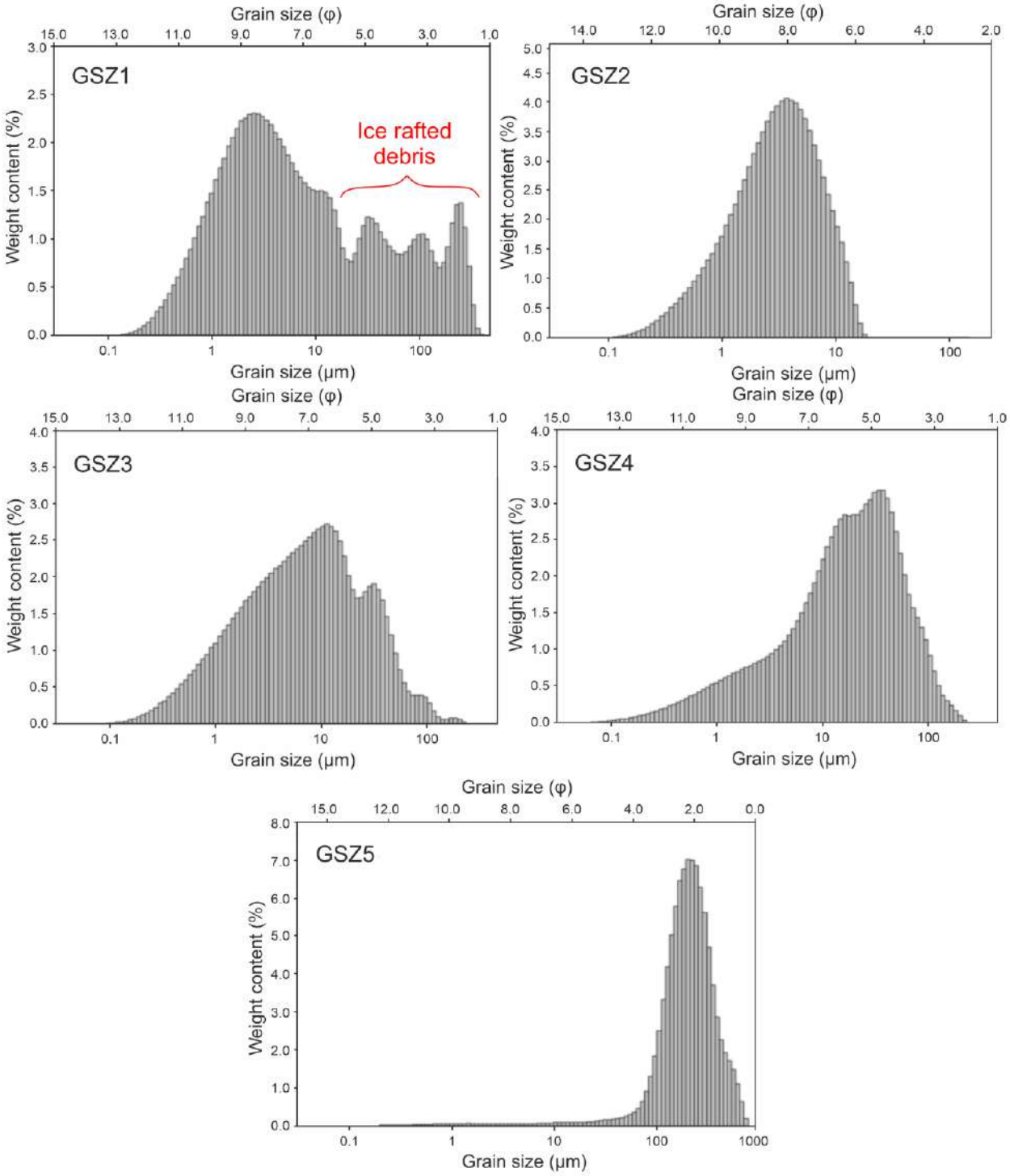

GSZ2 (-21.0 to -17.5 m asl)

Description

The zone is mainly composed of silt (39–68%), with higher percentages of clay (32–61%) and lower percentages of sand (0–1.8%) particles than in GSZ1. It comprises about 730 varves that enclose

gravel and pebbles. The varve thickness decreases upsection from 2 to 0.2 cm. The particle sizes show unimodal distribution, with a peak at ~3 μm (Fig. 4.19) and poor sorting (σ_1 = 1.3–1.7).

Interpretation

The deposition was in a glacial basin.

GSZ3 (-17.5 to -2.1 m asl)

Description

The zone begins in the upper part of the Sverdlov Fm., 1.8 m below the lithological boundary and includes the whole Mga Fm. composed of 74–80% silt, 16–23% clay, and 0–8% sand. The upper strata of the Sverdlov Fm. comprise ~350 varves. The particle sizes show bimodal distribution with peaks at ~11 and ~30 μm (Fig. 4.19) and poor to very poor sorting (σ_1 = 1.8–2.1).

Interpretation

The Mga Fm. has a uniform distribution of particle sizes over its entire thickness of 13.7 m. The deposition environment typical of the Mga Sea set in ~350 years before the interglacial.

GSZ4 (-2.1 to -1.8 m asl)

Description

The zone corresponds to the Mikulino/Lower Valdai lacustrine deposition. Most of the particles are of silt sizes 78–83%, clay percentages are 11–12%, while sand reaches 5–11%. The sediments show poor sorting (σ_1 = 1.9–2.0).

GSZ5 (-1.8 to -1.4 m asl)

Description

The zone falls within the Leningrad alluvial/lacustrine deposits and consists mostly of sand (94–95%), especially of finegrain sizes (125–250 μm), which reaches 82–83%. Silt particles are as low as 4–5% and clay is only 1.2–1.3%. The unimodal grain size distribution peaks at ~200 μm (Fig. 4.19). Sorting is moderate (σ_1 = 0.9).

4.6. Geochemistry and magnetic susceptibility

4.6.1. Water salinity and organic matter origin

4.6.1.1. Geochemical indicators

4.6.1.1.1. Total organic carbon (TOC) and C/N ratio

Total organic carbon (TOC) contents show the amount of organic matter (OM) in sediments, while the TOC/N ratio is an indicator of the OM origin. The ratio is expressed in atomic units equivalent to the respective weight ratio multiplied by 1.167 (Meyers and Teranes, 2001). The C/N <10 values are typical of organic matter mostly derived from plankton while C/N ratios above 20 represent OM originated from terrestrial vascular plants (Meyers and Teranes, 2001); intermediate values from 10 to 20 indicate a mixed origin.

4.6.1.1.2. Br/TOC ratio

Bromine in sediments is associated with plant detritus (Vinogradov, 1939, cited from Price et al., 1970; Shishkina, 1972; Malcolm and Price, 1984), but marine plants assimilate Br much better than the terrestrial taxa (Neufeld, 1936). Thus, the Br/TOC ratio may be another indicator of the OM origin (Mayer et al., 1981, 2007; Malcolm and Price, 1984). The Br/TOC ratio is 0.34–0.47 mg/g in plant detritus from alluvium and reaches 6.6–8.8 mg/g in shelf sediments deposited far from the continental provenance of clastic material (Mayer et al., 2007). The percentages of marine organic matter relative to the total amount (%-MAR) can be found using average Br/TOC values for terrestrial plant detritus and marine organic matter as end members, as suggested by Mayer et al. (2007):

$$\%-\mathrm{MAR} = 100 \times \frac{\frac{Br}{TOC} - 0.43}{7.7 - 0.43}, \quad (4.1)$$

where Br/TOC is the ratio of Br to TOC in a sample (mg/g); 0.43 and 7.7 are Br/TOC values in terrestrial and marine OM, respectively.

4.6.1.1.3. TOC/S ratio

Most of sulphur in organic-rich marine sediments resides in pyrite (e.g., Volkov, 1984). The percentages of diagenetic pyrite are lower in sediments deposited in freshwater conditions than in marine facies with similar TOC contents (Berner and Raiswell, 1984). The reason is that the formation of pyrite requires SO_4^{2-} which reaches 28 mmol/L in seawater and <1 mmol/L in fresh water. Correspondingly, the TOC/S ratio can be used to discriminate between marine (0.5 to 5 g/g), brackish (5–10 g/g), and freshwater (>10 g/g) deposition environments (Berner and Raiswell, 1984).

4.6.1.1. Zones of water salinity and organic matter origin

The above indicators were used to distinguish eight zones in the intermorainic deposits from the Sverdlov Factory quarry (Fig. 4.20).

SOZ1 (-21.9 to -19.5 m asl)

Description

The zone corresponds to the basal part of the visible Sverdlov Fm. section which includes about 70 varves. The TOC contents are moderate (0.34–0.50%) and the TOC/N ratio is 5.1–7.9 a/a; %-MAR is 3.0–7.4%; TOC/S = 2.6–6.6 g/g (5.0 g/g on average).

Interpretation

Organic matter in SOZ1 is mainly derived from phytoplankton, while the contribution of terrestrial vascular plants is minor (TOC/N < 10 a/a). The low contents of marine OM and TOC/S about 5 g/g indicate deposition in brackish water, i.e., seawater penetrated into the Late Moscow glacial lake already ~1100 years before the onset of the interglacial. The use of TOC/S ratio as an indicator of salinity for the lower basin strata requires caution though, as TOC is <1 % while the method works

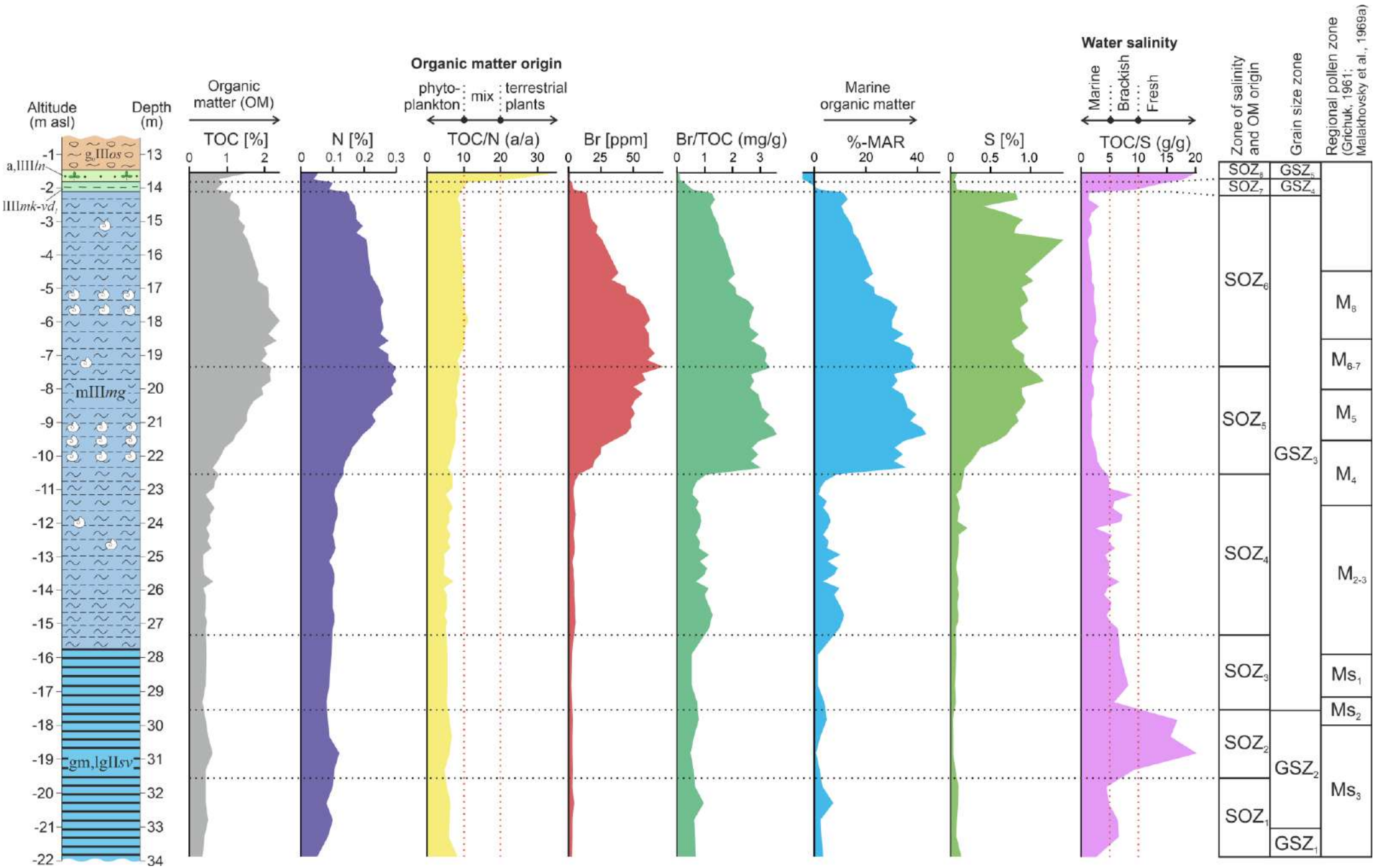

Fig. 4.20. Geochemical indicators of water salinity and organic matter origin in intermorainic deposits from the Sverdlov Factory quarry. For lithology legend see Fig. 4.1.

well only at TOC above 1 % (Berner and Raiswell, 1984). However, the inference is supported by the presence of marine OM up to 7.4%.

SOZ2 (-19.5 to -17.5 m asl)

Description

The zone corresponds to the middle portion of the visible Sverdlov Fm. section, with ~680 varves. TOC is low but slightly higher than in zone 1 (0.43–0.62%); TOC/N ranges from 4.7 to 6.5 a/a; %-MAR is 0.9–4.8%. The zone is distinguished on the basis of high TOC/S values of 9.2 to 20.3 g/g.

Interpretation

Judging by high TOC/S values (>10 g/g) and low marine OM contents, the sediments were deposited in freshwater conditions, at least a part of the time. A brief freshwater episode was also revealed by diatom analysis in the Upper Moscow sediments from BH 10 (Pleshivtseva et al., 1984). OM within the zone is mainly composed of phytoplankton (TOC/N < 10 a/a).

SOZ3 (-17.5 – -15.5 m asl)

Description

The zone encompasses the upper part of the Sverdlov Fm., with ~350 varves and the base of the Mga Fm. The TOC content is 0.36–0.50%; TOC/N is similar to that in zones 1 and 2 (5.2–5.5 a/a); %-MAR is 1.2–4.0%; TOC/S = 5.8–8.3 g/g (7.0 g/g on average).

Interpretation

The TOC/S ratio ranging from 5.8 to 8.3 g/g, along with the presence of marine OM, indicates brackish deposition conditions. OM is mostly derived from phytoplankton (TOC/N <10 a/a).

SOZ4 (-15.5 to -10.4 m asl)

Description

The zone corresponds to the lower portion of the Mga Fm. (pollen zones M_{2-3}–M_4). TOC ranges from 0.37 to 0.79%, increasing gradually up the section. TOC/N = 4.3–7.1 a/a; marine OM reaches 11.7% at the base of the zone but decreases gradually to 1.8% in the upper part. TOC/S varies from 4.4 g/g at the base to 9.1 g/g near the top.

Interpretation

Higher contents of marine OM and lower TOC/S ratios in the beginning of the zone may indicate higher salinity of the Mga basin which was gradually decreasing judging by progressively lower marine OM and higher TOC/S up the section. Moderate TOC/N values (<10) show predominant phytoplankton contribution to OM. Most likely, the time span of the zone correlated with the lagoonal phase of the Mga Sea history (Cheremisinova, 1960).

SOZ5 (-10.4 to -7.3 m asl)

Description

The zone covers the middle portion of the Mga Fm. (pollen zones M_4–M_{6-7}). TOC increases from 0.6 % at the base to 2.2% at the top. The TOC/N increases as well, though more slowly, from 5.4 to 8.6 a/a. Marine OM changes dramatically in the middle of the zone from 8.6% at -10.5 m asl to 35.9% at -10.3 m asl. The TOC/S is stable around 2 g/g after a slightly lower value at the base.

Interpretation

The slowly increasing TOC/N ratio indicates that organic matter consists mainly of phytoplankton. The onset of TOC growth in pollen zone M_4 records an increasing amount of phytoplankton in the Mga Sea. The sea apparently became deeper and more saline very rapidly, which is evident in many sections from diatom data (e.g., Cheremisinova, 1959; Malakhovsky et al., 1969a; Pleshivtseva et al., 1984) and accounts for the markedly higher marine OM percentage. The stable low TOC/S ratios averaging around 2.1 g/g within the zone provide more evidence for high water salinity in the basin. Marine sediments commonly have an average TOC/S ratio of 2.8±1.5 g/g but salinity variations above 18‰ are poorly resolvable by the estimation method (Berner and Raiswell, 1984). Therefore, the seawater salinity during the middle Mga deposition was at least 18‰. The zone can be correlated with the marine phase of the basin evolution (Cheremisinova, 1960).

SOZ6 (-7.3 to -2.1 m asl)

Description

The zone falls within the upper part of the Mga Fm. (pollen zones M_{6-7}–M_8). The TOC values reach a maximum of 2.41% at -5.9 m asl and then decrease gradually to 1.13% at the top. The TOC/N ratio varies in the range 8.0–11.0 a/a. The contribution of marine OM decreases upsection from 40.3 % to 11.3 %, while TOC/S averages about the level of zone 5 (1.1–3.2 g/g).

Interpretation

The relative content of marine OM decreases gradually above -7.3 m asl (pollen zone M_{6-7}), possibly, as a result of beginning regression evident in many sections within zone M_6 (Cheremisinova, 1959; Malakhovsky et al., 1969a; Pleshivtseva et al., 1984). Nevertheless, it remains relatively high at the top of the zone (11.3%), i.e., the sediments were deposited in marine conditions during the whole time span of the zone. This inference agrees with the TOC/S values. The TOC/N ratio indicates that organic matter in the Mga Fm. is derived mainly from phytoplankton.

SOZ7 (-2.1 to -1.8 m asl)

Description

The zone was distinguished in the Mikulino/Lower Valdai deposits. The contents of organic carbon (0.71–0.91%) are slightly lower than at the top of the Mga Fm. (1.13%). The TOC/N ratio (9.2–10.6 a/a) remains about the same level as in SOZ6. The %-MAR value within the zone is negative (-

2.0%) as the Br/TOC ratio (0.28 mg/g) is lower than the plant detritus value in equation 4.1. The TOC/S ratio reaches 9.6 to 14.7 g/g.

Interpretation

The TOC/N ratio indicates predominance of phytoplankton as a source of OM. The negative %-MAR values, along with high TOC/S values (>10 g/g), record freshwater conditions of deposition.

SOZ8 (-1.8 to -1.4 m asl)

Description

The interval of the zone fits the Leningrad sand. The TOC content reaches 1.63%. The TOC/N ratio is up to 22.9–34.6 a/a, which is much higher than in zone 7. Marine OM is likewise negative, because the Br/TOC ratio is as low as 0.08–0.10 mg/g. The TOC/S ratio ranges from 17.9 to 20.1 g/g.

Interpretation

The high TOC/N ratio exceeding 20 a/a shows that the plant detritus in sediments belongs to terrestrial vascular plants. The absence of marine OM and TOC/S values above 10 g/g confirm the limnic/alluvial origin of the Leningrad sand. Note that the TOC/S indicator was successfully applied to sand, though Berner and Raiswell (1984) limited its applicability to clay and silt sediments.

4.6.2. Redox conditions

4.6.2.1. Indicators

4.6.2.1.1. Sulphur and magnetic susceptibility

Sulphur in marine deposits is associated with OM (e.g., Volkov, 1984). Reducing diagenetic alteration in sediments begins at TOC = 0.5% and sediments lack active oxygen (compounds of Mn^{4+}) in mud water at higher TOC values (Volkov, 1984). High S contents in marine sediments record anoxic conditions in bottom water, with precipitation of diagenetic pyrite FeS_2 (e.g., Blanchett et al., 2007; Harff et al., 2011). Pyrite forms in the upper part of the anoxic zone by a reaction of iron-bearing minerals with hydrogen sulphide (H_2S) resulting from anaerobic bacterial reduction of SO_4^{2-}. The process involves OM as a reducing agent and an energy source (Berner, 1984) and produces greigite (Fe_3S_4) as an intermediate component (Berner, 1970; Wilkin and Barnes, 1997). Pyrite is a paramagnetic mineral with magnetic susceptibility 11.30×10^{-9} to 70.36×10^{-9} m^3/kg (Tang et al., 1995, cited from Wu et al., 2016), while greigite is ferromagnetic with a higher magnetic susceptibility of 3.2×10^{-4} m^3/kg (Roberts et al., 2011). At insufficient sulphur contents, pyritization is incomplete and stops at the stage of greigite formation (Volkov, 1961, cited from Berner, 1967; Wilkin and Barnes, 1997). Thus, low magnetic susceptibility in organic-rich (>0.5%) marine sediments is evidence for the presence of diagenetic pyrite and, correspondingly, anoxic conditions in bottom water.

4.6.2.1.2. Molybdenum

Molybdenum is another indicator of anoxic conditions: it is the highest in anoxic basins and much lower in the presence of oxygen (Calvert and Pedersen, 2007). At high concentrations of H_2S in water, Mo becomes immobilized in sediments (Calvert and Pedersen, 2007), largely in diagenetic pyrite (Huerta-Diaz and Morse, 1992).

4.6.2.1.3. Iodine

Iodine, like bromine, is associated with OM (Shishkina and Pavlova, 1965, cited from Price and Calvert, 1977; Price et al., 1970). The I and Br contents are proportional to TOC in oxic basins (Price and Calvert, 1977; Pedersen and Price, 1980; Malcolm and Price, 1984), but I is lower in anoxic conditions (Price and Calvert, 1973; 1977). Thus, low I/TOC values in sediments at an increasing or gradually decreasing Br/TOC ratio represent anoxic bottom water conditions.

4.6.2.1.4. Manganese

Relatively high Mn/Fe values in the bottom sediments of the Baltic Sea were shown (Neumann et al., 1997) to record large inputs of oxygenated water from the North Sea. Three episodes of such influx occurred in the 20th century and were confirmed by hydrographic data (Neumann et al., 1997). In stagnant conditions, Fe is bound in iron sulphides of bottom sediments while Mn accumulates in water as Mn^{2+}. Influx of oxygenated water leads to Mn^{2+} oxidation to Mn^{4+} and precipitation of pyrolusite (MnO_2), which degrades as Mn^{2+} migrates to pore water when bottom water becomes anoxic again. At the same time, mineralization of OM provides higher pH levels and allows precipitation of Ca-rich rhodochrosite ($Mn(Ca)CO_3$), which is stable in anoxic environments, at the water-sediment boundary. Thus, sedimentary layers with notable percentages of rhodochrosite record influx of oxygenated water into the basin which led to additional Mn accumulation in sediments. The Mn/Fe ratio can be used as an indicator of such layers and a tracer of Mn excess relative to iron.

4.6.5.5. Factor analysis

To amalgamate all indicators of redox conditions, factor analysis was conducted using the principal component method. The subsequent factors were determined from the following indicators: TOC (%), S (%), Mo (ppm), Mn/Fe (g/g), χ/Fe ($10^{-8}\times m^3/g$), Ca (%), average grain size (μm), Si (%), Zr (ppm), K (%), Ti (%) and Rb (ppm). Principal components were analysed using the R packages *FactoMineR* (Lê et al., 2008; Husson et al., 2022), *factoextra* (Kassambara, 2017; Kassambara and Mundt, 2022) and *missMDA* (Josse and Husson, 2016; Husson and Josse, 2022). Two principal components account for ~75% of variance, while the first one refers to particle sizes and explains 45.2% of variance (Figs. 4.21, 4.22). Relatively high Si and Zr values represent sand and coarse silt fractions, while K, Ti, and Rb concentrations correlate with the contents of clay and fine silt (e.g., Cuven et al., 2010; Kylander et al., 2011). The second principal component refers to redox conditions and is responsible for 29.5% of variance. Ca correlates with Mn, possibly, because they co-precipitated in

rhodochrosite when oxygen-rich water penetrated into the stagnant basin. Other components were not considered.

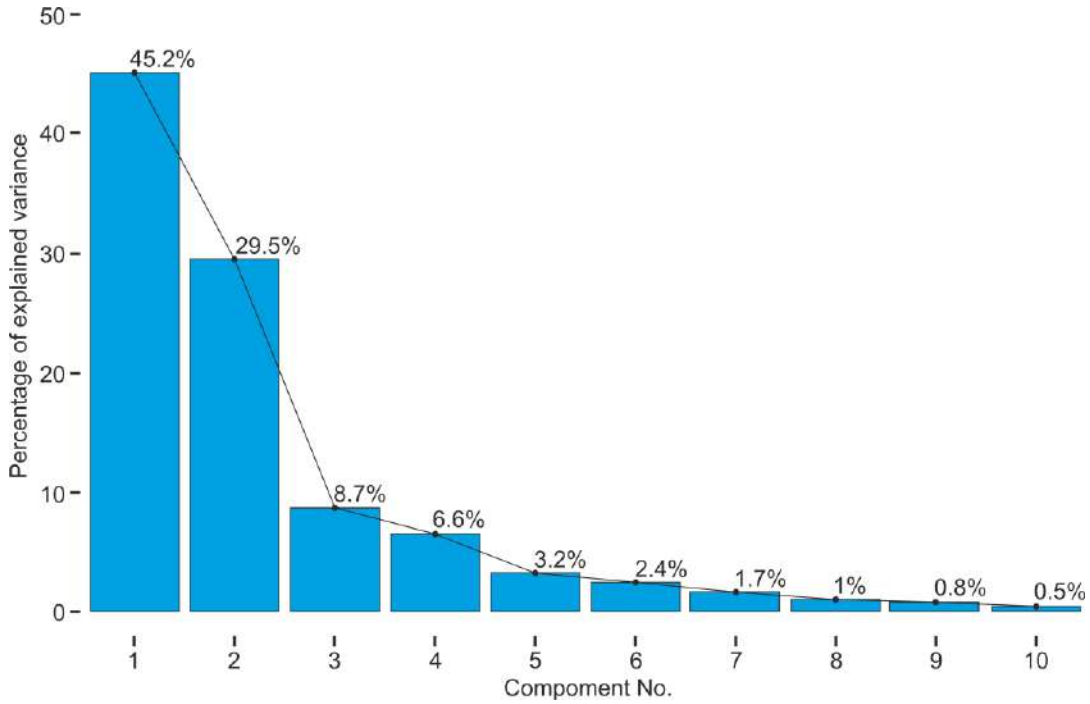

Fig. 4.21. Percentage of explained variance for principal components.

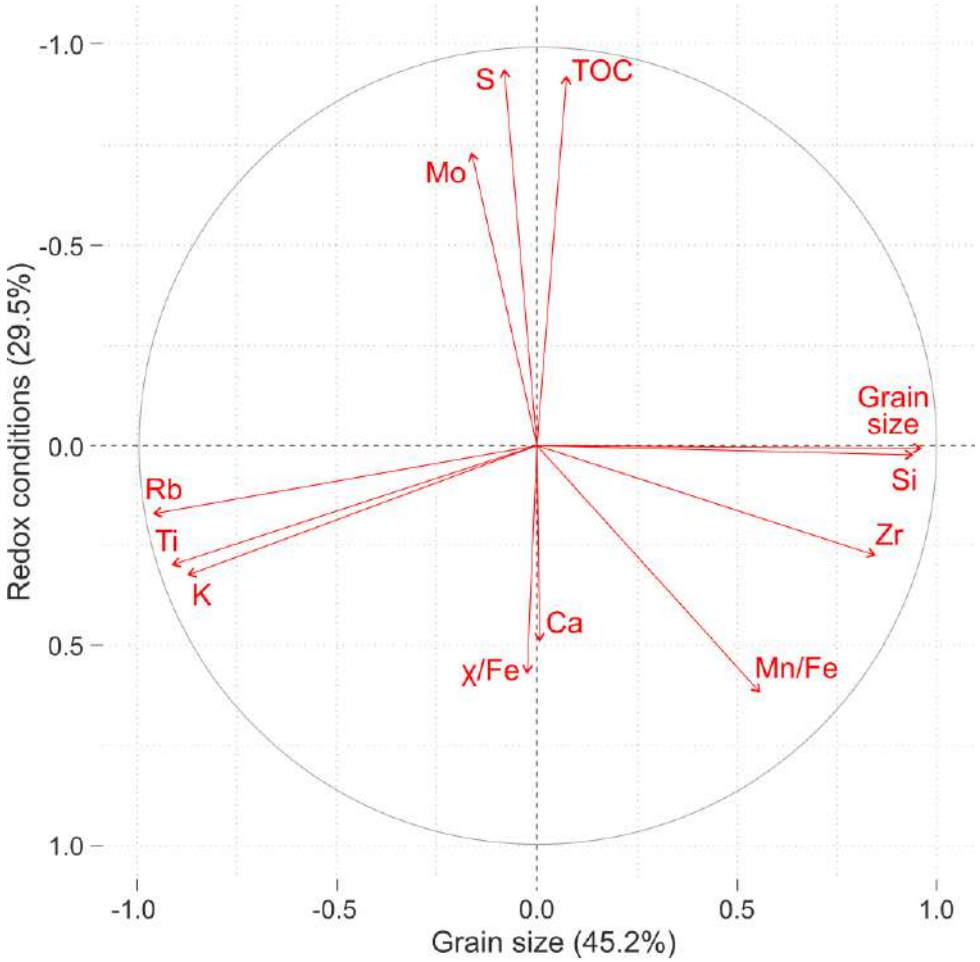

Fig. 4.22. Correlation circle of variables for the first and second components.

4.6.2.2. Redox zones

The interglacial sediments in the Sverdlov Factory section comprise three redox zones distinguished on the basis of indicators that record different redox conditions during deposition, with reference to factor analysis results (Fig. 4.23).

RZ1 (-21.9 to - 9.3 m asl)

Description

The interval encompasses the visible portion of the Sverdlov Fm. and the lower half of the Mga Fm. to the beginning of pollen zone M_5. The TOC content within the zone fluctuates about 0.5% and reaches 1.25% only in its upper part. Sulphur contents are likewise moderate: 0.1% on average and 0.7% in the upper strata. The concentration of Mo averages about 1 ppm and increases to 2–3 ppm near the top. The Mn/Fe ratio ranges from 9.0 to 24.1 mg/g and peaks between -10.3 and -10.1 m asl, with more than two-fold increase. The χ/Fe ratio varies about 0.5×10^{-8} m^3/g but increases rapidly to 2.1×10^{-8} m^3/g between -12.5 and -10.3 m asl.

Interpretation

Low TOC, S, and Mo contents suggest that sediments within the identified zone accumulated at sufficient oxygen availability, which is consistent with the results of factor analysis (Fig. 4.23, score of principal component 2). The Mn/Fe values in the lower part of the Mga Fm. may mark inputs of oxygenated water into the Mga Sea. The highest Mn/Fe peak correlates with the onset of rapid increase in marine OM at the beginning of SOZ5 (Fig. 4.20), which provides another argument for large inputs of saline oxic water into the Mga Basin in the middle of pollen zone M_4. Furthermore, the sediments within the -10 to -9 m asl interval also contain most abundant marine mollusc fossils and show times higher magnetic susceptibility than in other layers. High magnetic susceptibility may be due to incomplete pyritization with formation of greigite as an intermediate phase, as complete pyritization was impeded by deficit of sulfur (Volkov, 1961 cited from Berner, 1967; Wilkin and Barnes, 1997). The presence of diagenetic greigite at this level is confirmed by data of Dudanova (2023).

RZ2 (- 9.3 to - 2.1 m asl)

Description

The zone corresponds to the upper half of the Mga Fm. (pollen zones M_5–M_8). TOC in the zone is 1.13 to 2.41% and sulphur is 0.4 to 1.4%. The concentration of Mo is markedly higher in the lower half of the zone, reaches 10.6 ppm at -7.7 m asl and then decreases to 2–3 ppm. The Mn/Fe ratio is lower than in RZ1 and varies slightly around 9.5 mg/g. The χ/Fe ratio is likewise stable over the zone approaching 0.2×10^{-8} m3/g, though increasing to 0.4×10^{-8} m^3/g at the top. The I/TOC ratio starts decreasing in the beginning of the zone, after an increasing trend in the zone below.

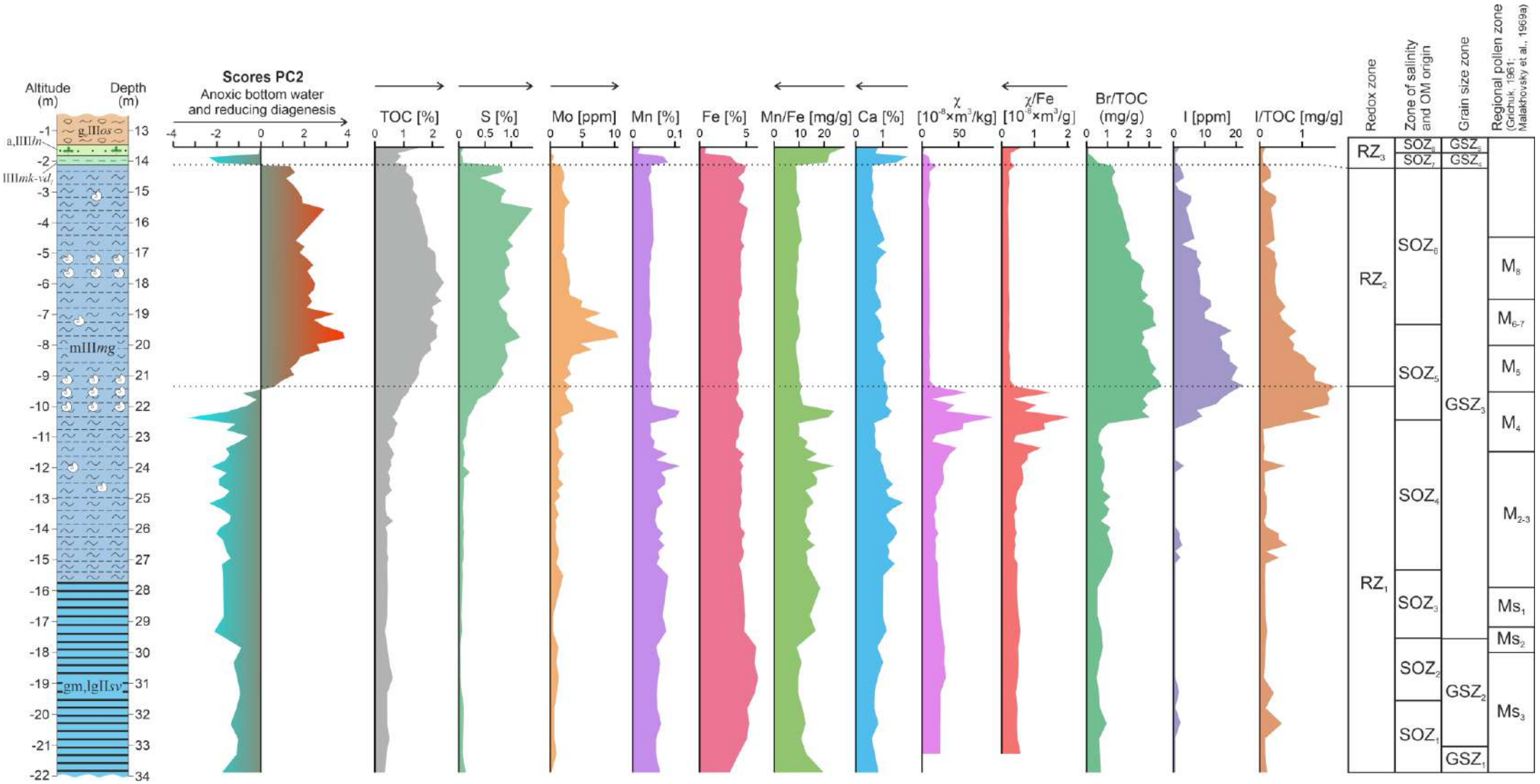

Fig. 4.23. Indicators of redox conditions in sediments from the Sverdlov Factory quarry correlated with grain size and regional pollen zones as well as zones of salinity and organic matter origin. Magnetic susceptibility (χ) data are borrowed from Dudanova et al. (2021). For lithology legend see Fig. 4.1.

Interpretation

The base of the zone is marked by rapid I/TOC decrease, while the Br/TOC ratio decreases slowly, which is evidence of anoxic conditions in the bottom water (Price and Calvert, 1973, 1977). This inference is supported by the Br vs TOC and I vs TOC plots (Fig. 4.24): the Br vs TOC relationship fits the linear function (R^2=0.85) at all TOC values, whereas I increases linearly only as far as TOC reaches1.25% but decreases upon its further growth. The I/TOC ratio remains low all over the zone, thus indicating, together with high TOC, that low oxygen contents persisted in the basin till the end of the Mga Sea lifespan. Reducing diagenetic processes begin acting at TOC = 0.5% (Volkov, 1984), while its value is much higher in the zone. Low values of the Mn/Fe ratio throughout the zone show limited inputs of oxygen-rich water into the basin. High S concentration and low magnetic susceptibility evidence for precipitation of pyrite as a result of reducing diagenetic reactions. The onset of anoxia within the zone is consistent with the PC2 score changes from negative to positive at -9.4 m asl according to factor analysis (Fig. 4.23).

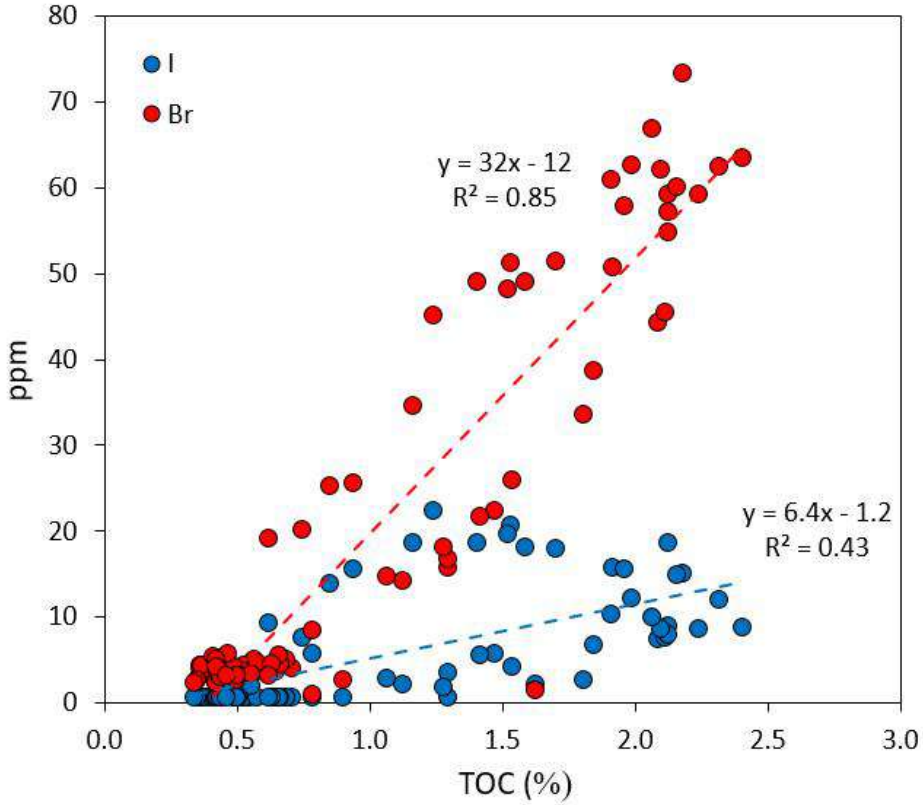

Fig. 4.24. Br vs TOC and I vs TOC plots for intermorainic sediments from the Sverdlov Factory quarry.

RZ3 (- 2.1 to - 1.4 m asl)

Description

The zone encompasses the Mikulino/Lower Valdai and Leningrad Fm. sediments. The concentrations of S and Mo decrease markedly to 0.04–0.08% and 0.2–0.6%, respectively, while the Mn/Fe ratio reaches as high as 21.4–28.2 mg/g. At the same time, the Mikulino/Lower Valdai rocks

show much higher Ca enrichment than the sediments of zones 1 and 2. The χ/Fe ratio is slightly higher than before. The TOC content in the Mikulino/Lower Valdai lacustrine facies is lower than in the Leningrad Fm. (0.71–0.91% against 0.79–1.63%).

Interpretation

Markedly lower S and Mo, along with higher Mn/Fe ratios, represent oxic bottom waters. The TOC content is higher in the Leningrad sand, but its organic matter consists of coarse plant detritus rather than the colloidal OM observed in the sediments below, and the criteria for interpretation of deposition environments are inapplicable in this case.

4.7. Diatom analysis

The diatom analysis (by Z. Pushina, VSEGEI, St. Petersburg) revealed 72 species of diatoms and two species of silicoflagellates (*Dictyocha fibula* and *Dictyocha speculum*) in ten samples of intermorainic deposits from the Sverdlov Factory quarry (Fig. 4.25). The diatom flora consists of several successive assemblages that belong to three diatom zones. The results of the analysis are reported below.

The depth interval between 32.8 and 26.7 m (-20.8 to -14.7 m asl) is free from diatoms.

DZ1 (-11.1 to -10.4 m asl)

Sediments at the depth 23.1 m (-11.1 m asl) contain an assemblage with modest abundances and poor diversity of diatoms, mostly of marine benthic (*Diploneis smithii*, *Cocconeis scutellum*) and freshwater (*Epithemia turgida*, etc.) taxa, as well as few species that live in fresh cold water and relict species *Cocconeis disculus* and *Diploneis domblittensis*. Benthic cosmopolitan species predominate in the assemblage. The diatom flora records deposition in shallow water of low-salinity, during the lagoonal stage of the basin evolution (Cheremisinova, 1960).

DZ2 (-10.4 – -5.5 m asl)

Unlike the previous interval, the diatom flora at depths from 22.4 to 17.5 m (-10.4 to -5.5 m asl interval) is rich. The diatom assemblage from the 22.3 m depth (-10.3 m asl) includes brackish benthic species *Hyalodiscus scoticus* (48% of assemblage total), as well as marine species *Grammatophora oceanica* (14%) and *Grammatophora macilenta* (8%). The diatoms coexist with marine sublittoral epiphyte *Achnanthes groenlandica* (0.3%), brackish to marine *Diploneis didyma* (3%), *Diploneis smithii* (3%) and other species. Among other findings, there are a few skeletons of *Dictyocha fibula* silicoflagellate, an inhabitant of warm water. The taxonomic composition of the assemblage records deposition in water of medium salinity in the marine intertidal or possibly subtidal zone.

The diatom assemblage from the 21.3 m depth (-9.3 m asl) consists of predominant planktonic neritic species *Chaetoceros* sp. (33%) and lower percentages of other taxa: *Thalassiosira gravida* (11%);

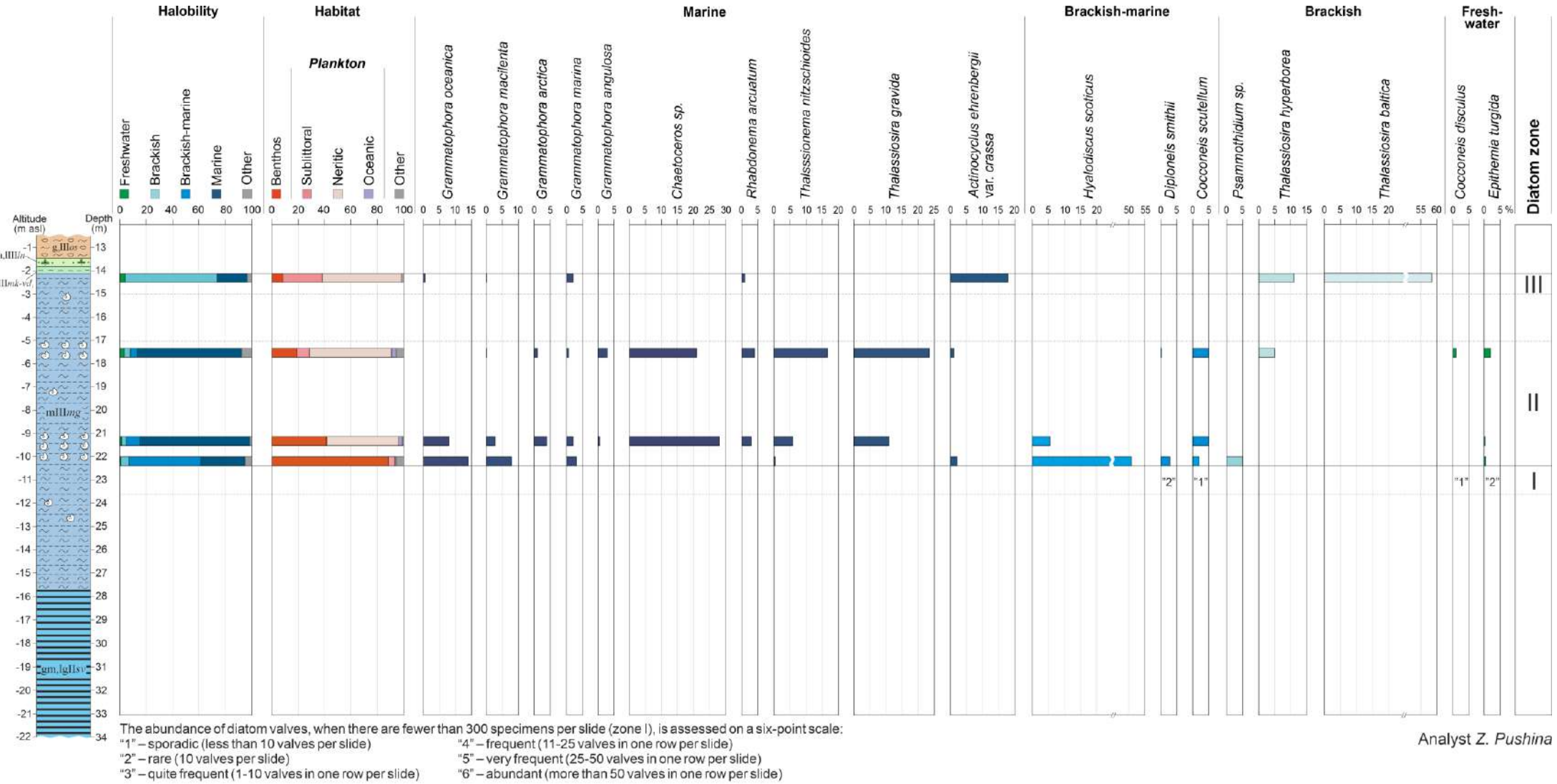

Fig. 4.25. Diatom analysis of interglacial deposits from Sverdlov Factory quarry (by Z. Pushina, VSEGEI). For lithology legend see Fig. 4.1.

brackish to marine benthic species *Hyalodiscus scoticus* (7%); five species of marine *Grammatophora* genus, especially *Grammatophora oceanica* (9%) and *Grammatophora angulosa* (3%) found in this assemblage only. The taxonomy corresponds to deposition in marine neritic conditions, at larger sea depths and in more saline water than the sediments of the -10.3 m level.

The diatom assemblage from the 17.5 m depth (-5.5 m asl) contains almost equal percentages of predominant *Chaetoceros* sp. (21%), *Thalassionema nitzschioides* (22%), and *Thalassiosira gravida* (24%) species. Less abundant taxa include sublittoral species of *Thalassiosira hyperborea* (5%), *Cocconeis costata* (3%), etc. The diatoms coexist with associate benthic plants: marine epiphyte *Caloneis brevis*, brackish to marine *Diploneis didyma*, *Diploneis smithii*, brackish *Tabularia fasciculata*, epiphyte *Cocconeis placentula* typical of fresh and brackish water, etc. The assemblage represents sediments deposited in marine neritic conditions, in quite saline water, which correspond to the marine phase according to Cheremisinova (1960). Note that this assemblage is very similar to the one described previously from sample 1/9 (Bolshiyanov et al., 2016).

DZ3 (-2.7 to -2.1 m asl)

Sediments at the 14.1 m depth (-2.1 m asl) contain dominant brackish planktonic species *Thalassiosira baltica* (59%) and two subdominant species of brackish water diatoms: *Actinocyclus ehrenbergii var. crassa* (17%) and *Thalassiosira hyperborea* (11%). The associate taxa are marine *Grammatophora marina*, brackish *Tabularia fasciculata*, sublittoral epiphyte *Cocconeis placentula* that grows in brackish water, and others. The diatom assemblage records shallow-marine deposition in low-salinity water during regression (Cheremisinova, 1960).

No diatoms were found in the 14.0–13.8 m interval (-1.8 to -2.0 m asl).

Thus, the salinity and sea depth patterns of the Mga basin, as inferred from diatom analysis, changed in the course of its history. The conditions of shallow moderate-salinity water (lagoon phase) changed to a marine neritic environment (marine phase) and then to a phase of regression, with shallow and low-salinity water.

Chapter 5. Duration of the Mikulino (Eemian) Interglacial

The LIG is correlated with the Eemian in Central and Western Europe and Mikulino Interglacial in the East European Plain. The division of the LIG in northwestern Europe is based on pollen assemblages (Fig. 3.1). At present it is generally accepted that the LIG correlates with MIS5e (e.g., LIGA Members, 1991; CAPE-LIP Members, 2006) as first suggested by Shackleton (1969) who divided MIS 5 into five substages. In that interpretation, the Eemian is considered as a single climatic cycle, from extremely cold to cold and a spell warmer than at present (Shackleton, 1969). Thus, the Eemian cannot be correlated with the entire MIS5 which comprises three climatic cycles. Shackelton (1969) estimated the duration of the Eemian at about 11 ka. Müller (1974) confirmed this conclusion by comparison of annual lamination counts with a pollen record from the Bispingen section in Northern Germany. Later, similar estimations were made for two other sections in Northern Germany: Quakenbrück (Hahne et al., 1994) and Gross Todtshorn (Caspers, 1997), which supported the results from Bispingen. The reliability of these estimations is limited to absence of varves in the final phases of the Eemian at these sites. Therefore, the duration of several pollen zones was determined using extrapolation. The correlation of the Eemian with MIS5e was also discussed by Mangerud (1989).

The MIS5/6 and MIS 5e/d transitions were timed as ~130 ka (Lisiecki and Raymo, 2005) and ~115 ka (Shackleton et al., 2002). Direct comparison of pollen spectra and the $\delta^{18}O$ isotope curve in core MD952042 sampled in the Atlantic Ocean ~130 km southwest of Lisbon revealed misfit between the MIS5/6 transition and the onset of the Eemian (Sánchez Goñi et al., 1999; Shackleton et al., 2003). Correspondingly, the interglacial conditions in the Iberian Peninsula were established approximately 6 ka later than the MIS6 termination, and the interglacial flora appeared in the Iberian Peninsula ~2 ka after the interglacial sealevel had reached the present stand. However, this conclusion contradicts a wealth of data on Eemian marine deposits from Northern Europe (Beets et al., 2006) placing the LIG high stand within the climatic optimum defined by pollen spectra (e.g., Zagwijn, 1983; 1996; Streif, 1990). Sier et al. (2011; 2015) concluded that the Eemian in Northern Europe began at ~121 ka, based on the correlation between terrigenous deposits and oceanic cores with respect to the paleomagnetic excursion Blake, and thus the beginning of the Eemian was marked by the sealevel fall. However, this interpretation is inconsistent with the results discussed above. The misfit between the isotopic and pollen data in core MD952042 may be due to the warming influence of the North Atlantic Deep Water (NADW) on the bottom waters, which caused a shift of the $\delta^{18}O$ record down the section. The discrepancy between the $\delta^{18}O$ plateau inception and the Holocene high stand in the North Atlantic is 3.7±1.1 ka (Waelbroeck et al., 2008).

Funder et al. (2002) timed the LIG high stand at 128±1 ka from the U/Th ages of corals, or ~500 years after the beginning of the *Carpinus* pollen zone, and dated the Eemian onset at 132.5 ka

using the Bispingen pollen zone chronology (Müller, 1974). Corrections for isostatic and tectonic effects made it possible to obtain a more precise estimate of 131 ka (Lambeck et al., 2006). A similar assessment of the LIG onset 131.2±2.0 (2σ) ka was made by Waelbroeck et al. (2008) based on the U/Th dating of corals. According to their data, the LIG inception was marked by sharp increase of the methane content in the Antarctic ice core and the sea level rose at 126.0±1.7 (2σ) ka. An alternatively, Hearty et al. (2007) concluded that the sea achieved the high stand 130±2 ka ago.

Correspondence between the endpoints of the Eemian and MIS5e was challenged by Kukla et al. (1997, 2002), Tzedakis (2003), Brauer et al. (2007), Allen and Huntley (2009). They demonstrated that interglacial conditions in southern Europe lasted until the second half of MIS 5d (111–107 ka ago). Tzedakis (2003) concluded that the difference in duration of the LIG in southern and northern Europe can be explained by divergence in timing of forest existence. Kukla et al. (2002) proposed to use the concept of "Last Interglacial *sensu stricto*" as a warm period identified in northwestern Europe and the concept of "Last Interglacial *sensu lato*" as the period of existence of temperate forests in southern Europe, which lasted throughout MIS5e and a part of MIS5d. They also suggested that “Eemian Interglacial” should be considered synonymous with the Last Interglacial *sensu stricto*. According to other scholars (Brigham-Grette, 2001; Helmens, 2014), the Last Interglacial, including the Eemian and Early Weichselian, encompasses the entire MIS5. However, this interpretation contradicts the author’s view since MIS5d-a was characterized by significant expansion of glaciation (Otvos, 2015). N. Bolikhovskaya and A. Molodkov (Bolikhovskaya and Molodkov, 2002; Molodkov and Bolikhovskaya, 2009; Molodkov, 2020) suggested that the Mikulino Interglacial, defined as the Last Interglacial *sensu stricto* according to J. Kukla (2002), lasted throughout MIS5 (145-70 thousand years ago), based on ESR dating of molluscs from northern Eurasian sediments. This viewpoint, though being refuted by the presence of significant ice sheets in northern Eurasia during MIS5d-a (e.g. Svendsen et al., 2004), as well as by varve chronology (Müller, 1974; Hahne et al., 1994; Caspers, 1997) and instrumental dating (Table 5.1).

Correlation of the Eemian with MIS 5e has not been confirmed by direct instrumental dating of palynologically constrained sections. Even though separate pollen zones were dated, the results do not allow an univocal conclusion on the LIG duration and its possible correlation with MIS5e (Table 5.1; Fig. 5.1). Ages from the same regional pollen zones expectedly vary from section to section as age uncertainties are often comparable with the LIG duration. Furthermore, the boundaries between successive vegetation phases within northern Europe were asynchronous: main LIG broadleaved species in the central and northwestern East European Plain emerged later than in Central Europe (Chepurnaya, 2009a,b).

Table 5.1. Summary of Uranium-Thorium (U/Th), Electron Spin Resonance (ESR), Optically Stimulated Luminescence (OSL), Infrared Stimulated Luminescence (IRSL) and Infrared Radiofluorescence (IR-RF) ages obtained for the LIG regional pollen zones in Northern Europe. When several ages are reported for an interval their weighted average is calculated. Ages and uncertainties are rounded to whole numbers. Asymmetric uncertainties are replaced by average symmetric uncertainties.

Site	Method	Age (ka)														Reference
		Saalian	**E1**	**E2a**	**E2b**	**E3a**	**E3b**	**E4a**	**E4b**	**E5**		**E6a**		**E6b**		Zagwijn, 1961
		Saalian	**I**	**IIa**	**IIb**		**IIIa**	**IIIb**	**IIIc**	**IVa**	**IVb**	**Va**	**Vb**	**VI**		Selle, 1962
		Saalian	**I**	**II**	**III**		**IVa**		**IVb**	**V**		**VI**		**VII**		Menke and Tunni, 1984
		M1	**M2**	**M3**	**M4**				**M5**	**M6**		**M7**		**M8**		Grichuk, 1961
Cheremoshnik	U/Th	122±6														Rusakov et al., 2019; Maksimov et al., 2020
Nizhnyaya	U/Th	128±2														Maksimov et al., 2022
Banzin	U/Th	119±7														Börner et al., 2015; Maksimov et al., 2021
Beckentin	U/Th	116±4														Rother et al., 2019; Maksimov et al., 2021
Fili	U/Th		105±3													Maksimov and Kuznetsov, 2010; Kuznetsov and Maksimov, 2012
Neumark-Nord 2	IR-RF			122±13												Strahl et al., 2010
Netiesos	ESR			112±10												Baltrūnas et al., 2013
Cheremoshnik	U/Th			115±8												Rusakov et al., 2015; Maksimov et al., 2020
Kileshino	U/Th				115±3											Maksimov et al., preprint
Jonionys	ESR				110±2											Gaigalas and Molodkov, 1998
Sverdlov Factory	ESR				110±9											Bolshiyanov et al., 2016
Netiesos	ESR/IRSL				96±7											Baltrūnas et al., 2013
Zaton	ESR				112±5											Molodkov and Raukas, 1988; Molodkov, 2020
Roer Valley Graben	OSL					114±12										Schokker et al., 2004
Rutten	IRSL							109±6								Sier et al., 2015
Dagebüll	U/Th/ESR								131±1							Hoffman et al., 1999; Winn et al., 2000
Nizhnyaya	U/Th								109±2							Maksimov et al., 2022
Zaton	ESR								89±3							Molodkov and Raukas, 1988; Molodkov, 2020
Neubrandenburg-Hinterste Mühle	U/Th								116±12							Börner et al., 2018; Maksimov et al., 2021
Nizhnyaya Boyarschina	U/Th									99±3						Maksimov et al., 2022
Mikulino	U/Th									110±5						Maksimov and Kuznetsov, 2010; Maksimov et al., 2021
Murava	U/Th									103±5						Maksimov and Kuznetsov, 2010; Kuznetsov and Maksimov, 2012
Kelkolovo	ESR									137±16						Molodkov and Krasnov, 1998
Dagebüll	ESR										127±15					Hoffman et al., 1999
Snaigupėlė	U/Th											129±12				Baltrūnas et al., 2015
Rutten	IRSL											112±11				Sier et al., 2015
Plyos	IR-RF													124±12		Degering and Krbetschek, 2007;

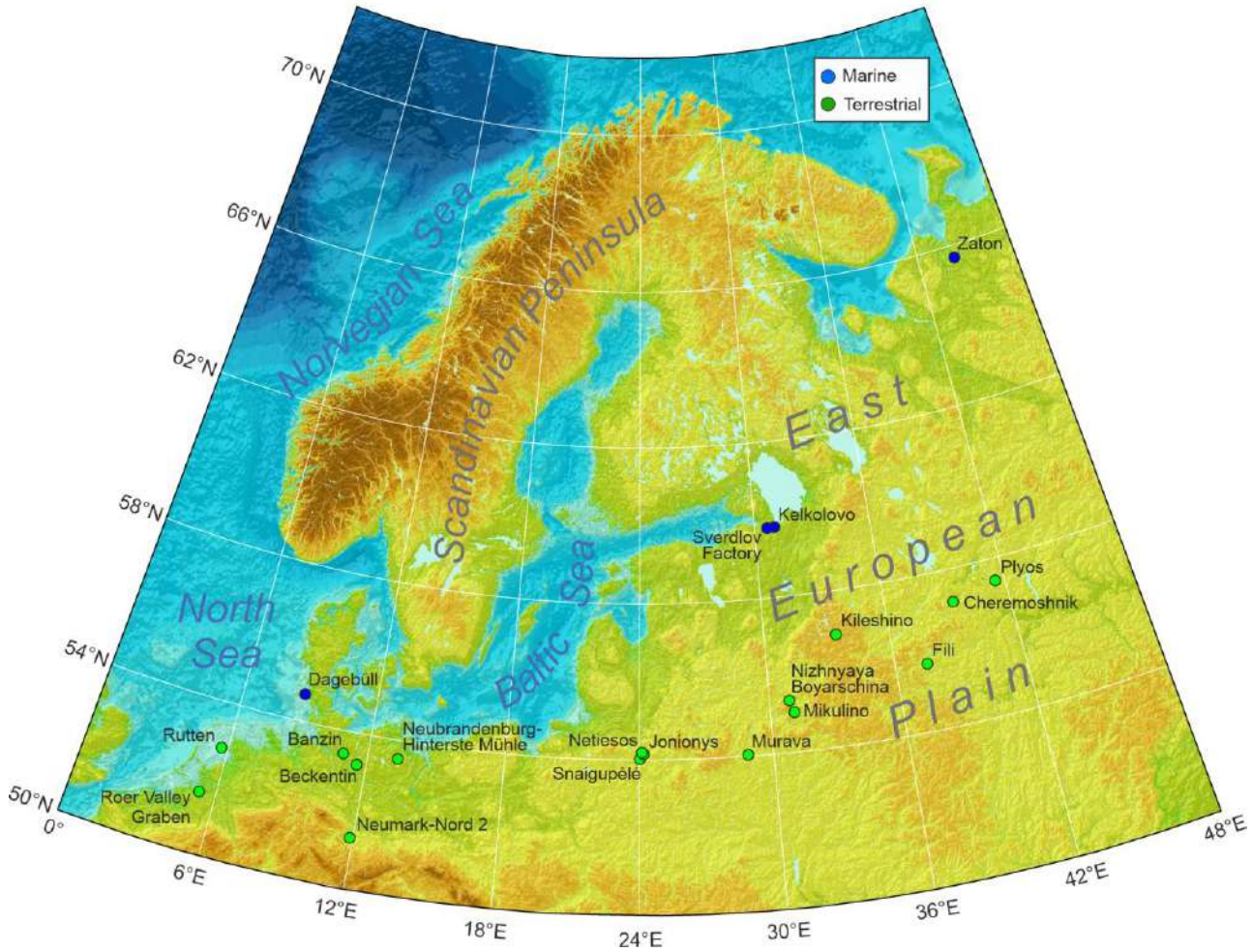

Fig. 5.1. Locations of dated palynologically characterized sections of terrestrial and marine Mikulino (Eemian) deposits (Table 5.1). Based on ETOPO1digital elevation model .

The sequence of OSL ages the author obtained from the Mga Fm. at Sverdlov Factory covers all Mikulino pollen zones and thus can be used to estimate the Mikulino duration. Our Bayesian model gives ages of the Mikulino onset and termination at 133±8 and 109±7, respectively. These estimates (taking into account measurement uncertanities) do not contradict the Eemian duration determined before from varve chronology (9.5–11 ka) (Müller, 1974; Hahne et al., 1994; Caspers, 1997). Moreover, they are consistent with correlation between the Mikulino Interglacial and MIS5e (130–115 ka, Shackleton et al., 2002; Lisiecki and Raymo, 2005).

It is important to note that the obtained results contradict those of Molodkov and Bolikhovskaya (2022) for the Voka section in Estonia. They reported IRSL ages in a range from ~94 to ~70 ka for Mikulino pollen zones M_6–M_8. However, correlation of these deposits with the Mikulino is questionable. A cross-section of the Vasavere ancient buried valley is exposed in the Voka outcrop (Raukas et al., 2007). From the classical point of view (Raukas, 1978; Tavast and Raukas 1982; Miidel 2003; Raukas et al., 2007), the Vasavere valley is filled with glaciofluvial and glaciolacustrine sediments accumulated during the retreat of the last glaciation. However, first attempts to date them gave ambiguous results.

Raukas (2004) obtained five feldspar IRSL ages in the range of 75–9.8 ka for the Pannjärve section. Raukas and Stankowski (2005) obtained two quartz OSL ages of 12.5 (18.5) ka and 25 ka at the Voka section. Raukas with coauthors believe that the youngest ages are the most accurate, and the sediments were mainly accumulated in the end of last glaciation.

Later a series of feldspar IRSL dates from ~94 to ~8 ka (Molodkov et al., 2007; Molodkov, 2007; Molodkov and Bolikhovskaya, 2022) for the Voka section was published. Scientists divided the section into two units and correlated the lower unit with Mikulino pollen zones M_6–M_8 and MIS4 and the upper one with the Middle Valdai and Holocene. However, the author considers the correlation of the lower unit with the Mikulino doubtful; the pollen spectra differ from the spectra of key interglacial sections around the Gulf of Finland, including the Mga (Znamenskaya, 1959; Pleshivtseva et al., 1984; Pleshivtseva, 2011a), Rybatskoye (Lavrova and Grichuk, 1960), Prangli (Liivrand and Valt, 1966), Sinyavino (Malakhovsky et al., 1969a), Krasnoselskoye (Sokolova et al., 1972), Yukki (Vishnevskaya et al., 1973), Röngu (Raukas, 1978), and several others. Firstly, the low content of tree pollen within the interglacial climatic optimum (zone M_6) is noteworthy: 40–65% at Voka against 80–95% in all Mikulino sections of the region. . Secondly, pollen of *Artemisia* and Chenopodiaceae is present throughout the unit at Voka identified as the Mikulino optimum, whereas it is absent or occurs only sporadically in typical Mikulino sections. It should be noted that *Artemisia* and Chenopodiaceae pollen are characteristic of periglacial landscapes in Eastern Europe during the Valdai Stage (Grichuk and Grichuk, 1960; Novenko, 2016). Thirdly, a key diagnostic sign of the Mikulino deposits is a sequence of culminations *Quercus*-*Ulmus*-*Corylus*-*Tilia*-*Carpinus* (Malakhovsky et al., 1969a). In the Voka section, pollen of broad-leaved species was found, but the sequence of culminations was not observed. Many Valdai (Weichselian) sections typically contain pollen of broad-leaved trees redeposited from older Mikulino (Eemian) sediments(Andersen, 1957; 1961; Malakhovsky et al., 1969b; Liivrand, 1976; 1982). For example, at Sinyavino (Malakhovsky et al., 1969b), pollen of broad-leaved species occurs throughout the 55-m Valdai deposits overlying the Mikulino sediments. Therefore, correlation of the lower unit at Voka with the Mikulino has not been proven. More probably, it correlates with the Lower Valdai or Late Glacial, as it was proposed earlier by Miidel (2003) and Raukas et al. (2007).

Chapter 6. Evolution of the Mga Sea: evidence from the Sverdlov Factory quarry

In this study, the history of the Mga Sea is assumed to comprise four main events distinguished according to geochemical and diatom data, following the previous interpretation (Cheremisinova, 1960; Znamenskayaa and Cheremisinova, 1962; Malakhovsky et al., 1969a): glaciomarine, lagoonal (after Cheremisinova) or brackish, marine, and regressive phases (Fig. 6.1). The names of the phases reflect the most prominent features characterising each stage of Mga Sea evolution. The glaciomarine phase corresponds to the start of transgression and the penetration of sea waters into the Late Moscow glacial basin. The brackish phase occurs at the beginning of the Mikulino Interglacial and is characterised by low salinity. The marine phase corresponds to the peak of the marine transgression, during which the Mga Sea had a maximum salinity, similar to that of normal marine salinity. The regressive phase corresponds to the retreat of the Mga Sea, accompanied by a gradual decrease in salinity.

6.1. Glaciomarine phase

The chemical compositions and varve chronology of sediments from the Sverdlov Factory quarry indicate that seawater first penetrated into the Late Moscow glacial basin no later than ~1100 years before the onset of the Mikulino Interglacial (subphase *a* of the glaciomarine phase, Fig. 6.1). Varved deposits of that period contain abundant ice-rafted debris (IRD) and thus may correlate with the 11th Heinrich event (Heinrich, 1988; McManus et al., 1998). In the model of Beets et al. (2006), the 11th Heinrich event correlates rather with the Kattegat Stadial, but the interval corresponding to the Kattegat Stadial in the Sverdlov Factory section lacks signatures of ice rafting. There is some probability that the level of IRD in the Sverdlov varved clay represents changes in local conditions at the glacier front and has no relation to the 11th Heinrich event.

In the end of the Moscow cryochron, the coast of the Mga Sea was mainly grown with pine and spruce communities that included periglacial flora elements. The ice-rafting activity stopped about 970 years before the onset of the interglacial, when the connection of the Mga Sea with the ocean apparently became impeded. This inference agrees with data on water salinity: the sea water salinity decreased markedly ~1030 years before the interglacial, i.e., the connection with the ocean may have interrupted for some time (subphase *b* of the glaciomarine phase, Fig. 6.1). However, the salinity decrease was reconstructed from a single parameter of the TOC/S ratio, at TOC in the sediments as low as <1%. Thus, the TOC/S ratio alone is not very reliable evidence (Berner and Reiswell, 1984), and the existence of the event remains insufficiently proven. A brief spell of low salinity was also inferred from diatom analysis for the Upper Moscow strata in BH 10 (Pleshivtseva et al., 1984), but it was timed at the latest Kasplya Interstadial (pollen zone Ms_2). According to the results from the Sverdlov Factory quarry, the

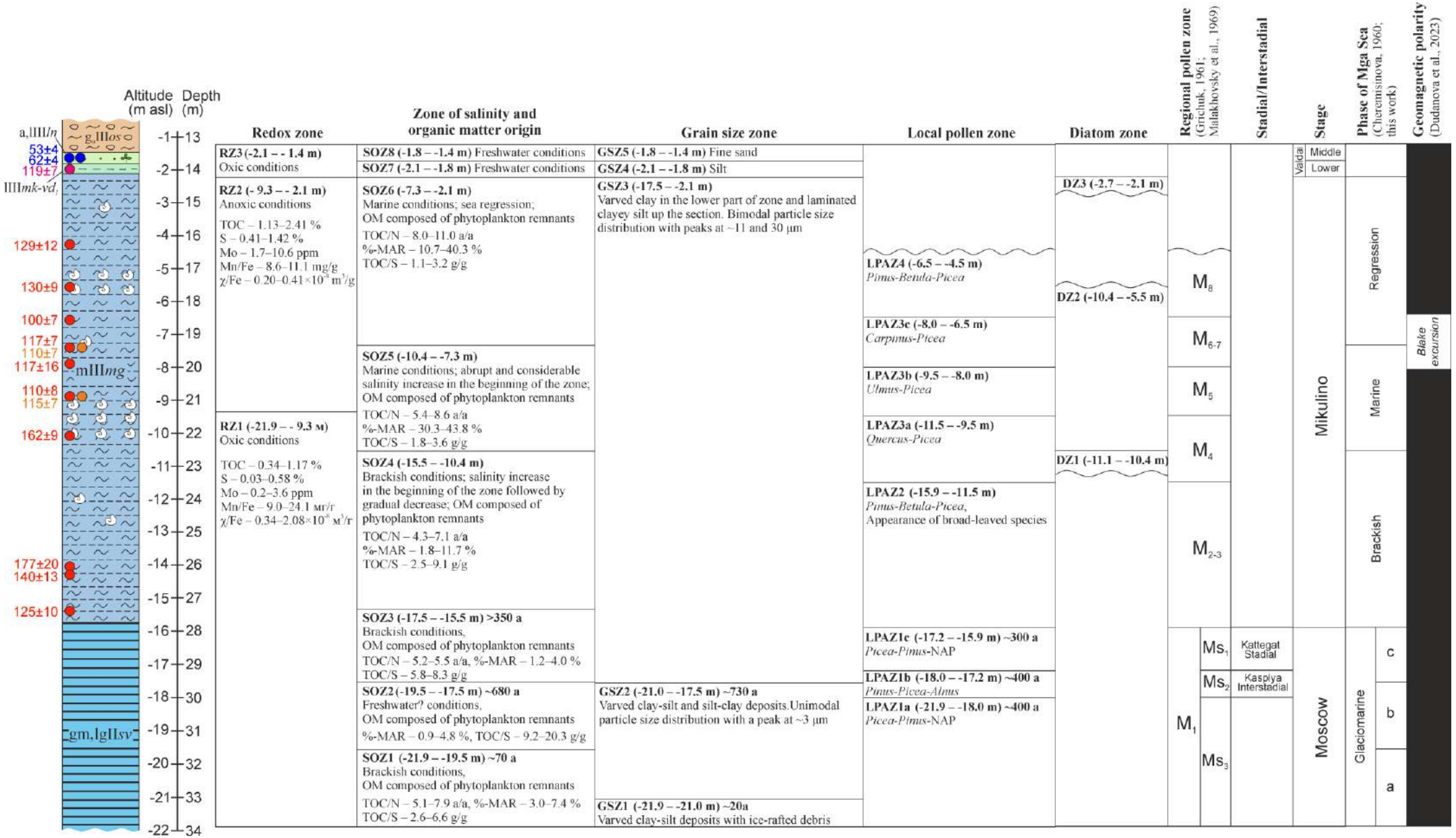

Fig. 6.1. Synthesized data on intermorainic deposits from the Sverdlov Factory quarry. For lithology legend see Fig. 4.1.

desalination period lasted about 680 years and ended ~350 years before the LIG. Interestingly, the age bounds of the presumed freshwater subphase almost perfectly match the boundaries of the grain size zone GSZ2 (Fig. 6.1), where the varved sediments have higher clay contents and the varves are thinner than in other intervals.

About 700 years before the LIG, the climate began to warm, probably correlating with the Kasplya Interstadial. The plant communities of the warmer climate contained lower percentages of *Picea* and periglacial flora elements but had greater percentages of *Pinus* and *Alnus* and also included *Corylus*. The Kasplya Interstadial lasted about 400 years, though the duration of its equivalent Zeifen Interstadial in Anholt Island (Denmark) was estimated as ~1000 years (Seidenkrantz, 1993). The Kasplya Interstadial was named by V. Grichuk after the Kasplya River in the Smolensk Oblast (Malakhovsky et al., 1966; Buslovich et al., 1969) and distinguished by Malakhovsky et al., (1966, 1969a) in several sections: Nizhnyaya Boyarschina (Chebotaryova, 1954; Grichuk and Grichuk, 1960) on the Kasplya River, Petrokrepost' (Nedrigailova et al., 1965; Pleshivtseva, 2011a), Sinyavino (Malakhovsky et al., 1969a) in the Leningrad Oblast, and Felitsianova (Krukle et al., 1963) in Latvia. The interstadial warming in the latest Saalian Glacial of West Europe was called Zeifen after a locality in Bavaria (Jung et al., 1972). The name was suggested by Woillard (1978) who discovered signatures of similar warming in the deposits of the Grand Pile section in northeastern France.

About 350 years prior to the LIG, the water salinity in the Mga Sea again reached the brackish level (subphase *c* of the glaciomarine phase, Fig. 6.1). At that time, the grain size distribution changed toward smaller percentages of clay and larger amounts of silt particles.

The Kasplya Interstadial was followed by the Kattegat Stadial, quite a short (300 years) cooling spell. A similar estimate for the duration of the cold event that preceded the Eemian interglacial (250 year) was based on varve chronology of the Lago Grande di Monticchio section in southern Italy (Brauer et al., 2007). On the other hand, the Kattegat Interstadial recorded in the Island Anholt (Denmark) data lasted ~1200 years (Seidenkrantz, 1993). The plant communities in the Mga Sea coast during the Kattegat Stadial were again dominated by *Picea*, while the contribution of *Pinus* reduced and periglacial flora increased slightly.

6.2. Brackish (lagoon) phase

The brackish phase of the Mga Sea roughly coincided with the onset of the Mikulino Interglacial. Pollen data show greater percentages of *Pinus* and smaller contributions of *Picea*, *Betula nana*, and *Artemisia* to the earliest interglacial plant communities. Lithologically, the onset of the interglacial was marked by the absence of rhythmic bedding and by color changes of clay and silt sediments to black (bluish). In terms of fauna, marine molluscs appeared at the respective level in the section. The brackish phase continued till the middle of pollen zone M_4. At that time, mixed forests of coniferous and

broadleaved trees were present on the coast of the Mga Sea. Diatom data for the beginning of pollen zone M_4 record shallow-marine deposition at low salinity. The diatom assemblage of the latest brackish phase included typical inhabitants of brackish (*Diploneis smithii*, *Cocconeis scutellum*) and fresh (*Epithemia turgida*, *Cocconeis disculus* and *Diploneis domblittensis*) waters. The low salinity of the basin also shows up in geochemical data.

6.3. Marine phase

The onset of the marine phase is easily detectable from geochemical and diatom evidence which records abrupt increase in salinity and sea depth at the -10.4 m asl level. The diatom assemblage at the -10.3 m level corresponds to deposition in marine (possibly, subtidal) conditions, at moderate salinity. The sediments at -9.3 m asl were deposited in marine neritic conditions of salinity and sea depths greater than at the -10.3 m asl level. The diatoms are mainly of marine and brackish species: *Hyalodiscus scoticus, Chaetoceros* sp., *Grammatophora oceanica, Thalassiosira gravida* and *Grammatophora macilenta*. Geohemical data indicate large inputs of saline oxygenated water into the Mga Sea in the beginning of the marine phase. TOC/S ratio values of about 2.1 g/g within the marine and subsequent regressive phases indicate a salinity of at least 18‰. The Mga sediments deposited during the early marine phase contain abundant shells of molluscs, which proliferated in oxic near-bottom water, but the mollusc fauna is poor in the overlying strata deposited in anoxic conditions. The oxygen contents reduced, possibly, when the basin became stagnant. The marine phase lasted till the middle of pollen zone $M_{6\text{-}7}$ and thus corresponded to the climate optimum of the Mikulino Interglacial. The plant communities of that time included broad-leaved species and *Picea*. Pollen zone $M_{6\text{-}7}$ approximately correlates with the Blake geomagnetic excursion (Dudanova, 2023).

6.4. Regressive phase

The onset of regression can be reconstructed from decrease in marine organic matter in the middle of pollen zone $M_{6/7}$ at -7.7 m asl. The OM contents decrease gradually till the top of the Mga Fm. Diatom data from the -5.5 m asl level record moderate-salinity neritic marine conditions, but the top of the Mga Fm. was already deposited in a notably less saline shallow basin. This inference is based on the taxonomy of diatoms with predominant brackish species in the end of the regression phase: *Thalassiosira baltica*, *Actinocyclus ehrenbergii* var. *crassa* and *Thalassiosira hyperborea.* According to geochemical data, the bottom-water conditions in the Mga Sea were anoxic and thus unfavorable for mollusc fauna, during the whole regression event.

6.5. Lacustrine phase

The water of the Mga basin became fresh in the end of pollen zone M_8, or in the beginning of the Early Valdai, judging by the TOC/S ratio (9.6–14.7) and the absence of the marine OM component (Fig. 4.20). The TOC/N ratio indicates that organic matter in lacustrine sediments mainly consists of

phytoplankton (Fig. 4.20). Low S and Mo, together with higher Mn/Fe ratios, provide evidence for oxic bottom-water conditions in the freshwater basin. Freshwater conditions are also inferred for pollen zone M_8 in the Krasnoselskoye (Sokolova et al., 1972), Yukki (Vishnevskaya et al., 1973) and Peski (Miettinen et al., 2014) sections of the Karelia Isthmus.

6.6. Concluding remarks

The obtained geochemical and diatom data from the Sverdlov Factory section have revealed four evolution phases of the Mga Sea: glaciomarine, brackish (lagoonal), marine, and regressive. The input of saline waters into the glacial basin during the Moscow Late Glacial occurred up to ~1100 years prior to the onset of the Mikulino Interglacial. Between ~1030 and 350 years prior to the LIG, the Mga Sea experienced substantial desalination, followed by the restoration of its connection to the ocean. The Sverdlov deposits in the Sverdlov Factory section provided reference for identification of three RPZ: Ms_3, Ms_2 (Kaslya Interstadial) and Ms_1 (Kattegat Stadial). According to varve chronology, the Kasplya Interstadial lasted approximately 400 years (~700-300 years prior to the onset of the LIG) whilst the duration of the Kattegat Stadial was around 300 years.

Furthermore, the glaciomarine phase of the Mga Sea evolution continued until the start of the Mikulino Interglacial before the transition to the brackish (lagoonal) phase characterized by slightly higher salinity. The termination of the brackish phase falls at the midpoint of the M_4 RPZ.

The beginning of the marine phase is marked by a steep rise in salinity and water depth of the Mga Sea, which catalyzed swift proliferation of marine diatoms and molluscs. Evidenced by geochemical scrutiny, the salinity of the Mga Sea during the marine episode and the ensuing regressive phase remained at a minimum of 18‰. At the start of the M_5 RPZ, anoxic conditions were established in the bottom waters of the Mga Sea, resulting in substantial reduction of faunal assemblages. The anoxic conditions persisted till the end of the LIG.

The regressive stage began in the middle of the M_{6-7} RPZ, lasted till the end of the LIG, and was succeeded by the lacustrine phase at the termination of the M_8 RPZ or Early Valdai.

Chapter 7. Last Interglacial vegetation and sea evolution in the Baltic and Onego-Ladoga regions

7.1. Eemian (Mikulino) chronology of vegetation in North Europe

The only available Eemian (Mikulino) vegetation chronology is based on data from the Bispingen section in North Germany (Müller, 1974). The duration of the Bispingen zones E_{4a}–E_5 (Menke and Tunni, 1984) approximately corresponds to that of the respective zones estimated from the number of annual varves in the Quakenbrück and Gross Todshorn sections (Table 7.1) (Hahne et al., 1994; Caspers, 1997). Additionally, the duration of the *Pinus-Picea* pollen zone, the last one in the Eemian Interglacial (E_7), was evaluated in the Krumbach section in Bavaria (Frenzel and Bludau, 1987, cited from Turner, 2002) as at least 1650 years, which is commensurate with the ~2000 a value for Bispingen (Table 7.1).

Table 7.1. Chronology of Eemian pollen zones in the Bispingen (Müller, 1974), Quakenbrück (Hahne et al., 1994), Gross Todshorn (Hahne et al., 1994; Caspers, 1997), and Krumbach (Frenzel and Bludau, 1987, cited from Turner, 2002) sections. Zone duration is according to count (bold) or to extrapolation from deposition rates (italic), modified after Caspers (1997).

Pollen zone (Menke and Tunni, 1984)	Pollen zone (Selle, 1962)	Duration, a				
		Bispingen (Müller, 1974)	Quakenbrück (Hahne et al., 1994)	Quakenbrück (recalculated, Caspers, 1997)	Gross Todshorn (Caspers, 1997)	Krumbach (Frenzel and Bludau, 1987)
E1	I	**~100**	-	-	-	-
E2	IIa	**200**	-	-	-	-
E3	IIb	**450**	-	-	-	-
E4a	IIIa	**450**	-	-	**345-386**	-
	IIIb	**700**	*1368 (1038)*	*1230 (900)*	**641-692**	-
E4b	IIIc	**1000-1200**	*1579*	*1063*	*1268-1469* **(1043-1244)**	-
E5	IV	*~4000*	*3300*	*4391*	-	-
E6	V	*~2000*	*1500 (700)*	*925 (125)*	-	-
E7	VI	*~2000*	-	-	-	**≥1650**

The varve chronology for the Bispingen section has some drawbacks though (Müller, 1974; etc.): zones E_5–E_7 lack varves and their duration has to be inferred by extrapolation from deposition rates; zone *Betula* (E_1) may be incomplete and its duration may be underestimated.

The boundaries of pollen zones before the *Carpinus* (E_5) zone were concluded (Zagwijn, 1996) to be almost synchronous in West and Central Europe, with an age difference of 200 to 500 years. Therefore, the Bispingen chronology has been often used for reference to estimate the duration of phases in the vegetation history of Germany, as well as in Denmark (e.g., Kristensen et al., 2000; Gibbard and Glaister, 2006), the Netherlands (e.g., Beets et al., 2006), Poland (e.g., Head et al., 2005; Knudsen et al., 2012; Marks et al., 2014), and other countries of the two regions. The Bispingen chronology was also used for East Europe sections, including those of the Leningrad Oblast (Miettinen et al., 2002, 2014),

Karelia (Funder et al., 2002), and the White Sea area (Grøsfjeld et al., 2006; Rudenko et al., 2023). Meanwhile, the latter reconstructions appear to be poorly justified because the boundaries of pollen zones can be synchronized only between relatively closely spaced sections. The diachrony of the vegetation phases and the dynamics of the tree species distribution have been studied in more detail for the Holocene (Firbas, 1954; Serebryanny, 1971; Savelieva, 2007; Giesecke et al., 2011), but only few publications on the subject are available for the LIG time span (Chepurnaya, 2009 a,b). In both Holocene and LIG, the distribution of main broad-leaved species was shifted to the east and north-east relative to Central Europe. Assuming that *Carpinus* reached the White Sea coast in the time of maximum expansion in Central Europe, its migration between the two areas during the LIG was inferred (Chepurnaya, 2009 a,b) to have taken no more than 2500–3000 years.

The lag of vegetation phases can be estimated with reference to a level synchronous in all Eemian (Mikulino) sections throughout North Europe. The North Sea and White Sea basins were connected in the LIG and any marked change in sea depth or salinity is expected to show up all over the region, from

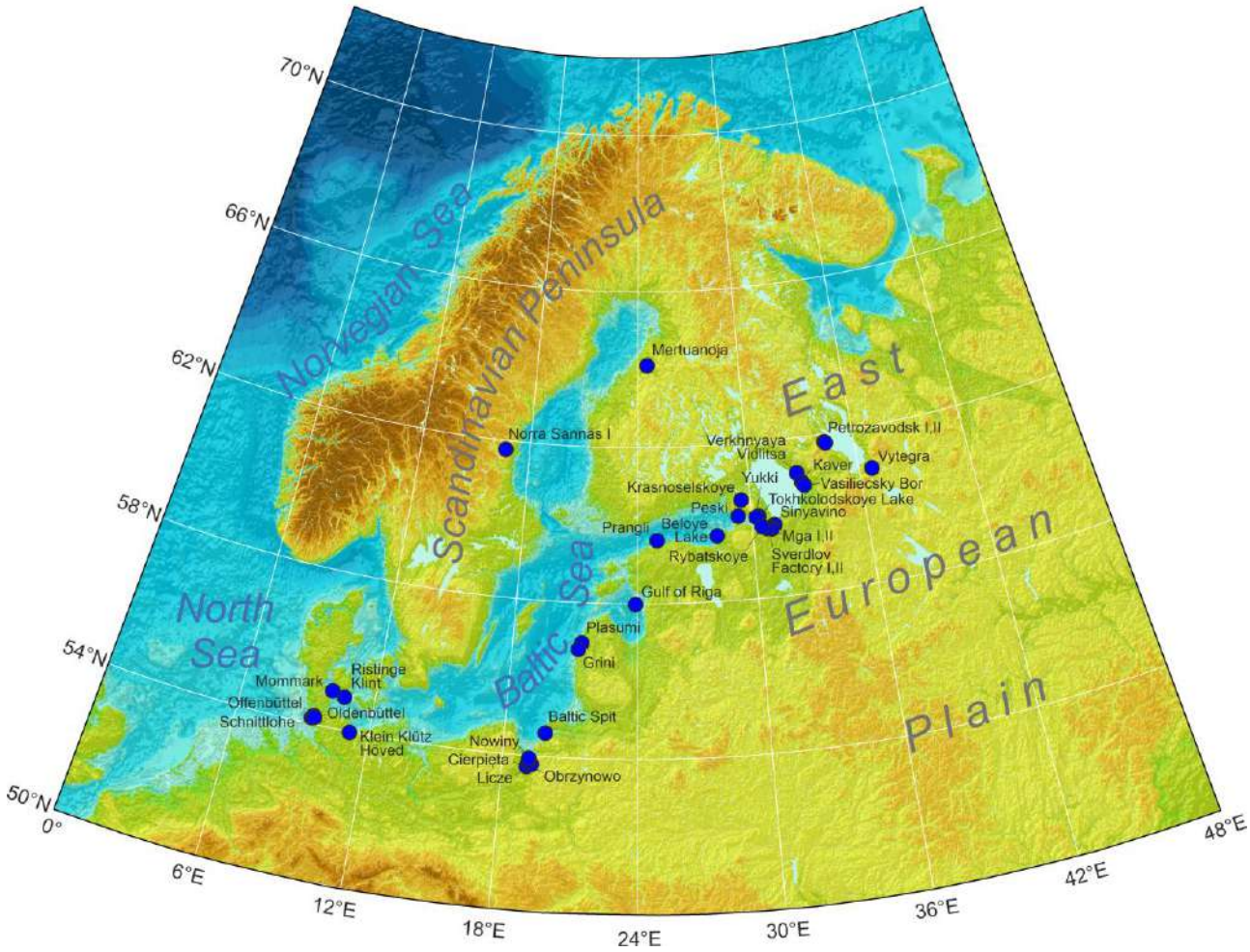

Fig. 7.1. Location map of reference Eemian (Mga) sections. The section examined by the author is titled ‘Sverdlov Factory II‘. Based on the ETOPO1 digital elevation model.

its westernmost to easternmost parts. According to data from the Sverdlov Factory quarry, the rapidly increasing marine influence in the *Quercus* zone (M_4) can be such a reference event, which appears in diatom and geochemical analytical data (Figs. 4.20, 4.21) and can be correlated with the boundary between the brackish (lagoonal) and marine phases in the Mga Sea history. Furthermore, the prominent Mn/Fe peak which records significant influx of oxygenated oceanic water into the Mga Sea likewise corresponds to this level (Fig. 4.23). The event was traced in different Mga Fm. localities, as well as elsewhere in the Baltic area, in 34 reference sections from the Kiel Canal (Germany) in the west to Lake Onego (Russia) in the east (Fig. 7.1). In addition to the above objectives, the cross correlation of the sections can reveal common trends in the LIG evolution of the Baltic and Mga Seas.

7.2. Reference sections of the Eemian (Mga) marine deposits in the Baltic and Onego-Ladoga regions

Reference sections of Eemian (Mga) marine sediments were selected proceeding from the availability of spore-pollen spectra for LIG deposits and were additionally characterized palaeontologically (diatoms, foraminifers, malacofauna, ostracods) to trace the development of the sea basin during the LIG. The obtained data for all sections allowed identifying the phases of the sea evolution, with reference to the division of E. A. Cheremisinova (1960): glaciomarine, brackish (lagoonal), marine, and regressive phases correlated then with regional pollen zones (Fig. 7.2). The basin history records in the Mga, Baltic, North, and White seas were cross correlated for the first time by Lavrova (1961), but the number of sampled sections has increased considerably since then and a more detailed review, with more numerous highlighted trends, has become possible.

7.2.1. Lake Onego

7.2.1.1. Vytegra

The Vytegra section (Figs. 7.1, 7.2) was stripped in two boreholes on the bank of the Vytegra River southeast of Lake Onego, near Novinki and Ivanovskoye Villages (Cheremisinova, 1952, 1962). The Mga marine deposits in the section may belong to an outlier of the upper moraine (Buslovich et al., 2002). The change from lacustrine to brackish deposition environments shows up in the *Pinus-Betula* zone (M_{2-3} in Grichuk, 1961). In this interval, freshwater diatoms (*Melosira (Aulacoseira) islandica* subsp. *helvetica*, *Melosira (Aulacoseira) distans*, *Melosira (Aulacoseira) granulata*) disappear being succeeded by brackish (*Coscinodiscus (Thalassiosira) lacustris* and *Thalassiosira baltica* var. *fluviatilis*) and marine (*Chaetoceros* spp., spores) species (Cheremisinova, 1962). *Thalassiosira baltica* var. *fluviatilis* represents 1–2°C water temperature and 8‰ salinity conditions (Cheremisinova, 1962).

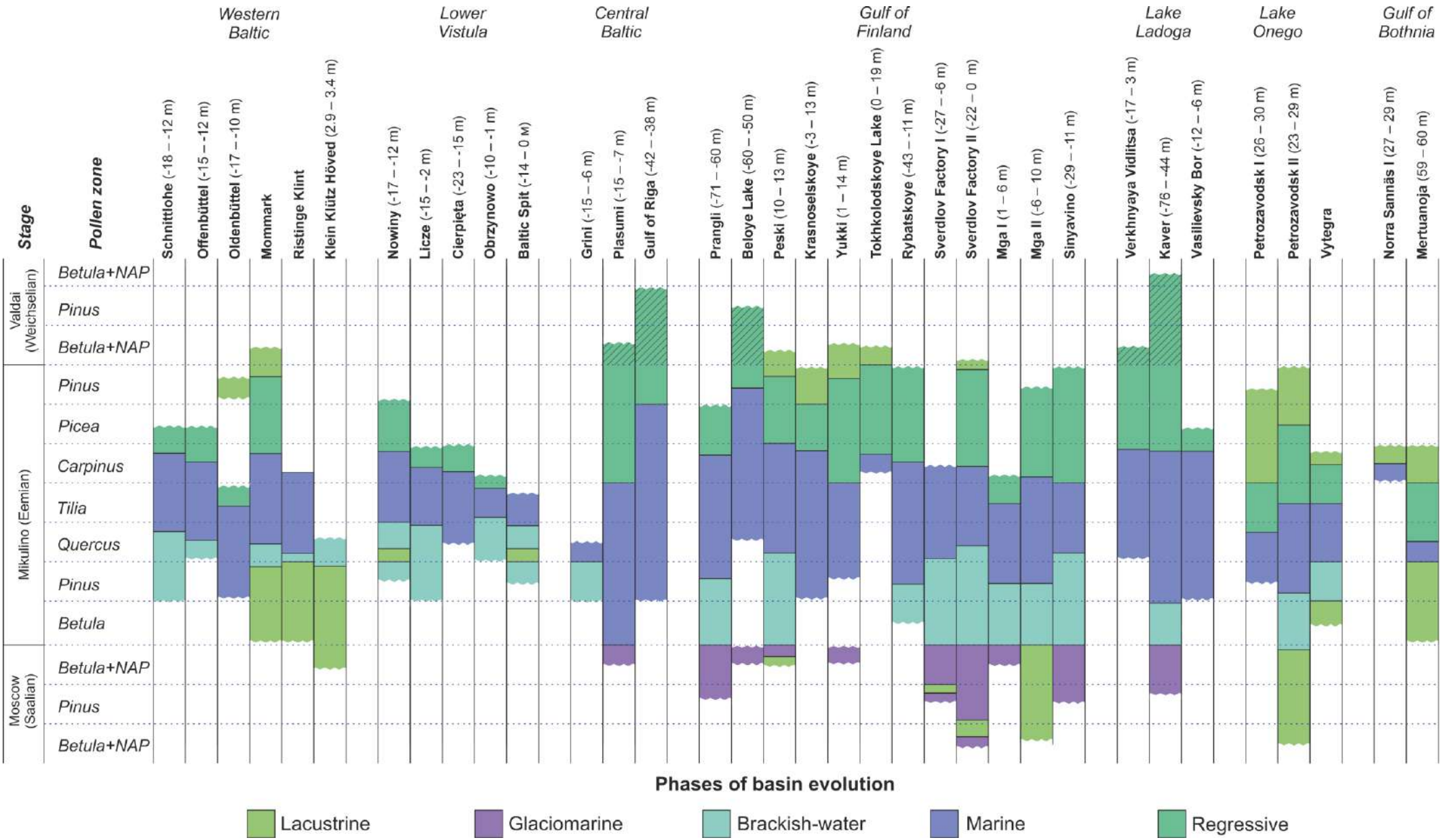

Fig. 7.2. Evolution of the Baltic and Mga basins during the LIG and the corresponding regional pollen zones, according to combined data from 34 reference sections. Numbers in parentheses are asl elevations of exposed marine sediments. Hatching indicates intervals of Lower Valdai (Lower Weichselian) deposits, the marine origin of which is uncertain.

The onset of the marine phase correlates with the appearance of deciduous forests (zones M_3–M_4). The clay deposited during maximum transgression contains abundant neritic plankton diatoms: *Coscinodis cus antiquus (Thalassiosira antiqua)*, *Coscinodiscus perforatus*, *Thalassiosira gravida*, *Chaetoceros* spp. (spores), and some other species.

The numbers and diversity of marine diatoms reduce in zone M_5 while brackish species, such as *Cosciodiscus (Thalassiosira) lacustris*, *Thalassiosira baltica, Thalassiosira baltica* var. *fluviatilis*, etc. become more abundant as evidence of beginning regression. Limnic conditions resume in zone M_6, judging by the presence of freshwater diatoms: *Melosira (Aulacoseira) islandica* subsp. *helvetica*, *Stephanodiscus astraea* and others.

7.2.1.2. Petrozavodsk I

The Petrozavodsk I section (Figs. 7.1, 7.2) was stripped by BH 3604 in Petrozavodsk city, on terrace I of Lake Onego, at 35.4 m asl (Devyatova, 1972). Diatoms appear above a core depth of 8.4 m corresponding to the *Pinus-Betula* (M_2 in Grichuk, 1961) zone (Devyatova, 1972; Devyatova, 1968, cited from Ikonen and Ekman, 2001). The diatom assemblage is dominated by marine species that record the marine phase of the Mga basin evolution: *Hyalodiscus scoticus, Opephora marina*, *Chaetoceros holsaticus, Chaetoceros mitra, Thalassionema nitzschioides*, etc. (Devyatova, 1968, cited from Ikonen and Ekman, 2001). Foraminifers appear at a slightly higher level (8.15 m), with *Buccella* ex gr. *frigida*, *Protelphidium orbiculare (Haynesina orbicularis), Elphidium subclavatum* and *Ammonia flevensis* as dominant species (Abrukina and Krasilnikova, 1972).

The development of foraminifers reaches its peak at a depth of 7.5 m (zone *Quercus-Ulmus,* M_{4b}). At the same time, the composition of the dominant diatom species changes to the following: *Actinocyclus octonarius, Actinocyclus octonarius* var. *tenellus, Actinocyclus octonarius* var. *intermedius*, *Coscinodiscus lacustris* var. *septentrionalis (Thalassiosira hyperborea* var. *septentrionalis), Hyalodiscus scoticus* and *Thalassionema nitzschioides* (Devyatova, 1972; Devyatova, 1968, cited from Ikonen and Ekman, 2001). The most abundant foraminifers in the assemblage include *Ammonia flevensis*, *Protelphidium* sp. and *Elphidium subclavatum* (Abrukina and Krasilnikova, 1972). Large quantities of marine mollusc shells were discovered between 7.35 and 5.5 m, including *Mutilus edulis*, *Tellina (Macoma) baltica*, *Tellina (Macoma) calcarea* and *Leda (Nuculana) pernula* (Devyatova, 1972).

In the end of the *Quercus-Ulmus-Carpinus* (M_5) zone (core depth 5.5 m), marine and brackish diatoms disappear and give way to freshwater taxa: *Melosira (Aulacoseira) islandica subsp. helvetica, Melosira (Aulacoseira) granulata, Cyclotella (Lindavia) comta*, etc. (Devyatova, 1968, cited from Ikonen and Ekman, 2001). Foraminifers disappear at 6.2 m (Abrukina and Krasilnikova, 1972).

7.2.1.3. Petrozavodsk II

The Petrozavodsk II section is located 550 m south of BH 3604 (Figs. 7.1, 7.2). The interglacial Mga Fm. lies over the Upper Moscow varved sediments containing *Aulacoseira islandica* as a dominant diatom species (40–100%) and some marine species: *Coscinodiscus lacustris f. septentrionalis (Thalassiosira hyperborea var. septentrionalis), Grammatophora arctica, Grammatophora marina* and *Grammatophora oceanica var. subtilissima* (Ikonen and Ekman, 2001). The percentages of marine and brackish diatoms vary in the range 1–22 %, but they may be allochthonous species (Ikonen and Ekman, 2001). Most of marine and brackish diatoms occur in the lower strata of the section corresponding to a warming interval, possibly correlated with the Kasplya Interstadial. Warmer conditions show up in pollen diagrams as higher percentages of *Pinus* and *Picea* and lesser amounts of *Betula sect. Albae*, *Betula nana, Betula humilis* and Chenopodiaceae.

Marine signatures are found in the *Pinus-Betula-NAP* zone, prior to the LIG, at a depth of 12.2–12.3 m, where *Thalassionema nitzschioides* diatoms common to marine environments appear and coexist with sporadic *Cibicides lobatulus (Lobatula lobatula)*, *Globigerina (Neogloboquadrina) pachyderma*, and *Guttulina (Laryngosigma) lactea*.

Higher salinity is reconstructed in the *Pinus–Betula* (M_{2-3} in Grichuk, 1961) zone at a depth of 11.0 m proceeding from the taxonomic change from freshwater to brackish and to marine diatom species. The assemblage is dominated by *Grammatophora oceanica* var. *subtilissima* (41 to 88%) in the early marine phase and by *Thalassionema nitzschioides* (up to 86%) in the second half. *Buccella tenerrima* and *Retroelphidium clavatum* are the most abundant among foraminifers.

The percentages of marine diatoms and formainifers peak in the *Alnus-Corylus* (M_5) zone and then decrease rapidly indicating the onset of regression. The regression diatom assemblage consists of *Coscinodiscus lacustris* f. *septentrionalis (Thalassiosira hyperborea* var. *septentrionalis)* reaching 70% and notable percentages of *Grammatophora oceanica* var. *subtilissima* and *Tabularia tabulata*. Foraminifers are mainly *Protelphidium pauciloculum* subsp. *albiumbilicatum (Cribroelphidium albiumbilicatum)* and *Buccella tenerrima*. No foraminifers were found above the 7.1 m depth, while marine and brackish diatoms almost disappear at 6.6 m (zone *Picea-Alnus-Carpinus*, M_{6-7}) where freshwater taxa appear (*Aulacoseira islandica, Ellerbeckia arenaria, Epithemia turgida*, etc.).

7.2.2. Lake Ladoga

7.2.2.1. Verkhnyaya Vidlitsa

BH 22 was drilled in the village of Verkhnyaya Vidlitsa on the eastern coast of Lake Ladoga. The wellhead is situated at an altitude of 18.5 m. Nedrigailova et al. (1971) identified a diatom flora with abundant development of marine forms in the depth range of 32.7–26.5 m, corresponding to the *Quercus – Carpinus* pollen zones (M_4–M_6 in Grichuk, 1961) (Nedrigailova et al., 1971; Devyatova, 1982;

Pleshivtseva, 2011b). The complex comprises of *Thalassiosira antiqua, Thalassiosira gravida, Coscinodiscus oculus-iridis, Coscinodiscus radiatus, Actinoptychus areolatus, Chaetoceros* sp. and *Thalassionema nitzschioides*. Additionally, littoral planktonic species such as *Hyalodiscus scoticus*, *Actinoptychus undulatus (senarius)* and *Actinocyclus echrenbergii (octonarius)* were observed in large numbers. This depth interval corresponds to the maximum transgression.

At a depth of 25.5 m in the *Carpinus* zone (M_6), the number of neritic diatom forms decreases while the littoral-planktonic species *Coscinodiscus (Lineaperpetua) lacustris* rapidly develops. The contribution of marine forms decreases markedly and that of freshwater forms increases. This complex indicates the beginning of sea regression. Diatoms were found up to a depth of 16.0 m, which corresponds to the base of the Lower Valdai sediments. However, the poor preservation of diatom valves in the depth range 20.5–16.0 m suggests possible redeposition of the material (Nedrigailova et al., 1971).

7.2.2.2. Kaver

In borehole section 78 on the eastern shore of Lake Ladoga, near Lake Kaver, marine planktonic diatoms occur in the Upper Moscow brown clays underlying the Mga Fm. (Nedrigailova et al., 1971). This interval belongs to the glaciomarine phase of the basin evolution.

The *Betula* zone (M_2 in Grichuk, 1961) corresponds to the brackish phase, and at the beginning of the *Pinus-Betula* zone (M_3) the rapid development of marine diatoms is observed (Nedrigailova et al., 1971; Pleshivtseva, 2011b). The dominant position is occupied by littoral planktonic *Actinoptychus undulatus (senarius)*, *Actinocyclus echrenbergii (octonarius), Melosira moninliformis* and the benthic *Diploneis interrupta*. Higher up in the section, neritic forms are most developed: *Thalassiosira antiqua*, *Thalassiosira gravida, Thalassiosira excentrica (eccentrica), Coscinodiscus oculus-iridis, Chaetoceros mitra, Chaetoceros* sp., *Actinoptychus areolatus, Thalassionema nitzschioides*, – as well as silicoflagellates and the littoral planktonic species *Actinoptychus undulatus (senarius)*.

In the upper part of the *Carpinus* zone (M_6), the deep-sea forms are replaced by littoral-planktonic species with a predominance of *Thalassiosira baltica, Coscinodiscus (Lineaperpetua) lacustris* and *Coscinodiscus curvatulus*, as well as the deep-sea form *Coscinodiscus divisus*. The change of complexes indicates the beginning of the regressive phase. In the upper half of the *Pinus* zone (M_8) the diatom flora is severely depleted, although individual valves are also found in the overlying Lower Valdai sediments (Nedrigailova et al., 1971; Pleshivtseva, 2011b).

7.2.2.3. Vasilievsky Bor

In the borehole section 83 drilled on the eastern shore of Lake Ladoga, in the village of Vasilievsky Bor, the brown and gray-green varved clay underlying the Mga Fm. contains fragments of valves of marine centric diatoms (Nedrigailova et al., 1971).

In the *Betula-Pinus* zone (M_2-M_3 in Grichuk, 1961) there is a sharp development of the diatom flora (Nedrigailova et al., 1971; Devyatova, 1982; Pleshivtseva, 2011b), which probably indicates the establishment of the marine phase. In the sediments of this phase, the most abundant species are *Thalassiosira gravida, Thalassiosira excentrica (eccentrica), Thalassiosira antiqua, Coscinodiscus lacustris (Thalassiosira hyperborea)* var. *septentrionalis, Actinoptychus undulatus (senarius)*, *Actinoptychus areolatus, Chaetoceros* sp. and *Thalassionema nitzschioides*.

In the *Carpinus* zone (M_6), the quantitative and species diversity of diatoms decreases, which may indicate the onset of marine regression.

7.2.3. Gulf of Finland

7.2.3.1. Mga I

The Mga I section in BH 3 on the bank of the Mga River (Figs. 7.1, 7.2) contains marine diatoms in the Upper Moscow varved clay beneath the Mga Fm. (Cheremisinova, 1959). The diatom assemblage of the glaciomarine phase consists of cold-water (*Cocconeis disculus*, *Diploneis domblittensis*) and some marine (*Hyalodiscus scoticus*, *Grammatophora oceanica* var. *macilenta*) species. Diatoms are mainly benthic, i.e., the sea depth of that time was around 20 m (Cheremisinova, 1959). Marine foraminifers appear at the top of the varved sequence, with *Elphidium subclavatum* reaching 100% (Nedesheva, 1972).

The brackish phase begins from the early Mikulino Interglacial. The respective diatom assemblage includes predominant *Thalassiosira baltica, Achnanthes taeniata, Coscinodiscus curvatulus*, and some other species which record 1–3°C water temperatures and 4–8‰ salinity (Cheremisinova, 1959). *Protelphidium parvum* makes up to 83% of brackish foraminifers (Nedesheva, 1972).

The marine phase corresponds to the *Pinus-Betula* (M_3 in Grichuk, 1961) interval and is recorded in the diatom assemblage as the presence of marine neritic and oceanic taxa (*Thalassiosira gravida, Chaetoceros* spp. (spores) and *Coscinodiscus* genus reaching 90 % in total). The assemblage indicates high salinity (25–30‰) and a sea depth at least 50–75 m (Cheremisinova, 1959). Foraminifers become notably more abundant in the beginning of the marine phase, and their assemblage includes *Elphidium subclavatum, Protelphidium parvum, Bucella frigida, Miliolinella* cf. *subrotunda* and *Quinqueloculina (Miliolinella) circularis* as dominant species (Nedesheva, 1972).

The onset of regression falls within the middle *Quercus-Ulmus-Corylus* (M_{4-5}) zone. The diatom assemblage of the regressive phase consists of brackish euryhaline species (*Coscinodiscus lacustris* var. *septentrionalis, Thalassiosira baltica* var. *fluviatilis, Coscinodiscus curvatules, Achnanthes taeniata*) coexisting with freshwater to brackish species of *Epithemia sorex*, *Epithemia turgida*, which record decreasing salinity. Foraminifers are mainly (73%) *Elphidium subclavatum* (Nedesheva, 1972).

7.2.3.2. Rybatskoye

The Rybatskoye section stripped in BH 47 near Rybatskoye Village (Figs. 7.1, 7.2) contains saline-water species in the lower strata of the Mga Fm. (beginning of *Pinus-Betula* or M_{2-3} zone in Grichuk, 1961) (Lavrova and Grichuk, 1960; Znamenskaya and Cheremisinova, 1962). The diatom assemblage of the brackish phase is dominated by marine (*Grammatophora* and *Melosira moniliformis*) and brackish (*Diploneis smithii* and *Synedra tabulate*) species.

The base of the marine phase is easily detectable 2 m further upsection in the middle of the *Pinus-Betula* (M_{2-3}) zone from the appearance and growing abundance of marine and brackish diatoms: *Thalassiosira gravida, Thalassionema nitzschioides, Chaetoceros* spp. (spores), *Rhabdonema arcuatum, Coscinodiscus* spp., etc. The depth of the Mga basin during the maximum transgression inferred from the diatom taxonomy is at least 80–100 m (Znamenskaya and Cheremisinova, 1962).

In the *Carpinus* (M_6) zone, marine diatoms become markedly less abundant and are succeeded by brackish taxa: *Synedra tabulata, Thalassiosira baltica, Coscinodiscus lacustris*, etc. Freshwater species appear at higher levels, in the *Pinus-Betula-Picea* (M_8) zone: *Pinnularia* spp., *Diploneis domblittensis* and some others, while the counts of brackish species reduce.

7.2.3.3. Sinyavino

The Sinyavino section (Figs. 7.1, 7.2) contains freshwater and brackish (*Epithemia sorex, Epithemia turgida, Epithemia zebra (adnata)*), as well as sporadic marine (*Thalassiosira gravida, Chaetoceros* spp., spores) diatoms in the Kasplya Interstadial of the Moscow Glacial (Malakhovsky et al, 1966, 1969a). Moreover, the glaciomarine phase is marked by cold-loving freshwater species, such as *Cocconeis disculus, Diploneis domblittensis* var. *subconstricta (Diploneis burgitensis)* and *Navicula (Cavinula) scutelloides.*

The onset of the brackish phase corresponds to the base of the *Pinus-Betula* (M_{2-3} in Grichuk, 1961) zone, i.e., to the beginning of the Mikulino Interglacial. The diatom assemblage is dominated by marine and brackish species: *Diploneis didyma, Diploneis interrupta, Campylodiscus echeneis, Chaetoceros* spp. (spores), etc.

Marine signatures become notable in the beginning of the *Quercus-Ulmus* (M_4) zone. The marine phase is marked by the presence of marine planktonic taxa, especially *Thalassiosira gravida, Thalassionema nitzschioides, Chaetoceros* spp. (spores) and some others.

The onset of regression shows up in the upper portion of the *Carpinus-Tilia* (M_{5-6}) zone, where marine diatoms become less abundant while brackish taxa increase. Diatoms are mainly *Thalassiosira baltica, Thalassiosira baltica* var. *fluviatilis, Coscinodiscus lacustris* var. *septentrionalis (Thalassiosira hyperborea var. septentrionalis), Coscinodiscus (Thalassiosira) lacustris*, etc.

7.2.3.4. Sverdlov Factory I

The Sverdlov Factory I section stripped in BH 10 (Figs. 7.1, 7.2) contains brackish diatoms within the Kasplya Interstadial (Pleshivtseva et al., 1984). The diatom assemblage at a core depth of 38.0 m mainly consists of benthic species *Fragilaria inflata (Pseudostaurosira brevistriata* var. *inflata)*, *Diploneis domblittensis, Navicula (Cavinula) scutelloides*, etc. and *Nitzschia (Tryblionella) navicularis* common to brackish habitats. At a depth of 37.6 m, in the end of the Kasplya Interstadial, species that live in brackish and brackish to freshwater environments are absent from the diatom assemblage while freshwater benthic *Epithemia zebra (adnata)* becomes a dominant species. This change indicates dilution with fresh water (Pleshivtseva et al., 1984). The conditions change again during the Kattegat Stadial, when freshwater diatoms are sporadic but *Grammatophora oceanica* and other marine species predominate in the assemblage.

The Mga interglacial clay deposition began with the onset of the brackish phase. The diatom assemblage of that time is taxonomically poor, limited to sporadic marine taxa of *Melosira (Paralia) sulcata, Melosira moniliformis* and some others.

The greater role of marine deposition shows up in higher abundances of marine diatoms and in the appearance of neritic (sublittoral) and littoral species in the beginning of the *Quercus-Ulmus-Alnus* (M_{4-5} in Grichuk, 1961) zone (Pleshivtseva et al., 1984, Pleshivtseva, 2023). The assemblage of maximum transgression has highest percentages of *Coscinodiscus lacustris* var. *septentrionalis (Thalassiosira hyperborea* var. *septentrionalis)* and *Chaetoceros* sp.

The beginning of regression is hard to time in the Sverdlov Factory I section, because the upper strata of the Mga Fm. bear both marine and freshwater diatoms, with overlapping peaks. The second peak of the *Carpinus* in the *Picea* (M_7) zone indicates that the pollen was redeposited from the sediments below (Pleshivtseva et al., 1984, Pleshivtseva, 2023). Therefore, marine diatoms are partly allochthonous as well.

7.2.3.5. Mga II

Sediments in the Mga II section (Figs. 7.1, 7.2) lie over varved clay that bear both freshwater and marine diatom species, though the frustules of marine diatoms are poorly preserved and were considered (Pleshivtseva et al., 1984) to be allochthonous. Meanwhile, freshwater diatoms (*Pinnularia lata*, *Pinnularia borealis, Hantzschia amphioxys*, etc.) remain well preserved. The deposition patterns in this section are similar to those observed in other sections from the Neva Lowland (Mga I, Sinyavino, Sverdlov Factory), with the upper Sverdlov Fm. deposited in brackish water conditions.

The marine effect becomes slightly better pronounced in the *Pinus-Betula* (M_2 in Grichuk, 1961) zone (Pleshivtseva et al., 1984; Pleshivtseva, 2011a), where the brackish diatom assemblage contains predominant *Thalassiosira gravida, Hyalodiscus scoticus, Actinocyclus ehrenbergii (octonarius)* and some other species. At the same time, freshwater diatoms, such as *Cocconeis disculus* var. *diminuta*

(Cocconeis neodiminuta), *Navicula (Cavinula) scutelloides* and *Epithemia zebra (adnata)*, become more abundant in the upper M_2 zone.

The onset of the marine phase falls within the *Pinus-Betula-Quercus* (M_3) zone where marine diatoms reach 60–80 species in a sample while freshwater species are fewer. The main assemblage of marine diatoms consists of *Melosira (Paralia) sulcata*, *Hyalodiscus scoticus, Cocconeis scutellum, Grammatophora oceanica, Chaetoceros* sp., *Thalassiosira gravida*, and *Actinoptychus undulatus (senarius)*.

The sea level fall began in the interval of the *Carpinus-Picea* (M_{6-7}) zone, judging by rapid decrease in littoral and sublittoral species, greater abundances of brackish *Cyclotella caspia* and *Synedra (Tabularia) tabulata*, and appearance of some freshwater diatoms.

7.2.3.6. Krasnoselskoye

The Krasnoselskoye section in the Karelian Isthmus (Figs. 7.1, 7.2) bears signatures of deepwater marine conditions in the beginning of the *Pinus-Betula-Quercetum mixtum* (M_3 in Grichuk, 1961) zone (Sokolova et al., 1972) but lacks any record of the glaciomarine and brackish phases. The maximum transgression diatom assemblage consists mainly of *Hyalodiscus scoticus*, *Thalassiosira gravida*, *Chaetoceros affinis, Chaetoceros mitra, Chaetoceros subsecundus*,and *Dictyocha fibula.*

In the end of the *Carpinus* (M_6) zone, marine diatoms reduce while brackish euryhaline *Coscinodiscus lacustris* var. *septentrionalis (Thalassiosira hyperborea* var. *septentrionalis)* and cold-loving marine *Coscinodiscus curvatulus* var. *minor* that lives within the shelf become predominant. This taxonomic change marks the onset of regression. Marine and brackish species almost disappear in the beginning of the *Pinus-Betula* (M_8) zone and give way to freshwater diatoms, such as *Cocconeis pediculus*, *Cocconeis placentula, Diploneis domblittensis* var. *subconstricta (Diploneis burgitensis)* and others, which represent the conditions of a shallow cold lake (Sokolova et al., 1972).

7.2.3.7. Yukki

In the Yukki section (Figs. 7.1, 7.2), marine diatoms are found in varved clay of the Moscow Late Glacial (Vishnevskaya et al., 1973). The diatom assemblage of the glaciomarine phase contains predominant cold-loving inhabitants of freshwater glacial lakes (*Cocconeis disculus* and *Diploneis domblittensis* var. *subconstricta (Diploneis burgitensis)*) coexisting with marine *Thalassiosira gravida*.

The section lacks any record of the brackish phase, possibly, because the basal strata were eroded, and interglacial sediments begin from the *Pinus-Betula-Quercetum mixtum* (M_3 in Grichuk, 1961) zone. The marine phase of the Mga basin shows up in typical diatom species of *Hyalodiscus scoticus*, *Thalassiosira gravida* and *Distephanus (Octactis) speculum*.

Marine species become fewer while brackish species increase in the end of the *Quercus-Ulmus-Corylus-Alnus* (M_{4-5}) zone. The regression diatom assemblage is dominated by brackish *Diploneis*

didyma, Diploneis interrupta, Coscinodiscus lacustris var. *septentrionalis (Thalassiosira hyperborea var. septentrionalis), Coscinodiscus curvatulus var. minor*, marine *Hyalodiscus scoticus* and freshwater *Epithemia turgida*. However, the brackish and marine species almost disappear in the end of the *Pinus* (M_8) zone while freshwater diatoms appear instead: *Cocconeis pediculus*, *Diploneis domblittensis var. subconstricta (Diploneis burgitensis)*, and *Cymbella (Reimeria) sinuate*.

7.2.3.8. Lake Tokhkolodskoye

A diatom assemblage of the maximum transgression in the Lake Tokhkolodskoye section (Figs. 7.1, 7.2) was found in the *Carpinus-Picea* (M_{6-7} in Grichuk, 1961) zone (Pleshivtseva et al., 1984). The diatoms are mainly neritic *Thalassiosira gravida* and *Chaetoceros sp.,* littoral plankton *Hyalodiscus scoticus* and benthic *Grammatophora oceanica* taxa.

The taxonomic diversity of marine diatoms reduces in the second half of the *Carpinus-Picea* (M_{6-7}) zone, possibly, as a result of beginning regression; *Coscinodiscus lacustris var. septentrionalis (Thalassiosira hyperborea* var. *septentrionalis)* and *Thalassiosira baltica* become predominant in the *Pinus* (M_8) zone. *Thalassiosira baltica* is common to sea domains with less saline water or to river estuaries (Pleshivtseva et al., 1984).

7.2.3.9. Peski

The Upper Moscow deposits of the Peski section in the northern coast of the Neva Bay (Figs. 7.1, 7.2) contain a brackish assemblage of dinoflagellates that record water salinity of 10–15 ‰ (Miettinen et al., 2014), mainly *Operculodinium centrocarpum (Protoceratium reticulatum)* and less abundant *Lingulodinium machaerophorum (Lingulodinium polyedra)*, coexisting with *Pediastrum* algae. The brackish deposits lie over a clay layer free from dinoflagellates but containing freshwater *Pediastrum* and *Botryococcus* microalgae.

The brackish phase corresponds to the time span of the *Pinus-Betula-Salix* (M_2) and *Pinus-Betula-Quercus* (M_3 in Grichuk, 1961) zones with a microflora composition similar to that of the glaciomarine phase (Miettinen et al., 2002; 2014).

The onset of the marine phase correlated with the lower half of the *Quercus-Ulmus* (M_4) zone marked by the appearance and wide spread of marine (mainly planktonic) diatoms, such as *Thalassionema nitzschioides, Grammatophora marina, Chaetoceros* spp., and *Thalassiosira gravida*. Dinoflagellates are mainly *Lingulodinium machaerophorum (Lingulodinium polyedra)* that live at water salinity above 15‰ (Miettinen et al., 2014). The assemblage of foraminifers with predominant *Elphidium excavatum* indicates that the sea water salinity exceeded 20‰ (Miettinen et al., 2014).

The percentages of brackish diatom species (*Thalassiosira hyperborea* + var., *Thalassiosira baltica*) increase in the beginning of the *Picea-Pinus* (M_{7-8}) zone while marine species become less abundant thus indicating shallower sea depths. In the end of the *Picea-Pinus* (M_{7-8}) zone, marine and

brackish diatoms disappear abruptly while freshwater species (*Pinnularia* spp., *Eunotia* spp.) appear in abundance.

7.2.3.10. Lake Beloye

The early LIG deposits in the Lake Beloye (White) section in the Kurgalsky Peninsula (Figs. 7.1, 7.2) were eroded (Shmayonok et al., 1962; Apukhtin and Sammet, 1967). The marine phase begins in the *Pinus-Betula-Quercetum mixtum* (M_3 in Grichuk, 1961) zone where diatom assemblages include species typical of transgression conditions: *Grammatophora oceanica* var. *macilenta (Grammatophora macilenta), Thalassiosira gravida, Hyalodiscus scoticus*, *Coscinodiscus (Thalassiosira) lacustris*, *Nitzschia (Tryblionella) punctata*. The maximum transgression apparently corresponds to the latest *Carpinus* (M_6) and earliest *Picea* (M_7) zones, when marine neritic species (*Dictyocha fibula* and *Chaetoceras* spp) become especially abundant.

The diatom count decreases considerably up the section: from 85 to 30% in the middle of the *Pinus-Picea-Betula* (M_8) zone, with largest percentages of freshwater to brackish species *Stephanodiscus astraea* and *Stephanodiscus astraea* var. *intermedius* (*Cyclostephanos mansfeldensis*). The freshwater taxa (*Melosira (Aulacoseira) islandica* subsp. *helvetica, Fragilaria spp.* and others) become predominant in the end of the *Pinus-Picea-Betula* (M_8) zone.

7.2.3.11. Prangli

The Prangli section in the neck of the Gulf of Finland, in northern Estonia (Figs. 7.1, 7.2), stores a record of the glaciomarine phase in the Mga deposits (Cheremisinova, 1961; Liivrand and Valt, 1966; Liivrand, 1987). Influx of seawater into the glacial lake occurred during the Kasplya Interstadial, as in the Neva Lowland. The glaciomarine diatom assemblage includes relict cold-loving freshwater species, typical inhabitants of glacial lakes, now almost extinct (*Cocconeis disculus*, *Diploneis domblittensis*, *Diploneis domblittensis var. subconstricta (Diploneis burgitensis)*), as well as shallow marine taxa, such as *Grammatophora* sp., *Hyalodiscus scoticus*, *Diploneis smithii*, etc.

The diatom flora of the brackish phase initiated with the onset of interglacial conditions is similar to that of the glaciomarine phase.

The change from the diatoms that live in fresh and low-salinity water to marine species is clearly detectable at a depth of ~75 m (Cheremisinova, 1961), in the interval of the *Pinus-Betula* (M_3 in Grichuk, 1961) zone (Liivrand and Valt, 1966). The maximum transgression is marked by *Melosira (Paralia) sulcata, Actinocyclus ehrenbergii (octonarius), Hyalodiscus scoticus*, *Chaetoceras* spp. (spores), *Rhabdonema arcuatum*, *Grammatophora sp*., *Synedra tabulata (Tabularia fasciculata)*, and some other diatom species, which live in normal salinity conditions (Cheremisinova, 1961).

The regressive phase apparently begins in the *Carpinus-Picea* (M_{6-7}) zone when marine diatoms reduce progressively and are succeeded by freshwater *Melosira arctica*, *Pinnularia* spp., etc.

7.2.4. Gulf of Bothnia

7.2.4.1. Mertuanoja

The Mertuanoja section in Finland, in the northern Gulf of Bothnia (Figs. 7.1, 7.2), contains diatoms that first appear in the *Betula* zone (Eriksson et al., 1999). The diatom assemblage is dominated by freshwater species (*Aulacoseira islandica*, *Aulacoseira valida, Cyclotella iris*) but also includes marine *Grammatophora oceanica* and *Hyalodiscus scoticus* species.

The maximum transgression corresponds to the beginning of the *Pinus-Betula-Quercus* zone, and the sediments deposited at that time contain an assemblage of marine and brackish diatoms, with especially frequent *Chaetoceros mitra*, *Grammatophora oceanica* and *Rhabdonema arcuatum*. The dinoflagellate assemblage of the interval comprises 54.5% *Chytroeisphaeridia (Leiosphaeridia) chytroeides* and 16.0% *Operculodiniurn centrocarpurn (Protoceratium reticulatum)*.

Diatoms (as well as dinoflagellates) become markedly fewer in the middle of the *Pinus-Betula-Quercus* zone and freshwater species of *Aulacoseira islandica, Cyclotella krammeri, Cyclotella iris* and *Pinnularia* spp. appear in the diatom assemblage. The percentage of marine diatoms decreases gradually till the beginning of the *Picea-Betula-NAP* zone where marine and brackish diatoms disappear almost completely while freshwater species become widespread (*Pinnularia borealis*, *Pinnularia lata*, *Orthoseira roseana*, etc.).

7.2.4.2. Norra Sannäs I

The Norra Sannäs I section in the southwestern coast of the Gulf of Bothnia in Sweden (Figs. 7.1, 7.2) includes sediments deposited during the Eemian maximum transgression correlated with the *Betula-Alnus-Picea-Corylus* (E_5 in Andersen, 1975) zone (Robertsson et al., 1997). Marine and brackish diatoms in these sediments reach 95% of the total count, with dominant species of *Chuctoceros* spp. (spores), *Grammatophora oceanica var. macilenta, Paralia sulcata* and *Hyalodiscus scoticus*; 79% of all diatoms are planktonic species.

Marine and brackish diatoms give way to freshwater species at a depth of 17.1 m, within the same pollen zone. No intermediate regression phase was detected in the section. The freshwater diatom assemblage is mainly composed of *Cyclotella operculata (distinguenda)* var. *unipunctata, Cyclotella (Pantocsekiella) ocellata*, *Cyclotella (Lindavia) comta* and *Aulacoseira italica*.

7.2.5. Central Baltic

7.2.5.1. Gulf of Riga

The Gulf of Riga section stripped by BH 21 (Figs. 7.1, 7.2) contains a rich diatom assemblage within the *Pinus-Quercetum mixtum* (E_3 zone in Liivrand, 1991) interval (Kalnina, 2001) but the sediments below this zone are free from diatoms. The most widespread marine diatoms are *Paralia sulcata, Grammatophora oceanica, Hyalodiscus scoticus* and *Thalassionema nitszchoides*.

Diatoms notably decrease in abundance and diversity in the second half of the *Picea-Abies* (E_7) zone, which is evidence of brackish conditions persisting as long as the end of the LIG.

7.2.5.2. Plasumi

The Plasumi section in the western coast of Latvia (Figs. 7.1, 7.2) contains brackish diatoms and foraminifers in the Upper Saalian varved clay lying beneath the Eemian deposits (Kalnina, 2001). The diatom assemblage of the glaciomarine phase is dominated by *Epithemia zebra (adnata)* and *Actinocyclus octonarius*. The assemblage of foraminifers consists of *Elphidium excavatum* f. *clavata (Elphidium clavatum)*, *Cassidulina reniforme*, *Buccella frigida*, *Bucella hannai arctica (Buccella floriformis)*, and *Elphidium (Cribroelphidium) albiumbilicatum*.

The brackish phase left no record in the Plasumi section, as marine conditions set in already early during the LIG, with the respective diatom assemblage composed of mesohalobous (salinity 5–18‰) and polyhalobous (salinity 18–30‰) species (Kalnina, 2001). The former are mainly *Grammatophora oceanica*, *Hyalodiscus scoticus*, *Paralia sulcata* and *Rhabdonema arcuatum* and the latter include *Actinoptychus senarius*, *Chaetoceros* spp, *Navicula (Lyrella) abrupta*, *Podosira* sp. and *Thalassionema nitzschioides*. The taxonomic composition of foraminifers (*Bulimina marginata*, *Cassidulina laevigata* var. *carinata (Cassidulina carinata)*, *Elphidium excavatum* subsp. *boreale (Retroelphidium boreale)*, etc.) likewise corresponds to marine conditions, while relatively high percentages of *Haynesina orbiculare (orbicularis)* indicate that the sea depth was about 15 m.

Foraminifers decrease in the beginning of the *Carpinus-Taxus-Ilex* (E_6 in Liivrand, 1991) zone, which may be evidence of beginning regression. The predominant species are the same as in the marine phase, and *Cibicides lobatulus (Cibicides lobatulus)* appears additionally. The diatom assemblage does not change much during the regression phase. The brackish conditions held as long as the latest LIG.

7.2.5.3. Grini

The Grini section located ~20 km south of Plasumi (Figs. 7.1, 7.2) contains marine diatoms in the beginning of the *Pinus* (E_2 in Liivrand, 1991) zone (Kalnina, 2001). Brackish diatoms are mainly *Cocconeis disculus*, *Diploneis domblittensis*, *Pinnularia* spp., *Epithemia* spp. and *Hyalodiscus scoticus.*

The diatoms show taxonomic changes in the *Alnus-Quercus-Corylus* (lower E_4) zone (Kalnina, 2001), where *Paralia sulcata*, *Hyalodiscus scoticus*, *Actinocyclus ehrenbergii (octonarius)* and *Grammatophora oceanica* are typical representatives of the assemblage, whereas the *Ulmus-Fraxinus* (upper E_4) zone lacks diatoms at all.

7.2.6. Lower Vistula

7.2.6.1. Baltic Spit

The interglacial sediments in the Baltic Spit section, Kaliningrad Oblast, stripped in BH 23 (Figs. 7.1, 7.2) lie over diatom-free varved clay. Marine diatoms first appear in the *Pinus-Betula-Quercetum*

mixtum (E_{2-3}, in Mamakova, 1988) zone (Znamenskaya and Cheremisinova, 1970). The brackish assemblage is dominated by *Opephora (Staurosirella) martyi, Fragilaria* spp.*, Melosira (Aulacoseira) granulata, Stephanodiscus astraea* and *Grammatophora* sp. The diatom taxonomy corresponds to a shallow low-salinity sea in the beginning of the interglacial transgression.

In the beginning of the *Corylus-Quercus-Tilia* zone (E_4), the sea receded, leading to the accumulation of peat that measures 75 cm in thickness. The peat comprises a variety of freshwater diatoms, with predominance of *Epithemia* spp., *Melosira (Aulacoseira) italica*, *Meridion circulare* and *Synedra (Ulnaria) ulna*. In the same pollen zone, a subsequent sea incursion happened.

The brackish phase continued to a depth of 11-12 m (*Corylus* peak), with the maximum development of marine diatoms such as *Coscinodiscus antiquus (Thalassiosira antiqua)*, *Coscinodiscus* spp., *Actinocyclus ehrenbergii (octonarius)*, and some others. Accordingly, there is a significant decrease in the percentages of freshwater forms.

7.2.6.2. Nowiny

The brackish deposits in the Nowiny section (Figs. 7.1, 7.2) were formed in the beginning of the Eemian Interglacial (Makowska, 1986). They contain a poor assemblage of molluscs with *Cardium paucicostatum (Acanthocardia paucicostata)*, *Corbula gibba (Varicorbula)*, and *Nassa (Tritia) reticulata*. Peat with freshwater mollusc fauna (mainly *Bithynia tentaculata*) at the boundary of the *Pinus-Betula-Ulmus* (E_2 in Mamakova, 1988) and *Quercus-Corylus* (E_3) zones indicates shoaling. In the *Quercus-Corylus* (E_3) zone, peat changes to sapropel and then to sand, while molluscs show an abrupt decrease in freshwater and increase in marine and brackish species. Up to 61.6 m in depth the dominant molluscs are consist of *Corbula (Varicorbula) gibba*, *Hydrobia (Peringia) ulvae*, *Rissoa membranacea*, *Spisula subtruncata*, *Nassa (Tritia) reticulata*, *Bittium reticulatum* and several others.

Deep-water conditions are observed in the *Corylus-Quercus-Tilia* (E_4) zone. The most widespread molluscs in the maximum transgression interval include *Corbula (Varicorbula) gibba*, *Cardium (Acanthocardia) paucicostatum, Cardium lamarcki (Cerastoderma glaucum)* and *Eulimella (Ebala) nitidissima* indicating seawater salinity around 25‰ (Funder et al., 2002).

Regression signatures appear in the *Carpinus-Corylus-Alnus* (E_5) zone (Makowska, 1986). The molluscs of the regression phase are mainly *Corbula (Varicorbula) gibba* and *Spisula subtruncata* in the lower strata and *Mytilus edulis* и *Cardium lamarcki (Cerastoderma glaucum)* up the section. The last marine molluscs and foraminifers appear in the beginning of the *Pinus* (E_7) zone.

7.2.6.3. Licze

The brackish phase in the Licze section (Figs. 7.1, 7.2) follows the limnic phase where freshwater molluscs (*Valvata piscinalis*, *Planorbis planorbis, Bithynia tentacula, Pisidium* sp.) (Makowska, 2001, cited from Head et al., 2005) and ostracods (Knudsen et al., 2012) are of broad occurrence. Brackish

dinoflagellates, foraminifers, and ostracods appear in the *Pinus-Betula* (E_1 in Mamakova, 1988) or *Pinus-Betula-Ulmus* (E_2) zones (Head et al., 2005; Knudsen et al., 2012). Dinoflagellates are mainly *Lingulodinium machaerophorum, Spiniferites bentorii (Gonyaulax digitale)* and *Spiniferites* indet. (Head et al., 2005). The salinity of near-surface water during that interval inferred from the dinoflagellate taxonomy was 10–15‰. The dominant foraminifers are *Ammonia beccarii, Elphidium excavatum* f. *selseyensis, Haynesina germanica, Elphidium (Cribroelphidium) gunteri, Buccella frigida*, etc. species (Knudsen et al., 2012), which coexist with marine molluscs *Hydrobia (Peringia) ulvae, Bittium reticulatum, Macoma balthica, Mytilus edulis*, etc. (Makowska, 2001, cited from Head et al., 2005).

The sediments in the *Corylus-Quercus-Tilia* (E_4) zone bear signatures of sealevel rise (Head et al., 2005; Knudsen et al., 2012). The diatom assemblage mainly consists of marine species, especially *Paralia sulcata*, *Cymatosira belgica*, *Diploneis didyma (didymus)* and *Plagiogramma minus* (Knudsen et al., 2012), but the percentages of freshwater diatoms (Knudsen et al., 2012) and *Pediastrum* (Head et al., 2005) are also significant, which is evidence of riverine inputs. According to the taxonomic composition of diatoms, the sea water salinity was the highest (~28‰) in the beginning of the marine phase and then decreased progressively (Knudsen et al., 2012). The count of dinoflagellates becomes tens of times greater in marine conditions (Head et al., 2005). The percentages of *Spiniferites bentori* (*Gonyaulax digitalis*) become 30% higher while *Lingulodinium machaerophorum* undergo 15% reduction. The salinity inferred from dinoflagellate data was also the highest in the beginning of the marine phase (> 22‰). The increase of dinoflagellate counts is synchronous with increase in foraminifers (Knudsen et al., 2012), especially, *Elphidium excavatum*, *Haynesina orbiculare (orbicularis)* and *Elphidium (Cribroelphidium) incertum* and ostracods (*Leptocythere* spp. and *Semicytherura sella*). The mollusc fauna includes *Cerastoderma edule*, *Corbula gibba*, *Venerupis (Polititapes) aurea senescens, Mytilus edulis*, etc. (Makowska, 2001, cited from Head et al., 2005).

The onset of regression apparently corresponds to the middle *Carpinus-Corylus-Alnus* (E_5) zone, where the dinoflagellate count decreases markedly, as well as *Spiniferites bentori* (*Gonyaulax digitalis*) (Head et al., 2005), while the percentages of *Spiniferites* indet. and *Pediastrum* increase. The dinoflagellate taxonomy records salinity above 15‰. The diatom assemblage contains higher percentages of freshwater species: *Fragilaria (Staurosira) construens, Fragilaria (Staurosirella) pinnata* and *Martyana (Staurosirella) martyi* (Knudsen et al., 2012). The salinity inferred from diatom data decreases gradually from ~20‰ in the beginning of the E_5 zone to ~7‰ in its end. The counts of foraminifers reduce considerably in the beginning of the E_5 zone, while the percentages of *Ammonia beccarii*, *Haynesina germanica, Elphidium excavatum* and *Elphidium (Cribroelphidium) albumbilicatum* increase (Knudsen et al., 2012). The taxonomy of foraminifers corresponds to water salinity at least 22‰. Furthermore, the deposits of the regression phase bear a rich ostracod assemblage

with predominant *Cyprideis torosa*, *Leptocythere* spp. and *Hirchmannia viridis* (Knudsen et al., 2012). The mollusc assemblage contains the same species as in the marine phase till the depth 94.55 m (upper zone E_5), but freshwater molluscs *Anisus spirorbis* and *Valvata piscinalis* predominate up the section (Makowska, 2001, cited from Head et al., 2005).

7.2.6.4. Obrzynowo

Signatures of brackish conditions are observed in the *Pinus-Betula-Ulmus* (E_2 in Mamakova, 1988) zone (Knudsen et al., 2012) in the Obrzynowo section located ~10 km ENE of the Licze site (Figs. 7.1, 7.2). The foraminifers of the brackish phase are mainly *Ammonia beccarii, Elphidium williamsoni, Haynesina germanica, Buccella frigida* and *Elphidium (Cribroelphidium) guntheri* in the lower strata, but the percentages of these species decrease up the section where *Elphidium (Cribroelphidium) albiumbilicatum* becomes predominant. Foraminifers record a salinity of <20‰. Brackish deposits also contain *Cyprideis torosa* ostracods and a diatom assemblage with dominant species of *Actinoptychus senarius, Paralia sulacata, Diploneis didyma (didymus)* and *Grammatophora oceanica* indicating ~20‰ salinity.

The salinity was slightly higher in the beginning of the *Corylus-Quercus-Tilia* (E_4) zone. The diatom assemblage including marine (*Paralia sulcata, Diploneis didyma (didymus), Grammatophora oceanica*), as well as brackish (*Tryblionella punctata, Catenula adhaerens*) and freshwater (*Fragilaria* spp.) species, records a trend toward slow salinity increase from ~18 to ~21‰ during the marine phase. The foraminifer assemblage, with *Elphidium excavatum*, *Haynesina orbiculare (orbicularis)*, *Elphidium (Cribroelphidium) incertum*, *Ammonia beccarii* and *Haynesina germanica* dominant species, indicates a salinity exceeding 22‰.

Salinity decreases from >20‰ in the second half of the *Corylus-Quercus-Tilia* (E_4) zone to ~3‰ in the beginning of the *Carpinus-Corylus-Alnus* (E_5) zone, judging by the upsection change from predominant brackish (*Catenula adhaerens*) to freshwater (*Fragilaria* spp., *Martyana (Staurosirella) martyi*, *Navicula scutelloides*) taxa. The salinity decrease is further confirmed by higher percentages of *Elphidium (Cribroelphidium) guntheri* foraminifers and by the appearance of freshwater ostracods.

7.2.6.5. Cierpięta

Marine conditions were reconstructed (Marks et al., 2014) in the *Corylus-Alnus-Tilia* (E_4) zone in the Cierpięta section (Figs. 7.1, 7.2), where *Paralia sulcata*, *Chaetoceros* spp. (spores), *Thalassionema nitzschioides* and *Punctastriata ovalis* predominate among diatoms and indicate a salinity reaching 26‰. The salinity remains >20‰ till the beginning of the *Carpinus-Corylus* (E_5) interval and decreases gradually to 14‰ in the middle of the zone. *Corbula (Varicorbula) gibba, Eulimella (Ebala) nitidissima, Nassarius reticulatus* (*Tritia reticulata*) and *Bittium reticulatum,* are the most abundant species in the mollusc assemblage, which corresponds to a salinity of >15‰ and a sea

depth of 20–30 m. The most abundant foraminifers are *Elphidium (Cribroelphidium) albiumbilicatum, Ammonia batavus (batava), Buccella frigida* and *Elphidium williamsoni.* The ostracod assemblage includes *Cyprideis torosa*, *Cytheromorpha fuscata*, *Leptocythere pellucida* and *Loxoconcha elliptica*

The taxonomy of diatoms changes markedly in the middle of the *Carpinus-Corylus* (E_5) zone, where marine and brackish species are fewer while freshwater diatoms are expanding. This change is synchronous with decrease in planktonic and increase in littoral and benthic taxa, with *Fragilaria (Staurosirella) martyi*, *Fragilaria (Pseudostaurosira) brevistriata*, *Fragilaria (Staurosira) construens*, *Punctastriata ovalis* and *Amphora pediculus* as dominant species. Salinity shows gradual reduction till ~7‰ in the *Pinus-Poacea* (E_7) zone corresponding to the regression phase (Marks et al., 2014), though there is a brief higher-salinity episode (up to ~17‰) in the end of E_5. Foraminifers and ostracods become less abundant but a rich mollusc assemblage persists, with predominant *Corbula (Varicorbula) gibba*. *Cyprideis torosa* ostracods reappear in abundance in the upper E_5 zone.

Marine and brackish diatoms disappear in the Early Weichselian NAP zone, and the diatom assemblage is limited to freshwater benthic taxa, especially *Amphora copulata*. The fauna includes also *Bithynia leachii* freshwater molluscs.

7.2.7. Western Baltic

7.2.7.1. Klein Klütz Höved

The Upper Saalian lacustrine sediments in the Klein Klütz Höved section (Figs. 7.1, 7.2) in the southern Bay of Mecklenburg (Germany) bear an assemblage of freshwater ostracods, such as *Limnocythere inopinata*, *Limnocytherina sanctipatricii* and *Ilyocypris* sp. (Kenzler et al., 2018), freshwater molluscs *Pisidium (Odhneripisidium) stewarti* (Menzel-Harloff and Meng, 2015; Kenzler et al., 2018), and terrestrial snails *Pupilla loessica*, *Vertigo genesii*, *Vallonia tenuilabris* (Krbetschek, 1995, cited from Kenzler et al., 2018). Brackish conditions correspond to the *Pinus-Betula* (E_2 in Menke and Tunni, 1984) – *Pinus-Betula-Quercetum mixtum* (E_3) zones reconstructed (Kenzler et al., 2018) from *Cyprideis torosa, Palmoconcha guttata* brackish and marine ostracods and *Ammonia parkinsonlana* and *Haynesina orbiculare (orbicularis)* foraminifers.

7.2.7.2. Ristinge Klint

The change from freshwater to brackish conditions in the Ristinge Klint section in southern Langelann Island in Denmark (Figs. 7.1, 7.2) is observed at the base of *Cyprina* clay with shells of *Arctica (Cyprina) islandica* molluscs, *Elphidium (Cribroelphidium) albiumbilicatum* foraminifers (Kristensen et al., 2000), as well as *Spiniferites* spp. and *Operculodinium centrocarpum (Protoceratium reticulatum)* as dominant dinoflagellates (Head, 2007) and mainly *Campylodiscus clypeus* and *Campylodiscus echeneis* diatoms (Knudsen et al., 2011). The *Cyprina* clay base corresponds to the boundary of the *Betula-Pinus-Alnus* (E_2 in Andersen, 1975) and *Quercus-Ulmus* (E_3) zones. The clay

bed lies over sand containing abundant *Cyprideis torosa* ostracods and mute early interglacial clay interpreted as limnic facies (Kristensen et al., 2000). Salinity on the sea surface did not exceed 3 ‰ in the beginning of the transgression episode (Head, 2007) but reached 15 ‰ in the end of the brackish phase, or in the second half of E_3 (Head, 2007; Knudsen et al., 2011).

An episode of considerably higher salinity shows up in the end of the *Quercus-Ulmus* (E_3) zone (Kristensen et al., 2000), where new foraminifer species appear: *Haynesina orbiculare (orbicularis), Elphidium excavatum, Buccella frigida, Elphidium williamsoni, Elphidium (Cribroelphidium) incertum,* along with two Lusitanian species of *Elphidium translucens* and *Elphidium lidoense (Porosononion granosum).* At the same time, all *Elphidium (Cribroelphidium) albiumbilicatum* tests disappear. The foraminifer assemblage records salinity above 22‰. The deposits of the marine phase also contain *Cyprideis torosa, Robertsonites tuberculatus*, and *Sarsicytheridea bradii* ostracods and molluscs, mainly *Paphia (Polititapes aureus) senescens* and *Mytilus edulis* in the lower strata and *Acanthocardia echinata* at higher levels (Nielsen et al., 2007). The salinity increase was accompanied by rapid progress of dinoflagellates (Head, 2007) with predominant *Lingulodinium machaerophorum*, which correspond to salinity values at least 15‰ in the beginning of the marine phase. The diatom assemblage of that time consists mainly of *Actinoptychus senarius* and *Coscinodiscus* cf. *asteromphalus* (Knudsen et al., 2011), but *Paralia sulcata* and *Stephanopyxis turris* become dominant species up the section. The diatom-based salinity of the surface seawater during the maximum transgression was 20–28‰ and remained high till the onset of the *Pinus-Picea-Corylus* (E_5) zone (Kristensen et al., 2000) at the section top.

7.2.7.3. Mommark

Data from the Mommark section in the southeastern shore of Denmark's Als Island (Figs. 7.1, 7.2) reveal a freshwater basin that existed in the earliest Eemian Interglacial, within the *Pinus-Betula* (E_{1-2} in Andersen, 1975) zone (Gibbard and Glaister, 2006; Kristensen and Knudsen, 2006). The limnic sediments contain freshwater ostracods *Cytherissa lacustris* (Kristensen and Knudsen, 2006). Seawater penetrated into the lake in the end of the E_{1-2} zone (Gibbard and Glaister, 2006; Kristensen and Knudsen, 2006). Early during transgression, the basin became inhabited with brackish ostracods, especially *Cyprideis torosa* (Kristensen and Knudsen, 2006); *Ellerbeckia arenaria*, *Campylodiscus* genus, appeared in the beginning of the *Quercus-Corylus* (E_4) zone (Haila et al., 2006). The upsection fauna change records gradual salinity increase till 5–10‰ (Kristensen and Knudsen, 2006).

The marine phase begins within the *Quercus-Corylus* (E_4) zone (Gibbard and Glaister, 2006; Haila et al., 2006; Kristensen and Knudsen, 2006), which is recorded in the appearance of marine diatoms, mainly *Paralia sulcata* and *Actinoptychus senarius* (Haila et al., 2006), some foraminifers (*Haynesina orbiculare (orbicularis), Buccella frigida, Elphidium excavatum, Haynesina nivea*, etc.) (Kristensen and Knudsen, 2006), as well as *Robertsonites tuberculatus* and *Sarsicytheridea bradii*

ostracods. Salinity is the highest (>25‰) in the middle of the *Picea-Carpinus-Pinus* (E_5) zone. The mollusc assemblage includes most abundant *Corbula (Varicorbula) gibba* in the first half of the marine phase, while *Arctica islandica* and *Mytilus edulis* become abundant as well in the second half (Funder and Balic-Zunic, 2006).

The subsequent regression episode was accompanied by gradual salinity decrease since the end of the *Picea-Carpinus-Pinus* (E_5) zone (Gibbard and Glaister, 2006; Haila et al., 2006; Kristensen and Knudsen, 2006). The foraminifer assemblage of that time is mainly composed of *Elphidium excavatum* (Kristensen and Knudsen, 2006), with notable percentages of *Haynesina orbiculare (orbicularis), Buccella frigida* and *Haynesina germanica*, as well as some other species (*Elphidium williamsoni* and *Elphidium (Cribroelphidium) albiumbilicatum*) that appear in the *Pinus-Betula* (E_7) zone. In the ostracod assemblage, *Robertsonites tuberculatus* and *Sarsicytheridea bradii* disappear and become succeeded by *Leptocythere pellucida* and *Palmoconcha laevata.* Diatoms of the *Paralia sulcata* species reduce markedly in the end of the *Picea-Pinus* (E_6) zone (Haila et al., 2006), while the dominant species include *Actinoptychus senarius*, *Pleurosigma angulatum*, and *Odontella rhombus (Zygoceros ehrenbergii)*. Among molluscs, *Corbula (Varicorbula) gibba* predominate within the regression interval and *Acanthocardia echinata* become abundant in the end of the E_6 zone (Funder and Balic-Zunic, 2006).

Brackish conditions changed to a limnic environment in the end of the *Pinus-Betula* (E_7) interval, which is recorded in the disappearance of foraminifers and ostracods present in the sediments below and in the appearance of freshwater species *Cytherissa lacustris* (Kristensen and Knudsen, 2006). The diatom assemblage of that time includes greater percentages of freshwater taxa, especially the genera *Aulacoseira* and *Pinnularia* (Haila et al., 2006). Other freshwater taxa are *Alona quadrangularis*, *Disparalona rostrata* and *Leydiga acanthoceroides* cladocera (Haila et al., 2006).

7.2.7.4. Oldenbüttel

The *Oldenbüttel section* (Figs. 7.1, 7.2) was stripped in BH 2 near Oldenbüttel city on the Kiel Canal coast and was first documented by Heck (1932). Marine diatoms, with *Navicula (Lyrella) lyra* and *Surirella fastuosa (Campylodiscus neofastuosus)* as dominant species, appear in the *Betula-Pinus* (c-d in Jessen and Milthers, 1928) zone. Other fauna groups include molluscs (*Corbula (Varicorbula) gibba, Tapes aureus* var. *eemiensis (Polititapes aureus senescens), Ostrea edulis, Bittium reticulatum, Cardium echinatum (Acanthocardia echinata)* and *Mytilus edulis*); foraminifers, with predominant *Nonionina (Haynesina) depressula* and *Polystomella striatopunctata* (*Elphidium striatopunctatum*); *Cythere papillosa* ostracods; and *Balanus* sp. crustaceans.

These taxa record quite high salinity (Heck, 1932), but it decreases within the *Quercus* (f) zone, judging by a high percentage of *Melosira moniliformis* diatoms that live in fresh of brackish water, as well as the presence of *Navicula (Pinnularia) interrupta*, *Navicula didyma* (*Diploneis bombus*),

Campylodiscus echeneis, *Melosira (Ellerbeckia) arenaria*, and some other diatom species. The composition of diatoms changes further to freshwater taxa (*Pinnularia*, *Cymbella* and *Fragilaria* genera) in the *Pinus-Picea* (i) zone, where they coexist with freshwater sponge *Ephydatia muelleri*.

7.2.7.5. Schnittlohe

In the Schnittlohe section in the Kiel Canal area, Germany (Figs. 7.1, 7.2), marine molluscs, with predominant *Bittium reticulatum, Cerastoderma edulis (edule), Venerupis (Polititapes aureus) senescens, Ostrea edulis* and some other species, appear first in the *Betula* (E_1 in Menke and Tunni, 1984) and *Betula-Pinus* (E_2) zones (Hinsch, 1985; Menke, 1985). The same strata contain freshwater molluscs: *Bithynia tentaculata*, *Valvata piscinalis*, *Planorbis planorbis* and *Sphaerium corneum*. Foraminifers appear in the E_1–E_2 zones as well (Knudsen, 1985) and are mainly *Ammonia batavus (batava)*, *Elphidium (Cribroelphidium) gunteri*, *Elphidium (Cribroelphidium) incertum*, *Elphidium (Cribroelphidium) albiumbilicatum*, *Elphidium williamsoni* and *Nonion germanicum (Haynesina germanica)*.

The onset of the marine phase shows up in the middle *Corylus-Quercetum mixtum* (E_{4a}) zone (Hinsch, 1985; Knudsen, 1985; Menke, 1985). The early marine phase is marked by the presence of most abundant *Ammonia batavus (batavus)* and *Elphidium (Cribroelphidium) gunteri* foraminifers, but *Nonion germanicum (Haynesina germanica), Elphidium williamsoni*, while *Elphidium (Cribroelphidium) incertum* reach higher significance later (Knudsen, 1985). The taxonomy of foraminifers corresponds to a sea depth of 10–20 m. The mollusc fauna of the maximum transgression mainly consists of *Varicorbula gibba, Bittium reticulatum, Venerupis (Polititapes aureus) senescens, Cerastoderma edulis (edule)* and *Hinia (Tritia) reticulata* (Hinsch, 1985).

Molluscs become fewer in numbers and less diverse in the second half of the *Carpinus-Picea* (E_5) zone, which records shoaling to 0–5 m water depths (Hinsch, 1985; Menke, 1985). *Venerupis (Polititapes aureus) senescens* and *Acanthocardia echinata* are dominant species in the mollusc assemblage of that time. Shoaling and salinity decrease are further confirmed by the presence of especially abundant *Ammonia batavus (batavus)* and *Nonion germanicum (Haynesina germanica)* foraminifers (Knudsen, 1985).

7.2.7.6. Offenbüttel

Brackish conditions are likewise recorded in the earliest LIG within the Offenbüttel section located ~1.5 km northeast of Schnittlohe (Figs. 7.1, 7.2), but the sediments are poor in pollen, and no pollen zones can be distinguished in this interval (Menke, 1985). Brackish foraminifers include abundant *Nonion germanicum (Haynesina germanica)*, *Ammonia batavus (batava), Elphidium gunteri (Cribroelphidium)*, *Elphidium williamsoni*, *Elphidium (Cribroelphidium) albiumbilicatum*, *Elphidium*

excavatum and *Buccella frigida* (Knudsen, 1985). The mollusc assemblage consists of *Hinia (Tritia) reticulata*, *Cerastoderma edulis (edule), Theodoxus fluviatilis*, and some other species (Hinsch, 1985).

The marine phase in the section begins at the boundary between the *Pinus-Quercetum mixtum* (E_3 in Menke and Tunni, 1984) and *Quercetum mixtum-Corylus* (E_{4a}) zones (Hinsch, 1985; Knudsen, 1985; Menke, 1985). As in the case of the Schnittlohe section, the onset of the marine phase is marked by high percentages of *Ammonia batavus (batavus)* and *Elphidium (Cribroelphidium) gunteri* foraminifers making up to 95% of the total count (Knudsen, 1985). As the sea grew deeper and more saline, *Elphidium williamsoni, Nonion germanicum (Haynesina germanica)* and *Bucella frigida* became predominant. During the maximum transgression, the sea depth was 10–20 m and the salinity was below the normal level. The marine mollusc assemblage is similar to that of the Schnittlohe section, but the dominant species additionally include *Ostrea edulis* (Hinsch, 1985).

The numbers and diversity of molluscs reduce in the *Carpinus-Picea* (E_5) zone (Hintsch, 1985), thus recording shallower-water conditions. The mollusc assemblage consists of *Bittium reticulatum, Varicorbula gibba, Acanthocardia echinata, Venerupis (Polititapes aureus) senescens, Mytilus edulis*, and *Cerastoderma edulis (edule)*. Among the regression-phase foraminifers, *Nonion germanicum (Haynesina germanica)*, *Ammonia batavus (batavus)* and *Elphidium translucens* are the most abundant (Knudsen, 1985).

7.3. Last Interglacial evolution of the Baltic and Mga seas

Upper Moscow (Upper Saalian) marine deposits are present in many East Baltic sections , but are generally unknown from the western Baltic Sea. The singular location where marine sediments of this age were found outside the Gulf of Finland is Plasumi on the west coast of Latvia (Kalnina, 2001). Note that clay with marine molluscs *Arctica islandica*, *Portlandia arctica*, *Mytilus* sp. and *Cardium* sp. in the Hiddensee, Arkona, and Greifswalder Oie coastal sections in northern West Pomerania (Germany) was timed (Obst et al., 2020) as Upper Saalian, proceeding from the presence of cold-water microfossils, mainly Arctic ostracods *Roundstonia globulifera* and foraminifers *Haynesina orbicularis*, the absence of Lusitanian molluscs and OSL ages between 153 and 115 ka. However, the age remains insufficiently constrained because no spore and pollen data are available yet for that section.

The Kattegat and other Danish straits were inferred (Obst et al., 2020) to have opened in the Late Saalian time and channeled North Atlantic oceanic water into the Baltic Sea after passing through the Norwegian trench. A similar interpretation was suggested in an earlier model (Kristensen and Knudsen, 2006) implying that the Kattegat strait was connected with the Baltic Sea via North Zealand, Öresund and South Sweden. A still earlier model (Lavrova, 1961) described influx of seawater into the Baltic Sea via tectonic lakes of Vänern and Vättern (Central Sweden) in the latest Middle Pleistocene.

Meanwhile, no geological proof for any of these hypotheses has been found yet. In this respect, the Petrozavodsk section is of special interest (Ikonen and Ekman, 2001) as it contains up to 22% of marine diatoms in the Upper Moscow varved clay. They were interpreted as allochthonous (Ikonen and Ekman, 2001) but marine diatoms peaked during the interstadial warming in the lower part of the section, which apparently correlates with the Kasplya Interstadial. This time interval bears signatures of increasing salinity in the Upper Moscow basin deposits in the Sinyavino, Sverdlov Factory, and Prangli sections. Thus, the Baltic Sea may have been connected with the ocean via the White Sea during the interstadial. This idea is consistent with a glacial isostaic model (Lambeck et al., 2006) showing a connection of the Baltic Sea with the North Sea via the Danish straits and South Sweden, as well as with the White Sea in Late Moscow time (135–134 ka ago).

In the earliest Eemian (Mikulino) Interglacial (zones E_1–E_2 after Menke and Tunni, 1984), a strait between the Baltic and North Seas was formed in the area of the present Kiel Channel: the Nordman Strait (Kosack and Lange, 1985). Judging by the presence of coarse coastal deposits with *Ostrea edulis* (Hinsch, 1985), the Nordman Strait of that time was warm and saline, which is evidence that the English Channel may have already existed (Funder et al., 2002). The connection between the Baltic and North Seas in the beginning of the LIG may account for increasing marine influence in many areas of the Baltic Sea, including in the studied Sverdlov Factory section (Fig. 4.20).

Slightly later (zones E_2–E_3), transgression reached the islands of the Danish Archipelago (Kristensen et al., 2000; Gibbard and Glaister, 2006; Kristensen and Knudsen, 2006), the Mecklenburg Bay (Kenzler et al., 2018) and the Lower Vistula area (Makowska, 1986; Head et al., 2005; Knudsen et al., 2012). The Baltic and Mga Seas of that time were cold and moderately saline while the seafloor was uplifted by glacial isostatic rebound, which became illustrated by sea retreat and peat deposition in the beginning of the *Corylus-Quercus-Tilia* zone (E_4 after Mamakova, 1988) observed in the Baltic Spit (Znamenskaya and Cheremisinova, 1970) and Nowiny (Makowska, 1986) sections of the Lower Vistula area.

In zones E_3–E_{4b} (M_3–M_5, according to Grichuk, 1961), numerous sections record marked and substantial increase in both sea depth and salinity corresponding to the transition from the brackish to the marine phase of basin evolution. Pollen data from the Ristinge Klint section show maximum abundances of *Quercus* and beginning of *Corylus* increase for that time interval (Fig. 7.3). Kristensen et al. (2000) linked this to the opening of the Danish Straits. The patterns of foraminifers in the Ristinge

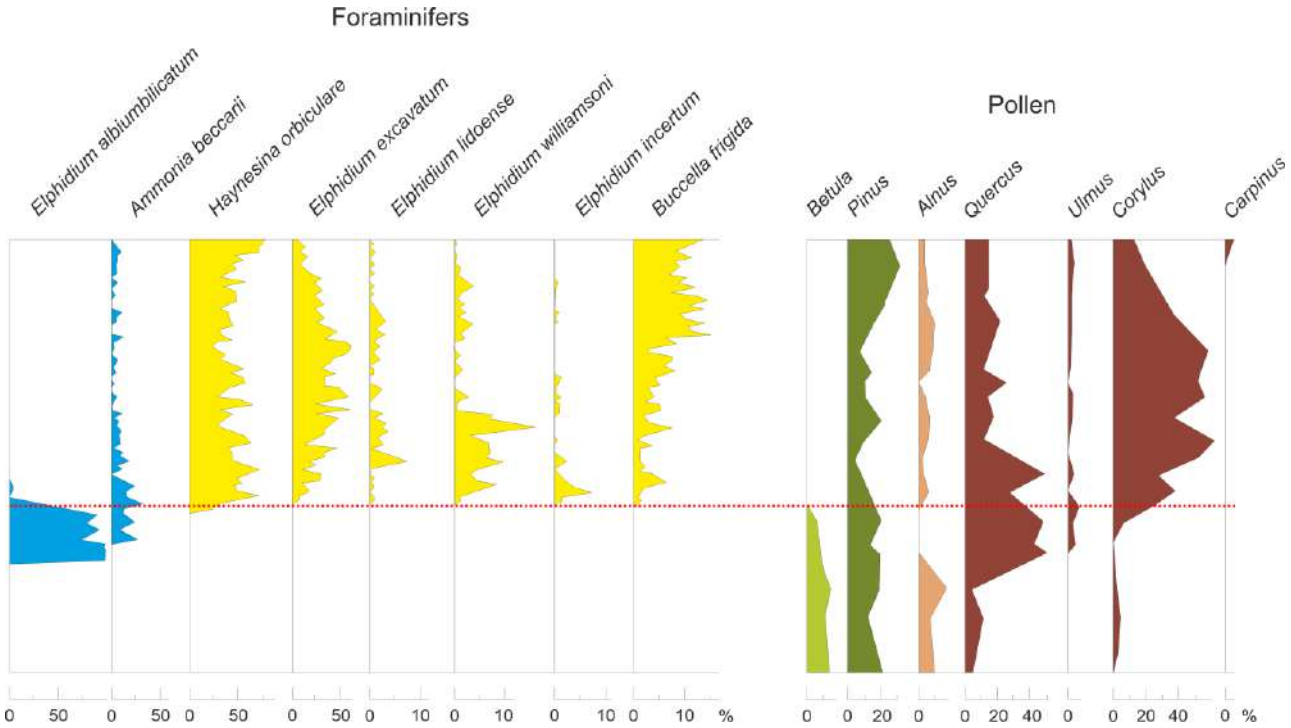

Fig. 7.3. Selected taxa of foraminifers and pollen in Eemian marine deposits from the Risting Klint section (Kristensen et al., 2000). Red dotted line marks the level of brackish-to-marine transition.

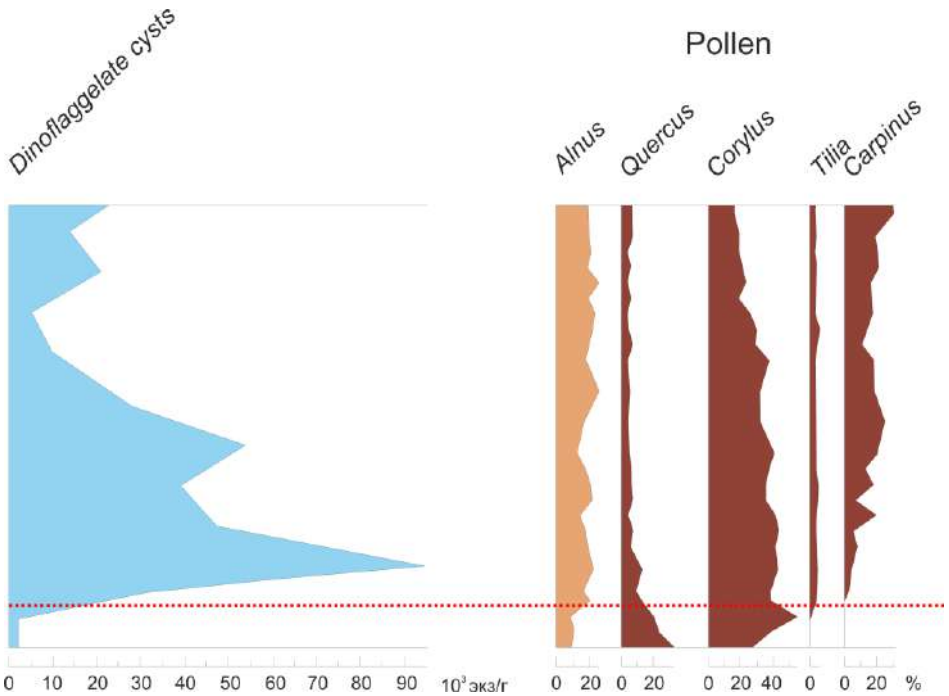

Fig. 7.4. Dinoflaggelates and selected pollen taxa in Eemian deposits from the Licze section (Head et al., 2005). Red dotted line marks the level of brackish-to-marine transition.

Klint section mark the onset of the marine phase evident in the disappearance of *Elphidium (Cribroelphidium) albiumbilicatum* and appearance of six new species: *Haynesina orbiculare (orbicularis), Elphidium excavatum, Elphidium lidoense (Porosononion granosum), Elphidium williamsoni, Elphidium (Cribroelphidium) incertum* and *Buccella frigida* (Fig. 7.3).

In the Licze section, which is situated in the Lower Vistula area, the inception of the marine phase is contemporaneous with the *Corylus* apex and the emergence of the *Tilia* (Fig. 7.4) (Head et al., 2005). The escalation of marine influence is indicated through a swift surge in the concentration of dinoflagellate cysts in the sediment from ~3 000 to ~95 000 sp./g (Fig. 7.4).

In the Prangli section (Fig. 7.5), in the gorge of the Gulf of Finland, the onset of deepwater marine conditions corresponds to the peak of *Pinus* (Cheremisinova, 1961; Liivrand and Valt, 1966). It is reconstructed based on abrupt disappearance of freshwater and freshwater to brackish diatoms *Stephanodiscus astraea, Navicula tuscula (Aneumastus tusculus), Epithemia spp., Cymatopleura elliptica, Melosira (Ellerbeckia) arenaria, Cocconeis disculus* and *Diploneis domblittensis, Diploneis domblittensis* var. *subconstricta (Diploneis burgitensis)* at simultaneous rapid growth of marine taxa (Fig. 7.5): *Melosira (Paralia) sulcata*, *Podosira* sp., *Hyalodiscus scoticus*, *Actinocyclus ehrenbergii (octonarius), Chaetoceros spp., Navicula lyra* var. *abrupta (Lyrella abrupta)*.

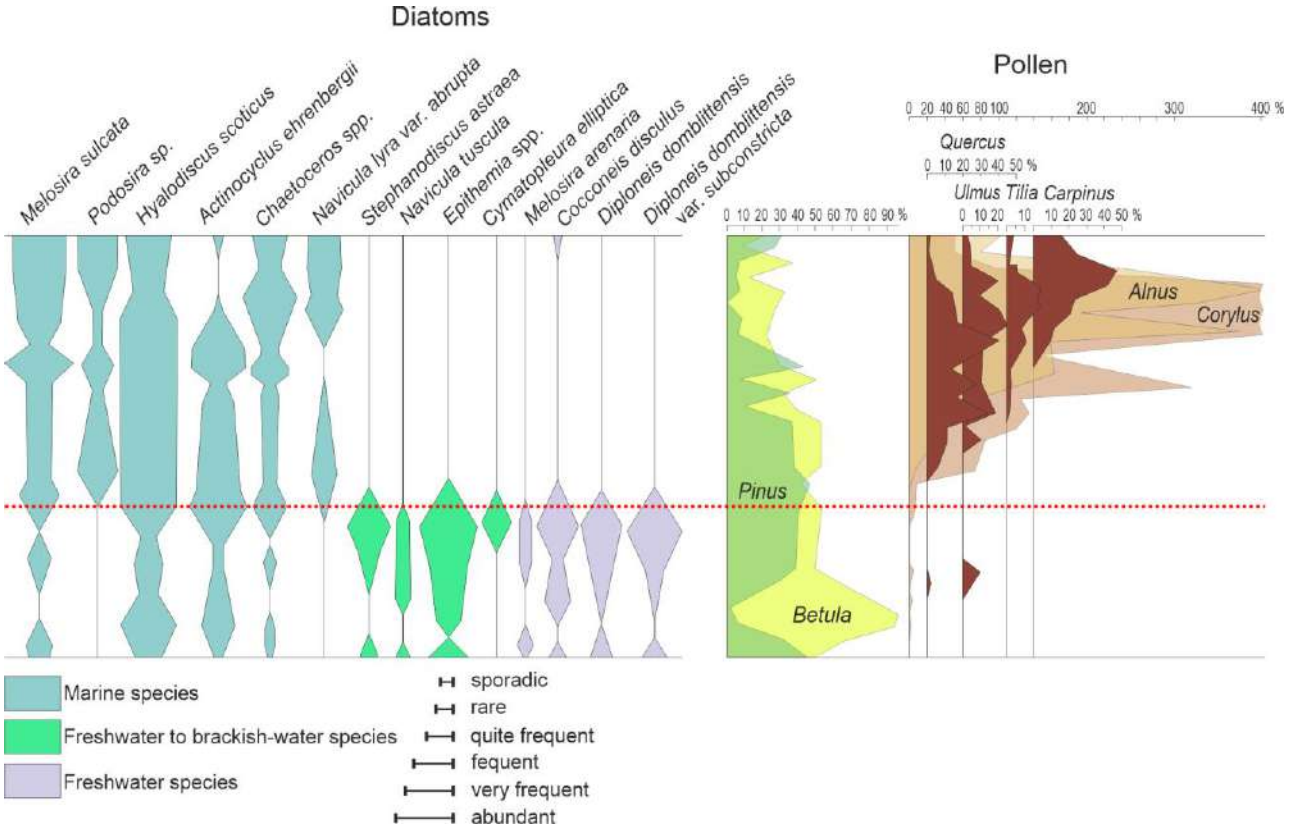

Fig. 7.5. Selected diatom taxa (Cheremisinova, 1961) and pollen spectra (Liivrand and Valt, 1966) for the Mga deposits in the Prangli section. The pollen diagram was plotted utilizing Grichuk's method (1961), excluding *Alnus* and hazel *Corylus* from the tree species composition. Red dotted line marks the level of brackish-to-marine transition.

Similar taxonomic changes in microfossils corresponding to the transition to deeper-water saline environments are observed in many other sections. The abrupt changes in the taxonomy of flora and fauna and in geochemical tracers (Fig. 4.20) found in different LIG sections indicate that water salinity and sea depths increased very rapidly as a result of voluminous inputs of oxygenated saline water,

apparently, after the Danish Straits had opened (Kristensen et al., 2000). Saline water can be expected to have spread over the Baltic and Mga Seas during the LIG for the time comparable with the modern water renewal cycle in the Baltic: 26–29 years (Döös et al., 2004), or much shorter than the vegetation evolution cycles (Table 7.1.) (Müller, 1974). Thus, the boundary between the brackish and marine phases was quasi-isochronous throughout the territory of the two seas.

Most of the sections show signatures of regression in the zone of *Carpinus*, which corresponds to the onset of the North Sea regression (Zagwijn, 1983; 1996; Strife, 1990). About that time, the Baltic-White Sea connection became disrupted, judging by the onset of freshwater deposition in the Petrozavodsk section (Ikonen and Ekman, 2001). In the Gulf of Bothnia sections (Mertuanoja, Norra Sannäs I), regression falls within zones E_5–E_6 of Andersen (1975), i.e., earlier than in other parts of the basin, possibly, because of more rapid glacial isostatic uplift. Signatures of freshwater conditions in most of the Mga sections in the Neva Lowland and the Karelian Isthmus appear in the *Pinus-Picea-Betula* zone (M_8).

In five sections (Upper Vidlitsa, Kaver, Beloye Lake, Plazumi and Gulf of Riga) the preservation of marine conditions in the Early Valdai (Early Weichselian) time is reconstructed (Fig. 7.2). Marine sediments accumulated in the north of the Jutland peninsula during the Herning Stadial and the Brørup Interstadial (Glaister and Gibbard, 1998), but it is unlikely that the connection between the Baltic and the North Sea was maintained during this period due to the low sea level. In MIS5d it fell to ~40 m below the modern level, and in MIS5c it rose no more than ~20 m (Waelbroeck et al., 2002). More likely, the Lower Valdai (Weichselian) deposits in the Lake Beloye, Gulf of Riga, and Plasumi sections contain allochthonous diatoms. Redeposition of microfossils from the Mga (Eemian) marine deposits in the Valdai is a known fact. Specifically, core samples of the Ladoga bottom sediments, ~30 km southeast of Priozersk, contain marine and brackish dinoflagellates, acritarchs and diatoms in the Lower Valdai deposits correlated to MIS 5d-a (Andreev et al., 2019; Ludikova et al., 2021). The marine microfossils were inferred (Ludikova, 2019; Ludikova et al., 2021) to be redeposited from the Mga deposits, i.e., the Lower Valdai sediments were accumulated in freshwater conditions in the Ladoga Basin. Allochthonous marine diatoms and foraminifers were found in the Valdai rocks of the Vääna-Jõesuu section in northern Estonia (Raukas and Liivrand, 1971, cited from Liivrand, 1991). The Karelian Isthmus sediments bearing brackish and marine diatoms were assigned to the Mga Fm., as in the case of the Denisovo (Apukhtin et al., 1959; Malyasova, 1960; Malakhovsky et al., 1969a), Zaostroviye in BH 33 (Grechko et al., 1972; Abakumenko et al., 1977) and Larionovo in BH 52 (Grechko et al., 1972; Abakumenko et al., 1977) sections. The Baltic Ice Lake deposits often contain redeposited brackish and marine diatoms as well, and their counts may approach those of the autochthonous freshwater diatoms (Zemlyakov et

al., 1941; Lak, 1976; Saarnisto et al., 1995; Ludikova, 2017). Sediments with redeposited diatoms are remarkable by simultaneous peaks of ecologically incompatible (marine and freshwater) species.

The intervals of the latest Mikulino (Eemian) Interglacial (*Pinus* zone) or the earliest Early Valdai (Early Weichselian) in both eastern (Krasnoselskoye, Yukki, Peski, Lake Tokhkolodskoye) and western (Mommark) sections were deposited in freshwater environments, while reliably assigned Lower Valdai (Lower Weichselian) marine deposits are unknown in the Baltic region. Furthermore, the Early Valdai sealevel never rose above ~ -20 m asl (Waelbroeck et al., 2002) and, hence, a lake basin most likely existed for the whole interval from the end of the LIG till the maximum of the Scandinavian Ice Sheet expansion ~60 ka ago (Svendsen et al., 2004). The lake level was below the present global sealevel, i.e., its strandlines must be hidden under the Baltic water.

7.4. Onset of marine conditions in different parts of the Baltic and Mga Seas

The pollen zones of the Baltic and Onego-Ladoga regions can be correlated with reference to the rigorously constrained onset of the marine phase in key sections. However, pollen zones were often distinguished from different criteria in specific areas, and the time constraints cannot be rigorous. In this study, the time when marine conditions set in the sections was estimated from characteristic points in pollen diagrams when main tree species (*Pinus*, *Quercus*, *Corylus*, *Tilia* and *Carpinus*) began to increase and culminate.

The southernmost reference sections are located in the Lower Vistula area. The onset of deep water and higher salinity conditions is reconstructed at a depth of 110.5 m after the *Corylus* maximum and in the beginning of *Tilia* increase in the Obzhinovo section (Fig. 7.6) (Knudsen et al., 2012) and at 97.5 m, likewise after the *Corylus* maximum and before the *Tilia* increase, in the Licze section (Figs. 7.4, 7.6) (Head et al., 2005). The respective depth in the Nowiny sections is 61.6 m, which corresponds to the *Corylus* maximum and precedes the *Carpinus* increase (Fig. 7.6) (Makowska, 1986), whereas marine diatoms in the Baltic Spit section appear already at the ~12 m depth, before the *Corylus* maximum (Fig. 7.6) (Znamenskaya and Cheremisinova, 1970). The brackish–marine boundary in the Cierpięta section remains unconstrained (Marks et al., 2014). In general, the marine phase in the Lower Vistula area correlates approximately with the *Corylus* maximum, in the middle of zone IIIb of the Bispingen chronology, or ~1500 a after the beginning of the Eemian Interglacial (Fig. 7.6) (Müller, 1974).

The sections of the Schleswig-Holstein area are located slightly north of the Lower Vistula area. In the Schnittlohe section, salinity increases since the 15.5 m depth, which correlates with lower abundance of *Quercus* and with the middle of the *Corylus* peak (Fig. 7.6) (Hintsch, 1985; Knudsen, 1985; Menke, 1985). The lower boundary of the marine phase in the Oldenbüttel section has not been constrained (Heck, 1932), and the resolution of the pollen spectra in the Ofenbüttel section is too low for estimating precisely the onset of the marine phase (Hintsch, 1985; Knudsen, 1985; Menke, 1985).

According to the Bispingen chronology, the middle of the *Corylus* peak corresponds to the IIIa-IIIb zone boundary, 1200 years after the beginning of the LIG (Fig. 7.6) (Müller, 1974).

In the Ristinge Klint section, located ~100 km northeast of Schnittlohe, marine conditions appear at a depth of 1.8 m, corresponding to the *Quercus* maximum and the beginning of the *Corylus* peak (Fig. 7.3, 7.6) (Kristensen et al., 2000; Knudsen et al., 2011). Stronger influence of marine conditions in the Mommark section, slightly farther northward, is reconstructed at a larger depth (9.5 m) which likewise coincides with the *Quercus* maximum and the *Corylus* increase (Fig. 7.6) (Gibbard and Glaister, 2006; Haila et al., 2006). According to the Bispingen chronology, *Corylus* increases from the beginning of zone IIIa, about 900 years after the Eemian began (Fig. 7.6) (Müller, 1974).

The Central Baltic sections cannot be used to time the onset of the marine phase: the brackish-water-to-marine transition was not distinguished in the Plasumi and Gulf of Riga sections, and is unclear in the Grini section, because the depths in Table 11 from Kalnina (2001) misfit those in the pollen diagram of Fig. 34b in the same publication (Kalnina, 2001).

Meanwhile, the onset of marine conditions is detectable in the Gulf of Finland sections located 6° north of the Lower Vistula sections. The depths corresponding to the beginning of the marine phase are 75 m (Figs. 7.5, 7.6) in the Prangli section (Cheremisinova, 1961; Liivrand and Valt, 1966), correlated with the *Pinus* maximum and preceding the increase of *Quercus* and *Corylus*; 29.8 m in the Peski section, or in the beginning of the *Corylus* peak (Fig. 7.6) (Miettinen et al., 2002; 2014); 70.75 m in the Sinyavino section, likewise in the beginning of the *Corylus* peak (Fig. 7.6) (Malakhovsky et al., 1969a); 41 m in the Rybatskoye section, where diatom counts increase extremely fast. As in the Prangli section, this depth corresponds to the *Pinus* maximum and precedes the increase of *Quercus* and *Corylus* (Fig. 7.6) (Lavrova and Grichuk, 1961; Znamenskaya and Cheremisinova, 1962); 5.75 m in the Mga II section, in the beginning of the *Quercus* peak and before the increase of *Corylus* (Fig. 7.6) (Pleshivtseva et al., 1984). On the other hand, this boundary is uncertain in the Mga I section because the spore-pollen (Znamenskaya, 1959) and diatom (Cheremisinova, 1959) data correlate poorly. In the Sverdlov Factory II section, marine signatures are detectable at a depth of -10.4 m (Fig. 6.1) corresponding to the middle of the *Quercus* peak, when *Corylus* is already widespread but has a long low peak (Fig. 4.16). Note that all deciduous tree species in the Sverdlov Factory I section culminate synchronously (Pleshivtseva et al., 1984), and thus the pollen may be redeposited, which obscures the brackish-to-marine transition. The lower boundary of the marine phase has not been constrained in the Lake Beloye, Krasnoselskoye, Yukki, and Lake Tokhkolodskoye sections (Fig. 7.2). On the average, the onset of the marine phase in the Gulf of Finland area is reconstructed slightly before the *Corylus* peak, or in zone IIb of the Bispingen chronology, ~600 years after the LIG began (Fig. 7.6) (Müller, 1974).

For the Lake Onego area, the beginning of the marine phase could be accurately determined in the Petrozavodsk II section only, in the absence of published diatom data for the Petrozavodsk I section and spore-pollen diagram for the Vytegra section. In the Petrozavodsk II section, freshwater diatoms disappear completely at a depth of 11 m or slightly below the *Pinus* peak (Fig. 7.6) (Ikonen and Ekman, 2001). In the Bispingen chronology, this is pollen zone IIa, ~250 years after the onset of the LIG (Fig. 7.6) (Müller, 1974).

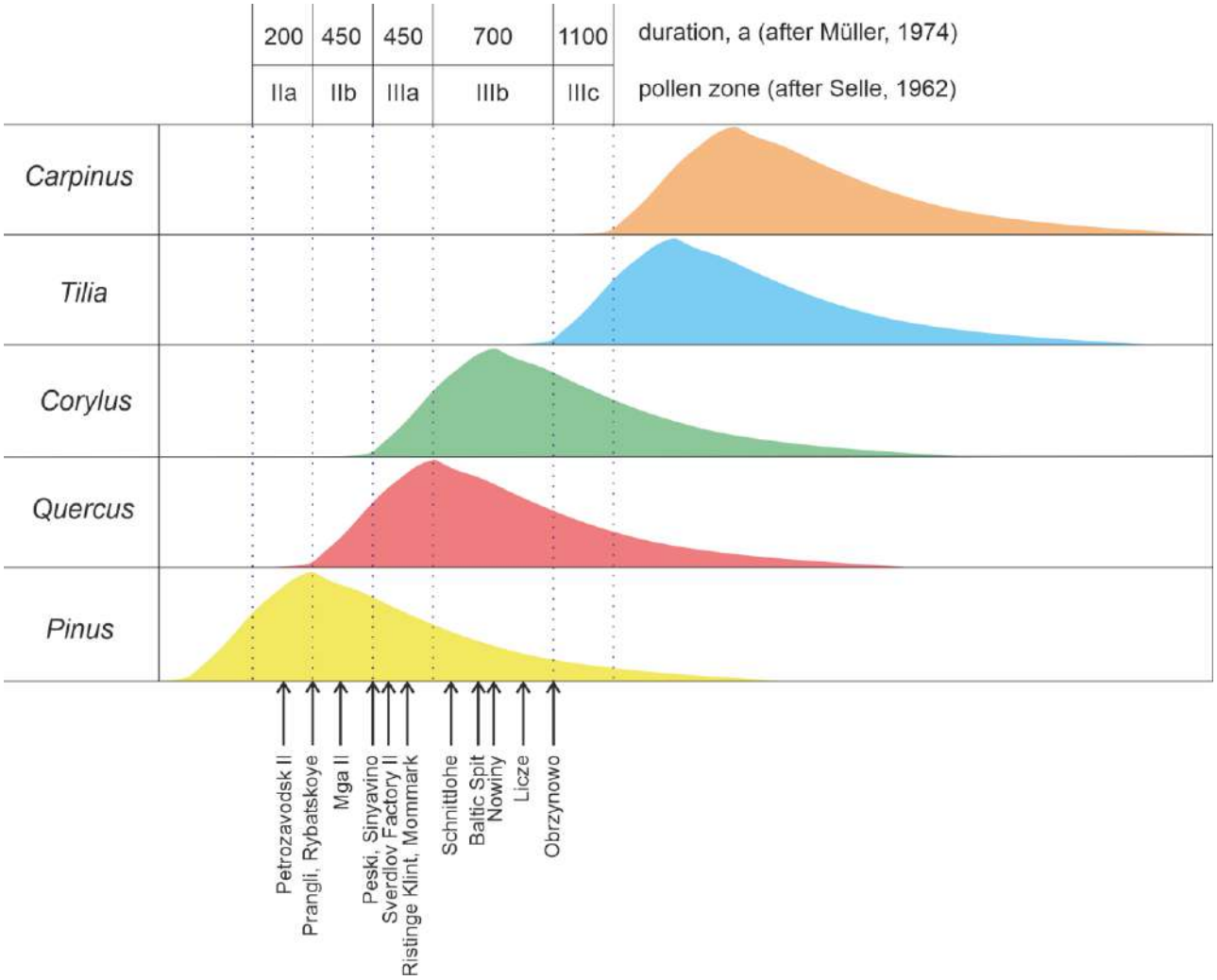

Fig. 7.6. Location of boundary between the brackish and marine phases correlated to LIG pollen peaks of main tree species in the reference sections of the Eemian (Mga) marine sediments from the Baltic and Onego-Ladoga regions.

On the eastern shore of Lake Ladoga, three sections (Verkhnyaya Vidlitsa, Kaver, and Vasilyevsky Bor) have been studied using both spore-pollen and diatom methods, but the frequency of sampling is insufficient to accurately determine the boundary between the brackish and marine phases.

The brackish-to-marine transition also remains unconstrained in the northernmost reference sections Norra Sannäs I and Mertuanoja on the Bothnia Gulf coast.

The synthesized data on the place of the transition relative to the pollen peaks of main tree species in reference Eemian (Mga) marine sections (Fig. 7.6) show that the vegetation phases in the Baltic and

Onego-Ladoga lagged behind those of Central Europe in the northern and northeastern directions. Since the Lower Vistula sections are located at approximately the same latitude as Bispingen, the boundaries of pollen zones in these areas may be considered isochronous. The lag behind Bispingen and Lower Vistula was ~600 years in South Denmark, ~900 years in the Gulf of Finland, and ~1250 years in Petrozavodsk areas. Therefore, the Bispingen chronology cannot be used directly for timing the boundaries between the Mikulino pollen zones in the sections of the East European Plain.

7.5. Concluding remarks

The only avaibale evidence of the vegetation evolution during the Eemian (Mikulino) Interglacial comes from the varve chronology of the Bispingen section, as well as other sections located in Northern Germany. This chronology has been largely used to to time pollen zone boundaries in both Central and Western Europe and the East European Plain. Nevertheless, the applicability of the Bispingen chronology to distant sections is doubtful because pollen zone boundaries are diachronous.

The spore-pollen and paleontological data from the reference sections of the sections of the marine deposits in the Baltic and Onego-Ladoga regions allowed the author to hypothesize that the boundary between the brackish and marine phases of sea basin evolution is located at the same chronostrtigraphic level throughout the specified terrain. Correlation of this boundary with the LIG peaks of main tree pollen species in various sections shows that the phases of vegetation history in the beginning of the LIG in the Gulf of Finland region lagged approximately 900 years behind those of Central Europe. Furthermore, the Petrozavodsk area witnessed a delay of around 1250 years. Therefore, the Bispingen chronology cannot be used directly for determining the age of palynozone boundaries in the sections of the East European Plain.

Conclusion

The Mga marine sediments deposited during the Mikulino Interglacial, as well as the sediments below and above the interglacial formation, have been studied for the first time with an integrated approach, using several combined methods: facies analysis, spore-pollen analysis, OSL dating, geochemical analyses, grain-size analysis, diatom analysis and varve chronology. The studies allowed constraining the age of the Mikulino Interglacial, reconstructing the deposition conditions in the Neva Lowland, and tracing main events in the evolution of the Mga Sea basin.

The interglacial deposits were sampled from the quarry of the Etalon (formerly Sverdlov) Brick Factory which exposes a continuous sequence of Middle-Upper Pleistocene sediments. The author of the present thesis, together with his colleagues, performed a pioneering minute study of the Upper Moscow varved clay beneath the Mga Fm. (distinguished by the author as the Sverdlov Fm.), which stores a record of the transition from the Moscow Glacial to the Mikulino Interglacial. The Sverdlov Fm. comprises three local pollen zones correlated with regional pollen zones Ms_3–Ms_1 (after Malakhovsky et al., 1969a) of the respective durations ~400 years (both for Ms_3 zone and for Ms_2 corresponding to the Kasplya Interstadial) and ~300 years (Ms_1, Kattegat Stadial). The varved clay formed during the time span between ~1100 and ~1080 years prior to the LIG contains abundant ice-rafted debris, and its deposition can be thus correlated with the 11th Heinrich event. The Sverdlov Fm. was deposited during the glaciomarine stage of the Mga Sea, where brackish conditions prevailed 1100 to 1030 years before the LIG. Between ~1030 and ~350 years before the onset of the LIG, the Mga Sea underwent significant desalination, but its connection with the ocean was later restored.

The lithological boundary between the Sverdlov and Mga Fms. detectable from the disappearances of varves and the appearance of black (bluish) hue of sediments in the Sverdlov Factory quarry approximately coincides with the base of the regional pollen zone M_2, and thus corresponds to the base of the Mikulino Stage. The Mga Fm. encompasses all Mikulino regional pollen zones M_2–M_8 which record the succession of climatic conditions from temperate in the beginning of the interglacial to warmer than the present climate during the optimum (zones M_4–M_6), and back to temperate in the end of the LIG. The sea setting changed from brackish (lagoonal) conditions between the beginning of zone M_2 and the middle of zone M_4, when the sea depth and salinity increased rapidly. The change from shallow diluted water, quite highly oxygenated near the bottom, to a saline marine environment shows up in diatom and geochemical data, as well as in the appearance of abundant mollusc fauna. The similarity of conclusions based on diatom and geochemical analyses indicates that the contents of elements can be a reliable proxy of salinity in paleobasins. As evidenced by geochemical study, the salinity of the Mga Sea during the marine episode and the ensuing regressive phase, remained at a minimum of 18‰. The mollusc fauna almost disappeared in the beginning of zone M_5 as the Mga bottom

water became anoxic. The marine phase lasted till the middle of pollen zone M_{6-7}, and then the sea began shoaling gradually. The regression, with its onset marked by lower contents of marine organic matter in the Mga sediments, lasted as long as the end of pollen zone M_8. The bottom water of the Mga Sea was mainly anoxic over the greater part of the marine phase and during the whole regression phase, which accounts for low numbers and poor taxonomic diversity of the mollusc fauna (e.g., Funder et al., 2002). The conditions changed to freshwater in the end of pollen zone M_8 or in the Early Valdai.

The K-feldspar luminescence ages for the Sverdlov Fm. samples are overestimated, apparently because the feldspar grains had not been bleached completely before burial. The incomplete bleaching is additionally confirmed by dating of deposits from the Baltic Ice Lake showing an up to 250 Gy remnant dose in K-feldspar from glaciolacustrine sediments. The bleaching degree may be the same in the respective Sverdlov and Baltic sediments, which were deposited in similar conditions. The age of the Mga Fm. has been constrained by fifteen OSL dates on K-feldspar, with an average of 123±10 (2σ) ka, as well as the 119±7 ka age for the Mikulino/Lower Valdai limnic facies lying above the Mga Fm. The ages obtained for the Mga and Mikulino/Lower Valdai sediments made basis for an age-depth model in which the Mga interglacial deposition is bracketed between 133±8 (1σ) and 109±7 (1σ) ka ago. These age bounds apply to the onset and end of the Mikulino Interglacial, as the Mga Fm. in the Sverdlov Factory quarry encompasses all Mikulino pollen zones. These estimates are consistent with approximate correlation between the Mikulino (Eemian) interglacial and MIS 5e, with regard to a large measurement uncertainty.

Sampling and comparative analysis of thirty one Eemian (Mga) sections in the Baltic and Onego-Ladoga regions revealed a well-pronounced boundary between the brackish and marine phases at the same chronostratigraphic level in most of the sections throughout the territory, as a marker for correlating pollen zones in the beginning of the LIG. The the vegetation evolutions phases in the studied territory were found out to be shifted in the northern and northeastern directions relative to Central Europe. The lag behind the respective phases of the Bispingen (Germany) and Lower Vistula (Poland) sections reaches ~900 years, i.e., the Bispingen chronology (Müller, 1974) cannot be used directly for timing pollen zones in the sections of the East European Plain.

The obtained results allow several inferences:

1. The Mga marine interglacial deposition in the territory of the Neva Lowland lasted within a period corresponding to Mikulino pollen zones M_2–M_8, from 133±8 to 109±7 ka ago. The beginning of the Mikulino Stage in the Neva Lowland coincides roughly with the top of the Sverdlov varved clay.

2. The evolution of the Mga Sea comprised four main phases of glaciomarine (pollen zones Ms_3–Ms_1), brackish (M_2–M_3), marine (M_4–M_6), and regressive (M_6–M_8) environments. Seawater penetrated into the Late Moscow periglacial basin in the territory of the present Neva Lowland no later than ~1100

years before the Mikulino Interglacial. Between ~1030 and ~350 years before the LIG, the Mga Sea became much less saline (or freshwater), but then the connection with the ocean resumed.

3. The bottom water of the Mga Sea became anoxic in the beginning of pollen zone M5, and these conditions lasted till the end of zone M_8. The lack of oxygen in the bottom water accounts for low numbers and poor diversity of molluscs in the Mga sediments.

4. The isochronous boundary between the brackish and marine phases detectable clearly in most of the Eemian (Mga) marine sections all over the Baltic and Onego-Ladoga regions marks abrupt increase in the sea depth and salinity of the Baltic and Mga basins.

5. The early interglacial vegetation phases in the Gulf of Finland area lagged ~900 years behind the respective phases of Central Europe.

List of abbreviatures

asl – above sea level

BH – borehole

CN analysis – carbon and nitrogen analysis

D_e – equivalent dose

DRC – dose response curve

ESR – electron-spin resonance

Fm. – Formation

IRD – ice-rafted debris

IRSL – infrared stimulated luminescence

LIG – Last Interglacial

LPZ – local pollen zone

MIS – marine isotopic stage

OM – organic matter

OSL – optically stimulated luminescence

pIR-IRSL – post infra-red IRSL

RPZ – regional pollen zone

SAR protocol – single-aliquot regenerative-dose protocol

TOC – total organic carbon

XRF – X-ray fluorescence

References

1. Abakumenko G.S., Ladyshkina T.E., Saltykova V.F., Semicheva V.I., Usikova T.V. Marine interglacial deposits in the north of the Karelian Isthmus // Stratigraphy and paleogeography of the Quaternary period of the North of the European part of the USSR / ed. Biske G.S. Petrozavodsk: Karelskij filial AN SSSR, 1977. P. 93–97 (in Russian).

2. Abrukina R.E., Krasilnikova G.N. Foraminifers of marine interglacial deposits of the Kola-Karelian region, their stratigraphic significance and history of development // Quaternary geology and geomorphology of the eastern part of the Baltic Shield / ed. Biske G.S. Leningrad: Nauka, 1972. P. 39–58 (in Russian).

3. Ailio J. Die geographishe Entwicklung des Ladogases in Postglazialer Zeit und ihre Beziehung zur stenzeitlichen Besiedelung // Fennia. 1915. Vol. 38, No. 3. P. 157–157.

4. Aitken M.J. Thermoluminescence Dating. London etc.: Academic press, 1985. 359 p.

5. Aitken M.J. Optical dating: a non-specialist review // Quaternary Science Reviews. 1994. Vol. 13, No. 5–7. P. 503–508.

6. Alexanderson H., Murray A.S. Luminescence signals from modern sediments in a glaciated bay, NW Svalbard // Quaternary Geochronology. 2012. Vol. 10. P. 250–256.

7. Allen J.R.M., Huntley B. Last Interglacial palaeovegetation, palaeoenvironments and chronology: a new record from Lago Grande di Monticchio, southern Italy // Quaternary Science Reviews. 2009. Vol. 28, No. 15–16. P. 1521–1538.

8. Andersen S. Th. New Investigations of Interglacial Fresh-Water Deposits in Jutland: A Preliminary Report // Quaternary Science Journal. Copernicus GmbH, 1957. Vol. 8, No. 1. P. 181–186.

9. Andersen S. Th. Vegetation and its Environment in Denmark in the Early Weichselian Glacial (Last Glacial) // Danmarks Geologiske Undersøgelse II. Række. Geological Survey of Denmark and Greenland, 1961. Vol. 75. P. 1–175.

10. Andersen S. Th. The Eemian freshwater deposit at Egernsund, South Jylland, and the Eemian landscape development in Denmark // Danmarks Geologiske Undersøgelse. Årbog 1974 / ed. Rasmussen L.B., Michelsen O. København: I kommission hos C.A. Reitzels Forlag, 1975. P. 49–70.

11. Andreev A.A., Shumilovskikh L.S., Savelieva L.A., Gromig R., Fedorov G.B., Ludikova A.V., Wagner B., Wennrich V., Brill D., Melles M. Environmental conditions in northwestern Russia during MIS 5 inferred from the pollen stratigraphy in a sediment core from Lake Ladoga // Boreas. 2019. Vol. 48, No. 2. P. 377–386.

12. Anechitei-Deacu V., Timar-Gabor A., Constantin D., Trandafir-Antohi O., Valle L.D., Fornós J.J., Gómez-Pujol L., Wintle A.G. Assessing the maximum limit of SAR-OSL dating using quartz of different grain sizes // Geochronometria. 2018. Vol. 45, No. 1. P. 146–159.

13. Ansberg E.A., Znamenskaya O.M. On marine sediments in the watershed of the Tosna and Sablinka Rivers // Doklady Akademii Nauk SSSR. 1941. Vol. 30, No. 9. P. 822–823.

14. Apukhtin N.I., Ekman I.M. Stratigraphy. Murmansk Oblast, Karelia, west of Arkhangelsk, north-west of Vologda and north of Leningrad Oblasts // Quaternary geology of the North-West of the European part of the USSR / ed. Apukhtin N.I., Krasnov I.I. Leningrad: Nedra. Leningrad Branch, 1967. P. 48–110 (in Russian).

15. Apukhtin N.I., Petrova E.A., Semyonova O.I., Shostak Z.A., Garkusha V.I., Perevozchikova V.A., Diakonova E.V. Report on geological survey of sheet P-36-XXXI on a scale of 1:200,000 (Karelian Isthmus). Leningrad, 1959 (in Russian).

16. Apukhtin N.I., Pokrovskaya I.M., Sharkov V.V., Yakovleva S.V. Stratigraphy of Quaternary deposits of the North-West of the USSR // Chronology and climates of the Quaternary period. International Geological Congress, XXI session. Moscow: Nauka, 1960 (in Russian).

17. Apukhtin N.I., Sammet E.Y. Pskov, Novgorod, western and southern parts of the Leningrad Oblast // Geomorphology and Quaternary deposits of the north-west of the European part of the USSR / ed. Apukhtin N.I., Krasnov I.I. Leningrad: Nedra. Leningrad Branch, 1967. P. 111–160 (in Russian).

18. Arslanov K.A., Breslav S.L., Zarrina E.P., Znamenskaya O.M., Krasnov I.I., Malakhovsky D.B., Spiridonova E.A. Climatostratigraphy and chronology of the Middle Valdai of the North-Western and Central Russian Plain // Pleistocene glaciations of the East European Plain / ed. Velichko A.A., Faustova M.A. Moscow: Nauka, 1981. P. 12–27 (in Russian).

19. Ashkroft N., Mermin N. Solid state physics. Volume 2. Moscow: Mir, 1979. 185 p (in Russian).

20. Astakhov V.I., Arslanov K.A., Maksimov F.E., Kuznetsov V.Y., Razina V.V., Nazarov D.V. Age of the interglacial peat section on the Lower Ob // Doklady Earth Sciences. 2005. Vol. 401, No. 2. P. 298–302.

21. Astakhov V.I., Nazarov D.V. Correlation of Upper Pleistocene sediments in northern West Siberia // Quaternary Science Reviews. 2010. Vol. 29, No. 25–26. P. 3615–3629.

22. Auslender V.G., Afanasov M.N., Andreeva N.G., Andriyanov V.D., Blankfeld K.S., Bogomolova T.V., Borovikova N.A., Garbar L.D., Fedko G.N., Fedotova E.S., Kabakov L.G., Karagodina M.V., Khazanovich-Vulf K.K., Koff G.L., Kotlov V.F., Mukhina I.A., Nagaisky A.F., Pleshivtseva E.S., Poluektov L.N., Popova O.V., et al. Report on complex geological, hydrogeological and engineering-geological further studies of scale 1:50 000 with general search and geoecological mapping of the territory of St. Petersburg and its vicinity. St. Petersburg, 2001 (in Russian).

23. Auslender V.G., Pleshivtseva E.S. Modern perspectives on the structure of the land Quarter in St. Petersburg and its surroundings // Collection of articles of FGUP “Petersburg Complex Geological

Expedition" employees devoted to the 60th organisation anniversary / ed. Vasin O.V., Korovkin V.A. St. Petersburg: Petersburg Complex Geological Expedition, 2011. P. 82–87 (in Russian).

24. Auslender V.G. Modern concepts regarding the structure of Quaternary strata in St. Petersburg and its surrounding areas // All-Russian Conference "The mainest investigation results of the Quaternary period and main directions of research in 21st century". Abstracts. St. Petersburg: VSEGEI, 1998. P. 311–312 (in Russian).

25. Autzen M., Andersen C.E., Bailey M., Murray A.S. Calibration quartz: An update on dose calculations for luminescence dating // Radiation Measurements. Elsevier Ltd, 2022. Vol. 157. P. 106828.

26. Bailey R.M., Smith B.W., Rhodes E.J. Partial bleaching and the decay form characteristics of quartz OSL // Radiation Measurements. 1997. Vol. 27, No. 2. P. 123–136.

27. Ballarini M., Wallinga J., Wintle A.G., Bos A.J.J. A modified SAR protocol for optical dating of individual grains from young quartz samples // Radiation Measurements. 2007. Vol. 42, No. 3. P. 360–369.

28. Baltrūnas V., Maksimov F.E., Kuznetsov V.Y., Karmaza B., Katinas V. Geochronology and palaeomagnetic records of the snaigupėlė section in South Lithuania // Geochronometria. Walter de Gruyter GmbH, 2015. Vol. 42, No. 1. P. 172–181.

29. Baltrūnas V., Šeiriene V., Molodkov A.N., Zinkute R., Katinas V., Karmaza B., Kisieliene D., Petrošius R., Taraškevičius R., Piličiauskas G., Schmölcke U., Heinrich D. Depositional environment and climate changes during the late Pleistocene as recorded by the Netiesos section in southern Lithuania // Quaternary International. 2013. Vol. 292. P. 136–149.

30. Banerjee D., Murray A.S., Bøtter-Jensen L., Lang A. Equivalent dose estimation using a single aliquot of polymineral fine grains // Radiation Measurements. 2001. Vol. 33, No. 1. P. 73–94.

31. Banham P.H. Glacitectonites in till stratigraphy // Boreas. 1977. Vol. 6, No. 2. P. 101–105.

32. Barré M., Lamothe M. Luminescence dating of archaeosediments: A comparison of K-feldspar and plagioclase IRSL ages // Quaternary Geochronology. Elsevier B.V., 2010. Vol. 5, No. 2–3. P. 324–328.

33. Beets D.J., Beets C.J., Cleveringa P. Age and climate of the late Saalian and early Eemian in the type-area, Amsterdam basin, The Netherlands // Quaternary Science Reviews. 2006. Vol. 25, No. 9–10. P. 876–885.

34. Bennett M.R., Glasser N.F. Glacial geology: ice sheets and landforms. 2nd Edition. Wiley-Blackwell, 2009. P. 385385 p.

35. Berner R.A. thermodynamic stability of sedimentary iron sulfides // American Journal of Science. American Journal of Science (AJS), 1967. Vol. 265, No. 9. P. 773–785.

36. Berner R.A. Sedimentary pyrite formation // American Journal of Science. American Journal of Science (AJS), 1970. Vol. 268, No. 1. P. 1–23.

37. Berner R.A. Sedimentary pyrite formation: An update // Geochimica et Cosmochimica Acta. 1984. Vol. 48, No. 4. P. 605–615.

38. Berner R.A., Raiswell R. C/S method for distinguishing freshwater from marine sedimentary rocks // Geology. 1984. Vol. 12, No. 6. P. 365–368.

39. Blaauw M., Christen J.A. Flexible paleoclimate age-depth models using an autoregressive gamma process // Bayesian Analysis. 2011. Vol. 6, No. 3. P. 457–474.

40. Blaauw M., Christen J.A., Aquino Lopez M.A., Esquivel Vazquez J., Gonzalez V. O.M., Belding T., Theiler J., Gough B., Karney C. Package ‘rbacon’. Version 2.5.8. Age-Depth Modelling using Bayesian Statistics. 2022.

41. Blanchet C.L., Thouveny N., Vidal L., Leduc G., Tachikawa K., Bard E., Beaufort L. Terrigenous input response to glacial/interglacial climatic variations over southern Baja California: a rock magnetic approach // Quaternary Science Reviews. 2007. Vol. 26, No. 25–28. P. 3118–3133.

42. Blott S.J., Pye K. Gradistat: A grain size distribution and statistics package for the analysis of unconsolidated sediments // Earth Surface Processes and Landforms. 2001. Vol. 26, No. 11. P. 1237–1248.

43. Boettger T., Novenko E.Y., Velichko A.A., Borisova O.K., Kremenetski K.V., Knetsch S., Junge F.W. Instability of climate and vegetation dynamics in Central and Eastern Europe during the final stage of the Last Interglacial (Eemian, Mikulino) and Early Glaciation // Quaternary International. 2009. Vol. 207, No. 1–2. P. 137–144.

44. Bolikhovskaya N.S., Molodkov A.N. Dynamics of Pleistocene Paleoclimatic Events: A Reconstruction Based on Palynological and Electron Spin Resonance Studies in North Eurasia // Archaeology Ethnology and Anthropology of Eurasia. 2002. Vol. 2, No. 10. P. 2–21.

45. Bolshiyanov D.Yu., Krylov A.V., Molodkov A.N., Savelieva L.A., Anikina N.Yu., Pushina Z.V., Rashke E.A., Nikitin M.Yu., Klevtsov A.S. New data about age, structure, faunal composition of marine sediments in the vicinity of St. Petersburg // Proceedings of the Russian Geographical Society. 2016. Vol. 148, No. 3. P. 25–46 (in Russian).

46. Borisova O.K., Novenko E.Y. Reconstruction of vegetation and climate during the pre-Mikulino late ice age according to pollen data analysis // Vestnik Moskovskogo Universiteta. Seria 5, Geografia. 2014. Vol. 5. P. 30–35.

47. Börner A., Hrynowiecka A., Kuznetsov V.Y., Stachowicz-Rybka R., Maksimov F.E., Grigoriev V.A., Niska M., Moskal-del Hoyo M. Palaeoecological investigations and 230Th/U dating of

Eemian interglacial peat sequence of Banzin (Mecklenburg-Western Pomerania, NE-Germany) // Quaternary International. Elsevier Ltd, 2015. Vol. 386. P. 122–136.

48. Börner A., Hrynowiecka A., Stachowicz-Rybka R., Niska M., Moskal-del Hoyo M., Kuznetsov V.Y., Maksimov F.E., Petrov A.Yu. Palaeoecological investigations and 230Th/U dating of the Eemian Interglacial peat sequence from Neubrandenburg-Hinterste Mühle (Mecklenburg-Western Pomerania, NE Germany) // Quaternary International. 2018. Vol. 467. P. 62–78.

49. Bøtter-Jensen L., Andersen C.E., Duller G.A.T., Murray A.S. Developments in radiation, stimulation and observation facilities in luminescence measurements. 2003. Vol. 37, No. 4–5. P. 535–541.

50. Bøtter-Jensen L., Bulur E., Duller G.A.T., Murray A.S. Advances in luminescence instrument systems // Radiation Measurements. 2000. Vol. 32, No. 5. P. 523–528.

51. Bøtter-Jensen L., Duller G.A.T., Murray A.S., Banerjee D. Blue light emitting diodes for optical stimulation of quartz in retrospective dosimetry and dating // Radiation Protection Dosimetry. Nuclear Technology Publishing, 1999. Vol. 84, No. 1–4. P. 335–340.

52. Bøtter-Jensen L., Thomsen K.J., Jain M. Review of optically stimulated luminescence (OSL) instrumental developments for retrospective dosimetry // Radiation Measurements. 2010. Vol. 45, No. 3–6. P. 253–257.

53. Brander G. Ein Interglazialfund bei Rouhiala in Südostfinnland // Bulletin de la Commission géologique de Finlande. 1937. No. 118. P. 1–75.

54. Brander G. Zur Deutung der intramoränen Tonablagerung an der Mga, unweit von Leningrad // Bulletin de la Commission géologique de Finlande. 1937. No. 119. P. 93–112.

55. Brauer A., Allen J.R.M., Mingram J., Dulski P., Wulf S., Huntley B. Evidence for last interglacial chronology and environmental change from Southern Europe // Proceedings of the National Academy of Sciences of the United States of America. 2007. Vol. 104, No. 2. P. 450–455.

56. Brigham-Grette J. New perspectives on Beringian Quaternary paleogeography, stratigraphy, and glacial history // Quaternary Science Reviews. 2001. Vol. 20, No. 1–3. P. 15–24.

57. Buslovich A.L., Garkusha V.I., Nikolaev B.A., Savanin V.S., Shipunova V.K., Starodub Yu.V., Dymov V.A., Makariev A.A., Makarieva E.M., Pogorelsky A.I., Serov E.K. Information report on the further geological study of the Onega area on a scale of 1:200 000 and preparation for the publication of the Gosgeolmap-200 set (second edition) sheets P-36-XXX, P-37-XXV. Onego object. St. Petersburg, 2002 (in Russian).

58. Buslovich A.L., Spiridonova E.A., Rukhina E.V., Malakhovsky D.B. Middle Pleistocene deposits // Geomorphology and Quaternary deposits of the North-West of the European part of the USSR

(Leningrad, Pskov and Novgorod regions) / ed. Malakhovsky D.B., Markov K.K. Leningrad: Nauka. Leningrad branch, 1969. P. 104–111 (in Russian).

59. Buylaert J.-P., Jain M., Murray A.S., Thomsen K.J., Thiel C., Sohbati R. A robust feldspar luminescence dating method for Middle and Late Pleistocene sediments // Boreas. 2012. Vol. 41. P. 435–451.

60. Buylaert J.-P., Murray A.S., Thomsen K.J., Jain M. Testing the potential of an elevated temperature IRSL signal from K-feldspar // Radiation Measurements. 2009. Vol. 44, No. 5–6. P. 560–565.

61. Buylaert J.-P., Vandenberghe D.A.G., Murray A.S., Huot S., De Corte F., Van Den Haute P. Luminescence dating of old (>70 ka) Chinese loess: A comparison of single-aliquot OSL and IRSL techniques // Quaternary Geochronology. 2007. Vol. 2, No. 1–4. P. 9–14.

62. Calvert S.E., Pedersen T.F. Chapter Fourteen Elemental Proxies for Palaeoclimatic and Palaeoceanographic Variability in Marine Sediments: Interpretation and Application // Developments in Marine Geology. 2007. Vol. 1. P. 567–644.

63. CAPE-LIP Members: Anderson P., Bennike O., Bigelow N., Brigham-Grette J., Duvall M., Edwards M., Fréchette B., Funder S., Johnsen S., Knies J., Koerner R., Lozhkin A., Marshall S., Matthiessen J., Macdonald G., Miller G., Montoya M., Muhs D.R., Otto-Bliesner B., et al. Last Interglacial Arctic warmth confirms polar amplification of climate change // Quaternary Science Reviews. Elsevier Ltd, 2006. Vol. 25, No. 13–14. P. 1383–1400.

64. Caspers G. Die eem- und weichselzeitliche Hohlform von Groß Todtshorn (Kr. Harburg; Niedersachsen) — Geologische und palynologische Untersuchungen zu Vegetation und Klimaverlauf der letzten Kaltzeit // Schriftenreihe Deutsche Geologische Gesellschaft. 1997. Vol. 4. P. 7–59.

65. Chapot M.S., Roberts H.M., Duller G.A.T., Lai Z.P. A comparison of natural- and laboratory-generated dose response curves for quartz optically stimulated luminescence signals from Chinese Loess // Radiation Measurements. 2012. Vol. 47, No. 11–12. P. 1045–1052.

66. Chebotaryova N.S. A new section with Dnieper-Valdai interglacial deposits on the Kasplya River near the Verkhnyaya Boyarshchina Village // Materials on paleogeography. Vol. 1. Moscow: Moscow State University, 1954. P. 69–81 (in Russian).

67. Chepurnaya A.A. Migration of Broadleaf Species of the East European Plain during the Mikulino Interglacial // Izvestiya RAN (Akad. Nauk SSSR). Seriya Geograficheskaya. 2009. Vol. 4. P. 69–77 (in Russian).

68. Chepurnaya A.A. Spatio-temporal analysis of vegetation dynamics within the forest zone of the East European Plain in the Mikulino interglacial (according to palynological data): Dissertation for

an academic degree Candidate of Geographical Sciences. Moscow: Institute of Geography, 2009. 192 p (in Russian).

69. Cheremisinova E.A. Marine diatom flora of interglacial deposits in the valley of the Mgi and Vytegra Rivers and in the basin of Lake Ladoga. Abstract of the dissertation for the degree of Candidate of Biological Sciences. 1952. P. 21–21 (in Russian).

70. Cheremisinova E.A. Marine diatom flora of Quaternary sediments of the Lake Ladoga basin // Bulletin of the Commission for study of the Quaternary. 1957. Vol. 21. P. 105–112 (in Russian).

71. Cheremisinova E.A. Paleogeography of the Mga Sea (based on diatom analysis data) // Doklady Akademii Nauk SSSR. 1959. Vol. 129, No. 2. P. 416–419 (in Russian).

72. Cheremisinova E.A. On the question of the age of marine interglacial deposits on the Mge River, Leningrad Oblast // Bulletin of the Commission for study of the Quaternary. 1960. Vol. 25. P. 50–70 (in Russian).

73. Cheremisinova E.A. Diatoms of marine interglacial sediments of the Estonian SSR // Doklady Akademii Nauk SSSR. 1961. Vol. 141, No. 3. P. 698–700 (in Russian).

74. Cheremisinova E.A. Marine diatom flora in the area of the Vytegra River (Onego-Beloye Lake watershed) // Doklady Akademii Nauk SSSR. 1962. Vol. 145, No. 4. P. 891–894 (in Russian).

75. Cleve-Euler A. Das letztinterglaziale Baltikum und die Diatomeenanalyse // Beihefte zum Botanischen Centralblatt. Abteilung B. 1940. Vol. 60, No. 3. P. 287–334.

76. Constantin D., Begy R., Vasiliniuc S., Panaiotu C., Necula C., Codrea V., Timar-Gabor A. High-resolution OSL dating of the Costineşti section (Dobrogea, SE Romania) using fine and coarse quartz // Quaternary International. Elsevier Ltd, 2014. Vol. 334–335. P. 20–29.

77. Cresswell A.J., Carter J., Sanderson D.C.W. Dose rate conversion parameters: Assessment of nuclear data // Radiation Measurements. Elsevier Ltd, 2018. Vol. 120. P. 195–201.

78. Cunningham A.C., Buylaert J.-P., Murray A.S. Attenuation of beta radiation in granular matrices: implications for trapped-charge dating // Geochronology. 2022. Vol. 4. P. 517–531.

79. Cunningham A.C., Wallinga J. Selection of integration time intervals for quartz OSL decay curves // Quaternary Geochronology. 2010. Vol. 5, No. 6. P. 657–666.

80. Cuven S., Francus P., Lamoureux S.F. Estimation of grain size variability with micro X-ray fluorescence in laminated lacustrine sediments, Cape Bounty, Canadian High Arctic // Journal of Paleolimnology. 2010. Vol. 44, No. 3. P. 803–817.

81. Degering D., Krbetschek M.R. Dating of interglacial sediments by luminescence methods // The Climate of Past Interglacials. Developments in Quaternary Science / ed. Sirocko F., Claussen M., Sanchez Goni M.F., Litt T. Amsterdam: Elsevier, 2007. P. 157–172.

82. Devyatova E.I. Late Pleistocene environments as related to human migrations in the Severnaya Dvina basin and in Karelia. Petrozavodsk, 1982. 156 p (in Russian).

83. Devyatova E.I. Palynological characteristics of the Upper Quaternary deposits of Karelia // Quaternary geology and geomorphology of the eastern part of the Baltic Shield / ed. Biske G.S. Leningrad: Nauka, 1972. P. 59–96 (in Russian).

84. Devyatova E.I., Abrukina R.E., Starova N.N. Report on the topic: "Studying the patterns of development of the Quaternary flora and fauna in order to clarify the paleontological criteria for the stratigraphy of the Upper Quaternary deposits of Karelia." Petrozavodsk, 1968 (in Russian).

85. Döös K., Meier H.E.M., Döscher R. The Baltic haline conveyor belt or the overturning circulation and mixing in the Baltic // Ambio. Kluwer Academic Publishers, 2004. Vol. 33, No. 4–5. P. 261–266.

86. Dudanova V.I. Magnetostratigraphy of the Middle–Upper Neopleistocene of the Neva area (section "Etalon"). Master's dissertation. 2023. 77 p (in Russian).

87. Dudanova V.I., Sheetov M.V., Biske Yu.S. New data on the history of the Neva River. Moscow: Geographical faculty of Lomonosov Moscow State University, 2020. P. 117–122 (in Russian).

88. Dudanova V.I., Veselovskiy R.V., Ruchkin M.V., Sheetov M.V. The Blake geomagnetic excursion recorded in the Mikulino interglacial sediments of the Neva Lowland // Doklady Earth Sciences (in press, in Russian).

89. Dudanova V.I., Veselovskiy R.V., Sheetov M.V. First results of petro- and paleomagnetic study from the key section of the Middle-Upper Pleistocene in the Sverdlov (Etalon) Factory / ed. Panin A.V., Borisova O.K., Konstantinov E.A., Kurenkova E.I., Timireva S.N., Kononov Yu.M. Moscow: Institute of Geography, RAS, 2021. P. 318–322 (in Russian).

90. Duller G.A.T. Distinguishing quartz and feldspar in single grain luminescence measurements // Radiation Measurements. 2003. Vol. 37, No. 2. P. 161–165.

91. Duller G.A.T. The Analyst software package for luminescence data: overview and recent improvements // Ancient TL. 2015. Vol. 33, No. 1. P. 35–42.

92. Duller G.A.T. Analyst v4.57 User Manual. Aberystwyth, 2018. P. 1-111-1–111.

93. Durcan J.A., Duller G.A.T. The fast ratio: A rapid measure for testing the dominance of the fast component in the initial OSL signal from quartz // Radiation Measurements. 2011. Vol. 46, No. 10. P. 1065–1072.

94. Durcan J.A., King G.E., Duller G.A.T. DRAC: Dose Rate and Age Calculator for trapped charge dating // Quaternary Geochronology. 2015. Vol. 28. P. 54–61.

95. Duval M., Guilarte V., Campaña Lozano I., Arnold L.J., Miguens Rodríguez L., Iglesias Cibanal J., González-Sierra S. Quantifying hydrofluoric acid etching of quartz and feldspar coarse grains

based on weight loss estimates: implication for ESR and luminescence dating studies // Ancient TL. 2018. Vol. 36, No. 1. P. 1–14.

96. Eriksson B. The Eemian pollen stratigraphy and vegetational history of Ostrobothnia, Finland // Bulletin - Geological Survey of Finland. 1993. Vol. 372. P. 1–36.

97. Eriksson B., Grönlund T., Uutela A. Biostratigraphy of Eemian sediments at Mertuanoja, Pohjanmaa (Ostrobothnia), western Finland // Boreas. Scandinavian University Press, 1999. Vol. 28, No. 2. P. 274–291.

98. Feathers J.K. Single-grain OSL dating of sediments from the Southern High Plains, USA // Quaternary Science Reviews. Elsevier Ltd, 2003. Vol. 22, No. 10–13. P. 1035–1042.

99. Firbas F. Die Synchronisierung der mitteleuropaischen Pollendiagramme // Danmarks Geologiske Undersøgelse. II. Række. 1954. Vol. 80. P. 12–21.

100. Fleming S.J. The acquisition of radioluminescence by ancient ceramics: PhD Thesis. 1969.

101. Folk R.L., Ward W.C. Brazos River bar [Texas]; a study in the significance of grain size parameters // Journal of Sedimentary Research. Society for Sedimentary Geology, 1957. Vol. 27, No. 1. P. 3–26.

102. Folz E., Mercier N. Single-aliquot OSL protocol using bracketing regenerative doses to accurately determine equivalent doses in quartz // Radiation Measurements. Elsevier Science Ltd, 1999. Vol. 30, No. 4. P. 477–485.

103. Frechen M., Schweitzer U., Zander A. Improvements in sample preparation for the fine grain technique // Ancient TL. 1996. Vol. 14, No. 2. P. 15–17.

104. Frenzel B., Bludau W. On the duration of the interglacial to glacial transition at the end of the Eemian interglacial (Deep Sea Stage 5 E): botanical and sedimentological evidence // Abrupt climatic change. Proc. 1985. Reidel; NATO ASI Series C, 216, 1987. P. 151–162.

105. Funder S., Balic-Zunic T. Hypoxia in the Eemian: Mollusc faunas and sediment mineralogy from Cyprina Clay in the southern Baltic region // Boreas. Taylor and Francis A.S., 2006. Vol. 35, No. 2. P. 367–377.

106. Funder S., Demidov I.N., Yelovicheva Y. Hydrography and mollusc faunas of the Baltic and the White Sea-North Sea seaway in the Eemian // Palaeogeography, Palaeoclimatology, Palaeoecology. 2002. Vol. 184, No. 3–4. P. 275–304.

107. Gaigalas A.Yu., Molodkov A.N. ESR dating of the age of the Likhvin and Mikulino interglaciations in the West of the East European Plain. Saint Petersburg: VSEGEI, 1998. P. 19–19.

108. Gerasimov I.P., Markov K.K. Ice Age on the territory of the USSR // Trudy Instituta geografii AN SSSR. 1939. Vol. 33. P. 1–462 (in Russian).

109. Gibbard P., Glaister C. Pollen stratigraphy of the Late Pleistocene sediments at Mommark, Als, South Denmark // Boreas. Taylor and Francis A.S., 2006. Vol. 35, No. 2. P. 332–348.

110. Giesecke T., Bennett K.D., Birks H.J.B., Bjune A.E., Bozilova E., Feurdean A., Finsinger W., Froyd C., Pokorný P., Rösch M., Seppä H., Tonkov S., Valsecchi V., Wolters S. The pace of Holocene vegetation change - testing for synchronous developments // Quaternary Science Reviews. 2011. Vol. 30, No. 19–20. P. 2805–2814.

111. Glaister C.G., Gibbard P.L. Pollen stratigraphy of late pleistocene marine sediments at Norre Lyngby and Skagen, North Denmark // Quaternary Science Reviews. 1998. Vol. 17, No. 9–10. P. 839–854.

112. Godfrey-Smith D.I., Huntley D.J., Chen W.H. Optical dating studies of quartz and feldspar sediment extracts // Quaternary Science Reviews. 1988. Vol. 7. P. 373–380.

113. Goretsky G.I. Karelian Interglacial Sea // Voprosy geografii. 1949. Vol. 12. P. 97–132 (in Russian).

114. Govin A., Capron E., Tzedakis P.C., Verheyden S., Ghaleb B., Hillaire-Marcel C., St-Onge G., Stoner J.S., Bassinot F., Bazin L., Blunier T., Combourieu-Nebout N., El Ouahabi A., Genty D., Gersonde R., Jimenez-Amat P., Landais A., Martrat B., Masson-Delmotte V., Parrenin F., et al. Sequence of events from the onset to the demise of the Last Interglacial: Evaluating strengths and limitations of chronologies used in climatic archives // Quaternary Science Reviews. 2015. Vol. 129. P. 1–36.

115. Grechko A.E., Abakumenko V.E., Panova O.A., Oganesova A.M. Report on complex geological and engineering geologic mapping of scale 1:50 000 for land reclamation undertaken in the Priozersk district of the Leningrad region in 1969-1971. Leningrad, 1972 (in Russian).

116. Grichuk M.P., Grichuk V.P. On periglacial vegetation in the territory of the USSR // Periglacial phenomena in the territory of the USSR / ed. Markov K.K., Popov A.I. Moscow: Moscow University, 1960. P. 66–100 (in Russian).

117. Grichuk V.P. Fossil flora as a paleontological basis for stratigraphy of Quaternary deposits // Relief and stratigraphy of the Quaternary deposits in the North-Western part of the Russian Plain / ed. Markov K.K. Moscow: Akademia nauk SSSR, 1961. P. 25–71 (in Russian).

118. Grichuk V.P. Vegetation of Europe in the Late Pleistocene // Paleogeography of Europe during the last one hundred thousand years / ed. Gerasimov I.P., Velichko A.A. Moscow: Nauka, 1982. P. 92–109 (in Russian).

119. Grichuk V.P., Zaklinskaya E.D. Analysis of fossilized pollen and spores and its application in paleogeography. Moscow: Geographgiz, 1948. 222 p (in Russian).

120. Gromig R., Wagner B., Wennrich V., Fedorov G.B., Savelieva L.A., Lebas E., Krastel S., Brill D., Andreev A.A., Subetto D.A., Melles M. Deglaciation history of Lake Ladoga (northwestern Russia) based on varved sediments // Boreas. Blackwell Publishing Inc., 2019. Vol. 48, No. 2. P. 330–348.

121. Grøsfjeld K., Funder S., Seidenkrantz M.S., Glaister C. Last interglacial marine environments in the White Sea region, northwestern Russia // Boreas. 2006. Vol. 35, No. 3. P. 493–520.

122. Hahne J., Kemle S., Merkt J., Meyer K.-D. Eem-, weichsel- und saalezeitliche Ablagerungen der Bohrung ”QuakenbrückGE2” // Geologisches Jahrbuch A. 1994. Vol. 134. P. 9–69.

123. Haila H., Miettinen A., Eronen M. Diatom succession of a dislocated Eemian sediment sequence at Mommark, South Denmark // Boreas. Taylor and Francis A.S., 2006. Vol. 35, No. 2. P. 378–384.

124. Hansen V., Murray A.S., Buylaert J.-P., Yeo E.Y., Thomsen K.J. A new irradiated quartz for beta source calibration // Radiation Measurements. 2015. Vol. 81. P. 123–127.

125. Harff J., Endler R., Emelyanov E., Kotov S., Leipe T., Moros M., Olea R., Tomczak M., Witkowski A. Late Quaternary Climate Variations Reflected in Baltic Sea Sediments // The Baltic Sea basin: Central and Eastern European development studeis. Springer, 2011. P. 99–132.

126. Hart J.K., Boulton G.S. The interrelation of glaciotectonic and glaciodepositional processes within the glacial environment // Quaternary Science Reviews. 1991. Vol. 10, No. 4. P. 335–350.

127. Head M.J. Last Interglacial (Eemian) hydrographic conditions in the southwestern Baltic Sea based on dinoflagellate cysts from Ristinge Klint, Denmark // Geological Magazine. Cambridge University Press, 2007. Vol. 144, No. 6. P. 987–1013.

128. Head M.J., Pillans B., Zalasiewicz J.A., the ICS Subcommission on Quaternary Stratigraphy. Formal ratification of subseries for the Pleistocene Series of the Quaternary System // International Union of Geological Sciences. 2021/09/01 ed. International Union of Geological Sciences, 2021. Vol. 44, No. 3. P. 241–247.

129. Head M.J., Seidenkrantz M.S., Janczyk-Kopikowa Z., Marks L., Gibbard P.L. Last Interglacial (Eemian) hydrographic conditions in the southeastern Baltic Sea, NE Europe, based on dinoflagellate cysts // Quaternary International. Elsevier Ltd, 2005. Vol. 130, No. 1. P. 3–30.

130. Hearty P.J., Hollin J.T., Neumann A.C., O’Leary M.J., McCulloch M. Global sea-level fluctuations during the Last Interglaciation (MIS 5e) // Quaternary Science Reviews. 2007. Vol. 26, No. 17–18. P. 2090–2112.

131. Heck H.-L. Die Eem- und ihre begleitenden Junginterglazial-Ablagerungen bei Oldenbüttel in Holstein // Abhandlungen der Preußischen Geologischen Landesanstalt. Berlin, 1932. Vol. 140. P. 80–80.

132. Heinrich H. Origin and consequences of cyclic ice rafting in the Northeast Atlantic Ocean during the past 130,000 years // Quaternary Research. 1988. Vol. 29, No. 2. P. 142–152.

133. Helmens K.F. The last interglacial-glacial cycle (MIS 5-2) re-examined based on long proxy records from central and northern europe // Quaternary Science Reviews. Elsevier Ltd, 2014. Vol. 86. P. 115–143.

134. Hinsch W. Die Molluskenfauna des Eem-Interglazials von Offenbüttel—Schnittlohe (Nord-Ostsee-Kanal, Westholstein) // Geologisches Jahrbuch Reihe A. 1985. No. 86. P. 49–62.

135. Hoffmann D., Woda C., Lomitschka M., Mangini Ä. Untersuchungen zur ESR-Datierung eemzeitlicher Muscheln aus Schleswig-Holstein // Meyniana. 1999. Vol. 51. P. 113–124.

136. Huerta-Diaz M.A., Morse J.W. Pyritization of trace metals in anoxic marine sediments // Geochimica et Cosmochimica Acta. 1992. Vol. 56, No. 7. P. 2681–2702.

137. Huntley D.J., Baril M.R. The K content of the K-feldspars being measured in optical dating or in thermoluminescence dating // Ancient TL. 1997. Vol. 15. P. 11–13.

138. Huntley D.J., Godfrey-Smith D.I., Haskell E.H. Light-induced emission spectra from some quartz and feldspars // Nuclear Tracks and Radiation Measurements. 1991. Vol. 18, No. 1/2. P. 127–131.

139. Huntley D.J., Godfrey-Smith D.I., Thewalt M.L.W. Optical dating of sediments // Nature. 1985. Vol. 313, No. 5998. P. 105–107.

140. Huntley D.J., Hancock R.G.V. The Rb contents of the K-feldspar grains being measured in optical dating // Ancient TL. 2001. Vol. 19. P. 43–46.

141. Huntley D.J., Lamothe M. Ubiquity of anomalous fading in K-feldspars and the measurement and correction for it in optical dating // Canadian Journal of Earth Sciences. 2001. Vol. 38, No. 7. P. 1093–1106.

142. Husson F., Josse J. Package ‘missMDA’: Handling Missing Values with Multivariate Data Analysis. Version 1.18. 2022. P. 1-41-1–41.

143. Husson F., Josse J., Le S., Mazet J. Package ‘FactoMineR’: Multivariate Exploratory Data Analysis and Data Mining. Version 2.7. 2022. P. 1-106-1–106.

144. Hütt G.I., Jaek I.V., Tchonka J. Optical dating: K-feldspars optical response stimulation spectra // Quaternary Science Reviews. 1988. Vol. 7, No. 3–4. P. 381–385.

145. Hyyppä E. Bemerkungen über G. Branders Aufsatz „Ein Interglazialfund von Rouhiala in Südost-finnland" und zwei neue Tonfunde auf der karelischen Landenge // Bulletin de la Commission géologique de Finlande. 1937. No. 119. P. 145–170.

146. Ikonen L., Ekman I. Biostrategraphy of the Mikulino interglacial sediments in NW Russia: the Petrozavodsk site and a literature review // Annales Academiae Scientiarum Fennicae A III Geologica-Geographica. 2001. Vol. 161. P. 1–88.

147. IPCC. Climate Change 2022: Impacts, Adaptation and Vulnerability. Contribution of Working Group II to the Sixth Assessment Report of the Intergovernmental Panel on Climate Change / ed. Pörtner H.-O., Roberts D.C., Tignor M.S., Poloczanska E., Mintenbeck K., Alegría A., Craig M., Langsdorf S., Löschke S., Möller V., Okem A., Rama B. Cambridge, New York: Cambridge University Press, 2022. P. 30563056 p.

148. Jacobs Z., Wintle A.G., Duller G.A.T. Optical dating of dune sand from Blombos Cave, South Africa: I - Multiple grain data // Journal of Human Evolution. Academic Press, 2003. Vol. 44, No. 5. P. 599–612.

149. Jain M., Ankjærgaard C. Towards a non-fading signal in feldspar: Insight into charge transport and tunnelling from time-resolved optically stimulated luminescence // Radiation Measurements. 2011. Vol. 46, No. 3. P. 292–309.

150. Jain M., Murray A.S., Bøtter-Jensen L. Characterization of blue-light stimulated luminescence components in different quartz samples: Implications for dose measurement. 2003. Vol. 37, No. 4–5. P. 441–449.

151. Jakowleff S.A. Zur Einteilung der Quartärablagerungen der Umgebung von Petersburg // Centralblatt fur Mineralogie, Geologie und Palĭontologie. 1923. No. 19–20. P. 593–634.

152. Jessen K., Milthers V. Stratigraphical and palaeontological studies of interglacial flresh-water deposits in Jutlanda nd northwest Germany // Danmarks geologiske undersøgelse Række II. 1928. Vol. 48. P. 379–379.

153. Josse J., Husson F. missMDA: A package for handling missing values in multivariate data analysis // Journal of Statistical Software. American Statistical Association, 2016. Vol. 70.

154. Jung W., Beug H.-J., Dehm R. Das Riß/Würm-Interglazial von Zeifen, Landkreis Laufen a.d. Salzach. München, 1972. P. 131131 p.

155. Kalnina L. Middle and Late Pleistocene environmental changes recorded in the Latvian part of the Baltic Sea basin // Quaternaria. Seria A: Theses and Research Papers. 2001. Vol. 9. P. 1–173.

156. Kars R.H., Wallinga J., Cohen K.M. A new approach towards anomalous fading correction for feldspar IRSL dating - tests on samples in field saturation // Radiation Measurements. 2008. Vol. 43, No. 2–6. P. 786–790.

157. Kassambara A. Practical Guide to Principal Component Methods in R Multivariate Analysis. 2017. P. 205205 p.

158. Kassambara A., Mundt F. Package ‘factoextra’: Extract and Visualize the Results of Multivariate Data Analyses. 2022. P. 84–84.

159. Kenzler M., Rother H., Hüneke H., Frenzel P., Strahl J., Tsukamoto S., Li Y., Meng S., Gallas J., Frechen M. A multi-proxy palaeoenvironmental and geochronological reconstruction of the Saalian-Eemian-Weichselian succession at Klein Klütz Höved, NE Germany // Boreas. Blackwell Publishing Inc., 2018. Vol. 47, No. 1. P. 114–136.

160. Knudsen K.L. Foraminiferal Faunas in Eemian Deposits of the Oldenbüttel Area near the Kiel Canal, Germany // Geologisches Jahrbuch Reihe A. 1985. Vol. 86. P. 27–47.

161. Knudsen K.L., Jiang H., Gibbard P.L., Kristensen P., Seidenkrantz M.S., Janczyk-Kopikowa Z., Marks L. Environmental reconstructions of Eemian Stage interglacial marine records in the Lower Vistula area, southern Baltic Sea // Boreas. 2012. Vol. 41, No. 2. P. 209–234.

162. Knudsen K.L., Jiang H., Kristensen P., Gibbard P.L., Haila H. Early Last Interglacial palaeoenvironments in the western Baltic Sea: Benthic foraminiferal stable isotopes and diatom-based sea-surface salinity // Boreas. 2011. Vol. 40, No. 4. P. 681–696.

163. Kosack B., Lange W. Das Eem-Vorkommen von Offenbiittel/Schnittlohe und die Ausbreitung des Eem-Meeres zwischen Nord- und Ostsee // Geologisches Jahrbuch Reihe A. 1985. Vol. 86. P. 3–17.

164. Krasnov I.I., Arslanov K.A., Kazartseva T.I., Tertychnaya T.V., Chernov S.B., Pleshivtseva E.S. The key section of the Upper Pleistocene deposits in the Neva Lowland in the Kelkolovo quarry // Regional Geology and Metallogeny. 1995. Vol. 4. P. 88–99 (in Russian).

165. Krasnov I.I., Reineke V.I. On the gas content of Quaternary deposits in the Leningrad Oblast // Prirodnye gazy. Sbornik 11. Leningrad-Moscow: ONTI NKTP. Glavnaya redakciya geologorazvedochnoj i geodezicheskoj literatury, 1936. P. 3–32 (in Russian).

166. Krause W.E., Krbetschek M.R., Stolz W. Dating Quaternary lake sediments from the Schirmacher oasis (East Antarctica) by infra-red stimulated luminescence (IRSL) detected at the wavelength of 560 NM. 1997. Vol. 16, No. 3–5. P. 387–392.

167. Krbetschek M.R. Lumineszenz-Datierung quartärer Sedimente Mittel-, Ost- und Nordostdeutschlands: PhD Thesis. 1995. 122 p.

168. Krbetschek M.R., Rieser U., Zöller L., Heinicke J. Radioactive disequilibria in palaeodosimetric dating of sediments // Radiation Measurements. 1994. Vol. 23, No. 2–3. P. 485–489.

169. Kreutzer S. calc_FadingCorr(): Apply a fading correction according to Huntley & Lamothe (2001) for a given g-value and a given tc. Function version 0.4.3. // Luminescence: Comprehensive Luminescence Dating Data Analysis. R package version 0.9.18. https://CRAN.R-project.org/package=Luminescence. 2022.

170. Kreutzer S., Schmidt C., Dewitt R., Fuchs M. The a-value of polymineral fine grain samples measured with the post-IR IRSL protocol // Radiation Measurements. Elsevier Ltd, 2014. Vol. 69. P. 18–29.

171. Kristensen P., Gibbard P.L., Knudsen K.L., Ehlers J. Last Interglacial stratigraphy at Ristinge Klint, South Denmark // Boreas. Taylor and Francis A.S., 2000. Vol. 29, No. 2. P. 103–116.

172. Kristensen P., Knudsen K.L. Palaeoenvironments of a complete Eemian sequence at Mommark, South Denmark: Foraminifera, ostracods and stable isotopes // Boreas. 2006. Vol. 35, No. 2. P. 349–366.

173. Krukle M.Ya., Lusinya L.A., Stelle V.Ya. Section of Pleistocene deposits near the settlement of Felitsianova // Trudy Instituta geologii AN Latvijskoj SSR. 1963. Vol. XI. P. 7–30 (in Russian).

174. Kukla G.J., Bender M.L., de Beaulieu J.L., Bond G., Broecker W.S., Cleveringa P., Gavin J.E., Herbert T.D., Imbrie J., Jouzel J., Keigwin L.D., Knudsen K.L., McManus J.F., Merkt J., Muhs D.R., Müller H., Poore R.Z., Porter S.C., Seret G., Winograd I.J. Last interglacial climates // Quaternary Research. Academic Press Inc., 2002. Vol. 58, No. 1. P. 2–13.

175. Kukla G.J., McManus J.F., Rousseau D.D., Chuine I. How long and how stable was the last interglacial? // Quaternary Science Reviews. 1997. Vol. 16, No. 6. P. 605–612.

176. Kupriyanova L.A., Aleshina L.A. Pollen and spores of plants of the flora of the European part of the USSR. Leningrad: Nauka, 1972. 171 p (in Russian).

177. Kupriyanova L.A., Aleshina L.A. Pollen of dicotyledonous plants of the flora of the European part of the USSR. Leningrad: Nauka, 1978. 184 p (in Russian).

178. Kuznetsov V.Y., Maksimov F.E. Methods of Quaternary geochronometry in palaeogeography and marine geology. St. Petersburg: Nauka, 2012. 191 p (in Russian).

179. Kylander M.E., Ampel L., Wohlfarth B., Veres D. High-resolution X-ray fluorescence core scanning analysis of Les Echets (France) sedimentary sequence: New insights from chemical proxies // Journal of Quaternary Science. 2011. Vol. 26, No. 1. P. 109–117.

180. Lak G.C. Diatom flora of marine and lacustrine super-moraine sediments in the basin of Lake Ladoga / ed. Biske G.S. Petrozavodsk: Karelia, 1976. 64 p (in Russian).

181. Lambeck K., Purcell A., Funder S., Kjær K., Larsen E., Möller P. Constraints on the Late Saalian to early Middle Weichselian ice sheet of Eurasia from field data and rebound modelling // Boreas. 2006. Vol. 35, No. 3. P. 539–575.

182. Lamothe M., Auclair M., Hamzaoui C., Huot S. Towards a prediction of long-term anomalous fading of feldspar IRSL // Radiation Measurements. 2003. Vol. 37, No. 4–5. P. 493–498.

183. Lapp T., Kook M., Murray A.S., Thomsen K.J., Buylaert J.-P., Jain M. A new luminescence detection and stimulation head for the Risø TL/OSL reader // Radiation Measurements. 2015. Vol. 81. P. 178–184.

184. Lavrova M.A. On the question of the age of marine intermoraine deposits of Petrozavodsk and the Mga River // Trudy Sovetskoj sekcii po izucheniyu chetvertichnogo perioda. 1939. Vol. 4. P. 59–61 (in Russian).

185. Lavrova M.A. On the geographical limits of the Boreal Sea distribution and its physical-geographical regime // Trudy Instituta geografii AN SSSR. 1946. Vol. 37. P. 64–79 (in Russian).

186. Lavrova M.A. On the Baltic-White Sea interglacial junction // Trudy II Vsesoyuznogo geograficheskogo s"ezda. Volume II. 1948. P. 177–187 (in Russian).

187. Lavrova M.A. Correlation between the Interglacial Boreal transgression of the northern USSR and Eemian transgression in Western Europe // Morskie berega. Trudy Instituta geologii AN SSSR. 1961. Vol. 8. P. 65–88 (in Russian).

188. Lavrova M.A. The main section of Upper Pleistocene deposits of the Leningrad region // Questions of Quaternary stratigraphy of the North-West of the European part of the USSR. Leningrad: Gostopotekhizdat, 1962. P. 125–139 (in Russian).

189. Lavrova M.A., Grichuk M.P. New data on the Mga marine interglacial deposits // Doklady Akademii Nauk. 1960. Vol. 135, No. 6. P. 1472–1475 (in Russian).

190. Lê S., Josse J., Husson F. FactoMineR: An R package for multivariate analysis // Journal of Statistical Software. American Statistical Association, 2008. Vol. 25, No. 1. P. 1–18.

191. Li B., Li S.H. Comparison of De estimates using the fast component and the medium component of quartz OSL // Radiation Measurements. Elsevier Ltd, 2006. Vol. 41, No. 2. P. 125–136.

192. Li B., Li S.H. Luminescence dating of K-feldspar from sediments: A protocol without anomalous fading correction // Quaternary Geochronology. Elsevier B.V., 2011. Vol. 6, No. 5. P. 468–479.

193. LIGA members: Anderson P., Borisova O.K., de Beaulieu J.L., de Vernal A., Eiriksson J., Funder S., Gibbard P.L., Hamilton T., Harrison S.P., Houmark-Nielsen M., Huntley B., Knudsen K.L., Larsen E., Maher L.J., Matthews J.V., Miller G., Raukas A.V., Reeh N., Robertsson A.M., et al. Report of 1st discussion group: The last interglacial in high latitudes of the Northern Hemisphere: Terrestrial and marine evidence // Quaternary International. 1991. Vol. 10–12, No. C. P. 9–28.

194. Liivrand E. Rebedded pollen and spores in Pleistocene deposits and their role in stratigraphy // Palynology in continental and marine geologic investigations / ed. Bartosh T., Kabailiene M., Raukas A. Riga, 1976. P. 166–178 (in Russian).

195. Liivrand E. Importance of the rebedded pollen of interglacial thermophilic trees in stratigraphy // Izvestiya Akademii Nauk Estonskoi SSR. Seriya Geologiya. 1982. Vol. 31, No. 2. P. 75–79 (in Russian).

196. Liivrand E. Regional type section of the Eemian marine deposits on Suur-Prangli // Proceedings of the Academy of Sciences of the Estonian SSR. Geology. 1987. Vol. 36, No. 1. P. 20–26 (in Russian).

197. Liivrand E. Biostratigraphy of the Pleistocene deposits in Estonia and correlations in the Baltic region. Stockholm, 1991. 114 p.

198. Liivrand E., Valt E. Results of the palynological investigations of marine intermorainic deposits on the Suur-Prangli island (Estonia) // Bulletin of the Commission for study of the Quaternary. 1966. Vol. 31. P. 117–119 (in Russian).

199. Liritzis I. A new dating method by thermoluminescence of carved megalithic stone builing // Computes Rendus - Academie des Sciences, Serie II: Sciences de la Terre et des Planetes. 1994. Vol. 319, No. 5. P. 603–610.

200. Liritzis I., Guibert P., Foti F., Schvoerer M. The temple of Apollo (Delphi) strengthens novel thermoluminescence dating method // Geoarchaeology - An International Journal. John Wiley and Sons Inc., 1997. Vol. 12, No. 5. P. 479–496.

201. Liritzis I., Stamoulis K., Papachristodoulou C., Ioannides K. A re-evaluation of radiation dose-rate conversion factors // Mediterranean Archaeology and Archaeometry. 2013. Vol. 13, No. 3. P. 1–13.

202. Lisiecki L.E., Raymo M.E. Pliocene-Pleistocene stack of globally distributed benthic stable oxygen isotope records // Paleoceanography. 2005. Vol. 20, No. PA1003. P. 1–17.

203. Lowick S.E., Valla P.G. Characterising the luminescence behaviour of ‘infinitely old’ quartz samples from Switzerland // Quaternary Geochronology. Elsevier B.V., 2018. Vol. 43. P. 1–11.

204. Ludikova A.V. Diatoms from Late Glacial sediments of Lake Ladoga / ed. Bolikhovskaya N.S., Klyuvitkina T.S. Moscow: Geographical faculty of Lomonosov Moscow State University, 2017. P. 163–165 (in Russian).

205. Ludikova A.V. Diatoms in the Early Weichselian (Valdai) sediments in Lake Ladoga // Voprosy sovremennoi algologii. 2019. Vol. 2(20). P. 225–228 (in Russian).

206. Ludikova A.V., Subetto D.A., Andreev A.A., Gromig R., Fedorov G.B., Melles M. The first dated preglacial diatom record in Lake Ladoga: long-term marine influence or redeposition story? // Journal of Paleolimnology. 2021. Vol. 65, No. 1. P. 85–99.

207. Lysakov V.S. About excitons in crystalline quartz // Vestnik Orenburg State University. 2003. Vol. 1. P. 37–40 (in Russian).

208. Makowska A. Morza plejstocenskie w Polsce - Osady, wiek i paleogeografia. // Prace Instytutu Geologicznego. 1986. Vol. 120. P. 1–74.

209. Makowska A. Palaeogeography of the Prabuty-Susz area (lower Vistula region) prior to,to time and after the Tychnowy Sea transgression,and malacological fauna of the deposits // Biuletyn Panstwowego Instytutu Geologicznego. 2001. Vol. 398. P. 25–67.

210. Maksimov F.E., Kuznetsov V.Y. New version of the 230Th/U dating method of the Upper and Middle Neopleistocene deposits // Vestnik of Saint-Petersburg University. Earth Sciences. 2010. Vol. 4. P. 94–107 (in Russian).

211. Maksimov F.E., Kuznetsov V.Y., Grigoriev V.A., Levchenko S.B., Petrov A.Yu., Baranova N.G. On the chronology of the Mikulinian interglacial on the base of 230Th/U dating of terrestrial deposits from the East European Plain (preprint, in Russian).

212. Maksimov F.E., Kuznetsov V.Y., Savelieva L.A., Grigoriev V.A., Petrov A.Yu., Fomenko A.P., Baranova N.G. On the question of the time limits of the Mikulinian interglacial and its individual phases / ed. Panin A.V., Borisova O.K., Konstantinov E.A., Kurenkova E.I., Timireva S.N., Kononov Yu.M. Moscow: Institute of Geography, RAS, 2021. P. 812–816 (in Russian).

213. Maksimov F.E., Savelieva L.A., Levchenko S.B., Grigoriev V.A., Petrov A.Yu., Fomenko A.P., Khrebtievsky V.V., Kuznetsov V.Y. On the chronology of Mikulino interglacial in the North-West Russian Plain / ed. Gusev E.A. St. Petersburg: AARI, 2020. P. 322–326 (in Russian).

214. Maksimov F.E., Savelieva L.A., Popova S.S., Zyuganova I.S., Grigoriev V.A., Levchenko S.B., Petrov A.Yu., Fomenko A.P., Pankratova L.A., Kuznetsov V.Y. Chronostratigraphic Position of the Mikulinian Deposits (Case of the Reference Section Near Nizhnyaya Boyarshchina Village, Smolensk Oblast) // Izvestiya RAN (Akad. Nauk SSSR). Seriya Geograficheskaya. 2022. Vol. 86, No. 3. P. 447–469 (in Russian).

215. Malakhovsky D.B., Bakanova I.P., Buslovich A.L., Aleksandrova T.B., Vigdorchik M.E., Kotlukova I.V., Rukhina E.V., Sammet E.Y., Spiridonova E.A., Karchevsky M.F., Korneeva T.L., Cukhacheva L.P., Urbanovskaya M.A. Report on the topic: “Compilation of a map of Quaternary deposits and a set of accompanying maps on a scale of 1:500000 for the territory of the Leningrad, Pskov and Novgorod Oblasts.” Quaternary deposits, geomorphology, paleogeography and mineral resources. Leningrad, 1966 (in Russian).

216. Malakhovsky D.B., Kotlukova I.V., Spiridonov M.A. Problems of stratigraphy and paleogeography of the Upper Pleistocene of the Northwestern Russia // Regional Geology and Metallogeny. 2000. Vol. 12. P. 24–33 (in Russian).

217. Malakhovsky D.B., Spiridonova E.A., Kotlukova I.V., Bakanova I.P., Buslovich A.L., Kvasov D.D. The Valdai Stage // Geomorphology and Quaternary deposits of the North-West of the

European part of the USSR (Leningrad, Pskov and Novgorod regions) / ed. Malakhovsky D.B., Markov K.K. Leningrad: Nauka. Leningrad branch, 1969. P. 133–177 (in Russian).

218. Malakhovsky D.B., Spiridonova E.A., Rukhina E.V. The Mikulino (Mga) Stage // Geomorphology and Quaternary deposits of the North-West of the European part of the USSR (Leningrad, Pskov and Novgorod regions) / ed. Malakhovsky D.B., Markov K.K. Leningrad: Nauka. Leningrad branch, 1969. P. 111–133 (in Russian).

219. Malakhovsky D.B., Znamenskaya O.M., Rukhina E.V. Mga marine interglacial formation of the Northwestern RSFSR // Paleaogeography of limnic and marine basins of the North-West in the Pleistocene / ed. Malakhovsky D.B., Kvasov D.D. Leningrad: ГО USSR, 1989. P. 44–60 (in Russian).

220. Malcolm S.J., Price N.B. The behaviour of iodine and bromine in estuarine surface sediments // Marine Chemistry. 1984. Vol. 15. P. 263–271.

221. Malyasova E.S. Results of using the method of spore-pollen analysis for the stratigraphic division of Quaternary deposits of the Kola Peninsula, Karelia and the Karelian Isthmus // Collection of paleogeography and stratigraphy of Quaternary and Tertiary deposits. Leningrad: Leningrad University, 1960. P. 42–91 (in Russian).

222. Mamakova K. Pollen stratigraphy of the Eemian and adjoining glacial deposits based on continuous sequences in Poland // Bulletin of the Polish Academy of Sciences. Earth Sciences. 1988. Vol. 36, No. 3–4. P. 299–307.

223. Mamakova K. Late Middle Polish glaciation, Eemian and early Vistulian vegetation at Imbramowice near Wroclaw and the pollen stratigraphy of this part of the Pleistocene in Poland // Acta Palaeobotanica. 1989. Vol. 29, No. 1. P. 11–176.

224. Mangerud J. The Late Interglacial/Glacial cycle in northern Europe // Quaternary landscapes / ed. Shane L.C.K., Cushing E.J. Minneapolis: University of Minnesota Press, 1991. P. 38–75.

225. Mangerud J. Correlation of the Eemian and the weichselian with deep sea oxygen isotope stratigraphy // Quaternary International. 1989. Vol. 3–4, No. C. P. 1–4.

226. Marks L., Gałaogonekzka D., Krzymińska J., Nita M., Stachowicz-Rybka R., Witkowski A., Woronko B., Dobosz S. Marine transgressions during Eemian in northern Poland: A high resolution record from the type section at Cierpieogonekta // Quaternary International. Elsevier Ltd, 2014. Vol. 328–329, No. 1. P. 45–59.

227. Mayer L.M., Macko S.A., Mook W.H., Murray S. The distribution of bromine in coastal sediments and its use as a source indicator for organic matter // Organic Geochemistry. 1981. Vol. 3, No. 1–2. P. 37–42.

228. Mayer L.M., Schick L.L., Allison M.A., Ruttenberg K.C., Bentley S.J. Marine vs. terrigenous organic matter in Louisiana coastal sediments: The uses of bromine:organic carbon ratios // Marine Chemistry. 2007. Vol. 107, No. 2. P. 244–254.

229. McManus J.F., Anderson R.F., Broecker W.S., Fleisher M.Q., Higgins S.M. Radiometrically determined sedimentary fluxes in the sub-polar North Atlantic during the last 140,000 years // Earth and Planetary Science Letters. Elsevier B.V., 1998. Vol. 155, No. 1–2. P. 29–43.

230. Mejdahl V. Thermoluminescence dating of partially bleached sediments // Nuclear Tracks and Radiation Measurements (1982). 1985. Vol. 10, No. 4–6. P. 711–715.

231. Mejdahl V. Internal radioactivity in quartz and feldspar grains // Ancient TL. 1987. Vol. 5. P. 10–17.

232. Mellett C.L. Luminescence Dating // Geomorphological Techniques. London: British Society for Geomorphology, 2014. P. 1–11.

233. Menke B., Tynni R. Das Eeminterglazial und das Weichselfrühglazial von Rederstall/ Dithmarschen und ihre Bedeutung für die mitteleuropäische Jungpleistozän-Gliederung // Geologisches Jahrbuch Reihe A. 1984. Vol. 76. P. 1–109.

234. Menke B. Palynologische Untersuchungen zur Transgression des Eem-Meeres im Raum Offenbüttel/Nord-Ostsee-Kanal // Geologisches Jahrbuch Reihe A. 1985. Vol. 86. P. 19–26.

235. Menzel-Harloff H., Meng S. Spätsaalezeitliche und eemzeitliche Makrofaunen aus dem Kliffaufschluss Klein Klütz Höved (NW-Mecklenburg) mit Erstnachweisen von Belgrandia germanica (Gastropoda: Hydrobiidae), Pupilla loessica (Gastropoda: Pupillidae) und Lagurus lagurus (Mammalia: Cric // E&G Quaternary Science Journal. 2015. Vol. 64, No. 2. P. 82–94.

236. Meyers P.A., Teranes J.L. 9. Sediment organic matter // Tracking Environmental Change Using Lake Sediments. Volume 2: Physical and Geochemical Methods / ed. Last W.M., Smol J.P. Springer Dordrecht, 2001. P. 239–269.

237. Miettinen A., Head M.J., Knudsen K.L. Eemian sea-level highstand in the eastern baltic sea linked to long-duration white sea connection // Quaternary Science Reviews. 2014. Vol. 86. P. 158–174.

238. Miettinen A., Rinne K., Haila H., Hyvärinen H., Eronen M., Delusina I., Kadastik E., Kalm V., Gibbard P.L. The marine Eemain of the Baltic: New pollen and diatom data from Peski, Russia, and Põhja-Uhtju, Estonia // Journal of Quaternary Science. 2002. Vol. 17, No. 5–6. P. 445–458.

239. Miidel A. Voka outcrop // International Symposium on Human Impact and Geological Heritage. Excursion Guide and Abstracts, 12 - 17 May 2003. 2003. P. 33–35.

240. Mokrienko Z.M., Stronskaya M.N., Khineiko K.P., Panova O.A. Report on a comprehensive engineering-geological survey on a scale of 1:50,000, carried out in the Tosno and

Volkhov Districts of the Leningrad Oblast (sheets O-36-3-Б, Г and A, B partially) in 1962-1963. Leningrad, 1963 (in Russian).

241. Möller P., Murray A.S. Drumlinised glaciofluvial and glaciolacustrine sediments on the Småland peneplain, South Sweden - new information on the growth and decay history of the Fennoscandian Ice Sheets during MIS 3 // Quaternary Science Reviews. 2015. Vol. 122. P. 1–29.

242. Molodkov A.N. IR-OSL dating of uranium-rich deposits from the new late Pleistocene section at the Voka site, North-Eastern Estonia // Quaternary Geochronology. 2007. Vol. 2, No. 1–4. P. 208–215.

243. Molodkov A.N. The Late Pleistocene palaeoenvironmental evolution in Northern Eurasia through the prism of the mollusc shell-based ESR dating evidence // Quaternary International. 2020. Vol. 556. P. 180–197.

244. Molodkov A.N., Bolikhovskaya N.S. Climate change dynamics in Northern Eurasia over the last 200 ka: Evidence from mollusc-based ESR-chronostratigraphy and vegetation successions of the loess-palaeosol records // Quaternary International. 2009. Vol. 201, No. 1–2. P. 67–76.

245. Molodkov A.N., Bolikhovskaya N.S. Palaeoenvironmental changes and their chronology during the latter half of MIS 5 on the south-eastern coast of the Gulf of Finland // Quaternary International. Elsevier Ltd, 2022. Vol. 616. P. 40–54.

246. Molodkov A.N., Bolikhovskaya N.S., Miidel A., Ploom K. The sedimentary sequence recovered from the Voka outcrops, northeastern Estonia: Implications for late Pleistocene stratigraphy // Estonian Journal of Earth Sciences. 2007. Vol. 56, No. 1. P. 47–62.

247. Molodkov A.N., Krasnov I.I. On absolute age of mollusc shells Portlandia Arctica from the Mga deposits of the Prinevskaya Lowland (in the vicinity of St. Petersburg). Saint Petersburg: VSEGEI, 1998. P. 323–324 (in Russian).

248. Molodkov A.N., Raukas A.V. The age of Upper Pleistocene marine deposits of the Boreal transgression on the basis of electron-spin-resonance (ESR) dating of subfossil mollusc shells // Boreas. 1988. Vol. 17, No. 2. P. 267–272.

249. Moore P.D., Webb J.A., Collinson M.E. Pollen Analysis. 3d Edition. Oxford: Blackwell, 1994. P. 216216 p.

250. Moska P., Adamiec G., Jary Z. High resolution dating of loess profile from Biały KoŚciół, south-west Poland // Quaternary Geochronology. 2012. Vol. 10. P. 87–93.

251. Moskvitin A.I. Mologa-Sheksna interglacial lake // Trudy Instituta geologicheskikh nauk. 1947. Vol. 88, No. 26. P. 5–18 (in Russian).

252. Moskvitin A.I. Pleistocene of the European part of the USSR (critical review of literature data) // Trudy geologicheskogo instituta. Москва: Наука, 1965. Vol. 123. P. 1–180 (in Russian).

253. Müller H. Pollenanalytische Untersuchungen und Jahresschichtenz ählung an der eemzeitlichen Kieselgur von Bispingen/Luhe // Geologisches Jahrbuch A. 1974. Vol. 21. P. 149–169.

254. Murray A.S., Arnold L.J., Buylaert J.-P., Guérin G., Qin J., Singhvi A.K., Smedley R.K., Thomsen K.J. Optically stimulated luminescence dating using quartz // Nature Reviews Methods Primers. Springer Nature, 2021. Vol. 1, No. 1.

255. Murray A.S., Buylaert J.-P., Henriksen M., Svendsen J.I., Mangerud J. Testing the reliability of quartz OSL ages beyond the Eemian // Radiation Measurements. 2008. Vol. 43, No. 2–6. P. 776–780.

256. Murray A.S., Olley J.M. Precision and accuracy in the optically stimulated luminescence dating of sedimentary quartz: A status review // Geochronometria. 2002. Vol. 21. P. 1–16.

257. Murray A.S., Svendsen J.I., Mangerud J., Astakhov V.I. Testing the accuracy of quartz OSL dating using a known-age Eemian site on the river Sula, northern Russia // Quaternary Geochronology. 2007. Vol. 2, No. 1–4. P. 102–109.

258. Murray A.S., Thomsen K.J., Masuda N., Buylaert J.-P., Jain M. Identifying well-bleached quartz using the different bleaching rates of quartz and feldspar luminescence signals // Radiation Measurements. 2012. Vol. 47, No. 9. P. 688–695.

259. Murray A.S., Wintle A.G. Luminescence dating of quartz using an improved single-aliquot regenerative-dose protocol // Radiation Measurements. 2000. Vol. 32, No. 1. P. 57–73.

260. Murray A.S., Wintle A.G. The single aliquot regenerative dose protocol: Potential for improvements in reliability // Radiation Measurements. 2003. Vol. 37, No. 4–5. P. 377–381.

261. Murray A.S., Wintle A.G., Wallinga J., Horowitz Y.S., Oster L. Dose estimation using quartz OSL in the non-linear region of the growth curve // Radiation Protection Dosimetry. Nuclear Technology Publishing, 2002. Vol. 101, No. 1–4. P. 371–374.

262. Murray-Wallace C.V., Woodroffe C.D. Quaternary sea-level changes: A global perspective. New York: Cambridge University Press, 2014. 484 p.

263. Nasonova L.D., Sammet E.Yu., Andreeva N.G., Savanina E.V., Krasnov I.I., Zarrina E.P. Information report on a set of geological, hydrogeological maps at a scale of 1:200000 of the territory of St. Petersburg and its vicinity with an explanatory note (Leningrad map-making facility). St. Petersburg, 1995 (in Russian).

264. Nazarov D.V. Quaternary deposits of the central part of the West Siberian Arctic: Dissertation for the scientific degree of Candidate of Geological and Mineralogical Sciences. 2011. 174 p (in Russian).

265. Nazarov D.V., Nikolskaia O.A., Gladysheva A.S., Zhigmanovskiy I.V., Ruchkin M.V., Merkuljev A.V., Thomsen K.J. Evidence for the intrusion of marine Atlantic waters into the West Siberian Arctic during the Middle Pleistocene // Boreas. 2022. Vol. 51, No. 2. P. 402–425.

266. Nedesheva G.N. Microfaunal characteristics of marine sediments of the Mga reference section // Vestnik Moskovskogo Universiteta. Seria geograficheskaya. 1972. No. 5. P. 108–110 (in Russian).

267. Nedrigailova I.S., Anischenkova O.N., Sokolova T.N., Savanin V.S., Kabakova I.M. Report on geological and hydrological survey of the central part of the Eastern Ladoga region on a scale of 1:200,000 for 1966-88. Leningrad: Leningrad complex geological expedition, 1971 (in Russian).

268. Nedrigailova I.S., Sokolova T.N., Savanin V.S., Yanovsky A.S. Report on comprehensive geological-hydrogeological survey of quadrangle O-36-II of scale 1 : 200 000 (Mga geological survey party 1962-64). Leningrad, 1965 (in Russian).

269. Neufeld A.H. Contributions to the biochemistry of bromine. I // Canadian Journal of Research. Canadian Science Publishing, 1936. Vol. 14b, No. 5. P. 160–194.

270. Neumann T., Christiansen C., Clasen S., Emeis K.C., Kunzendorf H. Geochemical records of salt-water inflows into the deep basins of the Baltic Sea // Continental Shelf Research. Elsevier Ltd, 1997. Vol. 17, No. 1. P. 95–115.

271. Nezhikhovsky R.A. Neva River and Neva Bay. Leningrad: Gidrometeoizdat, 1981. 112 p (in Russian).

272. Nielsen J.K., Helama S., Rodland D., Nielsen J.K. Eemian marine mollusks and barnacles from Ristinge Klint, Denmark: Hydrodynamics and oxygen defficiency // Geologie en Mijnbouw/Netherlands Journal of Geosciences. Stichting Netherlands Journal of Geosciences, 2007. Vol. 86, No. 2. P. 95–115.

273. Novenko E.Y. Vegetation and climate changes in the Central and Eastern Europe in the Late Pleistocene and Holocene at the Interglacial and transitional stages of climatic macro-cycles. Moscow: GEOS, 2016. 228 p (in Russian).

274. Novikov I.S., Nazarov D.V., Mikharevich M.V., Gladysheva A.S., Ruchkin M.V., Prudnikov S.G. The Azas ice sheet and its role in the formation of Late Pleistocene ice-dammed lakes in southern Siberia: case study of Upper Kharal paleolake // Geology and Geophysics. 2023. Vol. 64, No. 5. P. 595–606.

275. Obst K., Ansorge J., Thiel C., Frenzel P. The Late Saalian Cyprina clay of northeastern Germany and the following Weichselian sedimentation and deformation history – Review and new data // Boreas. Blackwell Publishing Inc., 2020. Vol. 49, No. 3. P. 488–513.

276. Olley J.M., Murray A.S., Roberts R.G. The effects of disequilibria in the uranium and thorium decay chains on burial dose rates in fluvial sediments // Quaternary Science Reviews. Elsevier Ltd, 1996. Vol. 15, No. 7. P. 751–760.

277. Otvos E.G. The Last Interglacial Stage: Definitions and marine highstand, North America and Eurasia // Quaternary International. Elsevier Ltd, 2015. Vol. 383. P. 158–173.

278. Panin P.G., Filippova K.G., Bukhonov A.V., Karpukhina N.V., Kalinin P.I., Ruchkin M.V. High-resolution analysis of the Likhvin loess-paleosol sequence (the central part of the East European Plain, Russia) // Catena. Elsevier B.V., 2021. Vol. 205. P. 105445.

279. Pawley S.M., Toms P., Armitage S.J., Rose J. Quartz luminescence dating of Anglian Stage (MIS 12) fluvial sediments: Comparison of SAR age estimates to the terrace chronology of the Middle Thames valley, UK // Quaternary Geochronology. 2010. Vol. 5, No. 5. P. 569–582.

280. Pedersen T.F., Price N.B. The geochemistry of iodine and bromine in sediments of the Panama Basin. // Journal of Marine Research. 1980. Vol. 38, No. 3. P. 397–411.

281. Pleshivtseva E.S. Report “Preparation for publication of the monograph “Palynology of the Pleistocene and Holocene of the North-West of the Russian Federation” (Leningrad, Pskov, Novgorod, Vologda Oblasts). In 3 books. Apatity-St. Petersburg, 2007 (in Russian).

282. Pleshivtseva E.S. History of palynological study of the Quaternary deposits stratigraphy (Leningrad, Pskov, Novgorod and Vologda Regions) // Collection of articles of FGUP “Petersburg complex geological expedition” employees devoted to the 60th organisation anniversary / ed. Vasin O.V., Korovkin V.A. St. Petersburg: Petersburg complex geological expedition, 2011. P. 53–81 (in Russian).

283. Pleshivtseva E.S. Palynological characteristic of the stratotypical section of the Mga marine deposits of the Mikulino Interglacial. Syktyvkar, 2011. P. 166–171 (in Russian).

284. Pleshivtseva E.S. Palinological study of the section of the Mga marine deposits of borehole 10 “Sverdlov Brick Factory” (Leningrad Oblast) / ed. Rozanov A.Yu., Petrov O.V., Rozhnov S.V., Arkadyev V.V., Bogdanova T.N., Bugrova E.M., Vuks B.Ya., Gavrilova V.A., Evdokimova I.O., Ivanova A.O., Kossovaya O.L., Modzalevskaya T.L., Popov E.V., Rayevskaya E.G., Sapelko T.V., Suyarkova A.A., Tesakov A.S., Titov V.V., Tolmachova T.Yu., Shurekova O.V., et al. St. Petersburg: VSEGEI, 2023. P. 176–177 (in Russian).

285. Pleshivtseva E.S., Abakumenko G.S., Gorshkova S.S. Report about studying of key Pleistocene sections in the vicinity of Leningrad. Leningrad, 1984 (in Russian).

286. Pokrovskaya I.M. About intermorainic deposits of the Mga River // Trudy Sovetskoj sekcii Mezhdunarodnoj associacii po izucheniyu chetvertichnogo perioda (INQUA). 1936. Vol. 2. P. 25–31 (in Russian).

287. Pokrovskaya I.M. The main stages in the development of vegetation during the Quaternary period on the territory of the European part of the USSR. 1954. P. 245–259 (in Russian).

288. Pokrovskaya O.A. Introduction to spore-pollen analysis. Leningrad: Nauka, 1950. 460 p (in Russian).

289. Porat N., Faerstein G., Medialdea A., Murray A.S. Re-examination of common extraction and purification methods of quartz and feldspar for luminescence dating // Ancient TL. 2015. Vol. 33, No. 1. P. 255–258.

290. Potulova N.V. Scientific chronicle // Geologichesky Vestnik. 1921. Vol. 4, No. 1–6. P. 187–187 (in Russian).

291. Potulova N.V. Geological structure of the Neva between Mga and Tosna. (Preliminary report on the summer work of 1921) // Izvestiya Geologicheskogo Komiteta. 1922. Vol. 41, No. 2–5. P. 109–126 (in Russian).

292. Potulova N.V. Some questions of the Quaternary deposits stratigraphy of the Leningrad Governorate // Izvestiya Geologicheskogo Komiteta. 1924. Vol. 43, No. 9. P. 1209–1236 (in Russian).

293. Potulova N.V. Interglacial deposits of the Mga River // Guide of excursions of the 2nd Quaternary Geological Conference. 1932. P. 2–33 (in Russian).

294. Prescott J.R., Hutton J.T. Cosmic ray contributions to dose rates for luminescence and ESR dating: Large depths and long-term time variations // Radiation Measurements. 1994. Vol. 23, No. 2–3. P. 497–500.

295. Price N.B., Calvert S.E. The geochemistry of iodine in oxidised and reduced recent marine sediments // Geochimica et Cosmochimica Acta. 1973. Vol. 37, No. 9. P. 2149–2158.

296. Price N.B., Calvert S.E. The contrasting geochemical behaviours of iodine and bromine in recent sediments from the Namibian shelf // Geochimica et Cosmochimica Acta. 1977. Vol. 41, No. 12. P. 1769–1775.

297. Price N.B., Calvert S.E., Jones P.G.W. Distribution of Iodine and Bromine in the Sediments of the Southwestern Barents Sea // Journal of Marine Research. 1970. Vol. 28, No. 1. P. 22–34.

298. Raukas A.V. Pleistocene deposits of the Estonian SSR. Tallin: Valgus, 1978. 310 p (in Russian).

299. Raukas A.V. Application of OSL and 10Be techniques to the establishment of deglaciation chronology in Estonia // Proceedings of the Estonian Academy of Sciences. Geology. Estonian Academy Publishers, 2004. Vol. 53, No. 4. P. 267–287.

300. Raukas A.V., Liivrand E.D. Pleistocene deposits in the section of the Vääna-Jõesuu borehole (Northern Estonia) and their genesis // Izvestiya Akademii Nauk Estonskoj SSR. Himiya i Geologiya. 1971. Vol. 20, No. 1. P. 60–72 (in Russian).

301. Raukas A.V., Stankowski W. Influence of sedimentological composition on OSL dating of glaciofluvial deposits: Examples from Estonia // Geological Quarterly. 2005. Vol. 49, No. 4. P. 463–470.

302. Raukas A.V., Tavast E., Vaher R. Vasavere ancient valley, its morphology, genesis and importance in the economy of North-East Estonia // Baltica. 2007. Vol. 20, No. 1–2. P. 13–18.

303. Readhead M.L. Absorbed dose fraction for 87Rb β particles // Ancient TL. 2002. Vol. 20, No. 1. P. 25–28.

304. Rees-Jones J. Optical Dating Of Young Sediments Using Fine-Grain Quartz // Ancient TL. 1995. Vol. 13, No. 2. P. 9–14.

305. Resolutions of the Interdepartmental Stratigraphic Committee and its standing commissions. Volume 33 / ed. Zhamoida A.I. Saint Petersburg: VSEGEI, 2002. 56 p.

306. Rhodes E.J., Bronk Ramsey C., Outram Z., Batt C., Willis L., Dockrill S., Bond J. Bayesian methods applied to the interpretation of multiple OSL dates: High precision sediment ages from Old Scatness Broch excavations, Shetland Isles // Quaternary Science Reviews. Elsevier Ltd, 2003. Vol. 22, No. 10–13. P. 1231–1244.

307. Roberts A.P., Chang L., Rowan C.J., Horng C.S., Florindo F. Magnetic properties of sedimentary greigite (Fe3S4): An update // Reviews of Geophysics. Blackwell Publishing Ltd, 2011. Vol. 49, No. 1.

308. Robertsson A.M., Svedlund J.O., Andrén T., Sundh M. Pleistocene stratigraphy in the Dellen region, central Sweden // Boreas. Taylor and Francis A.S., 1997. Vol. 26, No. 3. P. 237–260.

309. Rother H., Lorenz S., Börner A., Kenzler M., Siermann N., Fülling A., Hrynowiecka A., Forler D., Kuznetsov V.Y., Maksimov F.E., Starikova A. The terrestrial Eemian to late Weichselian sediment record at Beckentin (NE-Germany): First results from lithostratigraphic, palynological and geochronological analyses // Quaternary International. Elsevier Ltd, 2019. Vol. 501. P. 90–108.

310. Ruchkin M.V., Sheetov M.V., Dudanova V.I., Shukhvostov R.S., Belyaev P.Yu. Sverdlov (Etalon) Factory is a key Upper Pleistocene section in the North-West of the Russian Plain // Routes of Evolutionary Geography. Issue 2: Proceedings of the 2nd Scientific Conference in Memory of Professor A.A. Velichko (Moscow, November 22–25, 2021) / ed. Panin A.V., Borisova O.K., Konstantinov E.A., Kurenkova E.I., Timireva S.N., Kononov Yu.M. Moscow: Institute of Geography, RAS, 2021. P. 839–843 (in Russian).

311. Rudenko O.V., Taldenkova E.E., Bauch H.A., Ovsepyan Ya.S. New data on the palynostratigraphy of the Mikulinian (Eemian) deposits in the lower reaches of the Pyoza River (northeastern White Sea region) // Arctic and Antarctic Research. 2023. Vol. 69, No. 2. P. 206–227 (in Russian).

312. Rusakov A., Nikonov A., Savelieva L.A., Simakova A., Sedov S., Maksimov F.E., Kuznetsov V.Y., Savenko V., Starikova A., Korkka M., Titova D. Landscape evolution in the periglacial zone of Eastern Europe since MIS5: Proxies from paleosols and sediments of the Cheremoshnik key site (Upper Volga, Russia) // Quaternary International. Elsevier Ltd, 2015. Vol. 365. P. 26–41.

313. Rusakov A., Sedov S., Sheinkman V., Dobrynin D., Zinovyev E., Trofimova S., Maksimov F.E., Kuznetsov V.Y., Korkka M., Levchenko S.B. Late Pleistocene paleosols in the extra-glacial regions of Northwestern Eurasia: Pedogenesis, post-pedogenic transformation, paleoenvironmental inferences // Quaternary International. Elsevier Ltd, 2019. Vol. 501. P. 174–192.

314. Rzhonsnitskaya N.A., Kurochkina V.I. Report on engineering-geological research carried out in 1956 in the area of the village Otradnoe, Mga District, Leningrad Oblast (in 5 volumes). Leningrad, 1959 (in Russian).

315. Saarnisto M. Late Holocene land uplift/neotectonics on the island of Valamo (Valaam), Lake Ladoga, NW Russia // Quaternary International. 2012. Vol. 260. P. 143–152.

316. Saarnisto M., Grönlund T., Ekman I. Lateglacial of Lake Onega - Contribution to the history of the eastern Baltic basin // Quaternary International. 1995. Vol. 27, No. C. P. 111–120.

317. Salmi M. Imatra Stones in the Glacial Clay of Vuolenkoski // Bulletin de la Commission géologique de Finlande. 1959. Vol. 186. P. 1–27.

318. Sánchez-Goñi M.F., Eynaud F., Turon J.L., Shackleton N.J. High resolution palynological record off the Iberian margin: Direct land-sea correlation for the Last Interglacial complex // Earth and Planetary Science Letters. 1999. Vol. 171, No. 1. P. 123–137.

319. Sanderson D.C.W., Bishop P., Stark M., Alexander S., Penny D. Luminescence dating of canal sediments from Angkor Borei, Mekong Delta, Southern Cambodia // Quaternary Geochronology. 2007. Vol. 2, No. 1–4. P. 322–329.

320. Savelieva L.A. Migration specifics of spruce and alder in the Holocene in the north-west of European Russia: Dissertation for an academic degree Candidate of Geographical Sciences. St. Petersburg: St. Petersburg University, 2007. 145 p (in Russian).

321. Schielein P., Schellmann G., Lomax J., Preusser F., Fiebig M. Chronostratigraphy of the Hochterrassen in the lower Lech valley (Northern Alpine Foreland) // Quaternary Science Journal. Copernicus GmbH, 2015. Vol. 64, No. 1. P. 15–28.

322. Schokker J., Cleveringa P., Murray A.S. Palaeoenvironmental reconstruction and OSL dating of terrestrial Eemian deposits in the southeastern Netherlands // Journal of Quaternary Science. 2004. Vol. 19, No. 2. P. 193–202.

323. Seidenkrantz M.S. Benthic foraminiferal and stable isotope evidence for a “Younger Dryas-style” cold spell at the Saalian-Eemian transition, Denmark // Palaeogeography, Palaeoclimatology, Palaeoecology. 1993. Vol. 102, No. 1–2. P. 103–120.

324. Selivanova V.A. Geological map of the USSR (pre-Quaternary deposits). Scale 1:200 000. Ilmen Series. Sheet O-36-I. Moscow: Gosgeoltechizdat, 1962 (in Russian).

325. Selle W. Geologische und vegetationskundliche Untersuchungen an einigen wichtigen Vorkommen des letzten Interglazials in Nordwestdeutschland // Geologisches Jahrbuch. 1962. Vol. 79. P. 195–352.

326. Serebryanny L.R. Dynamics of proagation of some tree species in the north-west of the USSR in the postglacial time // Holocene Palinology. Moscow: Nauka, 1971. P. 17–31 (in Russian).

327. Shackleton N.J. The last interglacial in the marine and terrestrial records // Proceedings of the Royal Society of London. Series B. Biological Sciences. The Royal Society, 1969. Vol. 174, No. 1034. P. 135–154.

328. Shackleton N.J., Chapman M., Sánchez-Goñi M.F., Pailler D., Lancelot Y. The classic marine isotope substage 5e // Quaternary Research. Academic Press Inc., 2002. Vol. 58, No. 1. P. 14–16.

329. Shackleton N.J., Sánchez-Goñi M.F., Pailler D., Lancelot Y. Marine isotope substage 5e and the Eemian interglacial // Global and Planetary Change. Elsevier B.V., 2003. Vol. 36, No. 3. P. 151–155.

330. Sheshukova V.S. Diatoms of Quaternary sediments // Diatom analysis. Book 1 / ed. Proshkina-Lavrenko A.I. Moscow-Leningrad: Gosudarstvennoe izdatelstvo geologicheskoj literatury, 1949. P. 153–180 (in Russian).

331. Shishkina O.V. Geochemistry of marine and oceanic silt waters. Moscow: Nauka, 1972. 228 p (in Russian).

332. Shishkina O.V., Pavlova G.A. Iodine distribution in marine and oceanic bottom muds and their pore fluids // Geochem. Int. 1965. Vol. 2. P. 559-565.

333. Shmayonok A.I., Sammet E.Y., Belenitskaya G.A., Verbova G.N., Korneeva T.L., Ronshin N.I., Feigelson M.M. Geological structure of the area of the lower reaches of the Narva, Luga and Sista Rivers (report on a comprehensive geological survey, scale 1:200,000). Leningrad, 1962 (in Russian).

334. Sier M.J., Peeters J., Dekkers M.J., Parés J.M., Chang L., Busschers F.S., Cohen K.M., Wallinga J., Bunnik F.P.M., Roebroeks W. The Blake Event recorded near the Eemian type locality - A diachronic onset of the Eemian in Europe // Quaternary Geochronology. Elsevier B.V., 2015. Vol. 28. P. 12–28.

335. Sier M.J., Roebroeks W., Bakels C.C., Dekkers M.J., Brühl E., De Loecker D., Gaudzinski-Windheuser S., Hesse N., Jagich A., Kindler L., Kuijper W.J., Laurat T., Mücher H.J., Penkman K.E.H., Richter D., van Hinsbergen D.J.J. Direct terrestrial-marine correlation demonstrates surprisingly late onset of the last interglacial in central Europe // Quaternary Research. 2011. Vol. 75, No. 1. P. 213–218.

336. Skorokhod V.Z. Fauna of interglacial sediments of the Mga River // Materialy po chetvertichnoj geologii SSSR, chast' 1. Trudy Vsesoyuznogo geologorazvedochnogo ob"edineniya NKTP SSSR. 1932. Vol. 225. P. 82–93 (in Russian).

337. Smith B.W. Zircon from sediments: A combined OSL and TL auto-regenerative dating technique // Quaternary Science Reviews. 1988. Vol. 7, No. 3–4. P. 401–406.

338. Sohbati R., Murray A.S., Jain M., Thomsen K.J., Hong S.C., Yi K., Choi J.H. Na-rich feldspar as a luminescence dosimeter in infrared stimulated luminescence (IRSL) dating // Radiation Measurements. 2013. Vol. 51–52. P. 67–82.

339. Sokolova L.F., Malyasova E.S., Vishnevskaya E.M., Lavrova M.A. A new find of the Mga interglacial deposits in the central part of the Karelian Isthmus // Vestnik Leningradskogo Universiteta. 1972. Vol. 12. P. 124–131 (in Russian).

340. Sokolova L.F., Mokrienko Z.M. Report on a comprehensive engineering-geological survey on a scale of 1:50,000, carried out in the Vsevolozhsk District of the Leningrad Oblast (sheets P-36-133-Б and P-36-134-A, B, Г) in 1959. Leningrad, 1960 (in Russian).

341. Sokolova L.F., Mokrienko Z.M., Elkhanov Yu.L. Report on a comprehensive engineering-geological survey on a scale of 1:50,000, carried out in the Vsevolozhsk, Mga and Tosno Districts of the Leningrad Oblast (sheets O-36-2-Б, Г and O-36-3-A, B partially) in 1958. Leningrad, 1959 (in Russian).

342. Spooner N.A. Optical dating: Preliminary results on the anomalous fading of luminescence from feldspars // Quaternary Science Reviews. 1992. Vol. 11, No. 1–2. P. 139–145.

343. Spooner N.A. The anomalous fading of infrared-stimulated luminescence from feldspars // Radiation Measurements. 1994. Vol. 23, No. 2–3. P. 625–632.

344. Starik I.E., Arslanov K.A., Malakhovsky D.B. On the age of the Mga interglacial marine strata according to the radiocarbon method // Doklady Akademii Nauk SSSR. 1964. Vol. 157, No. 6. P. 1369–1372 (in Russian).

345. Stokes G.G. On the Change of Refrangibility of Light // Philosophical Transactions of the Royal Society of London. 1852. Vol. 142. P. 463–562.

346. Strahl J., Krbetschek M.R., Luckert J., Machalett B., Meng S., Oches E.A., Rappsilber I., Wansa S., Zöller L. Geologie, Paläontologie und Geochronologie des Eem-Beckens Neumark-Nord 2 und Vergleich mit dem Becken Neumark-Nord 1 (Geiseltal, Sachsen-Anhalt) // E&GQuaternary Science Journal. Copernicus GmbH, 2010. Vol. 59, No. 1/2. P. 120–167.

347. Streif H. Quaternary Sea-Level Changes in the North Sea, an Analysis of Amplitudes and Velocities // Earth's Rotation from Eons to Days / ed. Brosche P., Sündermann J. Springer-Verlag, 1990. P. 201–214.

348. Sukachov V.N. The main features of the Pleistocene vegetation history in the USSR // Materials on the Quaternary period of the USSR. Leningrad, Moscow: Izdatelstvo AN SSSR, 1936. P. 62–89 (in Russian).

349. Svendsen J.I., Alexanderson H., Astakhov V.I., Demidov I.N., Dowdeswell J.A., Funder S., Gataullin V., Henriksen M., Hjort C., Houmark-Nielsen M., Hubberten H.W., Ingólfsson Ó., Jakobsson M., Kjær K.H., Larsen E., Lokrantz H., Lunkka J.P., Lyså A., Mangerud J., Matiouchkov A., et al. Late Quaternary ice sheet history of northern Eurasia // Quaternary Science Reviews. 2004. Vol. 23, No. 11–13. P. 1229–1271.

350. Tang Y., Ren D., Zheng J., Guo M., Rong X., Ni Y. The research on magnetism and mechanism on pyrite in coal // Chinese Science Bulletin. 1995. Vol. 40, No. 16. P. 1483−1486-1483−1486.

351. Tarr W.A. Concretions in the Champlain formation of the Connecticut River valley // Bulletin of the Geological Society of America. Geological Society of America, 1935. Vol. 46, No. 10. P. 1493–1534.

352. Tavast E., Raukas A.V. Bedrock relief in Estonia. Tallin: Valgus, 1982. 193 p (in Russian).

353. Thiel C., Buylaert J.-P., Murray A.S., Terhorst B., Hofer I., Tsukamoto S., Frechen M. Luminescence dating of the Stratzing loess profile (Austria) - Testing the potential of an elevated temperature post-IR IRSL protocol // Quaternary International. 2011. Vol. 234. P. 23–31.

354. Thomsen K.J. Optically Stimulated Luminescence Techniques in Retrospective Dosimetry using Single Grains of Quartz extracted from Unheated Materials. PhD thesis. 2004. P. 176–176.

355. Thomsen K.J., Jain M., Murray A.S., Denby P.M., Roy N., Bøtter-Jensen L. Minimizing feldspar OSL contamination in quartz UV-OSL using pulsed blue stimulation // Radiation Measurements. 2008. Vol. 43, No. 2–6. P. 752–757.

356. Timar-Gabor A., Vasiliniuc S., Vandenberghe D.A.G., Cosma C., Wintle A.G. Investigations into the reliability of SAR-OSL equivalent doses obtained for quartz samples displaying dose response curves with more than one component. 2012. Vol. 47. P. 740–745.

357. Tsukamoto S., Rink W.J., Watanuki T. OSL of tephric loess and volcanic quartz in Japan and an alternative procedure for estimating De from a fast OSL component // Radiation Measurements. 2003. Vol. 37, No. 4–5. P. 459–465.

358. Tukey John.W. Exploratory Data Analysis. Reading, Massachusetts: Addison-Wesley Publishing Company, 1977. P. 688688 p.

359. Turner C. Problems of the duration of the Eemian interglacial in Europe North of the Alps // Quaternary Research. Academic Press Inc., 2002. Vol. 58, No. 1. P. 45–48.

360. Turney C.S.M., Jones R.T. Does the Agulhas Current amplify global temperatures during super-interglacials? // Journal of Quaternary Science. 2010. Vol. 25, No. 6. P. 839–843.

361. Tzedakis C. Timing and duration of Last Interglacial conditions in Europe: A chronicle of a changing chronology // Quaternary Science Reviews. Elsevier Ltd, 2003. Vol. 22, No. 8–9. P. 763–768.

362. Udden J.A. Mechanical composition of clastic sediments // Geological Society of America Bulletin. Geological Society of America, 1914. Vol. 25, No. 1. P. 655–744.

363. Usikova T.V., Malyasova E.S. On the question of the origin of the kame hills in the vicinity of Leningrad // Baltica. 1965. Vol. 2. P. 261–280 (in Russian).

364. Vandenberghe D.A.G., De Corte F., Buylaert J.-P., Kučera J., Van Den Haute P. On the internal radioactivity in quartz // Radiation Measurements. 2008. Vol. 43, No. 26. P. 771–775.

365. Velichko A.A., Novenko E.Y., Pisareva V.V., Zelikson E.M., Boettger T., Junge F.W. Vegetation and climate changes during the Eemian interglacial in Central and Eastern Europe: Comparative analysis of pollen data // Boreas. 2005. Vol. 34, No. 2. P. 207–219.

366. Verbitsky V.R., Yanovsky A.S., Verbitsky I.V., Vasilyeva O.V. State geological map of the Russian Federation of scale 1:1 000 000 (3rd generation). Cenral European Series. Sheet O-35 (Pskov), (N-35), O-36 (St. Petersburg). Geological map of pre-Quaternary deposits. St. Petersburg: VSEGEI, 2012 (in Russian).

367. Verzilin N.N., Gontarev E.A., Kalmykova N.A. Lithological and mineralogical characteristics of Late Glacial–Holocene deposits of the Neva River valley // Lithology and paleogeography. Vol. 5. Collection of scientific works dedicated to the 80th anniversary of Professor Nikolay Vasilyevich Logvinenko. St. Petersburg: St. Petersburg State University Publishing House, 1997. P. 206–219 (in Russian).

368. Vinogradov A.P. Iodine in marine muds. On the origin of iodine-bromine waters in oil regions // Trudy bio-geohimicheskoy laboratorii AN SSSR. 1939. Vol. 5. P. 19–32 (in Russian).

369. Vishnevskaya E.M., Malyasova E.S., Usikova T.V. A new section of the Mga interglacial deposits in in the vicinity of Leningrad // Vestnik Leningradskogo Universiteta. 1973. Vol. 24. P. 133–140 (in Russian).

370. Volkov I.I. Geochemistry of sulphur in ocean sediments. Moscow: Nauka, 1984. P. 272272 p (in Russian).

371. Volkov I.I. Iron sulfides, their relationships and transformations in sediments of the Black Sea // Trudy Instituta okeanologii AN SSSR. 1961. Vol. 50. P. 68–92 (in Russian).

372. Waelbroeck C., Frank N., Jouzel J., Parrenin F., Masson-Delmotte V., Genty D. Transferring radiometric dating of the last interglacial sea level high stand to marine and ice core records // Earth and Planetary Science Letters. 2008. Vol. 265. No. 1–2. P. 183–194.

373. Wagner G.A. Age determination of young rocks and artifacts: physical and chemical clocks in Quaternary geology and archaeology (translated from German). Berlin-Heidelberg, 1998. 466 p.

374. Wallinga J., Murray A.S., Duller G.A.T. Underestimation of equivalent dose in single-aliquot optical dating of feldspars caused by preheating // Radiation Measurements. 2000. Vol. 32, No. 5. P. 691–695.

375. Watanuki T., Murray A.S., Tsukamoto S. Quartz and polymineral luminescence dating of Japanese loess over the last 0.6 Ma: Comparison with an independent chronology // Earth and Planetary Science Letters. 2005. Vol. 240, No. 3–4. P. 774–789.

376. Wentworth C.K. A Scale of Grade and Class Terms for Clastic Sediments // The Journal of Geology. University of Chicago Press, 1922. Vol. 30, No. 5. P. 377–392.

377. Wilkin R.T., Barnes H.L. Formation processes of framboidal pyrite // Geochimica et Cosmochimica Acta. Elsevier Ltd, 1997. Vol. 61, No. 2. P. 323–339.

378. Winn K., Glos R., Averdieck F.-R., Erlenkeuser H. On the age of the marine Eem in northwestern Germany // Geologos. 2000. Vol. 5. P. 41–56.

379. Woillard G.M. Grande Pile Peat Bog: A Continuous Pollen Record for the Last 140,000 Years // Quaternary Research. Cambridge University Press, 1978. Vol. 9, No. 1. P. 1–21.

380. Wu X. qing, Xie X., Cao Y. fan. Self-magnetization of pyrite and its application in flotation // Transactions of Nonferrous Metals Society of China (English Edition). Nonferrous Metals Society of China, 2016. Vol. 26, No. 12. P. 3238–3244.

381. Yakovlev S.A. Sediments and relief of Leningrad and its vicinity. Leningrad: 2-ya tip. Transpechati NKPS im. t. Lokhankova, 1926. 186 p (in Russian).

382. Yakovlev S.A. On marine transgressions in the north of the Russian Plain in the Quaternary perod // Bulletin of the Commission for study of the Quaternary. 1947. Vol. 9. P. 5–14 (in Russian).

383. Yakovlev S.A. Fundamentals of the geology of Quaternary deposits of the Russian Plain (stratigraphy) // Trudy Vsesoyuznogo nauchno-issledovatelskogo geologicheskogo instituta VSEGEI Ministerstva geologii i ohrany nedr SSSR. Novaya Seriya. 1956. Vol. 17. P. 1–314 (in Russian).

384. Yanishevsky M.E. A brief preliminary report on geological work in the 41st sheet of the 10-verst map of European Russia in 1923 // Izvestiya Geologicheskogo Komiteta. 1924. Vol. 43, No. 6. P. 667–695 (in Russian).

385. Yanishevsky M.E. Geological sketch of the western part of the 41st sheet of the 10-verst map of the European part of the USSR // Trudy Glavnogo Geologo-Razvedochnogo Upravleniya VSNKh SSSR. 1931. Vol. 78. P. 1–38 (in Russian).

386. Yi S., Buylaert J.-P., Murray A.S., Lu H., Thiel C., Zeng L. A detailed post-IR IRSL dating study of the Niuyangzigou loess site in northeastern China // Boreas. 2016. Vol. 45, No. 4. P. 1–14.

387. Zagwijn W.H. Vegetation, climate and radiocarbon datings in the Late Pleistocene of The Netherlands. Part I: Eemian and Early Weichselian // Mededelingen van de Geologische Stichting. 1961. Vol. 14. P. 15–45.

388. Zagwijn W.H. Sea-level changes in The Netherlands during the Eemian. // Geologie en Mijnbouw. 1983. Vol. 62, No. 3. P. 437–450.

389. Zagwijn W.H. An analysis of Eemian climate in western and central Europe // Quaternary Science Reviews. Elsevier Ltd, 1996. Vol. 15, No. 5–6. P. 451–469.

390. Zander A., Hilgers A. Potential and limits of OSL, TT-OSL, IRSL and pIRIR290 dating methods applied on a Middle Pleistocene sediment record of Lake El'gygytgyn, Russia // Climate of the Past. 2013. Vol. 9, No. 2. P. 719–733.

391. Zans V. Das letzt Interglaziale Portlandia-Meer des Baltikums // Comptes Rendus de la Societé Gèologique de Finlande. 1936. Vol. 9. P. 231–250.

392. Zemlyakov B.F. Quaternary geology of Karelia. Petrozavodsk: Gosudarstvennaya tipografiya imeni Anokhina, 1936. 103 p (in Russian).

393. Zemlyakov B.F., Pokrovskaya I.M., Sheshukova V.S. New data on the Late Glacial marine Baltic-White Sea connection // Trudy Sovetskoj sekcii AICHPE. 1941. Vol. 5. P. 156–180 (in Russian).

394. Zhuze A.P., Proshkina-Lavrenko A.I., Sheshukova-Poretskaya V.S. Chapter VI. Research methodology // Diatoms in the USSR (fossil and modern). Vol. 1. Leningrad: Nauka. Leningrad branch, 1974. P. 50–79 (in Russian).

395. Zimmerman D.W. Thermoluminescence dating using fine grains from pottery // Archaeometry. 1971. Vol. 13. P. 29–52.

396. Znamenskaya O.M. Stratigraphical position of the Mga marine deposits // Doklady Akademii Nauk. 1959. Vol. 129, No. 2. P. 401–404 (in Russian).

397. Znamenskaya O.M., Cheremisinova E.A. Spreading of the Mga interglacial sea and the main features of its paleogeography // Questions of the Quaternary deposits stratigraphy of the North-West of the European USSR / ed. Lavrova M.A. Leningrad: Gostoptechizdat. Leningrad branch, 1962. P. 140–160 (in Russian).

398. Znamenskaya O.M., Cheremisinova E.A. New data on marine interglacial sediments in the Elbląg Upland region // Vestnik Leningradskogo Universiteta. 1970. Vol. 18. P. 86–101 (in Russian).